वार्षिक प्रतिवेदन 2009-2010
Annual Report 2009-2010

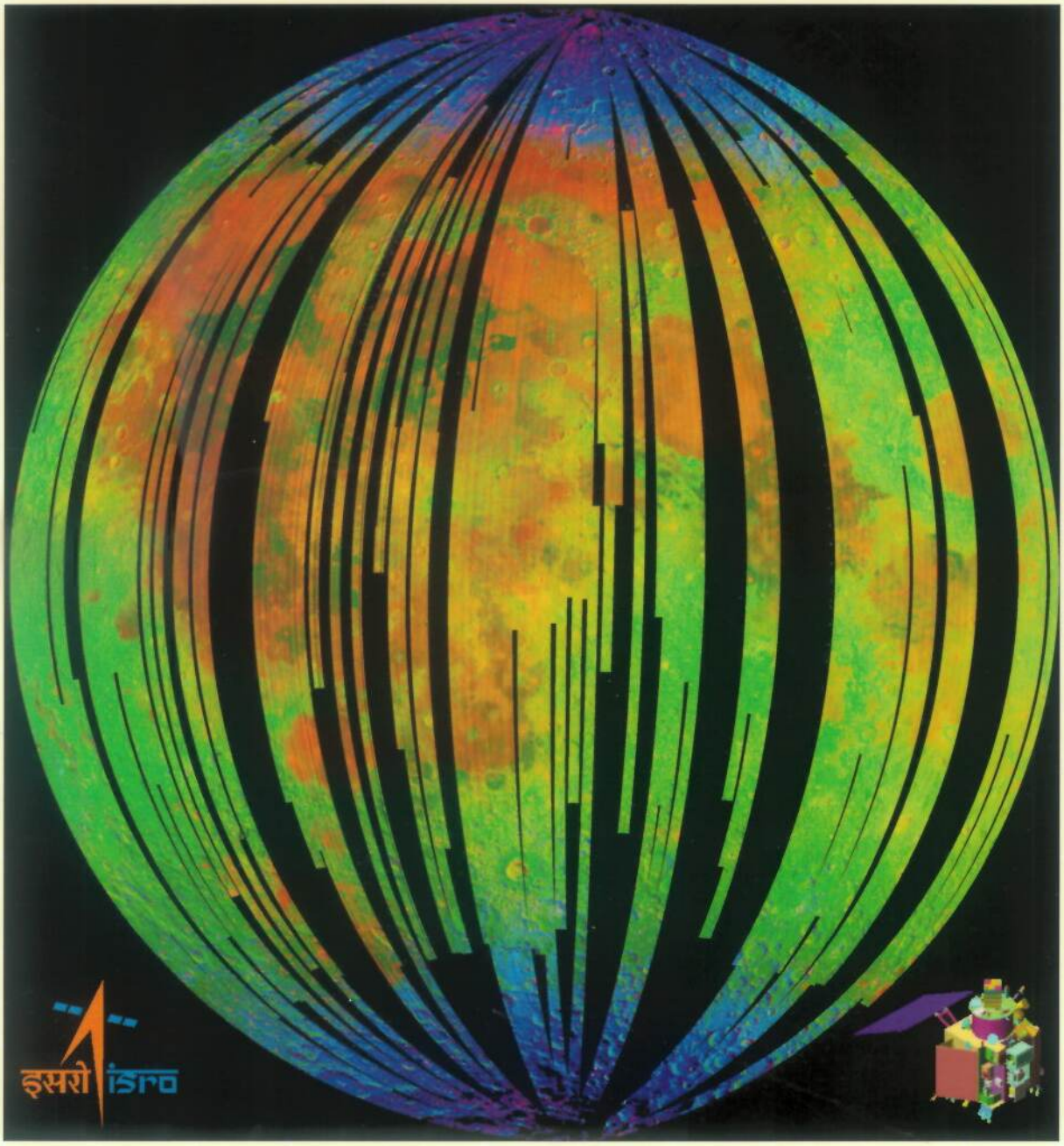

भौतिक अनुसंधान प्रयोगशाला, अहमदाबाद
Physical Research Laboratory, Ahmedabad

Director's Foreword

The discovery of presence of water molecules in lunar surface soils and rocks was a landmark achievement of the Chandrayaan-1 mission that received global acclaim. Association of PRL in the study that culminated in this major scientific result has made the last year a very eventful one for us. The Chandrayaan-1 mission has yielded a wealth of new data on lunar landform, mineralogy, chemistry and radiation environment that are being analyzed by eleven science teams across the globe. New findings from these studies were presented by the science teams at a Chandrayaan-1 Science Meet organized at PRL early this year. These findings have revealed new facets of lunar science and are providing newer insights about our nearest Solar System neighbour. The Chandrayaan-1 mission, in which PRL played a key role, has placed India in a pre-eminent position in the Global Planetary Exploration scene.

The pre-mature termination of Chandrayaan-1 mission did affect some of the planned scientific objectives. The High Energy X-ray Spectrometer, developed jointly by PRL and the ISRO Satellite Center, did perform as expected. However, the thermal constraints experienced during the mission reduced its operation time and the data collected were not sufficient to make definitive conclusions. Nonetheless, the activities in the field of Planetary Exploration at PRL are growing steadily and several proposals have been submitted to ISRO for the forthcoming Chandrayaan-2 mission. PRL is also continuing its efforts to enhance research in Planetary Sciences in the country by supporting and nurturing research programme at various academic and research institutes and universities through the ISRO sponsored PLANEX program.

Scientific activities conducted at PRL during the year yielded a significant number of new results. Some of these are outlined in the section on *"Scientific Highlights".* The "Science" section covers detail reports of scientific activities carried out by the different research divisions that include Astronomy and Astrophysics, Solar Physics, Planetary Sciences, Space and Atmospheric Sciences, Geosciences and Theoretical Physics. Several young scientists with strong academic credentials have joined PRL as faculty members during the year. A Computational Physics group was also formed to ensure efficient utilization of the recently commissioned cluster computational facility.

As parts of the 11th five year plan activities, several experimental facilities have been established during the year. These include a Multi-collector inductively-coupled plasma mass spectrometer for isotopic studies of terrestrial and planetary materials, an Aerosol time of flight mass spectrometer for physical and chemical characteristics of single aerosol particles, a Stable isotope mass spectrometer

for terrestrial and oceanic studies and a computer cluster for advanced computational work. The Multi-Application Solar Telescope (MAST) is anticipated to be commissioned at the Udaipur Solar Observatory by early 2011. Infrastructure upgrade at the observatory site to house MAST is nearing completion.

Design and engineering specifications of the Space Instrumentation facility, that will support development of space-borne payloads for studies in the areas of Planetary Exploration, Space and Atmospheric Sciences and Astronomy, have been finalized and construction will commence shortly. Several in house activities in the area of advanced techniques have yielded very good results. These include, successful demonstration of adaptive optics system for studies of sunspot activities and realization of a detection capability of a few meter per second in radial velocity excursions of sun like stars using the Echelle spectrograph, to be used for the search of exoplanets.

The total strength of faculty, post-doctoral fellow and research scholar is now close to one hundred and fifty and sustained endeavours to increase this number in the coming years will continue. Research conducted during the year resulted in publication of 129 papers in high impact peer reviewed journals, and 70 papers were published in the Proceedings of conferences. PRL faculty members authored 18 invited reviews and edited two conference proceedings. Eight research scholars have completed their Ph.D. studies during the year.

Recognition of the scientific work carried out by the faculty members and research scholars at PRL has come from both international and national academic forums. These include fellowship of National Science Academy, Honorary Fellowship of the Geological Society of London, INSA Young Scientist Medal, Krishnan Medal of Indian Geophysical Union, Goyal Prize for Physics, Membership of International Commissions, Adjunct and Honorary Professorships, J. C. Bose National fellowship and membership of Editorial Board of reputed journals. Eleven research scholars and young scientists were recognized for their work and were recipient of various national and international awards. I look forward to see this trend continue in the coming years with hope and anticipation.

Several Conferences/Workshops/Schools were held at PRL during the year. These include the International Workshop on High Energy Physics Phenomenology, The Second Asia-Pacific Conference on Luminescence and Electron Spin Resonance Dating, SERC School on Atomic and Molecular Physics, and the Sixth Chandrayaan-1 Science Meet. The colloquium and divisional seminar activities have been continued with vigour and apart from PRL faculty, 24 scientists from within the country and abroad were invited to present their scientific work in PRL colloquium series. Prof. Larry Ramsey of the Pennsylvania State University, USA, visited PRL during early 2010 as K. R. Ramanathan Professor.

As a part of Human Resource Development efforts, forty M.Sc. students and fifty B.Tech. students carried out project work at PRL under the guidance of academic and technical faculty during their summer vacation. PRL also conducted the Sixth UN Post-graduate Course of the Centre for Space Science & Technology Education in Asia and the Pacific (2009-10) in Space Sciences. Initiatives to increase interactions with school students in and around Ahmedabad have been continued through regular visits of students to PRL and interaction with Faculty members. The scope of the Science day activities was enhanced by organizing regional meets across Gujarat where PRL faculty interacted with students and selecting nearly 200 out of more than two thousand students, representing schools from all over the state, who were invited for the final meet on Science day at PRL. Talented students were offered scholarship and other incentives based on their performances in the events during the Science day. PRL scientists also carried out coordinated activities, in association with school and college students, at several centers spread over the states of Gujarat and Madhya Pradesh, for the observation of shadow bands during the long duration total solar eclipse in 2009. Progressive use of Hindi, particularly in administrative areas, is being pursued and realization of a bilingual PRL website is targeted within the coming year.

The PLANEX and RESPOND programmes of ISRO, administered by PRL, are progressing well. The PLANEX programme is aimed at fostering growth of research in Planetary Sciences and allied fields in the country, while the RESPOND programme supports research in the fields of Atmospheric and Space Sciences and in Astronomy and Astrophysics. Nearly fifty research groups in the country are being supported currently by these two programmes. Workshop on Planetary Sciences as well discussion meetings to formulate Science plans for future planetary missions to Moon and Mars were also organized as a part of PLANEX programme.

The dedication and hard work of all the members of PRL have led to a very successful and productive year for PRL and I thank and applaud all my scientific, technical, administrative colleagues and other members at PRL for their sincerity and devotion. The anticipation is high and there exists areas of concerns and we need to strive even harder to fully justify the unbounded confidence reposed on us by the Department of Space in terms of support received over the years. PRL needs to think ahead and formulate new and more challenging science objectives and chalk out appropriate plans and programmes to be pursued during the next five year plan.

In conclusion, I would urge all PRL members to continue to work with dedication and strive to further enhance the reputation of PRL as a major research center with a strong international credibility. I would like to thank the Chairman, Council of Management, PRL, and all the other members of the council for their sage advice, wise counsel that helped in smooth running of PRL and also for their support in implementation of several new academic and administrative initiatives.

J. N. Goswami

Director

Science Highlights

Astronomy & Astrophysics

- A high optical echelle spectrograph for detecting exo-planets by the radial velocity technique is undergoing commissioning tests at Mt. Abu Observatory. The spectrograph has reached a stability level of ~4m/ sec. The stability is expected to improve further when installation and fine tuning is complete by the end of 2010. Over 1000 dwarf stars upto visual magnitude of 10.5 are proposed to be studied over the next few years for exo-planet detections.

- The first overtone bands of carbon monoxide (CO) in Nova V2615 Ophiuchi (2007) were detected in 2.29-2.40 micron region from Mt. Abu Observatory. The CO bands are modeled to estimate temperature and mass of the gas emitting CO at several epochs enabling thereby the study of the formation and evolution of COtill the time of its rapid destruction.

- From Spitzer IRAC Imaging photometric study several new embedded young stellar objects (YSOs) have been identified near the central compact cluster of the massive star forming region AFGL 437.The outflow driving source in this cluster is a very young star that is not yet hot enough to form a HII region. Molecular hydrogen counterparts are detected in the outflow from this star.

- Near Infrared lunar occultations from Mt Abu Observatory of stars in the vicinity of the galactic centre region have yielded three resolved sources with angular sizes ranging from 7 to 18 milliarcseconds. A binary has also been detected with a projected separation between components of about 30 milliarcseconds. Two of the resolved sources are late type M giants while the third is a carbon star.

- Time series analysis on the latitude bins of solar full disc (SFD) images of Nobeyama Radioheliograph at 17 GHz for the period 1992-2001 show that solar corona rotates less differentially than the photosphere or chromosphere and has a smaller gradient in the rotation rate.

Solar Physics

- Analysis of satellite based and ground based data yielded several new results, which include: i) neutralization of net vertical current in individual

sunspots, ii) surface magnetic twist providing an upper limit for peak X-ray flux in solar flares, iii) sub-surface flow properties determining the flare productivity of an active region, iv) improvement in the prediction of arrival times at earth, of CMEs, with stereoscopic observations, and v) excitation of high frequency oscillations of whole sun by solar flares.

- A new telescope with a prototype collapsible dome was installed in the main USO campus, which was used to observe the partial solar eclipse of 16 January 2010.

Planetary Sciences and PLANEX Program

- Analysis of data from the Moon Mineral Mapper (M^3) on board Chandrayaan-1 has led to the first detection of hydroxyl and water molecule on lunar surface, a major discovery in the field of planetary sciences. Distinct absorption feature near 2.8 to 3.0 micrometers is widely seen and appears strongest at cooler high latitudes and also at several fresh feldspathic craters. These findings have been corroborated by later observations made by the Deep Impact mission and analysis of archival data obtained by this mission in 2007 and by Cassini mission in 1999. Interactions of solar wind ions with lunar surface soils and rocks is considered as the most probable cause for the observed OH and H_2O on lunar surface.

- Compositional and Topographic study of high altitude locations within Sculptured hills and Massifs surrounding Taurus-Littrow valley (Apollo 17 site) have revealed presence of numerous mafic anomalies on them, consistent with earlier findings from Clementine data. However, these are found to be morphologically different from each other and compositionally not all of them are either noritic or basaltic as envisaged earlier from spectral and compositional data, revealing greater geologic complexity for the region.

- Almahata Sitta is a recent meteorite fall, classified as a ureilite, and is the first meteorite to be associated with a known small asteroid of size ~4 m, called 2008 TC_3 (class F), whose fall was predicted and observed on Oct. 7, 2008 in the Nubian Desert of Sudan. This highly porous polymict ureilite has been studied for trapped N and noble gases and yielded a cosmic ray exposure ages of ~15 Ma in interplanetary space. Survival of a 4m object with high porosity, for such a long duration is a surprise and has implications for meteorite transport to inner solar system.

Space and Atmospheric Sciences

- Investigations of equatorial ionosphere during annular solar eclipse on 15 January 2010 using rocket borne probes indicate decrease in electric fields in addition to the conductivities during solar eclipse.

- Model calculations reveal that over urban regions black carbon aerosols alone can contribute 60% and 25% of shortwave and long-wave aerosol radiative forcing respectively, thereby, emphasizing the crucial role black carbon aerosols play in altering the Earth-atmosphere radiation budget.

- Simulation of tropospheric NO_2 column abundances over India using a global chemical transport model and comparison with satellite data revealed that the model overestimates the column NO_2 abundances, indicating uncertainties in emission inventory or errors in retrieval from the satellite data.

- The investigation of the response of solar X-ray flares on Martian atmosphere indicates that the sustenance of TEC (Total Electron Content) enhancement could be about a day.

Geosciences

- The chemical composition (involving water-soluble inorganic constituents, crustal elements and carbonaceous species) of size-segregated aerosols (PM_{10} and $PM_{2.5}$), collected from the marine atmospheric boundary layer (MABL) of the Bay of Bengal during 27th Dec' 08 – 28th Jan' 09, has provided the first field-based evidence for the increase

in the solubility of aerosol-Fe due to the acid processing of mineral dust during atmospheric transport from the Indo-Gangetic Plain. A temporal shift in the winds, representing the outflow from south-east Asia, and aerosol composition over the south Bay of Bengal also exhibit enhanced fractional solubility of aerosol-Fe, but associated with lower concentration of dust. These observations suggest the dominance of combustion sources (biomass burning and fossil-fuel) in dictating the aerosol-Fe solubility over the southern Bay.

- Simultaneous measurements of the surface level concentrations of sulphur dioxide (SO_2) and submicron sulphate aerosols (SO_4^{2-}), carried out from an urban region (Ahmedabad) and a high-altitude site (Mt. Abu), suggest that the ratio of SO_4^{2-} to SO_x (SO_x = SO_2 + SO_4^{2-}), termed as S-ratio, over an urban region is 0.37 and 0.55 during Aug-Sept'08 and Jan '09, respectively. In contrast, at Mt. Abu, the S-ratio is 0.28 during Feb '09 and 0.18 during Sept-Oct '09. An increase in the S-ratio during the high dust season is attributed to the enhancement in the oxidation efficiency of SO_2 due to the heterogeneous phase chemistry, in addition to the homogeneous gas phase reactions.

- The first results of daily measurements of stable oxygen and hydrogen isotopic compositions of atmospheric water vapor ($\delta^{18}O_{av}$, δD_{av}) and rain ($\delta^{18}O_r$, δD_r) during 2007-08 over Ahmedabad, India, based on satellite data, show that the onset of monsoon is marked by a dramatic decrease of ~ 2.9‰ and ~ 60‰, in $\delta^{18}O_{av}$, δD_{av}, respectively, and 46‰ in deuterium excess (δD-8$\delta^{18}O$) of vapor and $\delta^{18}O_{av}$, δD_{av}, $\delta^{18}O_r$ and δD_r exhibit correlated variations during the monsoon (15 June-15 September). The daily variations of $\delta^{18}O_{av}$ and δD_{av} are higher during large rain events, with sharp negative excursions from mean values.

- Studies on cosmic ray produced luminescence of meteorites using different emission spectral bands suggested the possibility of estimation of the duration of cosmic ray exposure using luminescence methods. Simulation and modeling of the interaction of cosmic radiation with a meteorite body, using a GEANT4 code, along with the determination of the efficiency of heavy charged particles in inducing luminescence provided the first realistic estimation of the annual cosmic ray dose to a meteorite body. Measurement of the thermal and athermal decay rates revealed a time dependence of the athermal decay factor (the g-factor), that offers the prospects of a direct estimation of cosmic ray exposure ages using luminescence.

- An imaging luminescence system comprising an electron multiplier CCD camera was developed in-house. The system offers spatial resolution of 25µm with provisions of measurements in specific spectral windows. The system can work in all luminescence modes and the command operations are developed with LABVIEW based interface. Images from repeat runs can be aligned within one pixel. This development will permit studies of natural samples that do-not permit extraction of requisite minerals used for luminescence analysis.

- A mathematical model has been developed to quantify the changes in isotopic ratios and concentration of an element in a parental magma during concurrent assimilation and fractional crystallization of silicate rocks combined with immiscible separation of carbonate melt (AFCLI), which leads to the formation of carbonatite and associated silicate rocks. AFCLI model successfully explains the isotopic ratio variations observed in most carbonatite-alkaline silicate complexes, which indicates that crustal assimilation, particularly of lower crust, plays a crucial role in the generation of carbonatites and alkaline silicate rocks and their diversification.

Theoretical Physics

- Equilibrium solutions of a boson star were studied in the mean field approximation using a general relativistic framework. Dynamics of the constituent matter in such a star was described by an elementary or composite scalar field and the statistical aspect of the matter

equilibrium is investigated by incorporating the effect of finite chemical potential in the equation of state. It was demonstrated that the introduction of finite chemical potential can lead to a new class of the solutions where the maximum mass and radius of a star change in a significant way.

- The generation of magnetic field in Higgs-inflation models, where the Standard Model Higgs boson has a large coupling to the Ricci curvature scalar has been studied. It is shown that during Higgs inflation magnetic fields with the present value and comoving coherence length of 100 kpc can be generated in the Einstein frame. The problem of large back-reaction which is generic in the usual inflation models of magneto-genesis is avoided as the back-reaction is suppressed by the large Higgs-curvature coupling.

- The amount of visible matter in our universe is comparable to the amount of dark matter in the universe. A model was proposed to explain the origin of both the visible and dark matter from the same mechanism and relate it to the neutrino masses and mixing. In this model the dark matter mostly decays into leptons, and can therefore explain the recent observations of cosmic positron and electron.

- A seesaw mechanism for generating quasi-degenerate neutrinos was proposed and extended to include all fermion masses within an SO (10) grand unified theory. A specific ansatz was shown to lead to the correct description of all fermion masses.

- In an attempt to find minimal scenarios for Dirac and Majorana mass matrices with texture zeros within the type–I seesaw mechanism it was found that 5-zero textures were the most minimal form that can successfully account for low energy phenomenology if the Majorana mass matrices are chosen minimal as well.

- A novel generalization of two Higgs doublet models which contains additional phases in the charged Higgs couplings to quarks was proposed and shown to follow from the study of the flavour symmetries of the quark mass matrices. The extra phases in the charged Higgs couplings were shown to lead to an explanation of the possible new phases seen in the mixing of B mesons.

- It is proposed that a search for top polarization in single-top production associated with charged Higgs at the Large Hadron Collider (LHC), measured through the secondary decay lepton distributions, would be a sensitive probe of the parameters of the theory. The charged-lepton azimuthal distribution, for a given value of charged-Higgs mass, is extremely sensitive to "tan β", the ratio of the scalar vacuum expectation values, which characterizes the model.

- The decay rate for the mode which has a CP-odd final state was calculated including the colour octet contribution and a large value was obtained for the branching ratio in contrast to naive expectations. This mode will thus be useful for a study of time-dependent CP asymmetry with high precision at LHC.

- When two dynamical systems are coupled, it is possible that one system (response system) can anticipate the behaviour of the other system (drive system). A new method of anticipatory synchronization based on variable delays is proposed, which may have applications in secure communications.

- The electric dipole moment of atomic ^{199}Hg induced by the nuclear Schiff moment and tensor-pseudotensor electron-nucleus interactions has been calculated using a novel method based on the relativistic coupled-cluster theory. The results demonstrate substantial changes in the results of earlier calculations which can be attributed to the more accurate inclusion of important correlation effects in the present work.

- Propagation in a Kerr medium has been studied for states of light such as (a) squeezed coherent states, (b) photon-added coherent states, (c) displaced number states, and (d) displaced squeezed number states. It is shown analytically that, like coherent states, at

certain instants of time, all the above states also will generate Schrödinger cat states and exhibit sub-Planck structures in both the Wigner distribution and the Kirkwood-Rihaczek distribution.

- The diffraction of an optical vortex through an iris diaphragm, which is a close approximation to a circular aperture, has been investigated experimentally and theoretically. The results are compared with those obtained from diffraction of a Gaussian beam through the same aperture. Very interesting new structures similar to vortices are seen; however unlike the vortex diffraction where the centre of diffracted beam is always dark, the resulting interference fringes do not show any signature of the presence of singularity in the diffracted Gaussian beam.

Awards and Honours

Faculty Members

U.R. Rao

1. Hari Om Ashram Prerit Senior Scientist Award-2008.

Jitendra Nath Goswami

2. Goyal Prize for Physics, Kurukshetra University.
3. TIFR Alumni Excellence Award, 2009.
4. Member, Commission-1 on Space and Physical Sciences, International Academy of Astronautics, 2009.

Anjan S. Joshipura

5. Member, Editorial Board, Pramana- Journal of Physics.

A.K. Singhvi

6. Lifetime Honorary Fellow, the Geological Society of London, 2009.

S.V.S. Murty

7. Member of the scientific organizing committee, COSPAR Capacity Building Workshop, held at Harbin, China, 6-19 September, 2009.

R. Ramesh

8. Member, the advisory board for the Handbook of Environmental Isotope Geochemistry, 2009.

S.D. Rindani

9. Fellow, The National Academy of Sciences, India, Allahabad, 2009.
10. J.C.Bose National Fellow, Department of Science and Technology, New Delhi, 2010.
11. Adjunct Professor, TIFR, Mumbai.

M. M. Sarin

12. Expert Member, UN/GESAMP (United Nation Group of Experts on Scientific Aspects of Marine Environmental Protection), 2009.

Utpal Sarkar

13. The Clark Way Harrison distinguished Visiting Professor, University of Washington in St. Louis, USA.

Y. B. Acharya

14. ISRO team excellence award for Chandrayaan-1 payload instruments for the year 2008.

Ashok Ambastha

15. Member, Editorial Board, Journal of Astrophysics and Astronomy.

S. A. Haider

16. Fellow, Indian Academy of Sciences Bangalore.

17. Visiting Professor, Foundation for the Promotion of Research in Sao Paulo (FAPESP), INPE, Brazil.

18. Convener, "Science and Exploration of Mars" 6th Annual AOGS Meeting, Singapore, 11-15 August 2009.

Srubabati Goswami

19. Adjunct Professor, TIFR, Mumbai.

D. Pallamraju

20. Convener, "Atmospheric Coupling Processes in the Sun-Earth System", 6th annual AOGS Meeting, Singapore, 11-15 August, 2009.

21. Member, Board of Studies on Atmospheric Sciences, Pune University, Pune.

22. Member, CAWSES-II Task Group 4.

S. Ramachandran

23. Invited by WMO - UNEP to act as a Co - author in writing a chapter on Stratospheric Ozone and Surface Ultraviolet radiation for the forthcoming Scientific Assessment of Ozone Depletion: 2010.

J.S. Ray

24. M.S. Krishnan Medal 2009, Indian Geophysical Union, Hyderabad.

S.K. Singh

25. Member, the Scientific Steering Committee, Ocean Science Section of Asia Oceania Geosciences Society, 2009.

Namit Mahajan

26. INSA Young Scientist Medal 2009.

Young Scientists

Arun Kumar Awasti

1. Best oral presentation award, National seminar on Effect of Space weather on and Human environment and Technological system, Durg, Chattisgarh, February 2010.

R.K. Das, et al.

2. Second pirze for the paper presented, "Near Infrared observation of Nova 574 Puppis", 16th National Space Science Symposium-2010,Saurashtra University, Rajkot, February 2010,

Suruchi Goel, et al.

3. Best paper award, "Ne and Ar isotopic analysis by a multicollector noble gas mass spectrometer", 11th Triennial International conference on Mass Spectrometry, Hyderabad, 24-28 November, 2009.

Vineet Goswami

4. Best Poster Presentation award by Fourth International SOLAS Summer School, Cargese, Corsica Island, France, 3-15 August, 2009.

Rajesh Kushawaha

5. Best Young Scientist's Presentation award "Dissociation Kinematics of CO_2^{3+}", Topical Conference on Atomic and Molecular Physics, RRCAT, Indore, 3-6 March 2010.

Ashwini Kumar

6. Planary Talk at SOLAS-Open Science Conference, Balcelona, Spain, 16-19 November, 2009.

Shreyas Mangave

7. First prize, Research Scholars' presentation at the XI ISMAS Triennial International Conference on Mass Spectrometry, Hyderabad, 24-28 November, 2009.

Jayesh P. Pabari

8. Elected Member of The Institution of Electronics and Telecommunication Engineers.

Durga Prasad, et al.

9. Best paper award "Understanding Some Physical Properties of Lunar Regolith using Laboratory test bed", 16th National Space Science Symposium,

Saurashtra University, Rajkot, 24-27 February, 2010.

Sumanta Sarkhel, et al.

10. Second best paper award for the paper entitled "On the role of collissions in the sodium airglow process", National Space Science Symposium, Saurashtra University, Rajkot, February 2010.

Arvind Singh

11. POGO-SCOR fellowship, Max Planck Institute for Marine Microbiology, Bremen, Germany, September-November 2009.

Theses submitted

1. **Ramakrishna Das**

   "Infrared Studies of Novae", (September 2009), Gujarat University, Ahmedabad.

2. **Shashikiran Ganesh**

   "Multi-wavelength Study of the Milky Way Galaxy", (October 2009), Gujarat University, Ahmedabad.

3. **Rajesh Kushawaha**

   "Study of Fragmentation Dynamics of Polyatomic Molecules",(October 2009) Mohanlal Sukhadia University, Udaipur.

4. **Akhilesh Nautiyal**

   "Imprint of Pre-inflation Universe From Sigtures in the cosmic Microwave Background Anisotropy Spectrum" (June 2009), Mohanlal Sukhadia University, Udaipur.

5. **Som Kumar Sharma**

   "Rayleigh Lidar Studies of Middle Atmospheric Density and Temperature Structures over Mount Abu", (April 2009) Gujarat University.

6. **Santosh Kumar Singh**

   "Neutrino Masses and Leptogenesis" (July 2009) Mohanlal Sukhadia University, Udaipur.

7. **Rohit Srivastava**

   " Stable isotope studies of atmospheric water vapour and clouds (July, 2009) Mohanlal Sukhadia University, Udaipur.

8. **Sanjiv Kumar Tiwari**

   "Helicity of the Solar Magnetic Field", (November, 2009) Mohanlal Sukhadia University, Udiapur.

Human Resource Development

Staff Structure

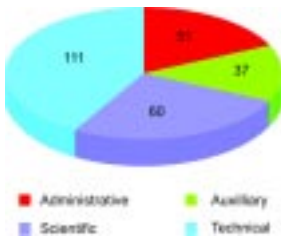

Doctoral, Post Doctoral and Other Programmes

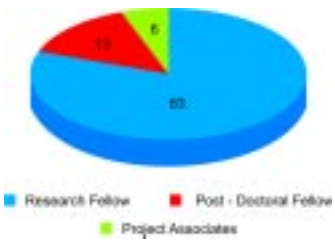

Technical Programmes

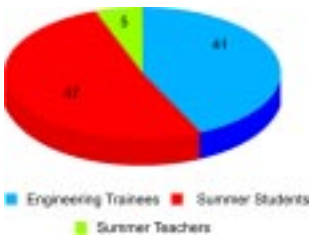

Scientific Publication

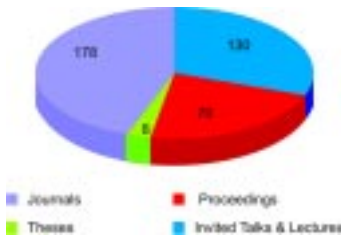

Administrative and Allied Services Trainee

Visitors/Colloquia/Public Lectures

Prof. M.D. Sastry
Gemmological Institute of India, Mumbai
Spectroscopy of Coloured Diamonds

Dr. Vinit Kumar
Raja Ramanna Centre for Advanced Technology, Indore
Free- Electron Lasers

Dr. Jayanta K. Pati
Nehru Science Centre, University of Allahabad, Allahabad
Terrestrial Impact Cratering: the Third Revolution in the Earth Sciences

Dr. S.N. Tripathi
IIT Kanpur, Kanpur
Non-Sphericity and Mixing State of Aerosols: Do they play a Major Role in their Radiative Effects?

Prof. G.S. Agarwal
Noble Foundation Chair & Regents Professor, Oklahoma State University, Oklahoma, USA.
Dipole Blockade

Dr. Gurbax Singh Lakhina
Indian Institute of Geomagnetism, Mumbai.
Electrostatic Solitary Waves in Planetary magnetospheres

Prof. M.N. Rao
NASA, Johnson Space Center, Houston,USA
Evidence for a Martian soil component in some Martian meteorites

Dr. H.S. Mazumdar
Dharmsinh Desai University, Nadiad
Computational Intelligence and Applications

Prof. Gregg Vane
Jet Propulsion Laboratory, Pasadena, USA
Jet Propulsion Laboratory and the Robotic Exploration of the Solar System

Prof. Baldev Raj Arora
Wadia Institute of Himalayan Geology, Dehra Dun
Road Map to Understand the Himalayan Seismicity

Dr. Jerome Lave
Centre de Recherches Petrographiques et Geochimiques, France
Life and death of mountain ranges

Dr. Kailash C. Sahu
Space Telescope Science Institute, Baltimore
Search for Extra-Solar Planets using the Hubble Space Telescope

Dr. Vikram Dalal
Iowa State University, USA
Global warming, Energy Problems, and strategies for India

Prof. Sunil Mukhi
Tata Institute of Fundamental Research, Mumbai
String Theory: A Frame For The Big Picture

Dr. Ishwar Chandra C.H.
Tata Institute of Fundamental Research, Pune
Exploring the infancy of the universe through radio window

Prof. M.A. Abdu
National Institute for Space Research, Brazil
Space Weather Research and Activity Program in Brazil

Prof. Ashok Kumar Sen
Assam University, Silchar, Assam
Star formation in dark clouds – some recent photopolarimetric studies in optical and sub-mm

Dr. Vinod K. Gaur
Indian Institute of Astrophysics and Centre for Mathematical Modelling (C-MMACS), Bangalore
A Frame work for India's Water Policy

Prof. Larry Ramsey
Pennsylvania State University, USA.
The Hobby Eberly Telescope, an experiment in low cost Astrophysics with an 8 meter class facility

Prof. A.N. Sekar Iyengar
Saha Institute of Nuclear Physics, Kolkata
Applications of Nonlinear Dynamics

Dr. R.S. Sharma
Honorary Scientist of Indian National Science Academy, University of Rajasthan, Jaipur
Tectono-thermal evolution of Himalayan rocks: A paradigm for the exhumation of the ultra high pressure (UHP) rocks at Tso-Morari

Prof. Tom Gehrels
University of Arizona, USA
Honorary Fellow Physical Research Laboratary, Ahmebadad
The History of our Universe and its Dark energy

Prof. Ranjan Gupta
The Inter-University Centre for Astronomy and Astrophysics, Pune
Artifical Neural Networks: A Robust Classification Tool for Astronomy

Dr. Amol S. Dighe
Tata Institute of Fundamental Research, Mumbai
The Elusive Neutrino

Dr. K. Sankarasubramanian
ISAC, Bangalore
Small-scale Magnetic Structures on the Solar Atmosphere

Dr. Raja Ganeshram
School of Geosciences, University of Edinburgh, UK
Biological Carbon Pump and Ocean Nutrient Variability on Glacial-Interglacial time scales

Conferences/Symposia/Workshops

Planetary Sciences and PLANEX Program

1. Sixth Chandrayaan-I Science Meeting, Physical Research Laboratory, Ahmedabad, 8-9 February 2010.

2. Tenth PLANEX Workshop on "Planetary Science and Space Instrumentation", Punjab University, Chandigarh, 1-5 February 2010.

Space and Atmospheric Sciences

3. Symposium on "Science and Exploration of Mars" Asia-Oceania Geosciences Society meeting, Singapore, 11-15 August 2009.

4. DST-sponspred "SERC school on Experimetal Techniques in Atomic and Molecular Physics", PRL, 15 April to 5 May 2009.

Geosciences

5. "Second Asia-Pacific Conference on Luminescence and Electron Spin Resonance dating", PRL, 12-14 November, 2009.

6. Seminar on "Climate Change: Causes, Measures and Preparedness", jointly organized by PRL and The University Centre for Earth and Space Sciences, University of Hyderabad, Hyderabad, 24-26 August 2009.

Theoretical Physics

7. National Seminar on "New Frontiers in Nuclear, Hadron and Mesoscopic Physics", jointly organized by PRL and The M.S. University of Baroda, at The M.S. University of Baroda, Vadodara, Gujarat, 3 December 2009.

8. "Workshop on High Energy Physics Phenomenology" (WHEPPXI) organized jointly by Physical Research Laboratory and the International Centre for Theoretical Science (ICTS), TIFR, 3-12 January, 2010.

Invited Talks

Astronomy and Astrophysics

B.G. Anandarao

1. "An Overview of astrophysical plasmas", DST-SERC School on Plasma Diagnostics, Institute of Plasma Research, Bhat, Gujarat, 20-31 July, 2009.

2. "Science with new facilities at Mt. Abu Observatory", International Workshop on "Interstellar matter and star formation: Multi wavelength perspective", as a part of Dr. Homi Bhabha Centenary celebrations, TIFR National Balloon Facility, Hyderabad 5-7 October, 2009.

3. "Molecular diagnostics in Astronomy", International Workshop on "Chemical evolution and origin of life', Indian Institute of Technology, Roorkee, 5-7 March, 2010.

T. Chandrasekhar

4. "Space and Ground based Astronomy of small bodies of the solar system", 10th PLANEX Workshop on "Planetary Sciences and Space Instrumentation", Punjab University, Chandigarh, 1-5 February, 2010.

P. Janardhan

5. "Studying our closest Stellar Neighbour – The Sun", One day Seminar on Current Trends in Physics, Gujarat University, Ahmedabad, 14 March, 2010.

U.C. Joshi

6. "Distribution of Interstellar Matter in the Direction of LN45", International Workshop on "Interstellar matter and star formation: Multi wavelength perspective", as a part of Dr. Homi Bhabha Centenary celebrations, TIFR National Balloon Facility, Hyderabad, 5-7 October, 2009.

S.V. Vadawale

7. "Monte Carlo simulations for the proposed Indian X-ray Polarization Measurement Experiment", International conference on 'The Coming of Age of X-ray Polarimetry', Rome, April 2009.

8. "Chandrayaan-1 X-ray Spectrometer", 8th IAA Conference on 'Low Cost Planetary Missions', Goa, September 2009.

9. "X-ray experiments onboard Chandrayaan-1", Workshop on 'Frontiers in Physics', PRL, Sept. 2009.

10. "Monitoring Space Radiation", 10th PLANEX Workshop, Chandigarh, February 2010.

11. "Remote sensing in X-rays and Gamma-rays", 10th PLANEX Workshop, Chandigarh, February 2010.

Solar Physics

Ashok Ambastha

12. "Magnetic and Doppler Transients associated with the White Light Flares in NOAA 10486", Chinese Astronomical Society-IAU Joint Meeting on "Dynamic Solar Corona", Suzhou, China, 24-26 July, 2009.

Bhuwan Joshi

13. "The Dynamic Sun", Recent Advances in Helio-Physics, DBF Dayanand College of Arts and Science, Solapur, Maharashtra, 5 February, 2010.

Brajesh Kumar

14. "Helioseismology : A tool for probing the solar interior", INSA Seminar on Current Trends in Physics, Dept. of Physics, MLS University, Udaipur, Rajasthan, 12 September, 2009.

15. "Seismology of the Sun", UGC National Seminar on Recent Advances in Helio-Physics, DBFD College of Science, Solapur, Maharashtra, 5-6 February, 2010.

Nandita Srivastava

16. "Estimation of true speed and direction of propagation of CMEs using SECCHI (STEREO) observations",EGU General Assembly, Vienna, 19-24 April, 2009.

Sanjiv Kumar Tiwari

17. "Solar Magnetic Fields"**,** in "National Seminar on Recent Advances in Helio-Physics", D.B.F. Dayanand College of Arts & Science, Solapur, 5 February 2010.

P. Venkatakrishnan

18. "The Mystery of Sunspots : From Galileo to Hinode", INSA Seminar on Current Trends in Physics, Dept. of Physics, MLS University, Udaipur, 12 September, 2009.

Planetary Sciences and PLANEX Program

J.N. Goswami

19. "Planetary Science and Exploration: An Indian Perspective", Distinguished Speaker, at IIT Kharagpur, 17 April 2009.

20. "Chandrayaan-1: Technology & Science Perspective", Jawaharlal Nehru Centre for Advanced Scientific Research, Bangalore, 21 April, 2009.

21. "Exploring the Moon", Technology Day Lecture at Wadia Institute of Himalayan Geology, Dehradun, 11 May, 2009.

22. "Chandrayaan-1 Mission: Initial results", 2nd Annual Lunar Science Forum, NASA Lunar Science Institute, California, 22 July, 2009.

23. "Planetary Exploration Programme of India: Opportunities and Challenges", Inaugural DST sponsored INSPIRE Meet, New Delhi, 12 August, 2009.

24. "Chandrayaan-1 and Planetary Exploration", Distinguished Lecture at Asia-Oceania Geological Society Meeting, Singapore, 14 August, 2009.

25. "Origin of Solar System: Stellar connection", Presidential Address, Astronomical Society of India Meeting, Bangalore, 19 August, 2009.

26. "Results from Chandrayaan-1 Mission" and "Planetary Exploration Programme of ISRO", International Conference on Low-cost Planetary Missions, Goa, 30 and 31 August, 2009.

27. "India's Planetary Exploration Programme", Foundation Day Lecture, Indian Institute of Tropical Meteorology, Pune, 17 November, 2009.

28. "Lunar Science from Chandrayaan-1 Mission", Plenary Talk, National Space Science Symposium-2010, Rajkot, 24 February, 2010.

29. "Over-view of Chandrayaan-1 Mission and Science Results", Key-Note Talk, International Symposium on Research and Application of Lunar Exploration Data, Maccau, 25-26 March, 2010.

Shiv Kumar Goyal

30. "Gamma Ray Spectrometer",10th PLANEX Workshop on "Planetary Sciences and Instrumentation", Panjab University, Chandigarh, 1-5 February, 2010.

K.K. Marhas

31. "Stardust and evolution of solar system" INSA-IAPT One day seminar, PRL 13 September 2009.

S.V.S. Murty

32. "Chandrayaan-1: Program overview and instruments" and "Moon: Chandrayaan Plans and Perspectives" two talks at COSPAR Capacity Building Workshop, on "Lunar and Planetary surface Science", Harbin, China, 6-18 September, 2009.

33. "Planetary Sciences and Instrumentation" two talks at the 10th PLANEX Workshop on Panjab University, Chandigarh, 1-5 February, 2010.

Durga Prasad

34. (i) "Sensors for Studying Surface Properties"; (ii) "Planetary Surface Measurements using Rovers"; (iii) "Properties of Lunar Regolith"; (iv) "Seismic and Thermal Probing of Moon", 10th PLANEX Workshop on "Planetary Sciences and Instrumentation", Panjab University, Chandigarh, 1-5 February, 2010.

Neeraj Srivastava

35. "Chandrayaan – 1 data analysis", 10th PLANEX Workshop on "Planetary Sciences and Instrumentation", Panjab University, Chandigarh, 1-5 February, 2010.

36. "Hyperspectral Remote Sensing in Planetary Exploration", HYPER SPACTRA 2010, DST Sponsored short term course on "Emerging Trends in Remote Sensing: Imaging Spectroscopy and Natural Resource Mapping", Dept. of Earth Sciences, IIT, Mumbai,12-16 January 2010.

Space and Atmospheric Sciences

Y. B. Acharya

37. "Chandrayaan-1 and ahead", Frontiers in Physics, SPU, Vallabh Vidhyanagar, 24 January, 2010.

38. "Solid State Detectors for Nuclear Instrumentation", Planex workshop 2010, Punjab University Chandigarh, 1-5 February, 2010.

B. Bapat

39. "Molecular Fragmentation Studies at Indus-1", Topical Conference on Atomic and Molecular Physics, RRCAT, Indore, 3—6 March, 2010.

D.Chakrabarty

40. "Effects of substorms over low latitudes: Case studies", National Space Science Symposium**,** Rajkot, February 2010.

41. "Impacts of the electric field of solar wind origin on the low latitude ionosphere-thermosphere system", General Session for Upper Atmosphere and Ionosphere, Sixth AOGS meeting**,** Singapore: 11-15 August, 2009.

S.P.Gupta

42. "Balloon and rocket borne sensors to measure electrical parameters in atmosphere and ionosphere", SERC School on electrodynamical coupling of atmospheric regions, IIG, Mumbai, 6-19 January, 2010.

S. A. Haider

43. "Comparative study of D, E, F layers in the daytime ionospheres of Mars and Earth: Modeling and observations", PS08-D4-AM1-303-027 Symposium, "Science and Exploration of Mars", AOGS, Singapore 11-15 August, 2009.

S. Lal

44. "Planetary Atmospheres", Planex Workshop, Punjab University, 2 February, 2010.

45. Atmospheric Science: Role of Trace Gases in Chemistry and Climate, Vallabh Vidhyanagar, 24 January, 2010.

46. "Atmospheric Trace Gases : Their Role in Chemistry and Climate",Teachers Workshop, ICCSIR, Ahmedabad, 23 January, 2010.

47. "Indo-US Collaboration to study Chemistry – Climate Interactions", Joint Executive Meeting of MoES and NOAA, Delhi, 6-7 October, 2009.

D. Pallamraju

48. "International perspectives of the Climate and Weather of the Sun-Earth System (CAWSES) Science", CAWSES-India Phase II Science Programme Workshop, NARL, Gadanki, 9-11 July, 2009.

49. "Short and long term wave dynamics as derived from daytime airglow observations from low-latitudes", 6th AOGS Meeting, Singapore, 11-15 August, 2009.

50. "Space weather and earth's upper atmospheric response", INSA-IAPT Seminar on Frontiers of Physics, PRL,19 September, 2009.

51. "Investigations of ionospheric disturbances", Brainstorming on 'Vision for R & D in Atmospheric Sciences' for a decade, Indian Institute of Sciences, Bangalore, 22-24 October, 2009.

52. "Space Weather effects in Geospace", Research & Training Unit for Navigational Electronics, Osmania University, 12th November 2009.

S. Ramachandran

53. "Ozone and Climate", International Ozone Day, Indian Meteorological Society- Ahmedabad Chapter, SAC, Ahmedabad, 16 September, 2009.

54. "Carbonaceous aerosols: Radiative and climate impacts", (Plenary Lecture) International Conference on Environmental Issues in Emerging and Advanced Economies, Gujarat University, 6-8 December, 2009.

55. "Global warming and air pollution", Pancham 2009, Zenith School, Vadodara, 12 December, 2009.

56. "Aerosol radiative forcing: Observations and Modeling", Brainstorming Session on Observational and Modeling Aspects of Aerosols, Clouds and Climate, IITM, Pune, 29 December, 2009.

57. "Black carbon aerosols over urban regions in India: Radiative forcing and climatic implications", Monsoon Asia Integrated Regional Study (MAIRS) Mega-city workshop, Academia Sinica, Taiwan,Taipei, 19-22 January, 2010.

58. "Radiative forcing and climate impact of black carbon aerosols over urban regions", International workshop on Frontiers of Black Carbon studies, Research Center for Advanced Science and Technology (RCAST), The University of Tokyo, Tokyo, Japan, 25 January, 2010.

59. "Spatiotemporal gradients in aerosol properties and radiative forcing over Bay of Bengal and Arabian Sea", NOAA Geophysical Fluid Dynamics Laboratory, Princeton University, Princeton, USA, 5 Feb., 2010.

60. "Aerosol characteristics and radiative forcing over Bay of Bengal and Arabian Sea: Spatial and temporal variations", ARIES, Nainital, 17 February, 2010.

61. Two lectures on Aerosols and Radiation Budget, SERC School on Atmospheric Chemistry and Air Pollution, NPL, New Delhi, March 2010.

62. "Global warming and air pollution, One-day seminar on current trends in Physics", Gujarat University, Ahmedabad, 14 March, 2010.

R.Sekar

63. "Radio and optical investigations of the low-latitude ionosphere-thermosphere system", IAGA 11th Scientific Assembly, Sopron, 24-29 August, 2009.

Varun Sheel

64. "Modeling Chemical Composition of Stratosphere & Troposphere", Vision for R&D in Atmospheric Sciences for a Decade: National Discussion Meeting on Atmospheric Sciences, IISc, Bangalore, 22-24 October 2009.

65. "Modeling the Changing Composition of the Atmosphere", 2nd Review Meeting of AT-CTM, ARIES, Nainital, 28-29 January, 2010.

66. "Stardust and evolution of solar system" INSA-IAPT One day seminar, Physical Research Laboratory 13 September 2009.

Geosciences

R.D. Deshpande

67. "Use of Delta V Plus IRMS with Gas Bench II for high throughput of isotopic analyses for IWIN National Programme", Thermo Scientific Isotope Ratio Mass Spectrometer (IRMS) User Meet, Kozhikode, Kerala.17 September 2009.

68. "IWIN National Programme for isotopic characterization of Indian hydrological cycle: Preliminary results", 11th ISMAS Triennial Conference,Hyderabad, 24-28 November, 2009.

Navin Juyal

69. "Himalaya: inception, growth and degradation" Doon University, Dehra Dun, 26th September, 2009.

70. "Luminescence chronology of Late Quaternary climatic events, southern desert margin and higher Central Himalaya", APLED 2009, PRL, 12-14 Nov., 2009.

Ashwini Kumar

71. "Mineral and anthropogenic aerosols over the Arabian Sea and the Bay of Bengal" Plenary Talk. SOLAS-

Open Science Conference, Barcelona, Spain, 16-19 November, 2009.

R. Ramesh

72. "Isotope dendroclimatology", Indo-Us workshop on Concepts in Quaternary Climate Studies with emphasis on Dendrochronology and Palynology, Birbal Sahni Institute of Paleobotany, Lucknow,12-13 May, 2009.

73. "Stable isotope methodology for climate reconstruction", Workshop on Proxies for Climate Change, Silver Jubilee of Marine Science Dept., Goa University, 8-10 March, 2010.

74. "Ocean Productivity", National Workshop on Climate Change: Status and Future Plans at Indian Institute of Tropical Meteorology, Pune, 18-19 May, 2009.

75. "Spatial and temporal coherence of paleomonsoon records from marine and land proxies in the Indian region during the past 30 ka", Seminar on Climate Change: causes, measures and Preparedness, University of Hyderabad, Hyderabad, 24-26 August, 2009.

76. "Applications of Stable Isotopes in Oceanography" keynote address in Thermo-Fisher Scientific meet at Kozhikode, 17-18 September, 2009.

77. "Holocene climate of India" Ecology and the Environment in India: Past, Present and Future, Silver Jubilee Symposium of CES, IISc, Bangalore, 22-24 October,2009.

78. "Paleomonsoon reconstructionusing stable oxygen isotopes in various proxies from India", ISMAS Triennial Conference, Hyderabad, 24-28 November, 2009.

79. "Direct solar Influence on Climate", 16th National Space science Symposium, Saurashtra University, Rajkot, 24-27 February, 2010.

80. "Paleomonsoon reconstruction using speleothems", National Seminar on Earth Resources-Role of Geologist in ameliorating the Environment", S.V. University, Tirupati, 29-30 March, 2010.

J.S. Ray

81. "Radiogenic isotopic ratio variations in carbonatites and associated silicate rocks", 47th Annual Convention of Indian Geophysical Union, Dehradun, 5 October 2009.

M.M. Sarin.

82. "Atmospheric input of chemicals to ocean", 36th session of the Joint Group of Experts on the Scientific Aspects of Marine Environment Protection (GESAMP), WMO, Geneva, Switzerland, 27 April – 1 May, 2009.

83. "Atmospheric mineral dust in western India: Temporal variability of coarse and fine size fractions and elemental characteristics", Int'l Workshop MOCA-09: IAMAS-IAPSO-IACS-2009 Joint Assembly, Montreal, Canada, 19-29 July, 2009.

84. "Site- specific mass absorption efficiency of EC in atmospheric aerosols from urban, rural and high altitude sites in India", Int'l Workshop MOCA-09: IAMAS-IAPSO-IACS-2009 Joint Assembly, Montreal, Canada, 19-29 July, 2009.

85. "Atmospheric Chemistry and Air Pollution" SERC School, National Physical Laboratory, New Delhi, 2-22 March, 2010 (2 Lectures).

S.K. Singh

86. "Understanding the natural processes using isotope tracers", ISMAS Conference, Hyderabad, 11th ISMAS-TRICON-2009 24-28 November, 2009.

A.K. Singhvi

87. "Quaternary Geochronology using Luminescence: The Indian Scenario" MR Sahni memorial lecture of the Paelontological Society of India, Lucknow, 16 March, 2009.

88. "Thermo- and Optically Stimulated Luminescence in Geosciences and Meteoritics: Applications and implications" National Seminar on Thermo Physics, MS University of Baroda, Vadodara, 8-10 Oct., 2009.

89. "Luminescence dating: new improvements in SAR protocol and new applications to Indian Archaeology" International symposium on Luminescence in Archeological Sciences, Athens Greece, 9-12 September, 2009.

M.G. Yadava

90. "Isotopic signatures of rainfall events in western India", Seminar on Climate Change: causes, measures and

Preparedness, University of Hyderabad, Hyderabad, 24-26 August, 2009.

91. "Usefulness of cave deposits in Climate reconstruction" in One-Day Seminar on Current Trends in Physics jointly organized by PRL, INSA and MLS University, Udaipur, 12th September, 2009.

Theoretical Physics

R.E. Amritkar

92. "Synchronization of time-varying networks", Workshop on Dynamics on Networks, IISER, Pune, 13-14 Nov 2009 and Third International Conference on Complex Systems and Applications, Le Havre, France, June 29 - July 02, 2009.

93. "Synchronization of Networks" at the Indo-Russian workshop on Complex Dynamical Networks: Dynamics and Synchronization, IICB, Kolkata, 1-2 December, 2009; International workshop on Nonlinear and Complex systems, Taipei, Taiwan, 10-15 December, 2009 and Conference on Evolution of Complex Systems, IISc, Bangalore,13-15January, 2010.

94. "Estimating Parameters of a Dynamical System from the Time Series", Conference on Computational Physics 2009, Kaohsiung, Taiwan. 16-19 December, 2009.

Jitesh R. Bhatt

95. "Quark-Gluon Plasma in Relativistic Heavy-Ion Collisions", National Plasma Physics Symposium (Plasma 09), NIT, Hamirpur, 8-11 December, 2009.

Srubabati Goswami

96. "Renormalization Group Effects and Precision Neutrino Data". IDS-NF Plenary meeting, TIFR, Mumbai, October, 2009.

97. "INO and Beams", INO meeting, Punjab University, Chandigadh, November, 2009.

98. "Renormalization Group Effects and large 1-3 leptonic mixing", NuHorizons, HRI, Allahabad, February 2010.

99. Four lectures on "Solar and Atmospheric Neutrinos in Nuclear Physics", SERC School, University of Calicut, February, 2010.

V.K.B. Kota

100. Modern Shell Model, School cum Workshop on "Yrast and Near-Yrast Spectroscopy", IIT, Roorkee, 26-30 October, 2009.

101. "Nuclear shell model: Past to Present", Workshop on Hadrons and Nuclei, SPU, Vallabh Vidyanagar, 12 February, 2010.

S.D. Rindani

102. "The Bhabha-Gupta equation", at the Bhabha Centenary Symposium, TIFR Centre for Applicable Mathematics, Bengaluru, July, 2009.

Utpal Sarkar

103. "Varieties of Leptogenesis", in Particle Physics and Cosmology, University of Oklahoma, Norman, USA, 18-22 May, 2009.

Angom Dilipkumar Singh

104. "Ground state geometry and dynamical evolution of binary condensates", One day seminar on Atomic, Molecular and Optical Physics (to celebrate Platinum Jubilee of IPS), IACS, Kolkata, 17 March, 2010.

105. "The cold frontier: bridging gaps and more", Advance Topics in Applied Physics SVNIT, Surat, 1-5 February 2010.

106. "The cold frontier: bridging gaps and more", Frontiers of Physics - an introductory seminar, SPU, Vallabh Vidyanagar, 24 January, 2010.

107. "Electric dipole moments—signature of time reversal violation", International School and Conference on Cold ions and atoms, Kolkata (one lecture and one tutorial), 6-21 January, 2010.

108. "Clusters: workhorse of high performance computing", NUCONE-09, Institute of Technology, Nirma University, 25 November, 2009.

109. "Bounds from Hg Electric Dipole Moment: CP violation parameters", DNAP seminar, TIFR, Mumbai, 10 July, 2009.

110. "AMO Physics: past, present and future", INSA-IAPT One-Day Seminar, PRL, 19 September, 2009 and DST-SERC School in atomic and molecular physics (Inaugural invited lecture), PRL, 15 April, 2009.

Manan Vyas

111. Random Interaction Matrix Ensembles in Mesoscopic Physics, National Seminar on "New Frontiers in Nuclear, Hadron and Mesoscopic Physics", MSU, Vadodara, 3 December, 2009.

Facilities and Services

R.S. Gupta

112. "Principles of Translation and its usage", Oil & Natural Gas Corporation (ONGC), Ahmedabad, 8 August 2009.

113. "Official Language Policy of Govt. of India", Food Corporation of India (FCI), Ahmedabad, 10 September, 2009.

114. "(i) Official Correspondence, (ii) Principles of Translation and its usage", Oil & Natural Gas Corporation (ONGC), Mt. Abu, 8-9 January, 2010.

115. "Annual Program & Various Committees", Indian Institute of Management Ahmedabad, 26 February, 2010.

116. "Principles of Translation and its usage", Oil & Natural Gas Corporation (ONGC), Ahmedabad 15 March, 2010.

Jigar Raval

117. "Linux Security", GCET, Vallabh Vidyanagar, 15 March 2009.

Nishtha Anilkumar

118. "Scientometrics", UGC Refreshers' Course, Gujarat University, Ahmedabad, November, 2009.

119. "(i) Internet History & Internet Functions. (ii) Free E-Resources available on Internet" ADINET, Ahmedabad 20 June, 2009.

Lectures at Universities / Institutions

Astronomy and Astrophysics

B.G. Anandarao

1. "Integral-field spectroscopy in Astronomy using Faby Perot Interferometers", lead talk in the discussion session, IUCAA. Pune, 15 June, 2009.

2. "New Worlds in the Universe", Physics Department, Saurashtra University, Rajkot, 3 July, 2009.

Rajmal Jain

3. "The Sun from the Earth and Space", Govt.Dr. W. W. Patankar Girls P. G. College, Durgh, Chattisgarh, 15 February, 2010.

A.K. Singal

4. "Maximum Brightness Temperature of an Incoherent Synchrotron Source: Inverse Compton Limit - A Myth!" RRI Bangalore, 1 June, 2009.

Solar Physics

Ashok Ambastha

5. "The Dynamic Sun", Zonal Meeting for Master Resource Persons' Training Programme on IYA and TSE2009, Vigyan Prasar and National Council for Science & Technology Communication, Gangtok, Sikkim, 8-10 July, 2009.

6. (1) "Probing the Structure and Dynamics of the Solar Interior", (2) "Solar Activity and Explosive Phenomena" and (3) "The Solar Corona and Beyond: The Space Weather", Three lectures at the State-level Camp for College Students under IYA2009, Pt. Ravishankar Shukla University, Raipur, 11-13 January, 2010.

7. "Understanding our Daytime Star from its deep Interiors to the Outer Corona", Bhilai Mahila Mahavidyalaya, Bhilai (C.G.), 14 January, 2010.

8. "Science of oscillations from the deep solar interior to the outer corona: helio and coronal seismology", MK Dasgupta Memorial seminar, Kolkata, Institute of Radio Physics and Electronics, University of Kolkata, 1 September, 2009.

Sanjay Gosain

9. "Coherent Lateral Motion of Penumbral Filaments during a X-class flare: Hinode Observations" in the Hinode-3 Science Meeting, Tokyo, Japan,1-4 December 2009.

10. "Magnetic Field Measurements: *From Hale to HMI"* in the INSA workshop at Mohan Lal Sukhadia University, Udaipur, 20 August, 2009.

Brajesh Kumar

11. "Helioseismic signatures of solar flares", AOGS 2009, Suntec, Singapore, 11-15 August, 2009.

Nandita Srivastava

12. "Coronal mass ejections: 3 D observations from SECCHI/STEREO", the Curtin Institute of Radio Astronomy, Perth, Australia,14 January, 2010.

Sanjiv Kumar Tiwari

13. "Helicity of the solar magnetic field", HAO, Boulder Co, USA, 21 December, 2009.

P. Venkatakrishnan

14. "The Solar Corona", Zonal Meeting for Master Resource Persons' Training Programme on IYA and TSE, Vigyan Prasar and NCSTC, Mumbai, 4 July, 2009.

15. "Measuring the Universe" and "Understanding the Sun", Indian School, Bahrain, 3-4 December, 2009.

16. "On the Absence of Net Vertical Current in Sunspots", LESIA, Observatoire de Paris, Meudon, 5 February 2010.

17. "Multi Application Solar Telescope of USO", IAS, Orsay, France, 11 February, 2010.

18. "Net Vertical Current in Sunspots", Max Planck Institute for Solar System Research, Lindau, Germany, 16 February, 2010.

Planetary Sciences and PLANEX Program

S.V.S. Murty

19. "Nitrogen and noble gases in individual chondrules" at Max Planck Institute für Chemie, Mainz, Germany, 23 July, 2009.

Space and Atmospheric Sciences

Y. B. Acharya

20. "Chandrayaan-1 mission", Dharmsinh Desai Institute of Technology, Nadiad, 6 October, 2009.

21. "A road to Moon", Govindram Sakseria Institute of Technology and Science, Indore, 17 November, 2009.

H Chandra

22. Gujarat University: 10 lectures on ionosphere and radio probing techniques.

23. Dibrugarh University: 14 lectures on ionosphere, 8-16 March, 2010.

24. A lecture on "Space weather" at Garhwal Universiry Srinagar, the DST scheme INSPIRE for bright school students,30 December, 2009.

25. "Coordinated rocket and MST radar studies of mesospheric turbulence" IIT Roorkee, 22 March, 2010.

S.P. Gupta

26. Delivered a popular talk on the topic of "Use of balloons and rockets for space research" to the school children during 16th National Space Science Symposium, at Rajkot during 24-27 February, 2010.

S. Lal

27. Two lectures on Atmospheric chemistry in SERC school on "Atmospheric Chemistry and Air Pollution'"at National Physical Laboratory, New Delhi sponsored by DST during 2-22 March, 2010.

R.Narayanan

28. "Study of upper atmosphere using artificially released vapor clouds and natural airglow using optical instruments" at Amritapuri School of Arts and Sciences, Karunagappalli, January, 2010.

S. Ramachandran

29. "Atmospheric aerosol: Sources and sinks, effects on the atmosphere, and Radiation", Gujarat University, Ahmedabad, September-October, 2009 (7 lectures).

30. "Aerosols", Gujarat University and Centre for Environment Education, Ahmedabad, November-December, 2009 (4 lectures).

31. "Atmospheric optics, Aerosols and Radiative Transfer", Aryabhatta Research Institute of Observational Sciences (ARIES), Nainital, February 2010 (5 lectures).

Varun Sheel

32. "Effect of Aerosols on the Martian Lower Ionosphere", 6th Annual Meeting of the AOGS, Singapore, 11-15 August, 2009.

33. "Effect of a Martian dust storm on ions in the lower atmosphere", 16th National Space Science Symposium, Saurashtra University, Rajkot, 24-27 February, 2010.

34. "Fundamentals of Chemical Transport Modeling" and "Modeling Chemistry & Dynamics of Trace gases in Stratosphere & Troposphere", (2 lectures), SERC School on Atmospheric Chemistry and Air Pollution, National Physical Laboratory, Delhi, 2-22 March,2010.

Geosciences

R.D. Deshpande

35. "Oxygen and hydrogen isotope systematics for hydrological applications", DST-SERC Short Term Training on Isotope Tracer Technique for Water Resources Development and Management, CWRDM, Kozhikode, Kerala,15-20 June.

36. "Quantification of Hydrological Processes using Oxygen and Hydrogen isotope systematics", M.G. Science College, Ahmedabad, November 2009.

37. "Global climate change and hydrological consequences", Pancham Science Exposition, Baroda, 11 December, 2009.

N. Juyal

38. "Late Glacial Fluctuations in Central Himalaya, India" Cold and Arid Regions Environmental Engineering Research Institute (CAREERI) and State Key Laboratory for Cryospheric Sciences (SKLCS), Lanzhou, China, 7th April, 2009.

39. "Centennial and millennial scale monsoon variability reconstruction based on high resolution sediment record collected from the relict proglacial lake sediments in the Higher Central" at field station of CAREERI located at Urumqui Glacier No. 1, China (Tienshan Mountain), 10th April, 2009.

J.S. Ray

40. "Third Rock from the Sun - the story of the Earth", workshop on Earth and Space Sciences, IIST, Trivandrum, 18 November, 2009.

R. Ramesh

41. "Paleoclimatic studies from various natural archives", six lectures in the Climate Change Course conducted jointly by CEE and Gujarat University, January, 2010.

42. "How much of the recent climate change is due to the sun?", NRSC, Hyderabad, 12 March, 2010.

43. "Monsoon during the Holocene: comparison of marine and terrestrial records", University of Hyderabad, 12 March, 2010.

44. "Solar Activity and Climate", IISER, Kolakata, 27 March 2010.

S.K. Singh

45. "Contribution from Salt: Overestimation of silicate weathering in the Ganga-Brahmaputra Basin", Workshop on Anthropogenic impacts on water resources and soils: An Indo-French perspective, IISc, Bangalore, India, 23-27 November, 2009.

A.K. Singhvi

46. "Luminescence Dating: An example of synergistic mutualism between Physics and Geology", National Workshop on Luminescence and its applications to Nonmaterial's, Radiation Dosimetry and Geosciences, Bhilai, 5-7 December, 2009.

47. "Paleoclimatology: The Indian Context", MoES workshop on Climate Research in India, 25th May, 2009.

Theoretical Physics

A.C. Das

48. "Solar-Terrestrial Relation and Space Weather" (10 lectures), part of a course on "Advanced P.G. Diploma in Geo-informatics and Satellite Communication", Gujarat University, November 17-December 11, 2009.

49. "The Sun and its interaction with the earth's magnetosphere" (20 lectures), Centre of Atmospheric Studies, Dibrugarh University, Assam, 15-29 March 2010.

V.K.B. Kota

50. "Random Matrix Ensembles with Random Interactions: Some Exact Results", SINP, Kolkata, 30 April, 2009.

51. "Shell Model Based DSM and SDM Methods for 7Double Beta Decay", Laurentian University, Sudbury, Canada, 27 May, 2009.

52. "Random Interactions Matrix Ensembles in Quantum Physics", Berhampur University, Berhampur, 13 October, 2009.

Raghavan Rangarajan

53. "Gravitino production in an inflationary Universe and implications for leptogenesis", Indian Conference on Cosmology and Galaxy Formation, IIT, Kanpur, 30 Oct - 1 Nov, 2009; IISER, Kolkata and IOP, Bhubaneswar, November, 2009.

54. "A Career as a Physicist" at S. P. Baria Science Institute, Navsari, August, 2009.

55. "Astroparticle Physics", S. P. Baria Science Institute, Navsari, Aug 2009 and IIT, Gandhinagar, February 2010.

Utpal Sarkar

56. "Astroparticle Physics, Neutrinos and LHC", St. Louis University, USA, 8 April, 2009, Washington University in St. Louis, USA 7 May 2009 and Colloquium at University of California, Riverside, USA, 28 May, 2009.

57. "Astroparticle Physics and Neutrinos", Oklahoma State University, Stillwater, USA, 23 April, 2009.

R.P. Singh

58. "Optical vortices: a study about darkness" at the Department of Physics, Allahabad University, 18 November, 2009.

Facilities and Services

Jigar Raval

59. "Open Source Technology-Linux and Internet and Security", B.S.Patel Polytechnic, Ganpat University, 12 November, 2009.

SCIENCE

Astronomy & Astrophysics

The activities of the Astronomy and Astrophysics Division cover a wide spectrum of research studying the evolution of explosive events like novae, imaging massive star forming regions, probing the highly obscured central region of our galaxy, studying variability in distant Active Galactic Nuclei (AGN). In addition polarimetric studies of bright comets, stellar occultations of asteroids and research on some aspects of solar physics like solar flares, solar rotation, solar wind and the interplanetary medium are also carried out. New activities include development of a sophisticated Echelle spectrograph (PARAS) for detecting exo-planets from Mt. Abu Observatory and developing satellite payloads for polarimetric and other studies in Xray astronomy.

A small 20 inch telescope is also being set up in Mt. Abu for continuous photometric monitoring of a few AGNs to detect transient outbursts as well as for studies of exo-planetary transits and transient events like GRB afterglows.

Rotational spectroscopy of AlO

The detection of rotational transitions of the AlO radical at millimeter wavelengths from the astronomical source VY CMa has recently been reported. In view of this, rotational transitions in the ground X2S+ state of AlO have been reinvestigated. A list of calculated rotational lines in v = 0, 1 and 2 of the ground state up to N' = 11 is presented which should aid astronomers in analysis and interpretation of observed AlO data and also facilitate future searches for this radical.

This work was done in collaboration with Dr. O. Launila of the KTH AlbaNova University Center, Stockholm, Sweden.

(Dipankar P.K. Banerjee)

Detection and evolution of the CO ($\Delta v = 2$) emission in Nova V2615 Ophiuchi (2007)

We present near-infrared (1–2.5 micron) spectroscopic and photometric results of the 2007 outburst of Nova V2615 Ophiuchi. The evolution of the spectra is studied from the initial P Cygni phase to an emission-line phase and finally to a dust formation stage. The characteristics of the JHK spectra are very similar to those observed in a nova outburst occurring on a carbon–oxygen white dwarf. We analyse an observed line at 2.088 micron and suggest that it could be due to Fe II excited by Lyman a fluorescence. The highlight of the observations is the detection of the first overtone bands of carbon monoxide (CO) in the 2.29–2.40 micron region. The CO bands are modelled to estimate the temperature and mass of the gas emitting CO and also to place limits on the 12C/13C ratio. The CO bands are recorded over several epochs, thereby allowing a rare opportunity to study its evolution from a phase of constant strength through a stage when the CO is destroyed fairly

rapidly. We compare the observed time-scales involved in the evolution of the CO emission and find a good agreement with model predictions that investigate the chemistry in a nova outflow during the early stages.

(R.K. Das, Dipankar P.K. Banerjee and N.M. Ashok)

Near-Infrared H and K band studies of the 2006 outburst of the recurrent nova RS Ophiuchi

We present near-infrared photo-spectroscopy in the H and K bands of the 2006 outburst of the recurrent nova RS Ophiuchi (RS Oph). Analysis of the HI line profiles show the presence of broad wings on both flanks of a strong central component indicating the presence of a bipolar velocity flow in the ejecta. We discuss the behaviour and origin of the observed Fe II lines at 1.6872 and 1.7414 μm and show that Lyman a and Lyman continuum fluorescence are viable mechanisms to excite these lines. As collisional excitation can also contribute in exciting and significantly enhancing the strength of these Fe II lines, we propose that these lines originate from a site of high particle density. Such a likely site could be the high-density, low temperature contact surface that should exist in the shockfront in between the shocked ejecta and red giant wind. Recombination analysis of the HI lines indicate deviations from Case B conditions during most of the span of our observations indicating optical depth effects. It appears likely that the breakout of the shockfront had not yet occured till the end of our observations. An analysis is made of the temporal evolution of the [Si VI] 1.9641 μm and the 2.0894 μm [Mn XIV] coronal lines. Assuming collisional effects to dominate in the hot coronal gas, estimates are made of the ion temperature in the gas.

(Dipankar P.K. Banerjee, R.K. Das and N.M. Ashok)

Spitzer IRAC Imaging photometric study of AFGL 437

AFGL 437 is a massive star forming region at a distance of 2.0 kpc containing compact young clusters of newly formed stars. Mid-infrared (and far-infrared) wavelength region is best suited for studying such highly embedded compact clusters. We have made a photometric study on AFGL 437 by using spitzer IRAC 4-band mid-infrared observations (3.6 – 8.0 μm). We identified several new embedded young stellar objects (YSOs) within 90 arc sec of the central compact cluster. Using a 2D radiative transfer model, we have derived physical parameters from the spectral energy distributions (SEDs) constructed for all the YSOs detected in the cluster. We showed that the outflow driving source WK 34 in the cluster is in fact a very young massive star deeply embedded and not yet hot enough to drive a HII region. From the ratio maps of the IRAC bands we detected the molecular hydrogen counterpart of the outflow/jet from this young star.We have also detected molecular hydrogen and PAH emission regions driven by the massive stars in the central compact cluster.

(Lokesh Dewangan and B.G. Anandarao)

Commissioning of the PRL Echelle Spectrograph (PARAS) at Mt. Abu Observatory

The PRL Echelle Spectrograph was recently installed at the Mt. Abu Gurushikar Observatory. It is a fiber-fed optical high-resolution cross-dispersed spectrograph capable of a single- shot spectral coverage of 3700A to 8600A at R ~ 60,000 and is under very stable conditions of temperature (±0.03°C at 25°C). Later on the spectrograph will be housed inside a low Vacuum Chamber for accurate pressure control.

The primary science goal of the spectrograph is to detect planets around Sun-like stars and for this we need the spectrograph to be stable down to a few meter/sec in terms of Doppler shifts. The spectrograph is currently in the testing phase. It is attached to the 1.2m telescope using two 50 micron core optical fibers (one for the star and another for simultaneous Thorium-Argon spectral calibration). This also includes F/13 to F/4 fiber transfer optics at the Cassegrain focus of the telescope, and vice-versa at the slit position of the spectrograph.

The spectrograph was commissioned in early January 2010, but various tasks for commissioning had begun at the Observatory as early as in May 2009 beginning with the installation of the thermal insulation outer and the inner chambers. The outer chamber is of the size of about 7.5m × 4.5m × 2.7m and the inner chamber has the dimensions of 6m × 3.6m × 2.55m which houses the spectrograph. The outer chamber achieves temperature control of ±0.8°C at 23°C, which has both heating and cooling by standard heaters and airconditioners.

However, the Inner chamber can achieve temperature control of ±0.03°C at 25°C by only heating and very finely controlled heaters. In future the temperature control unit will be made even more precise, down to ±0.01°C at 25°C. This system was designed and developed by PRL engineers (Figure 1).

Fig.1:The Echelle Spectrograph installed in the inner Chamber.

To determine the spectrograph stability over the night of observation, every night, spectral calibrations are taken T2, T3.... and the Doppler shifts of the drifts of the spectral lines are measured in terms of meters/sec. Ideally the drifts should be identical for calibration spectra of both the fibers, and therefore the intrinsic difference in drifts between the spectra from the two fibers defines the stability of the spectrograph.

The instrument will be ultimately used for radial-velocity searches of exoplanets around 1000 dwarf stars, brighter than 10.5 magnitude, for the next 5 years with a precision of 3-5m/s using the simultaneous Th-Ar spectral lamp reference technique beginning 2011.

(Abhijit Chakraborty)

Infrared observations of lunar impact of Kaguya Spacecraft from Mt. Abu Observatory

The impact of Japanese lunar orbiter Kaguya (Selene) on the lunar surface was successfully observed in the near infrared from Mt Abu Observatory. Apart from Mt Abu the impact flash was observed only at the Anglo-Australian Observatory near Sydney. Observations were made using the NICMOS IR Camera attached to the 1.2m telescope through a narrow band IR filter centered at 2.12 microns (Bandwidth 0.04 microns). Field of view on the sky was 2.2 arc min x 2.2 arc min or 256 km x 256 km on the moon. The impact flash was clearly recorded at 18:25:10:32 UT on June 10, 2009 at the predicted lunar position (80˚.4E, 65˚S). In the next frame taken one second later the flash is still recorded but with diminished intensity (Figure 2). A star calibration was carried out soon after the impact on a nearby star (SAO 188932, K5 III, m_k = 3.39 ± 0.30). The main flash magnitude was calculated to be 3.26 ± 0.3 which diminished to 5.55 ± 0.30 one second later. The intensity of the flash decreased to 12% of its peak value in one second and to < 2% of the peak value in the next second. In comparison lunar meteor impact events are more transient – the optical flash lasts only ~ 200 milliseconds.The flash energy at the impact site at 2.12 microns is inferred to be $(1.6 \pm 0.4) \times 10^{+5}$ Joules. Using a optical conversion efficiency of < 0.1% the impact energy could be > 10^8 Joules. For comparison the kinetic energy of impact of the 2000 kg spacecraft moving at I.73 km/s is ~ 3×10^9 Joules. In comparison to LCROSS impact on the moon which could not be observed in IR from ground based large telescopes, it has been suggested

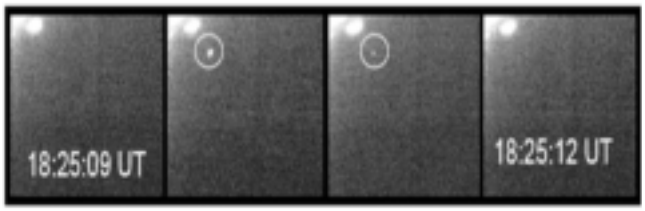

Fig. 2: Impact flash as recorded at 2.12 microns at Mt. Abu Observatory on June 10, 2009. Four consecutive frames at 1 second intervals are shown. The impact flash is seen within the circle in the middle two frames. North is up and West is to the right.

that Kaguya impact was unusually bright due to ~ 40 kg of unspent Hydrazine fuel which ignited on impact. However there is no spectroscopic evidence. The Kaguya impact should have created a crater 5 – 10m wide and about 1m deep which is yet to be confirmed.

(T. Chandrasekhar, R.R. Shah, S.N. Mathur and G.S. Rajpurohit)

Lunar Occultations of Galactic Centre region sources observed at Mt. Abu Observatory – Further analysis.

A detailed analysis of dozen lunar occultation events observed earlier within one degree of the Galactic Centre, from Mt. Abu Observatory in the K band has been completed. The analysis involves non linear least squares method, comprising five parameters – geometric time of occultation, star signal counts, background counts, velocity component of the moon in the direction of occultation and the uniform disk angular diameter of the source. The point source Fresnel diffraction pattern modulated by the finite bandwidth of the system, the finite telescope aperture, sampling time determined by the system electronics and the finite uniform disk angular size of the source are used to fit the observed data.

A serious effort was made to determine the limiting angular resolution of LO observations recorded with infrared sub

arrays. The limiting angular resolution in case of the 10 x 10 pixel (5" x 5") sub array normally used is derived to be 3 milli arc sec (mas) for a sampling time of 9ms for a source with K = 4.0.

Fig.3: 50cm automated telescope in the small telescope building at Gurushikar,Mt Abu.

Of the 12 successfully observed events, three sources (events 4, 5 and 14) are found to be clearly resolved with angular size ranging from 7 to 18 milliarc seconds. Another source (event 8) exhibits binarity with a separation of 30 ± 5 mas in the direction of occultation with a brightness ratio of 3.8 ± 0.2. Two of the resolved sources are late M giants while the third is a carbon star.

(T. Chandrasekhar and Tapas Baug)

Optical photo-polarimetry of Comet C/2007 N3 (Lulin)

Polarization study of the comets provides us the tool to understand their grain properties. We observed comet Lulin during the month of February 2009, for linear polarization using the optical polarimeter mounted at the 1.2 m telescope at Mt. Abu Observatory. The observations were carried out through the IHW narrow band (continuum) and R broad band filters and several apertures at phase angles ranging from 1.6 to 10.5 degree when comet was near opposition. Comet N3 Lulin was also closest (~ 0.41AU) to the Earth during the observing run. It showed negative polarization, expected at these phase angles, and a marginal enhancement in the flux at phase angles less than 2.5 deg. During our observing run, comet did not approach zero phase angle and hence no opposition surge was noticed. The first 'dip' at low phase angle, expected in the model, was noticed in our observations at ~ 6.5 deg. Our observations favour coherent back-scattering model for flux distribution. On the basis of these measurements, we infer comet C/2007 N3 (Lulin) to be a comet with a typical grain composition-mixture of silicates and organics.

(U.C. Joshi, S. Ganesh and K.S. Baliyan)

Photometry and polarimetry of Blazars : Polarisation variability in 3c454.3 and PKS 0716 + 71

Blazars are a subclass of active galactic nuclei (AGNs) with huge energy output, the mechanism for which is not well understood. Variability in total intensity and polarized flux is used as a tool to understand their properties. From Mt Abu IR Observatory, we monitored a sample of blazars in optical and near-IR for variability in flux and polarization using optical CCD (1296x1152 pixels), EMCCD (1000x1000 pixels), NICMOS IR array and photopolarimeter for about 44 nights during 2009-10. Monitoring was done mostly in R band with some images in other filters to study any wavelength dependent variation. The lightcurves generated from such observations are useful to determine variability timescales. The shortest timescale of variation provides upper limits on the size of the emission region. With a knowledge of the location of such emission regions, one can infer mass of the black hole using these timescales.

Optical linear polarization observations made on PKS 0716 + 71 and 3C454.3 during December 10-14, 2009 exhibited interesting activity in these two blazars. The observations were made with the PRL optical photopolarimeter on dark photometric nights. BL Lac PKS0716 + 71 showed variable degree of polarization. Most interestingly, during one night the degree of polarization decreased significantly by about 2.5% in about one hour and then remained at that level for about three hours. The position angle remained almost same during the night. These intra-night variations point to a relativistic shock moving down the jet with stable magnetic field orientation. The inter-night variation of degree of polarization and position angle rotation is perhaps due to geometric effects caused either by helical jet or light house effect. Drastic intra-night changes in degree of polarization (3 to 5 %) and position angle (5 to 8 deg) are also shown by 3c454 during Dec.11-14, 2009. A few days before these observations, a significant Gamma-ray flare was detected by Fermi Spacecraft. The source behaviour indicates shocks moving in turbulent jet with changing magnetic field. Efforts are on to understand any possible relationship between optical and the gamma-ray flare.

(Sunil Chandra, K. S. Baliyan, S. Ganesh and U. C. Joshi)

Automated telescope for precision photometric studies

Blazars, a subclass of AGNs show strong variability in their flux which can be used to study their energetics.However, for this long term continuous precision light curves are required. To cater to this need and for other programs (like exo-planet transit events), a 50 cm telescope suitable for automation was procured in 2009. The telescope is of the Corrected Dall-Kirkham (CDK) type with open truss design, mounted on an equatorial fork mount. The telescope has drives on both axes allowing tracking of the objects at sidereal as well as non-sidereal (eg. comets) rates. It was installed on January, 2010 in the existing small dome (Figure 3) behind main 1.2m telescope building at the Mt. Abu Observatory, Gurushikhar. The telescope has a focal ratio of f/6.8 . The telescope is equipped with a computer controlled filter wheel (with standard UBVRI filters) and Andor EMCCD camera (1024x1024 pixels), mounted at the focal plane as an imaging instrument.

Fig.4: First light image from the 50cm telescope – A 60 sec V band image of galaxy M65 taken with EM CCD.

First light image from the Telescope is shown in Figure 4 - A 60 second V band image of the M65 galaxy taken with EMCCD. The work is going on to integrate the complete system (dome + telescope + backend instrument) to make it a automated/robotic observatory. Once fully automated, it should prove very useful to also observe transient events, such as Gamma-Ray Bursts (GRBs), apart from programs outlined above.

(S. Ganesh, U.C. Joshi, K.S. Baliyan and S.N. Mathur)

Near-infrared Observations of Nova V574 Puppis

Extensive near-infrared spectroscopic and photometric observations of nova V574 Pup are reported. The observations were obtained over 4 months, starting from 2004 November 25 (4 days after the nova outburst) to 2005 March 20 using the 1.2 m telescope at Gurushikhar, Mt Abu. The near-infrared light curves in J, H, and K-bands show no evidence for dust formation during our observations. In the early decline phase, the JHK spectra of the nova are dominated by emission lines of hydrogen Brackett and Paschen series, O I, C I and He I. We also detect the fairly uncommon Fe II line at 1.6872 microns in the early part of our observations. The strengths of the He I lines at 1.0830 and 2.0585 microns are found to become very strong towards the end of the observations indicating a progression towards higher excitation conditions in the nova ejecta. The width of the emission lines do not show any significant change during the course of our observations. The slope of the continuum spectrum was found to have a $\lambda^{-2.75}$ dependence in the early stages which gradually becomes flatter with time and changes to a free-free spectral dependence towards the later stages. Recombination analysis of the H I lines shows deviations from case B conditions during the initial stages. However, towards the end of our observations, the line strengths are well simulated with case B model values with electron density $n_e = 10^{9\text{-}10}$ cm^{-3} and a temperature equal to 10000 K. Based on our distance estimate to the nova of 5.5 kiloparsec and the observed free-free continuum emission in the later part of the observations, we estimate the ionized mass of the ejecta to be between 10^{-5} and 10^{-6} M_{sun}.

(Sachindra Naik, Dipankar P. K. Banerjee, N. M. Ashok and R. K. Das)

An α-tagged X-ray source for the calibration of space borne X-ray detectors.

The characterization and measurement of X-ray emission from the astrophysical sources require well calibrated X-ray detectors. Calibration of X-ray detectors is very important to understand the performance characteristics of the detectors and their variation with time and changing operational conditions. This enables the most accurate translation of the measurements to absolute and relative values of the incident X-ray photon energy so that physical models of the source emission can be tested. It is a general practice to put a known X-ray source (radioactive source) in the detector housing for the calibration purpose. This, however, increases the background. Tagging the calibration source with the signal from a simultaneously emitted charge particle (like alpha particle) can identify the X-ray event used for calibration. We presented a new design for an alpha-tagged X-ray source using Am^{241} radioactive source for space application which is rugged, cheap and easy to

use. The alpha-tagging method selects only the calibration X-rays along with negligible contribution from the background, thus enabling the calibration with a low count rate source. Further, even if a small fraction of these X-rays enter the detector without getting tagged, they will have negligible impact on the overall background rates. This alpha-tagged X-ray calibration source is proposed to be used in the Astrosat satellite.

This work was done in collaboration with A.R. Rao and his group in TIFR, Mumbai.

(Sachindra Naik)

Suzaku Observation of GRS 1915+105: Evolution of Accretion Disc Structure during Limit-Cycle Oscillation.

GRS 1915+105 is the brightest microquasar in our Galaxy, providing us with a unique opportunity to study the accretion flow onto a black hole at high fractions of Eddington ratio. It was recognized to be a superluminal source by Very Long Baseline Array observations of radio outbursts, and hence making it a target of great importance for studying the formation mechanism of relativistic jets. From the kinetics of the radio jets, their intrinsic speed and inclination are determined to be 0.92-0.98c (where c is the speed of light) and 66°-70°, respectively. The near-infrared observations have revealed that the system consists of a black hole with a mass of 14 ± 4 solar-mass and a K III type companion star with an orbital period of 33.5 days. This indicates a huge size of the accretion disk with a continuously high mass transfer rate from the companion, which may account for many unique features of this source compared with the normal black hole binary systems. This microquasar was observed with Suzaku during the 2005 October multi-wavelength campaign.

The data, we analyzed and interpreted, include both stable state (class χ) and limit-cycle oscillation (class θ). Correct interstellar absorption as well as effects of dust scattering are fully taken into account in the spectral analysis. The energy spectra in the 2-120 keV band in both states are all dominated by strong Comptonization of disk photons by optically thick (τ ~ 7-10) and low-temperature (T_e ~ 2-3 keV) hybrid plasmas containing non-thermal electrons produced with 10% - 60% of the total power input. Absorption lines of highly ionized Fe ions detected during the oscillation indicate that a strong disk wind is developed. The ionization stage of the wind correlates with the X-ray flux, supporting the photo-ionization origin. The iron-K emission line shows a strong variability during the oscillation; the reflection is strongest during the dip but disappears during the flare. We interpret this as evidence for "self-shielding" that the Comptonizing corona becomes geometrically thick in the flare phase, preventing photons from irradiating the outer disk. The low-temperature and high-luminosity disk emission suggests that the disk structure is similar to that in the very high state of canonical black hole binaries. The spectral variability during the oscillation is explained by the change of the disk geometry and of the physical parameters of Comptonizing corona, particularly the fractional power supplied to the acceleration of non-thermal particles.

This work was done in collaboration with Japanese scientists.

(Sachindra Naik)

Monte-Carlo simulations for X-ray Polarimeter

The X-ray polarization measurement experiment is a collaborative project between PRL and RRI. It is under advance stages of consideration by ISRO for possible launch during 2013-14. It is based on classical method of X-ray polarization measurement based on Thomson scattering. The experiment employs the baseline design of a central low Z scatterer (typically Beryllium) surrounded by X-ray detectors to measure the angular intensity distribution of the scattered X-rays. It will have collecting area of approximately 800 cm^2 and will be sensitive in the energy range of 8 – 30 keV. The bright Galactic X-ray sources are the prime targets for this experiment. The design goal for the polarization measurement sensitivity of this experiment is ~ 1% MDP (Minimum Detectable Polarization) at 3 σ significance from one Crab source in ~1 Mega Sec exposure. However, the sensitivity of such experiment is critically dependent on the collecting area and the modulation fator which in turn are determined by the scattering geometry which can provide the highest modulation factor and thus highest sensitivity within the specified experimental constraints. The best way to determine optimum scattering geometry is by means of Monte Carlo simulations for various possible cases. We have carried out extensive Monte Carlo simulations using the Geant4 toolkit to determine the best scatterer shape as well as to determine the sensitivity of the experiment. We have considered two different detector arrangements as well as five different scatterer shapes which are feasible within the weight and size constraints of the available spacecraft platform. It was found that the conical shape of the scatterer provides the best sensitivity for a given

collecting area. More simulations are being carried out in order to further optimize conical shape in terms of the cone angle as well as base area.

(S.V. Vadawale, J. Pendharkar and S. Naik)

Interplanetary magnetic field: Modulation of solar rotation

The most extensive data set of interplanetary magnetic field in available from the Advanced Composition Explore (ACE). ACE orbits the L1 liberation point which is a point of Earth-Sun gravitational equilibrium about 1.5 million km from Earth and 148.5 million km from the Sun. From its location at L1 ACE has a prime view of the solar wind, interplanetary magnetic field and higher energy particles accelerated by the Sun, as well as particles accelerated in the heliosphere and the galactic regions beyond. We used the interplanetary magnetic field data to look for the periodicities in its three components. For year 2001 we prepared time series with a daily cadence of Bx, By and Bz. These time series are very regular with less than 3% missing data. These data gaps were filled with linear interpolation scheme. We performed correlation analysis with these time series. The analysis indicate that Bx and By component of the IMF have a very strong modulation of solar rotation (Figure 5).

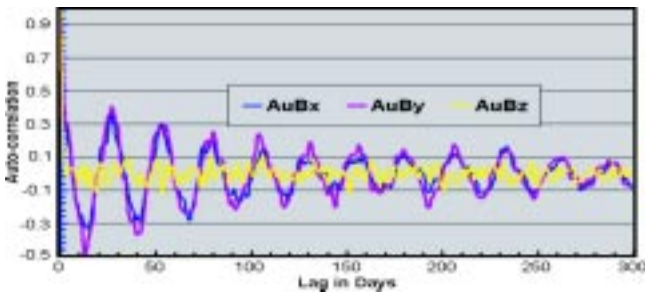

Fig.5: Auto-correlation of the Interplanetary Magnetic Field (IMF) for the year 2001. The auto-correlation of B_x and B_y components ($A_u B_x$, $A_u B_y$) are similar and periodic while that of B_z ($A_u B_x$) is low and aperiodic.

The auto-correlation curve of z component of IMF (AuBz) surprisingly has no rotational modulation. The estimated synodic rotation periods for the years 2000 and 2001 are 27.85 and 25.85 days respectively. Thus rotation in 2001 is faster than that in 2000. This is in contrast with the earlier measurements using other features on the solar surface. This work is being done in collaboration of Satish Chandra of PPN College Kanpur, U.P and Mehul Mehta of VP Science College, Vidyanagar, Gujarat.

(Hari Om Vats)

Radio and X-ray images of the Sun:

The sunspots and solar activity cycle through a complex manner are believed to be due to the differential rotation of the Sun. We report here the recent investigations of differential rotation during a solar cycle using radio images at 17 GHz and Yohkoh soft X-ray images. We split the images with daily cadence in 17 bins along the solar longitude separated by 10^0 in latitude. Thus images of one year give us a set of 17 time series which can be analyzed to estimate rotation period by correlation technique. The coronal sidereal rotation rate as a function of latitude for each year, extending from 1992 to 2001 for radio and soft X-ray images are obtained. The average for the whole duration is shown in Figure 6.

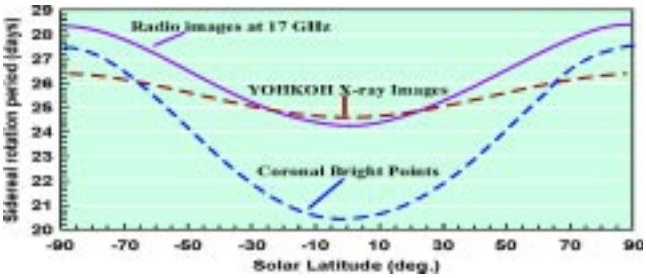

Fig.6: Differential rotation profiles obtained by three different observing methods.

The present analysis reveals that; (i) the equatorial rotation rate of the corona is comparable to the photosphere and the chromosphere, (ii) the latitude differential obtained byboth radio and X-ray images is variable throughout the period of the study, and (iii) the equatorial rotation period seems to vary systematically with sunspot numbers and indicates its dependence on the phases of the solar activity cycle. The results were compared with other measurements of differential rotation estimated by other techniques. There is a large variation for agreement, partial agreement and clear opposition with different observations.

This work is being done in collaboration with K N Iyer of Saurashtra University, Rajkot and Satish Chandra of PPN College Kanpur, UP.

(Hari Om Vats)

Evidence of periodicities in the disk integrated solar coronal rotation:

The present study is an attempt to investigate the long term variations in coronal rotation by analyzing the time series of the radio emission data at 2.8 GHz frequency for the period 1947–2009. The autocorrelation analysis of disk integrated radio intensity shows that the rotation The

present analysis reveals that; (i) the equatorial rotation rate of the corona is comparable to the photosphere and period varies between 17.2 to 29.4 sidereal days (mean sidereal rotation period is 24.5 days). This variation in the coronal rotation period shows evidence of three components in the variation; (1) 11-years component which is related to the sunspot cycle, (2) 22-years component which may be related to the solar magnetic field reversal or Hale's cycle, and (3) a component which is irregular in nature, but dominates over the other components. The cross correlation analysis between the annual average sunspots number and the coronal rotation period also shows evidence of its correlation with the 11-years sunspot cycle and the 22-years Hale's cycle. The two periodic components namely 11 years and 22 years, found in the temporal variation of the solar coronal rotation period are neither in phase nor out of phase with the corresponding periodicities in the variation of the sunspots number.This appears to be the reason that we do not see the solar activity in the entire data set of solar rotation (1947-2009) .

This work is being done in collaboration Satish Chandra of PPN College Kanpur, UP

(Hari Om Vats)

GMRT Deep Imaging at 150 MHz of High Redshift Radio Galaxies:

Since powerful radio sources reside in massive ellipticals, finding radio galaxies at high redshifts is important to understand the radio evolution of galaxies. It is known that the fraction of radio sources that can be optically identified is lower by a factor of 3 or more for steep spectrum radio sources ($\alpha > 1$; $S_\upsilon \propto \upsilon^\alpha$; where α is the spectral index) suggesting that the radio sources with steeper spectra at decimeter wavelengths are more distant compared to the ones with normal spectra ($1 > \alpha > 0.5$). Over the years, this correlation has been exploited to search for radio sources at high redshifts. Since radio emission does not suffer from dust absorption, selecting candidate high redshift radio galaxies (HzRGs) at radio frequencies provides an optically unbiased sample.

We have started a programme with the Giant Metrewave Radio Telescope (GMRT) to exploit this correlation at flux density levels ~100 times deeper than the known HzRG's which were identified primarily using the already available radio catalogues. In our programme, we have obtained deep, high resolution radio observations at 150 MHz with GMRT for a 'deep' field, called the "Deep2 Survey", which has been well studied at higher radio frequencies and in other bands of the electromagnetic spectrum. The aim is to detect candidate HzRG's. The 'Deep2 Survey' consists of four fields in the redshift range ($0.70 < z < 1.55$). The Deep2 Survey was carried out with the 10m optical Keck Telescope for detection HzRGs.

The 150 MHz band of GMRT is ideal for deep imaging as it provides a large field of view (half power beam width of 3^o), high angular resolution (~20") and a sensitivity of ~1 mJy. The chosen deep fields at 150 MHz contain thousands of sources in a single pointing. The observed GMRT deep fields at 150 MHz are processed through the standard astronomical imaging processing software (AIPS) to produce multi-facet maps. We aim to go well below the detection limit of SDSS (optical), WENSS, NVSS, FIRST and GB6 surveys (radio). The new sources that this analysis will find can be followed up, at a later date, for optical identification at other IR and optical facilities.

(Janardhan, P. and Susanta K. Bisoi)

Solar Polar Fields During Cycles 21 - 23: Correlation with Meridional Flows.

Detailed studies of solar magnetic features is an important area of research because solar magnetic fields have a profound and far reaching influence on the earth's near-space environment. With mankind's increased dependence on space based technology, much of which is at risk due to solar activity that waxes and wanes with the sunspot cycle, it is imperative that we understand the solar magnetic cycle and its effects on the near-space environment. In addition, due to the significant anthropogenic influence on climate change in recent times, it is becoming increasingly important to distinguish and delineate the degree to which the solar cycle can affect terrestrial climate.

We have examined polar magnetic fields for the last three solar cycles, viz., cycles 21, 22 and 23 using NSO Kitt Peak synoptic magnetograms. In addition, we have used SoHO/MDI magnetograms to derive the polar fields during cycle 23. Both Kitt Peak and MDI data at high latitudes (78^o – 90^o) in both solar hemispheres show a significant drop in the absolute value of polar fields from the late declining phase of the solar cycle 22 to the maximum of the solar cycle 23. We find that long term changes in the absolute value of the polar field is well correlated with changes in meridional flow speeds that have been reported recently. The behaviour of solar polar fields is shown to be a good indicator of the meridional flow speeds. We

have examined the implication of this in influencing the extremely prolonged minimum experienced at the start of the current cycle 24 and in forecasting the behaviour of future solar cycles.

(Janardhan, P. Susanta K. Bisoi and Sanjay Gosain)

Magneto hydrodynamic simulation for triggering of Solar Flares

The physical process of flare occurrence via reconnection of the magnetized loops in the corona has been well known However the physical process responsible for the reconnection that may lead to trigger the flare is not clear. Recent investigations suggest the evolution of an emerging flux in the pre-existing sunspot region might be the source of the flare. We study two-dimensional (2-D) magneto-hydrodynamic (MHD) model of emerging magnetic flux region in the solar photosphere/chromosphere and corona by using nonlinear 2-D MHD numerical simulations to explore the role of these emerging magnetic fluxes in triggering the solar flares. The sunspots are formed by the emergence of magnetic flux tubes from the interior of the Sun into the solar atmosphere. In this study we investigate nonlinear evolution of the "Parker instability" produced by the flux emergence parallel to pre-existing magnetic field. This instability is also known as the undular mode of the magnetic buoyancy instability.

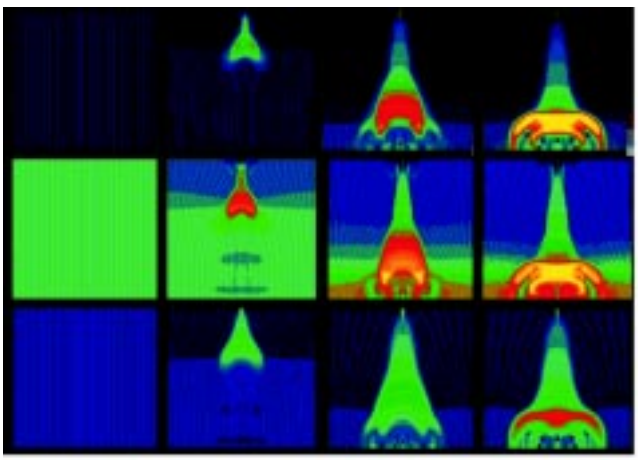

Fig.7:2-D MHD numerical simulation incorporating emerging flux in the solar plasma showing process of flare triggering via reconnection reveals *Top panel:* temperature *Middle panel*: resistivity and *Bottom panel*: Pressure, for evolution time t = 0,8,13,15 sec.

The rising magnetic loops resulting from the instability are identified as the emerging magnetic flux which with the help of highly resistive region drives the magnetic reconnection in corona that is followed by the solar flare. We simulate pressure, temperature and resistivity using Coordinated Astronomical Numerical Software (CANS) which includes the engines to solve the one-, two- and three-dimensional HD or MHD equations (Figure 7).

(Rajmal Jain and Arun Kumar Awasthi)

Estimating thermal and non-thermal energy budget in solar flares:

We investigate the physical implication of Neupert effect in 12 M-class flares observed by "Solar X-ray Spectrometer" (SOXS) onboard GSAT-2 to probe the fraction of energy converted from non-thermal to thermal component. For this purpose we have split up our investigation into two categories of solar flares viz. gradual flares (Rise time $t_r > 150$ sec) and impulsive flares ($t_r < 150$ sec. We found 5 gradual and 7 impulsive flares in our data sample of 12 flares.

The fraction Q_f of the thermal to non-thermal energy is defined as the ratio of soft X-ray flux in 4-25 keV energy band (F_{sxr}) to integrated hard x-ray flux in 25-50 keV energy band (F_{hxr}) modeled with empirical cooling time (τ_{cool}). We consider τ_{cool} approximately equal to the derived conduction cooling time by us for the rise time of the flares.

To estimate Q_f we employ 3 sec spectra from Si and CZT detectors of SOXS experiment, and then derive the cumulative integration of hard X-ray flux with the application of SolarSoft package. The cooling time in the magnetized flare loops has been estimated from the plasma codes derived by spectral analysis such as maximum temperature, emission measure, power-law index and electron density etc.We find Q_f in impulsive flares ~ 0.6, which suggests that approximately 60 percent of the energy of the accelerated electrons is deposited in chromosphere during thick-target bremmstrahlung and rest is emitted in the form of non-thermal hard X-ray, H-alpha emission etc. On the other hand, surprisingly, Q_f is > 1 for gradual flares This suggests that SXR emission in gradual flares is mainly due to pre-flare heating of the plasma in addition to conversion of non-thermal to thermal X-ray emission.

(Arun Kumar Awasthi and Rajmal Jain)

Spectral characteristics of Solar Energetic Particles (SEPs) to probe their geo-effectiveness

The energetic charge particle environment in interplanetary space of Sun-Earth-Moon system is comprised of solar wind, solar energetic particles (SEPs), co-rotating interacting regions (CIRs) and anomalous and galactic cosmic rays

(GCR). The charged particle spectroscopy gives an opportunity to understand the effect of SEPs on earth system. In this investigation we have analyzed 16 SEP events, which have also been identified as "Ground Level Enhancements (GLE)" events. We use observations made by ULEIS instrument onboard ACE satellite, which provides wide spectrum of elemental composition. We measured the elemental fluencies as a function of energy in order to study the acceleration mechanism The energy spectra of Fe^{56} of 13 December 2006 event reveal the break in the spectrum around 1 MeV, which suggests higher energy ions were accelerated by a different mechanism then lower energy ions. We are analyzing the data for this as well as other GLE events to probe the role of interplanetary shock versus earth's bow shock in further acceleration of high-z ions.

(Rajmal Jain, Subhash Kaushik, Arun Awasthi and Nipa J. Bhatt)

New technique to estimating flare plasma parameters using SOXS observations:

SOXS provides high-resolution spectral and temporal data on daily basis to study the physics of full disk integrated X-ray emission from the Sun in general and solar flares in particular. The solar coronal X-ray emission particularly during flares provides unique opportunity to measure flare plasma parameters viz. temperature, density, spectral index and elemental abundances etc., which in turn allows understanding the physical process that prevailing in the solar corona. We have developed a software based on the "Ratio Technique" of two energy windows to estimate the plasma parameters from SOXS data. We measure the photon flux in two energy bands viz. 4-10 and 10-15 keV, derive the ratio(R), and compare it with independently measured temperature from spectral fit techniques. The photon flux ratio R, theoretically becomes independent of emission measure, and therefore correlates well with temperature.

(Rajmal Jain and Arun Kumar Awasthi)

Radio Galaxies and Quasars

It has been shown that an upper limit of $\sim 10^{12}$ K on the peak brightness temperature for an incoherent synchrotron radio source, commonly referred to in the literature for the last 40 years as an inverse Compton limit, is not due to inverse Compton effects. It was shown that a somewhat tighter limit $T_{eq} \sim 10^{11}$ K is actually obtained for the condition of equipartition of energy between radiating particles and magnetic fields which happens to be a configuration of minimum energy for a self-absorbed synchrotron radio source. An order of magnitude change in brightness temperature from T_{eq} in either direction would require departures from equipartition of about eight orders of magnitude, implying a change in total energy of the system up to $\sim 10^4$ times the equipartition value. Constraints of such extreme energy variations mean that brightness temperatures may not depart much from T_{eq}. Higher brightness temperatures would also require many order of magnitude weaker magnetic fields. Diamagnetic effects do not allow such extreme conditions, thereby enforcing a tight upper brightness temperature limit in synchrotron sources $\sim 10^{11.5}$K making the inverse Compton limit arguments rather redundant.

(Ashok K. Singal)

Cosmological parallax-distance formula – A correction

A correction has been pointed out in the standard cosmological parallax-distance formula, as found in the literature, including text-books on cosmology. This correction arises from the fact that any chosen baseline in a gravitationally bound system does not partake in the cosmological expansion and therefore two ends of the baseline used by the observer for parallax measurements cannot form a set of co-moving co-ordinates, contrary to what seems to have been implicitly assumed in the standard text-book derivation of the parallax distance formula. At large redshifts, the correction in parallax distance could be as large as a factor of three or more, in the currently favoured cosmologies ($\Omega_\Lambda = 0.73$, $k = 0$). It has been further shown that even the most distant observable objects (i.e., redshift approaching infinity) have a finite parallax angle and which thus needs to be carefully accounted for when using such distant objects as the background field against which the parallax of a foreground object is measured.

(Ashok K. Singal)

Front-end and Back-end electronics development for X-ray detectors

We have designed and are developing front-end electronics - charge Sensitive Pre-Amplifier (CSPA), Shaping Amplifier (SA), Peak Detector (PD) and Analog-to-digital converter (ADC) - for Silicon Drift Detector (SDD), Silicon diodes and Silicon Pixellated Array. Field Programmable Gate Array (FPGA) based processing electronics is also under development for event data acquisition, real-time spectrum

generation, online data packaging and spectrum uploading to host system. Proto models are designed in a fashion that it can easily converted into space qualified models for satellite based applications. X-ray laboratory has been equipped with the state-of the-art testing and measuring instruments to characterise single pixel and multi-pixels x-ray detectors.

(A.B. Shah and S.L. Kayasth)

Solar Physics

The research and development activities of the Udaipur solar observatory revolve around the central theme of solar activity and solar eruptive processes. Helioseismology is used as a tool to dig into the sub-surface origins of eruptions. Surface magnetic field is measured to monitor magnetic energy storage and evolution of the potential triggers of the eruptions. Above the surface, chromospheric and coronal phenomena are used to predict the geoeffectiveness of these eruptions. A combination of analyses of archived data, mathematical modeling and construction of sophisticated instruments is employed to achieve the desired goals.

On the Absence of Photospheric Net Currents in Vector Magnetograms of Sunspots Obtained From Hinode (SOT/ SP):

Various theoretical and observational results have been reported regarding the presence/absence of net electric currents in the sunspots. The limited spatial resolution of the earlier observations perhaps obscured the conclusions. We have analyzed 12 sunspots observed from Hinode (SOT/SP) to clarify the issue. The azimuthal and radial components of magnetic fields and currents have been derived. The azimuthal component of the magnetic field of sunspots is found to vary in sign with azimuth. The radial component of the field also varies in magnitude with azimuth. While the latter pattern is a confirmation of the interlocking combed structure of penumbral filaments, the former pattern shows that the penumbra is made up of a "curly interlocking combed" magnetic field. The azimuthally averaged azimuthal component is seen to decline much faster than v in the penumbra, after an initial increase in the umbra, for all the spots studied. This confirms the confinement of magnetic fields and absence of a net current for sunspots (Figure 8) as postulated by Parker in 1996.

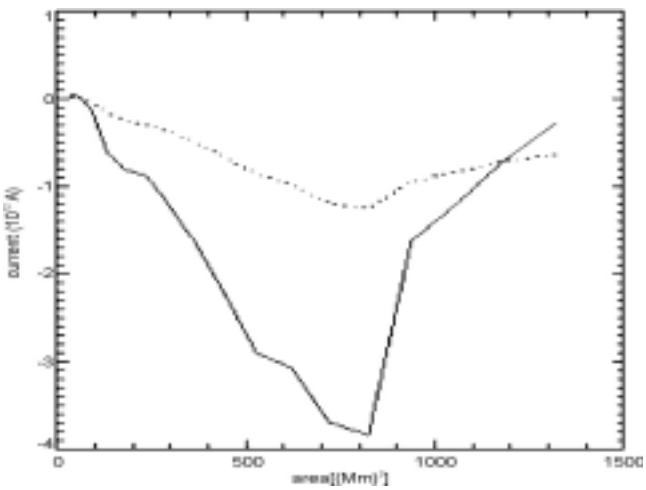

Fig.8:The net current variation with increasing area has been shown for our calcuation (solid line) and derivative mathod (dashed line).

The existence of a global twist for a sunspot even in the absence of a net current is consistent with a fibril-bundle structure of the sunspot magnetic fields.

(P. Venkatakrishnan, and Sanjiv Kumar Tiwari)

Magnetic Non-Potentiality of Solar Active Regions and Peak X-Ray Flux of the Associated Flares:

Predicting the severity of the solar eruptive phenomena like flares and Coronal Mass Ejections (CMEs) remains a great challenge despite concerted efforts for several decades.

The advent of high quality vector magnetograms obtained from Hinode (SOT/SP) has increased the possibility of meeting this challenge. In particular, the Spatially Averaged Signed Shear Angle (SASSA) seems to be an unique parameter to quantify the non-potentiality of the active regions. We wish to demonstrate the usefulness of SASSA for predicting the flare severity. For this purpose we present a case study of the evolution of magnetic non-potentiality in two active regions (ARs) namely NOAA AR 10930 and NOAA AR 10961 during 08-15 December, 2006 and June 28-July 5, 2007 respectively. The NOAA AR 10930 was very active and produced two X-class flares along with many smaller X-ray flares. On the other hand the NOAA AR 10961 was relatively less active and produced only very small (A and B class) flares. For this study we use a large number of high resolution vector magnetograms obtained from Hinode (SOT/SP). The study shows that the upper limit of the peak X-ray flux of solar flares emanating from the active regions depends on the magnitude of SASSA at the time of the flare (Figure 9). This discovery of the existence of an upper limit of the peak X-ray flux of a solar flare for a given value of the SASSA will be very useful for space weather forecasting.

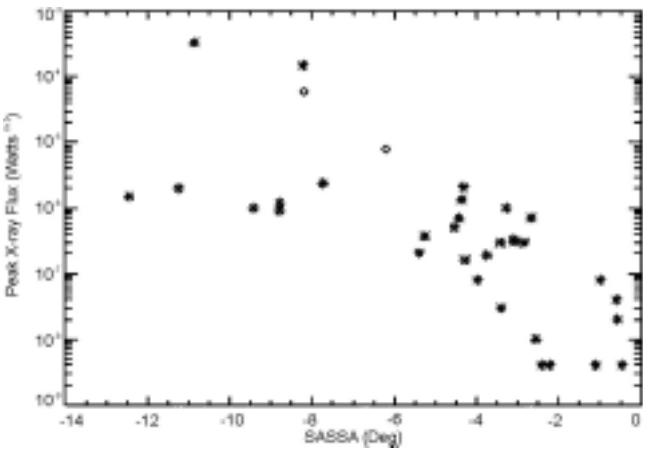

Fig.9: Scatter plot between SASSA and peak X-ray flux of GOES 12 satellite. Samples include all the events associated with both the active regions i.e., NOAA 10930 and NOAA 10961. The magnitude of SASSA at the time of the peak X-ray flux has been interpolated from the available sample of SASSA. Also, the approximate values of the SASSA corresponding to M-class flares in two cases have been taken from the Table 1 of Tiwari et al., (2009, ApJ, 702 L133-L137) and are shown by diamond symbols.

(Sanjiv Kumar Tiwari, P. Venkatakrishnan and Sanjay Gosain)

Magnetic Tension of Sunspot Fine Structures:

The equilibrium structure of sunspots depends critically on its magnetic topology and is dominated by magnetic forces. Tension force is one component of the Lorentz force which balances the gradient of magnetic pressure in force-free configurations. We employ the tension term of the Lorentz force to clarify the structure of sunspot features like penumbral filaments, umbral light bridges and outer penumbral fine structures. We compute vertical component of tension term of Lorentz force over two active regions namely NOAA AR 10933 and NOAA AR 10930 observed on 05 January 2007 and 12 December 2006 respectively. The former is a simple while latter is a complex active region with highly sheared polarity inversion line (PIL). The vector magnetograms used are obtained from Hinode(SOT/SP). We find highly inhomogeneous distribution of tension with both positive and negative signs in various features of the sunspots (Figure 10). The existence of positive tension at locations of lower field strength and higher

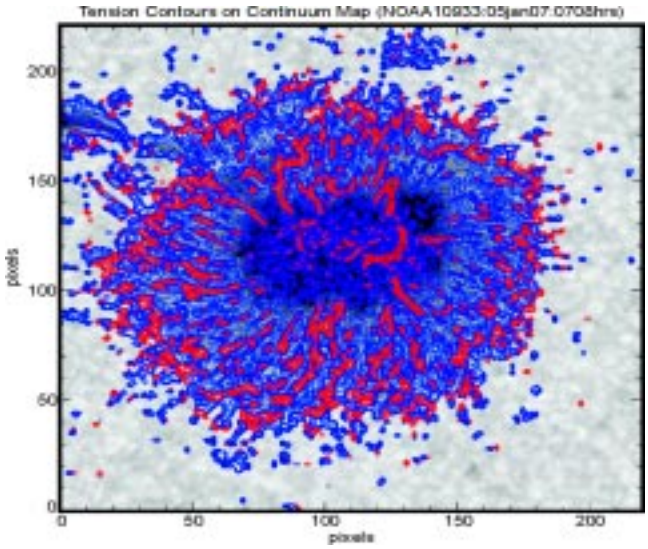

Fig.10: Contours of tension forces in terms of solar gravity overlaid on the continuum map of NOAA AR 10930. Blue and red colors show negative and positive values respectively.

inclination confirms the uncombed model of the penumbral structure. Positive tension is also seen in umbral light bridges which could be indication of uncombed structure of the light bridge. Like-wise, the upward directed tension associated with bipolar regions in the penumbra could be a direct confirmation of the sea serpent model of penumbral structures. Upward directed tension at the PIL of AR 10930 seems to be related to flux emergence. The magnitude of the tension force is comparable or greater than the force of gravity in some places, implying a force-free configuration for these sunspot features. The study of magnetic tension in various types of sunspot fine structures promises to yield new and exciting information on the equilibrium and dynamics of these structures.

(P. Venkatakrishnan and Sanjiv Kumar Tiwari)

Estimation of width and inclination of a filament sheet using He II 304 A observations by STEREO/EUVI

The STEREO mission has been providing stereoscopic view of the filament eruptions in EUV wavelengths. The most extended view during filament eruptions is seen in He II 304 A observations, as the filament spine appears darker and sharper. The projected filament width appears differently when viewed from different angles by STEREO satellites (Figure 11). Here, we present a method for estimating the width and inclination of the filament sheet using He II 304 A observations by STEREO-A and B satellites from the two viewpoints. The width of the filament sheet, when measured from its feet to its apex, gives estimate of filament height above the chromosphere.

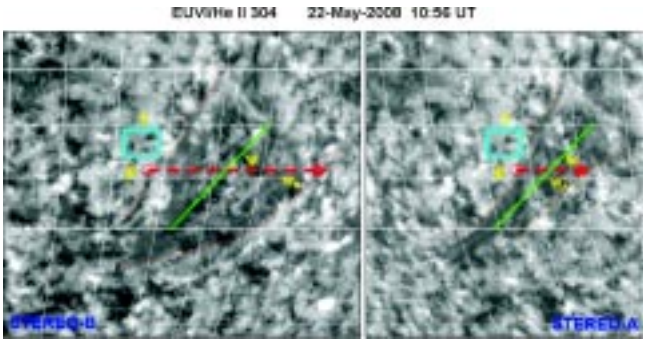

Fig.11: The He II 304 A observations of a filament on 22 May 2008 during its disappearance phase at 10:56 UT. The separation angle of about 52.4 degrees between STEREO satellites shows quite different view of the filament.

This work was done in collaboration with B. Schmieder of LESIA, Meudon, France.

(S. Gosain)

Magnetic Field Structures in a Facular Region Observed by THEMIS and *Hinode*

We build and compare vector magnetic maps obtained by two spectral polarimeters, i.e. THEMIS/MTR and Hinode SOT/SP, using two inversion codes (UNNOFIT and MELANIE) based on the Milne-Eddington solar atmosphere model. To this end, we used observations of a facular region within active region NOAA 10996 on 23 May 2008, and found consistent results concerning the field strength, azimuth and inclination distributions. Because SOT/SP is free from the seeing effect and has better spatial resolution, we were able to resolve small magnetic polarities with sizes of 1" to 2", and could detect strong horizontal magnetic fields, which converge or diverge in negative or positive facular polarities. These findings support models which suggest existence of small vertical flux tube bundles in faculae. A new method is proposed to get the relative formation heights of the multi-lines observed by MTR assuming the validity of a flux tube model for the faculae. We found that the Fe I 6302.5 A line forms at a greater atmospheric height than the Fe I 5250.2 A line.

This work was done in collaboration with Y. Guo, B. Schmieder and V. Bommier of LESIA, Meudon, France.

(S. Gosain)

On the estimate of magnetic non-potentiality of sunspots derived using Hinode SOT/SP observations: Effect of polarimetric noise.

We determine typical uncertainties in the M-E inverted field vector and its distribution over a real sunspot using Monte-Carlo method. We generate synthetic Stokes profiles using Hinode SOT/SP vector magnetogram as an input, add normally distributed polarimetric noise with (3-σ) level 0.5

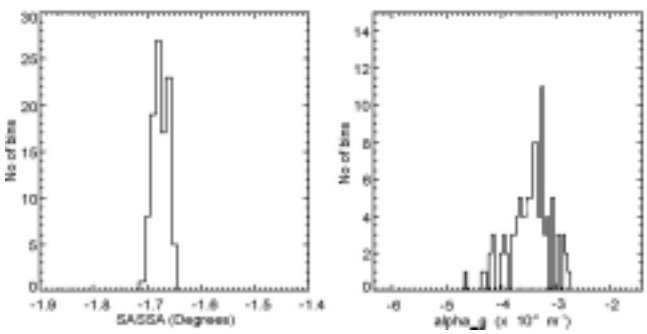

Fig.12: The histograms show distribution of SASSA and α_g corresponding to NOAA 10933. The vector maps were derived hundred times, and each time different realization of normally distributed noise (3σ = 0.5% of Ic) is added to the synthetic profiles.

% of continuum intensity and then invert them. This process is repeated 100 times with different realizations of noise. It is found that within most of the sunspot area (> 90\% area) the spread in the (i) field strength is less than 10 Gauss, (ii) field inclination is less than 2 degree, and (iii) field azimuth is less than 6 degrees. Further, we determine the uncertainty in the magnetic non-potentiality of a sunspot as determined by the force-free parameter α_g and Spatially Averaged Signed Shear Angle (SASSA). It is found that for the sunspot studied here these parameters are α_g = -3.5 ± 0.37 (x 10^{-9} m^{-1}) and SASSA = -1.68 ± 0.014 degrees (Figure 12). This suggests that the SASSA is a more reliable non-potentiality parameter as compared to α_g. By examining the effect of increasing noise levels, it is found that the SASSA of the sunspot is less vulnerable to noise as compared to α_g parameter.

(Sanjay Gosain, Sanjiv Kumar Tiwari and P. Venkatakrishnan)

Supersonic Downflows at the Umbra-Penumbra Boundary of Sunspots

High resolution spectropolarimetric observations of 3 sunspots taken with *Hinode* illustrate the presence of supersonic downflows at or close to the umbra-penumbra boundary. These downflows are located at the centre side penumbra being confined to large patches, usually encompassing bright penumbral filaments (Figure 13). Identification of these downflows was made by constructing magnetograms in the far red and blue wings of the Stokes *V* profile. While the downflows emanate from regions with multiple red-lobed Stokes *V* profiles, one also finds asymmetric circular polarization signals that are strongly red shifted. The nature of the strong velocities as well as strong magnetic fields and their proximity to the umbra-penumbra boundary rules out an association to the Evershed Flow, although the Evershed flow channels are clearly seen in the neighborhood of these downflows. We do however find evidence of intersecting filaments, similar to the post reconnection configuration presented by Ryutova et al. (2008). Chromospheric filtergrams acquired close to the time of the spectropolarimetric measurements, show large, strong brightenings/jets in the neighborhood of the downflows. The time scale of these chromospheric events is longer than those of penumbral microjets which are highly transient but ubiquitous in the penumbra. Our analysis suggests that while a slingshot reconnection mechanism may be responsible for the supersonic downflows, the process may be different from that believed to trigger microjets.

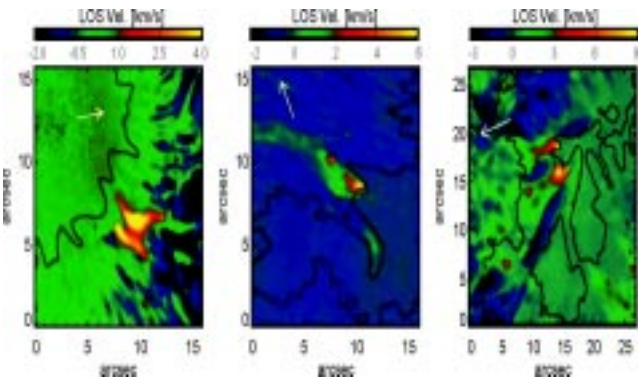

Fig.13: LOS velocities derived from the SIR inversion for NOAA ARs 10923, 10953 and 11029 shown from *left* to *right* respectively. The white arrow points to disc centre.

This work was done in collaboration with Dr. Luis R. Bellot Rubio, IAA, Granada, Spain.

(Rohan E. Louis, Shibu K. Mathew and P. Venkatakrishnan)

The Relationship Between Kinetic and Magnetic Helicities of Active Regions

Solar transient activities, viz., flares and CMEs, are associated with rapid changes in magnetic and velocity field topologies in the solar atmosphere. These changes are essentially brought about by the magnetic fields that are rooted beneath the photosphere where they interact and get affected by sub-surface flows. Therefore, we expect the twist in sub-surface flows to be correlated with the observable twist of magnetic fields at the photosphere and higher layers. In order to examine the correlation, if any, we have derived the kinetic helicity of sub-surface flows using ring diagram analysis and the magnetic helicity using photospheric vector magnetograms for a sample of 68 active regions (ARs) observed during Solar Cycle 23. This study reveals that there is a significant relationship between these twist parameters derived from the internal flows to the external magnetic fields. Their hemispheric trend is also further corroborated. A map of kinetic helicity density constructed using the GONG helioseismic data for the super-active region NOAA 10486 of 28 October 2003 is shown in Figure 14. It provides a clear evidence of large twist in the sub-photospheric flows of NOAA 10486 where the photospheric mean magnetic field is strong (top panel).

(R. A. Maurya, A. Ambastha and V. Reddy)

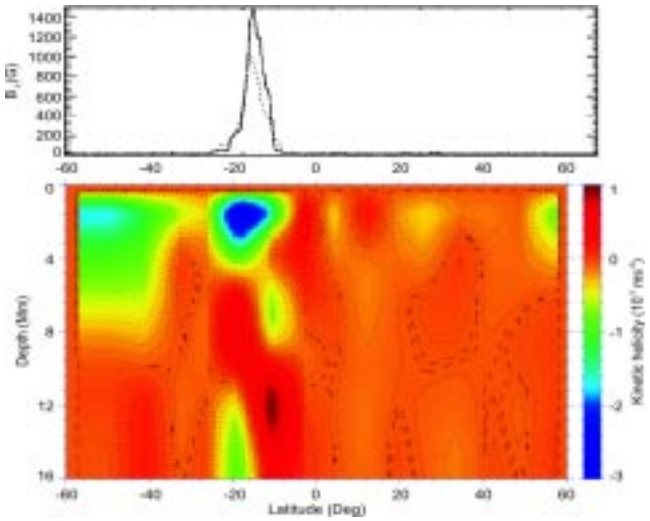

Fig.14: (top) Photospheric mean magnetic field, and (bottom) kinetic helicity density map constructed using GONG data from the surface to 16 Mm sub-surface depth corresponding to the super-active region NOAA 10486 of 28 October 2003.

Variation of p-mode Parameters with Energetic Transients

Our previous studies have shown that power in p-modes is amplified during high flare activity as compared to that in non-flaring regions of similar magnetic field strength.

However, changes of p-mode parameters during various phases of flares have remained unclear. In order to address this problem, we have obtained three-dimensional power spectra for super-active region NOAA 10486 during the long-duration energetic X17.2/4B flare of 28 October 2003, by placing the flare at different temporal positions in appropriately constructed data-cubes**.** Changing the temporal position of the flare within the Doppler data-cubes obtained for the active region amounts to changing the level of the pre- and post- effects in the data-set. The ring diagram analysis of the data-sets thus constructed provided the following important results : (1) Amplitude of p-modes increased up to 150% in the case of the flare placed in the beginning of the data-set as compared to the case when flare was placed near the end or outside the data-cube. A similar result is obtained for p-mode energy as expected due to its relation to the amplitude, manifesting the rate of energy supplied to the p-modes by the flare. (2) Amplitude and energy of the modes decreased with radial order indicating that the effect of the flare decreased with increasing depth. Furthermore, we found that the amplitude and energy of modes increased with frequency. This suggests that modes with high natural frequencies are amplified more by the flare as compared to the low frequency modes. (3) The kinetic helicity of sub-surface flow around the depth of 1 Mm changed from positive to negative during the pre- to the peak phases, and returned back to the pre-flare level after the post-flare phase. In summary, our study provides strong evidence about the role of a large flare in modifying various acoustic mode parameters.

This work was done in collaboration with Sushant Tripathy of NSO, Tucson, USA.

(R. A. Maurya and A. Ambastha)

Sub-photospheric flows in flaring and dormant active regions

Sub-photospheric or internal flows in active and quiet solar regions have been recently studied, however, an understanding of their distinctive characteristics in flare productive ARs as compared to that in dormant ARs is not well understood. Therefore, we have carried out a detailed investigation of the internal flows in a sample of 74 ARs of varying levels of flare productivity and magnetic complexity using the Doppler data obtained by the Global Oscillation Network Group (GONG) project. The sample of these ARs is taken from the Carrington rotations 1980—2052 covering the period August 2001-January 2007 which includes extremely large and complex ARs such as NOAA 10030, 10484, 10486, 10070 which are often termed as super-active regions (SARs). We have discovered the presence of steep gradients in meridional velocity at depths ranging from 1.5 to 5 Mm in flare productive ARs. The gradients showed an interesting hemispheric trend of negative (positive) signs in the northern (southern) hemisphere, i.e., directed toward the equator. We have discovered three sheared layers in the depth range of 0–10 Mm of 44 ARs, providing an evidence of their complex flow structures. The two extrema in meridional velocity and its gradient in these ARs were found to be located at the depths of 1.92 ± 0.15 and 4.69 ± 0.30 Mm. These ARs having only a single extremum were found to be less flare productive. The extremum gradient in meridional velocity was found to follow a hemispheric trend, viz., in the northern hemisphere, 24 (70%) out of 34 ARs had negative gradients while in the southern hemisphere, 29 (74%) out of 39 ARs had positive gradients. ARs of larger magnetic field strength possessed larger gradient in meridional velocity. Flaring activity of an AR is largely associated with the first extremum of vertical vorticity located closer to the surface.

(R. A. Maurya and A. Ambastha)

Sub-photospheric Flow topology and the Life-time of Active Regions.

Solar sub-surface fluid topology provides an indirect approach to examine the internal characteristics of active regions (ARs). Prevalence of strong flows has been found to prevail in the interior of ARs having complex magnetic fields. We have discovered that sub-photospheric flow topology may also decide the remaining life time of ARs. This study is based on the theoretical inferences that the connection between the magnetic structures at the photosphere and its underlying roots may get broken through a dynamical disconnection mechanism. We suggest that the zero vertical vorticity (ω_z) of sub-photospheric flows may be a signature of the flux rope being broken at these depths. Once flux ropes in the interior of an AR are disconnected, its remaining life time would depend upon the depth where ω_z vanishes, i.e., $\omega_z = 0$. To establish this idea further, we have studied 74 active regions of solar cycle 23, and found a linear relationship between the depth (d0) of zero vertical vorticity and the remaining life time (τ) of ARs given by, τ = 6.43 + 0.34 do (Figure 15). The fit is found to be good as 72.65% of the total variance in τ is explained by the linear regression model, suggesting that life time of ARs is correlated with the depth of deepest zero vertical vorticity. This inference may be useful in predicting the expected life time of ARs.

(R. A. Maurya and A. Ambastha)

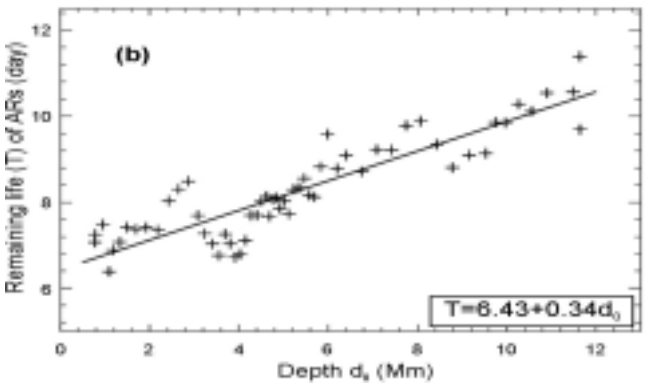

Fig.15: Variation of the remaining lifetime of the sample of 74 ARs with the depth of deepest zero vertical vorticity.

Spectro-Polarimetry and High Cadence Imaging of Solar Corona during the TSE 2009 from Anji, China.

During the July 22, 2009 Total Solar Eclipse (TSE) an expedition was carried out to Anji, China. The main goals of coronal observations were: (i) measurement of coronal emission line polarization in imaging and spectroscopy mode, and (ii) fast imaging in coronal green line channel for detection of coronal oscillations. For fast cadence imaging a Celestron 35-cm aperture telescope was used with a 5303 A filter. For polarization measurements in the white-light, Hα λ 656.3 nm, and the emission lines in green [Fe XIV λ530.3nm] and red [Fe X λ 637.4nm], we designed and fabricated a spectrograph-polarimeter instrument. It was equipped with a beam splitter to simultaneously work in imaging as well as spectroscopy modes. The optical set up was designed for imaging a field-of-view of 1.45° x 1.45° with plate scale of about 5 arc-sec per pixel. Narrow band interference filters (FWHM ~ 0.15 nm) were used for imaging mode while a grating spectrograph in Littrow configuration was used in spectroscopy mode. This simultaneous mode was helpful in tuning of filter transmission profile, which is tilt and temperature sensitive. A reflective blazed diffraction-grating with 1200 grooves per mm was used in first order to achieve dispersion of ~128 mÅ/pixel at 5303Å with spectral resolution of ~120000. The schematic of the instrument is shown in Figure 16.

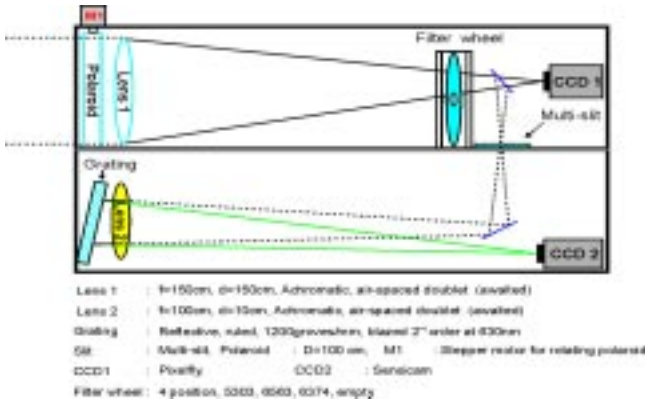

Fig.16: Schematic layout of the polarization measurement setup in imaging and spectroscopy mode.

The optical setup was mounted on a Celestron CGE series German-Equatorial mount to enable direct view of the Sun without any intermediate reflections. The narrow passband filters were kept in a temperature controlled oven with a temperature regulation accuracy of ± 0.5 degree C. Polarimetry was performed using a rotating Polaroid, placed as the first element in the optical train, right in front of the imaging lens, thereby avoiding instrumental polarization. During the TSE campaign, both the instruments performed as expected, however, the recording of the totality was hampered by clouds through the line-of-sight affecting the usability of the data for scientific analysis.

(Ashok Ambastha, Sanjay Gosain, Raja Bayanna and Sudhir Gupta)

Evolution of X-ray sources and magnetic reconnection in solar eruptive flares

Recent X-ray observations of the Sun made by Reuven Ramaty High Energy Solar Spectroscopic Imager (RHESSI) spacecraft have revealed a new phenomenon during the rise phase of flares in which the X-ray loop-top source (coronal source) exhibits a downward motion. In a few events, RHESSI observations have also confirmed the converging motion of HXR foot-points during the rise phase, simultaneously with the downward motion of loop-top source. The explanation of this 'rise phase' observed by RHESSI is beyond the scope of the standard model of solar flares.

Here we have made an attempt to understand the RHESSI perceptive of 'rise phase' of flares in terms of a specific model called "rainbow reconnection model".

In Figure 17, we show a schematic representation of the flare evolution. To understand the observed motion of X-ray sources during the flare, we consider the three-dimensional magnetic reconnection at a separator in the corona. In Figure 17a, we depict the process in which magnetic reconnection releases an excess magnetic energy related to the magnetic tensions which are generated before a flare by shear flows in the photosphere. The relaxation of the associated magnetic shear in the corona by magnetic

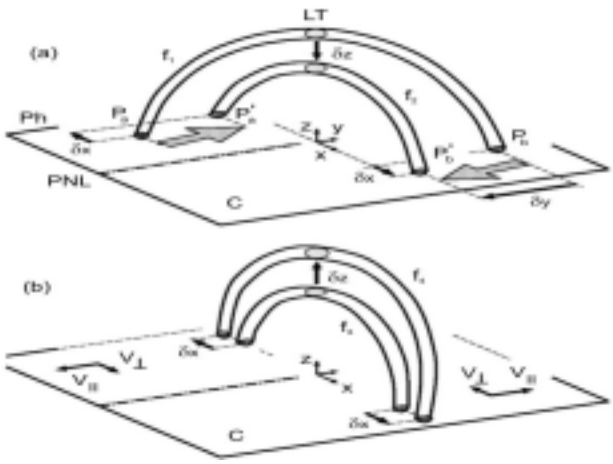

Fig.17: Schematic representation of the flare evolution in terms of rainbow reconnection model during its rise phase (top panel) and main phase (bottom panel).

reconnection explains the descending motion of the loop-top source and converging motion of the foot-point sources. Figure 17b shows the flare evolution during the main phase which is consistent with the standard model of solar flares. Here, flare involves reconnection of the magnetic field lines with foot-points located at larger distance from the PNL and, therefore, have a smaller shear or practically none. As the reconnection involves field lines rooted successively apart from the PNL, the X-ray loop-top source shows the upward motion and HXR foot-points separate from each other.

This work was carried out in collaboration with Astrid Veronig (University of Graz, Austria), K-.S. Cho and colleagues (KASI, Daejeon, South Korea) and Boris V. Somov (Moscow State University, Moscow, Russia).

(Bhuwan Joshi)

Rolling Motion in Erupting Prominences Observed By STEREO

We analysed large-scale dynamical forms of three erupting prominences (filaments) observed by STEREO spacecraft. The observations reveal evidence of the poorly understood "roll effect" i.e. sideways rolling motion beginning at the crest of the erupting filament (Figure 18). We found that all the three events were also highly non-radial and located adjacent to large coronal holes.

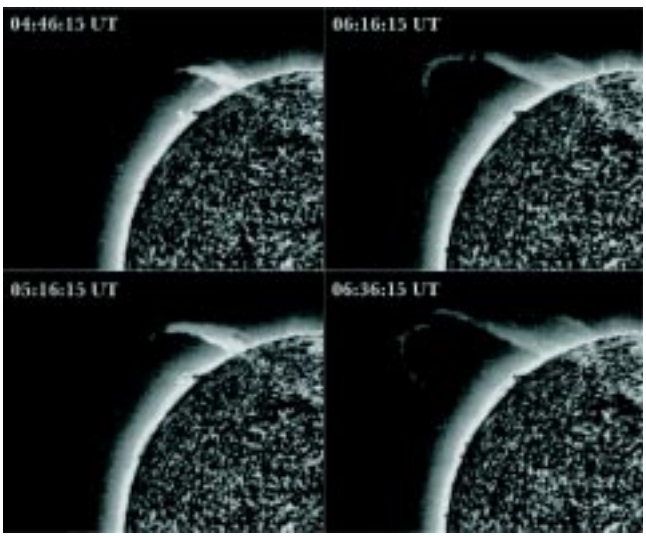

Fig.18: Images taken by STEREO A spacecraft in EUVI wavelength (304 Å) show roll effect in an erupting prominence observed on 12 December 2008.

The associated Coronal Mass Ejections (CMEs) were also found to be non-radial in the same direction as the erupting prominence. The 12 December 2008 eruption occurred underneath a large helmet streamer that extends across the equator and separates the north and south polar holes. The non-radial motion can be explained as due to the channeling of the erupting material by the magnetic tension along the closed loops toward the magnetic null point, which lies at the intersection of the closed and open field

domains. We have reconstructed the 3-D configuration of the CMEs and obtained the true coordinates of the top of the erupting prominences as seen in EUVI 304 Å images. In case of 12 December 2008 event, the prominence underwent a very gradual rise for more than an hour before its eventual eruption that started at 03:56 UT. This early eruptive phase was also found to be quite slow, its true speed being 51 km s^{-1} in the interval from 04:00 to 07:00 UT. A notable change is the decrease in latitude of the prominence from 47^0 to 24^0 once it starts to erupt. Later the prominence, however, was seen to erupt much more rapidly in the COR1coronagraphs, its true speed being around 187 km s^{-1}. However, consistent with the EUVI observations, the decrease in measured latitude concurrent with increasing height was observed in the coronagraphs for both the prominence and the CME. The change in latitude of the leading edge is because of the non-radial motion of the CME. The change in latitude of the prominence is a manifestation of the early phase of roll effect in the lower corona wherein the top of the prominence bends.

This work is done in collaboration with Olga Panasenco and Sara F. Martin, Helio Research, USA.

(Nandita Srivastava and Anand D. Joshi)

Estimation of arrival time of Coronal Mass Ejections at the Earth based on observations from STEREO

A number of CMEs that were observed by COR 1 & 2 coronagraphs on both the spacecraft and that also arrived at the earth were selected for this study. Applying different stereoscopic techniques to the leading edge of the observed CMEs by COR coronagraphs, the true speed and true direction of propagation were estimated. Assuming that the CMEs propagate in a self similar way i.e. its radius expand spherically with a velocity V_{exp} and its center propagate radially away from the Sun with V_{cent}, one can estimate the mean travel speed in the direction of the earth as given by

$$V_{tt} = V_{cent} \cos\alpha + \sqrt{(V_{exp}^2 - V_{cent}^2 \sin^2\alpha)}$$

where α is the propagation latitude angle or the angle between the propagation direction of the CME and the STEREO mission plane. The calculation of V_{tt} requires the estimation of reconstructed speeds of the CMEs which is determined from application of tie-pointing techniques to the CME leading edge in simultaneously recorded images by STEREO A & B and the expansion speeds can be estimated from single spacecraft images. From an analysis of six geo-effective CMEs, we find that the estimation of their arrival time significantly improves using STEREO images which lies within ± 6 hours of the actual arrival times at the earth. This is a significant improvement as compared to ± 24 hours uncertainty estimated from projected plane-of sky speeds obtained from CME observations by single spacecraft.

This work is done in collaboration with M. Mierla and L. Rodriguez of the Royal Observatory of Belgium.

(Nandita Srivastava)

Analysis of peculiar penumbral flows in the NOAA active region 10930 during a major solar flare

During the solar minimum phase between activity cycles 23 and 24, a complex active region NOAA 10930 gave rise to a major flare (of class X3.4) on 13 December 2006 during its passage on the solar disk. The photospheric observations taken in Ca II H and G-band by Solar Optical Telescope (SOT) on board *Hinode* satellite have shown elongated flare ribbons which separate apart with the progress of the flare. The hard X-ray (HXR) images obtained by *RHESSI* satellite show double-footpoint HXR sources located on the flare ribbons. There are also reports on the lateral motion of penumbral filaments in this active region during the flare. Motivated by the aforementioned examples, we have analyzed the velocity flows in different parts of this active region (AR) during the flare using the Dopplergrams obtained by the GONG telescope. We observe peculiar evolution of velocity flows in some localized portions of the penumbra of this AR during the flare. The aforementioned localized penumbral parts are observed to be located on the flare ribbon. Application of Wavelet and Fourier transforms to these flare induced penumbral velocity flows show strong high-frequency oscillations during the flare. We also plan to study the flare induced changes in the global velocity oscillations of the Sun as observed with GOLF instrument on board *SOHO* satellite in order to understand the epochs of local high-frequency enhancements and the global high-frequency enhancements.

This work is being done in collaboration with Savita Mathur of High Altitude Observatory, Boulder, USA, and R. A. Garcia of Laboratoire AIM, CEA/DSM-CNRS, Universite Paris, IRFU/SAp, Centre de Saclay, Gif-sur-Yvette, France.

(Brajesh Kumar, P. Venkatakrishnan, and Sanjiv Kumar Tiwari)

Three-dimensional Reconstruction of Solar Features using STEREO

The Solar TErrestrial RElations Observatory (STEREO) consists of two spacecraft orbiting the Sun ahead of (A) and behind (B) the Earth. The twin spacecraft provide simultaneous observations of the Sun from different angles. The Sun Earth Connection Coronal and Heliospheric Investigation (SECCHI) suite of instruments observe various transient events right from the solar chromosphere up to about 1 AU. This allows us to carry out stereoscopy, i.e. obtain 3-dimensional information of these transients as against the plane-of-sky information that can be obtained from a single spacecraft. We applied the reconstruction technique to a case each of an erupting filament on the disc observed in EUVI 304 Å on 2007 May 19 and a coronal mass ejection (CME) observed in COR1 on 2007 Jun 05. To validate the technique, we compared it with previously published results, and another well-established technique based on tie-pointing method, and found that they are in good agreement.

(Anand D. Joshi and Nandita Srivastava)

Global Twist of Sunspot Magnetic Fields Obtained from High Resolution Vector Magnetograms:

The presence of fine structures in the sunspot vector magnetic fields has been confirmed from Hinode as well as other earlier observations. We studied 43 sunspots and found fine structures in the vertical currents and force-free parameter alpha of each sunspot. They are distributed in positive and negative patches in the umbra, while they appear as alternately positive and negative filaments in the penumbra. We associate these filamentary patterns in the penumbra with the inclination variations along the azimuthal direction. However, we also find that these high amplitude variations in alpha in the penumbra have negligible contribution to global alpha value of the sunspots (Figure-19). Our results are based on the data sets taken from ASP/DLSP and Hinode spectro-polarimeters (SOT/SP). In this paper, (i) We introduce the concept of signed shear angle (SSA) for sunspots and establish its importance for non force-free fields. (ii) We find that the sign of global alpha is well correlated with the global SSA and the photospheric chirality of sunspots. (iii) Local alpha patches of opposite signs are present in the umbra of each sunspot. The amplitude of the spatial variation of the local alpha in the umbra is typically of the order of the global alpha of the sunspot. (iv) We find that the sunspots have filamentary structures and local opposite alpha values are present side

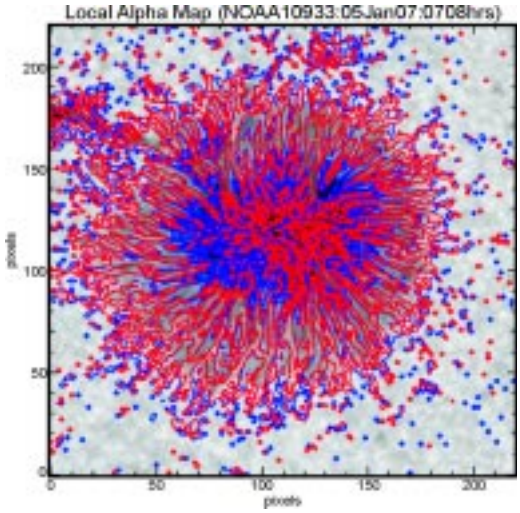

Fig.19. One examples of local a distribution observed in Hinode (SOT/SP) data. Background is the continuum image. Red and blue contours represent positive and negative values of alpha respectively. The contour levels are $\pm 1x10^{-8}m^{-1}$, $\pm 5x10^{-8}m^{-1}$, $\pm 10x10^{-8}m^{-1}$.

by side in the penumbra. The amplitude of azimuthal variation of the local alpha in the penumbra is approximately an order of magnitude larger than that in the umbra. The contributions of the local positive and negative currents and alpha in the penumbra cancel each other giving almost no contribution for the global values of current as well as alpha of the whole sunspot. (v) Arc-like structures (partial rings) with a sign opposite to that of the dominant sign of vertical current and alpha of the umbral region is seen at the umbral-penumbral boundaries of some sunspots. (vi) Most of the sunspots which we studied, belong to the minimum epoch of the 23rd solar cycle and do not follow the so-called hemispheric helicity rule.

This work has been done in the collaboration with Dr. K. Sankarasubramanian of ISAC/ISRO, Bangalore.

(Sanjiv Kumar Tiwari and P. Venkatakrishnan)

Choice of Shack-Hartmann wavefront sensor for optimum performance of Adaptive Optics system at Udaipur Solar Observatory

A prototype low-order AO system is being designed at the Udaipur Solar Observatory on a 15 cm Coudé telescope that utilizes a Shack-Hartmann lenslet array, along with a high speed camera (955 fps), as the wavefront sensor. The optimum number of lenslets for sensing the wavefront is decided by the diameter of the telescope and the seeing conditions prevalent over the site. The performance of such an AO system is evaluated through simulations for different

geometries and sizes of the lenslets. The simulations were carried out for four lenslet configurations, namely Sq(340), Sq(460), Hx(360) and Hx(520). 'Sq' and 'Hx' imply square and hexagonal lenslets respectively; while the numbers in parentheses indicate the lenslet pitch in μm (Figure 20).

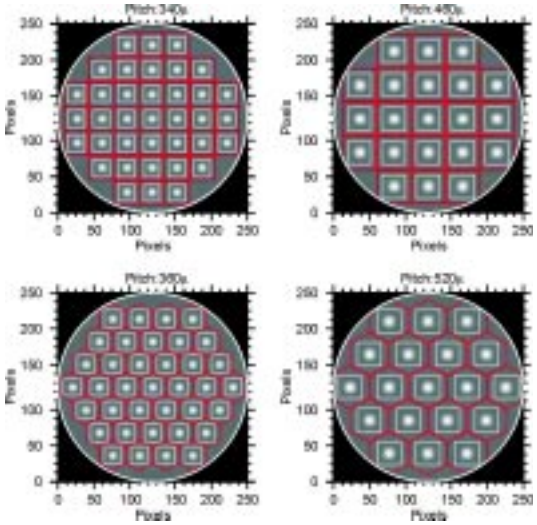

Fig. 20. Lenslet Configurations considered for the simulations. The top and bottom set of panels depict square and hexagonal LAs respectively. The grey area represents the pupil, while the sub-apertures are shown in red. The white boxes denote the central region from which the shift is estimated. The point source has been shown in negative for clarity.

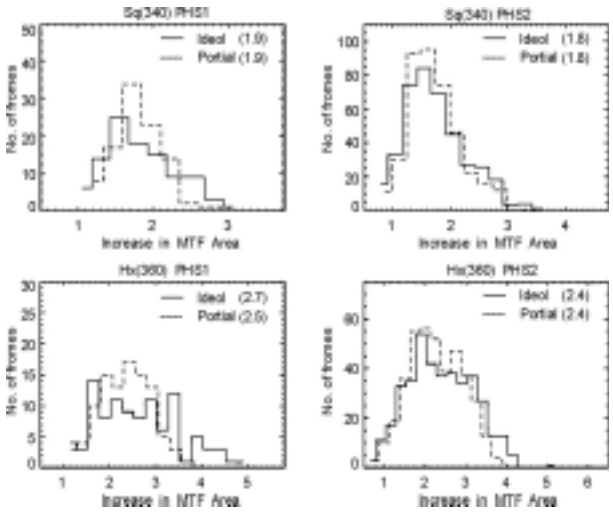

Fig.21. Histogram of the fractional increase in the azimuthally averaged MTF area for ideal (solid) as well as partial (dashed) AO compensation for phase screens PHS1 and PHS2 which correspond to an r_o of 3 cm and 5 cm respectively. Top Panels: AO correction for PHS1 and PHS2 using Sq(340). Bottom Panels: Same as above but for Hx(360). The numbers in the parentheses denote median values of the histogram. The bin size is 0.25.

The effectiveness of the lenslets was tested using 1000 random wavefronts generated from the first 20 Zernike terms. The lenslets Sq(340) and Hx(360) prove to be far more effective than the others in retrieving the random wavefronts. These lenslets were used to sense phase fluctuations derived from a Kolmogorov spectrum which mimic seeing conditions similar to that at Udaipur. It is observed that, the azimuthally averaged MTF area increases by a factor of 2.5; if the re-imaged telescope pupil is sampled with 37 lenslets having a hexagonal geometry (Figure 21).

(Rohan E. Louis, A. Raja Bayanna, Shibu K. Mathew and P. Venkatakrishnan)

Membrane based Deformable Mirror: Intrinsic aberrations and alignment issues

The Deformable Mirror (DM) is an important component of an Adaptive Optics (AO) system. A 37 channel Micro Machined Deformable Mirror (MMDM) is being used at the Udaipur Solar Observatory. It is known that an on-axis spherical/parabolic optical component, placed at an angle to the incident beam introduces defocus as well as astigmatism in the image plane. Although the former can be compensated by changing the focal plane position, the latter cannot be removed by mere optical re-alignment. Since the DM is also being used to compensate a turbulence-induced curvature term in addition to other aberrations, it is necessary to determine the aberrations induced by such (curved DM surface) an optical element when placed at an angle in the optical path. To this effect, we estimate to a first order, the aberrations caused by placing the DM at several angles of incidence and recording the subsequent images using a simple optical setup. It is observed that astigmatism is a dominant aberration which is determined by measuring the difference between the tangential and sagital focal planes. For very small angles of incidence this difference nearly remains a constant irrespective of the curvature of the mirror which is modified by applying the same voltage to all actuators. For large angles of incidence the difference increases with increase in voltage and subsequently the change in curvature (refer Figure 22).

Simulations of the above experiment were carried out using ZEMAX™, which also factored in the presence as well as absence of an intrinsic astigmatism in the DM. The simulation results are in agreement with the recorded images and we conclude that, by placing the DM at an angle of incidence of 10°, the induced astigmatism is insignificant

in comparison to the intrinsic astigmatism which can be compensated by a suitable set of voltages. This also facilitates biasing the DM surface to allow corrections in either direction.

(A.Raja Bayanna, Rohan E. Louis, S.K. Mathew and P. Venkatakrishnan)

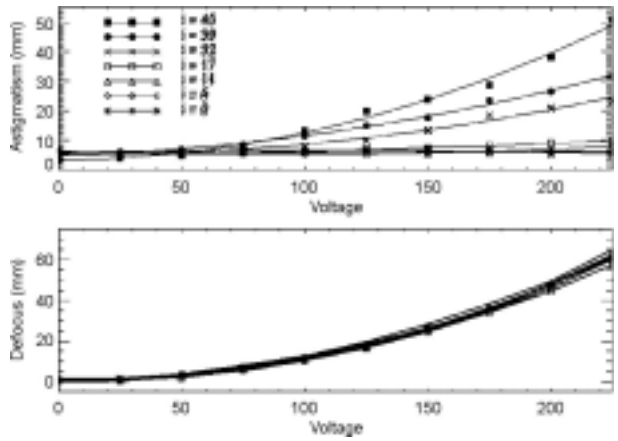

Fig.22. Top panel shows astigmatism with increase in radius of curvature for different angles of incidence. Bottom panels show the change in focal plane (circle of least confusion) with the increase in radius of curvature.

Issues with External Occultation of a Coronagraph

We addressed the issues related to externally occulted solar coronagraph; vignetting and achievable resolution due to an external occulter. The analytical expression by J.W.Evans is used to perform the initial calculations.

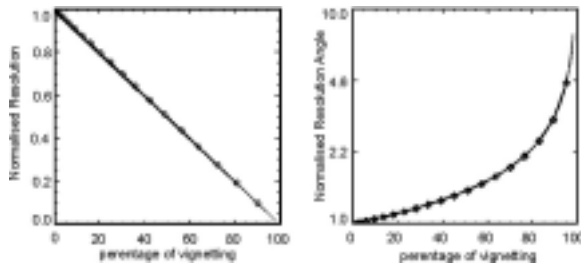

Fig. 23: Vignetting due to external occulter with varying boom length. Different curves from right to left are for boom lengths 10m, 30m, 50m, and 100m respectively. Data points shown in diamond are from the theoretical relation; where as the solid lines are from ZEMAX

An expression for the vignetting due to a given external occulter and for a given field angle is derived; the values obtained with the derived expression is verified with that of the values obtained from ZEMAX an Optical design software; values obtained from the relation and with the ZEMAX are in good agreement with each other(Figure 23). The degradation in angular resolution of the system due to vignetting is also presented; Telescope apertures with varied amount of vignetting are simulated and considered them as the effective aperture for different field angles and the resolution (volume under transfer function) of each effective aperture is calculated. An empirical relation to calculate the normalised resolution for a given amount of vignetting is derived (Figure 24).

This work is in collaboration with Dr K. Sankarasubramanian of ISAC and Profs J. Singh and B.R. Prasad of IIA.

(A. Raja Bayanna, Shibu, K. Mathew , and P. Venkatakrishnan)

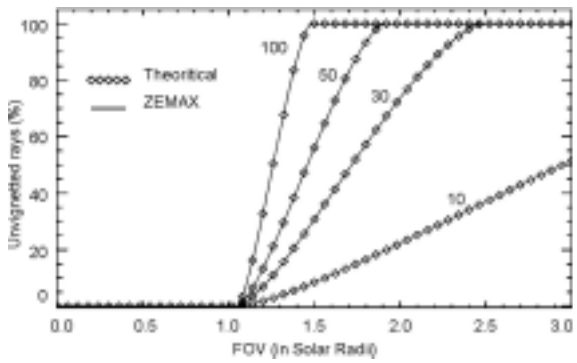

Fig.24: The degradation in the normalised resolution with respect to percentage of vignetting. As vignetting increases resolution decreases.

On the flare induced high-frequency global waves in the Sun

Recent research reports showed evidence of strong correlation between the energy in the high-frequency part ($5.3 < \nu < 8.3$ mHz) of the disk-integrated intensity observations of the Sun obtained from the VIRGO (Variability of solar IRradiance and Gravity Oscillations) instrument on board *SOHO* (Solar and Heliospheric Observatory) spacecraft and the solar X-ray flux. Similar signature of flares in velocity observations has not been confirmed till now. In this work, we analyzed the velocity observations of the Sun obtained from the MDI (Michelson and Doppler Imager) and the GOLF (Global Oscillations at Low Frequencies) instruments on board *SOHO* for some major flare events of the solar cycle 23. Application of wavelet techniques to the time series of disk-integrated velocity signals from the solar surface using the full-disk Dopplergrams obtained from the MDI clearly indicates that there is enhancement of high-frequency global waves in

the Sun during the flares with respect to quiet (non-flaring) condition. This signature of flares is also visible in the Fourier Power Spectrum of these velocity oscillations. On the other hand, the analysis of disk-integrated velocity observations obtained from the GOLF shows only marginal evidence of effects of flares on high-frequency oscillations. This work has been done in collaboration with Savita Mathur of Indian Institute of Astrophysics, Bangalore, and R. A. Garcia of Laboratoire AIM, CEA/DSM-CNRS, Universite Paris, IRFU/SAp, Centre de Saclay, Gif-sur-Yvette, France.

(Brajesh Kumar and P. Venkatakrishnan)

Planetary Sciences and PLANEX Program

The most significant result during the last one year is the spectacular discovery of water molecule and hydroxyl ion on the lunar surface, and water ice in the permanently shodowed polar regions, using Chandrayaan-1 payload data. The focus of the activities in the Planetary Sciences Division and the PLANEX program, during the year, are centered around investigations on meteorites to understand solar system processes, analysis of data from Chandrayaan-1 payloads to understand lunar surface features and surface processes and development of laboratory prototypes of instruments for planetary exploration. During the year we have spent considerable efforts in the installation and standardisation of the three newly acquired analytical tools. In this report, we provide a glimpse of these activities under three heads, Planetary Science and new analytical facilities, Chandrayaan-1 data analysis and Planetary Exploration.

Cosmic ray exposure age and trapped gases in Almahata Sitta ureilite, a fragment of asteroid 2008 TC_3

Ureilites are the second largest group of achondrites in our collection, although the number of observed falls is only 7. Almahata Sitta (hereafter AS) is the most recently fallen ureilite, the least weathered in our collection, and is classified as an anomalous polymict ureilite, rich in pores (> 20%) and carbonaceous matter. It is the first meteorite to be associated with a known small asteroid of size ~4 m, called 2008 TC_3 (class F), predicted and observed to hit the earth on Oct. 7, 2008 in the Nubian Desert of Sudan. AS has been studied for trapped N and noble gases to understand the nature of this anomalous polymict ureilite, as a part of international consortium. A bulk sample and an acid resistant residue have been analysed for noble gases and nitrogen by step-wise combustion/pyrolysis. Cosmic ray exposure ages of 13.8 and 16.0 Ma are calculated based on ^{3}He and ^{21}Ne respectively. Survival of a 4m object with high porosity, for ~15 Ma in the

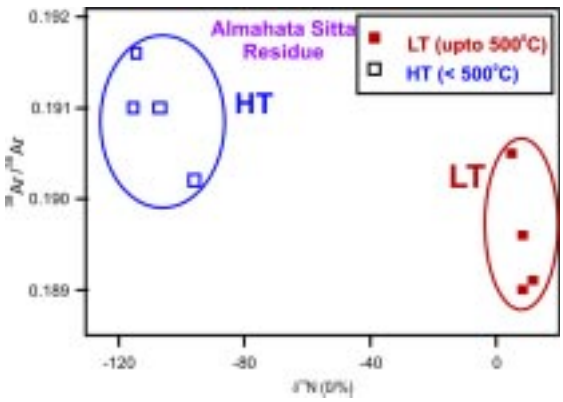

Fig. 25: $^{38}Ar/^{36}Ar$ vs. $\delta^{15}N$ for the individual temperature steps of AS residue. The low temperature (LT) and high temperature (HT) data cluster into two fields, indicating the presence of two different components.

interplanetary space is the surprise finding and has implications for meteorite transport to inner solar system. Ar, Kr and Xe in both the bulk and residue are dominated by a trapped component, but the elemental ratios are different. While the ratios of $^{36}Ar/^{132}Xe$ and $^{84}Kr/^{132}Xe$ are about 400 and 1, respectively, in all the combustion steps of the residue, the bulk sample has about an order of magnitude more ^{132}Xe in the corresponding combustion steps. It seems, an acid soluble phase is the host of this Xe-rich carrier. Nitrogen in the bulk sample and acid residue are 21.1 ppm (-36.8‰), and 249.5 ppm (-74.3‰), respectively. Peak release of C (monitored as CO + CO_2), N, Ar, Kr and Xe occurred at the 700°C combustion step of the residue, confirming diamond as the principal carrier for these gases. The most important finding is a monotonic increase of the isotopic ratio $^{38}Ar/^{36}Ar$ in the residue, with release temperature. The combined behaviour of N and Ar isotopic components in the low temperature (LT) and high temperature (HT) fractions suggest the occurance of two trapped Ar components in AS (Figure 25), the first such finding in ureilites.

(S.V.S. Murty and R.R. Mahajan)

Indian Meteorite studies

Recent Indian meteorite fall Karimati has been studied for chemical, petrological and isotopic composition. Karimati fell in Kanpur district, UP on May 28, 2009. It was immediately collected by Dr. Verma of IIT, Kanpur, and sent to PRL for further study. Chemical, mineralogical and petrological studies classify it as belonging to L Chondrite (Fa = 24.8, in olivine and Fs = 20.6 in low Ca pyroxene). Oxygen isotopic composition (measured at UCSD by Dr. Subrata Chakrabarty) further confirmed this classification ($\Delta^{17}O$ = 1.2 ‰). Trapped and cosmogenic noble gases suggest the metamorphic grade to be 5/6, and give a cosmic ray exposure age of 15 Ma.

(S.V.S. Murty, R.R. Mahajan and D. Panda)

Platinum Group Elements (PGEs) in Meteorites by ICP-MS

The platinum-group elements (PGEs) comprise a group of six rare metals – Os, Ir, Ru, Rh, Pt and Pd with similar physical and chemical properties. All six PGEs are distinguished by their refractory nature (except for Pd) and siderophile character. In a cooling solar nebula, five of the six platinum-group elements condense as refractory-metal alloys at temperatures above the condensation of Fe–Ni metal. Non-refractory Pd condenses in solid solution with Fe–Ni. The changes in relative distribution of PGEs in the metal phase reflect its formation environment in the nebula and/or the metal silicate fractionation process in the parent body. In the PLANEX Program at PRL, we have initiated the measurement of PGEs by ICP-MS, with the aim of applications in meteorite studies and planetary processes. We have worked out procedures to analyse about ~ 1 mg sample of a bulk chondrite and iron meteorite. The samples were prepared by conventional acid digestion procedures. Measurements were made using a Thermo X-Series II Quadrupole ICP-MS. The PGEs along with some other siderophile elements were analysed in about a dozen chondritic, iron and ureilite meteorites. The reproducibility and precision have been demonstrated by analysing 5 aliquots of (~ 1 mg each) Allende standard (Figure 26) as well as the cuttings of an iron meteorite. We plan to use this technique for analysing individual chondrules splits and metal phases in primitive meteorites.

(N.K. Agrawal, K. Durga Prasad, Suruchi Goel and S.V.S. Murty)

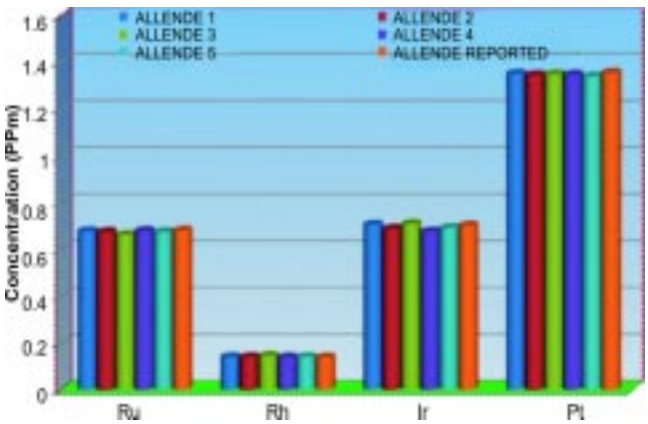

Fig. 26: Results of 5 Allende standard samples for the four PGEs Ru, Rh, Ir and Pt have been compared with reported values from literature, to demonstrate reproducibility and precision.

Mineralogical and petrological classification of CAIs

Calcium Aluminum Inclusions (CAIs) are the high temperature mineral condensates found in the primitive chondritic meteorites with size range from sub mm to few cm and with spheroidal to irregular shape. They are considered to be first forming solids in the solar system with a reported age of 4567 ± 0.6 Ma. Short lived radionuclides incorporated in CAIs during their formation, act as fine scale chronometers providing information regarding the formation and evolution of the early solar system. If the short-lived nuclides were injected into the

protosolar molecular cloud from a stellar source, their presence in early solar system solids puts a very stringent constraint on the time interval between the production of these nuclides in the stellar source and the formation of the early solar system solids. On the other hand, if the short-lived nuclides are products of solar energetic particle interactions with material in the solar nebula, provides us specific information about the energetic environment in the early solar system.

In order to identify the exact source of the short-lived nuclides present in the early solar system and to study the sequence of the early solar system processes, we have initiated study of multiple short-lived nuclides such as ^{26}Al, ^{10}Be, ^{7}Be, ^{36}Cl on individual CAIs from primitive meteorites of CV3 group. First step in this process is identification and classification of primitive CAIs and search of different phases available for short lived nuclide analyses.

An EPMA (Electron Probe Micro Analyzer) analysis including BSE (Backscattered electron) imaging and WDS (Wavelength dispersive x-ray spectrum) have been carried out on various probable CAIs [Allende (23), Bali (1)]. Classification according to their mineral composition scheme indicates, out of twenty three Allende CAIs, nine are of type B CAI (melilite ~ 5- 20%, anorthite ~ 20 - 45%) and rest are fine grained olivine and pyroxene aggregates. Sub-classification of nine identified Allende CAIs indicate five of them belong to type B1 with melilite rich mantle and well defined rim pattern and rest four fall in type B2 CAI (no rim) pattern. CAI from Bali has been classified as type B CAI.

(Y. Kadlag, K. K. Marhas and D. Panda)

Search for Presolar silicates

Presolar grains condense around different types of stars. Hence, isotopic study of presolar grains leads to understanding of nucleosynthesis taking place in individual parent stellar sources. Apart from this, abundance of presolar grains in primitive meteorite gives clue to the survival of these grains into the early solar system. With technical advancement of ion probe, in-situ search of presolar grains in thin/thick sections of meteorites has been possible. It's nearly impossible to separate presolar silicates by chemical separation procedure due to large amount of silicate material that meteorite is made up of and also because average size of presolar silicates is quite small (~ 200-300nm) to be detected by conventional ion probe. In this case, insitu search by nanoSIMS (nano Secondary Ion Mass Spectrometer) having a high spatial resolution of 50nm is a boon.

In-situ search of presolar grains from meteorites includes (a) Selection of primitive meteorites rich in presolar grains, (b) Preparation of meteorite thick sections, (c) Calculating percentage matrix using backscattered electron (BSE) images of the sample surface (d) nanoSIMS image analysis for oxygen isotopes to identify presolar silicates.

Five meteorites (Cold Bokkeveld, Mighei, Murray, Nogoya, Orguiel) rich in presolar grains based on their earlier noble gas isotopic composition and carbon content on bulk samples have been chosen for this study. Various back scattered electron probe images taken at a resolution of ~ 300X for each of the thick sections from five meteorites were used to make complete mosaic of the sections. Freeware 'ImageJ' used for matrix area calculation indicates, the chosen Orguiel section has highest percentage (~ 97%) of matrix area whereas rest four of the meteorite sections have matrix of around 70%. This matrix area will be raster analyzed in nanoSIMS in order to search for presolar silicates, if any.

(K. K. Marhas)

Simulation of solar wind implantation in enstatite grains

Ion implantation has played a very vital role in the delivery of volatile gases to meteorites and hence to precursors of terrestrial planets. Significant isotopic variations have been observed between the surface sited noble gases and they are also quite different from the volume sited trapped noble gases. These isotopic variations could be i) source related during the ionization and/or acceleration processes in solar photosphere ii) a mixture of different isotopic components *e.g.*, SW and SEP or iii) implantation artifact or iv) result of latter processing such as fractionation during surface erosion. In order to identify the exact cause of these isotopic variations, an ion implantation simulation study has been initiated. In this study we implanted one million ions of noble gases with random distribution of energy between 5-100 KeV in spherical enstatite grains of various sizes using SRIM (Stopping Range of Ions in Matter) Code.

Each ion starts from the surface of the spherical grain with random cosine angle *i.e.*, equal probability that 50% ions move inside/outside the grains. Each grain, is divided into a number of spherical shells of finite thickness and total number of ions in each spherical grain have been counted. Further we calculated depth variation of isotopic and elemental ratios and overall effect of surface erosion on

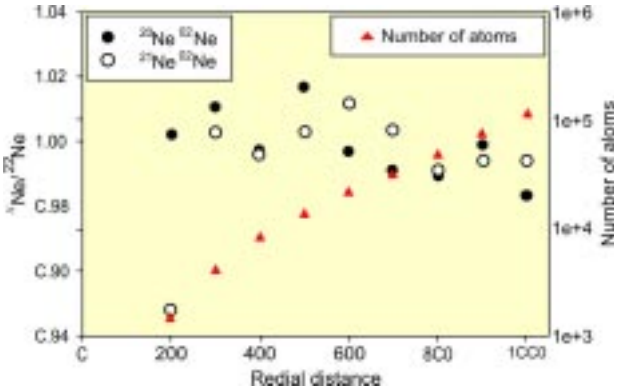

Fig. 27. The resultant atom density and isotopic ratios, as a function of depth due to implantation of Ne in a spherical grain of 0.1 µm size is shown, based on SRIM Code calculations

these ratios. We have observed significant isotopic and elemental fractionation with depth in the grain due to implantation. Figure 27 shows the variations in the number of atoms as well as isotopic ratios as a function of depth, in the grain. These results will aid in the understanding of surface gardening on small asteroids.

(Vinai K. Rai and S.V.S. Murty)

Co-injection of now-extinct short-lived nuclides into solar nebula

We have earlier demonstrated that the two now-extinct short-lived nuclides (SLNs), ^{26}Al and ^{60}Fe, present in the early solar system were co-injected from a single stellar source and a high mass supernova (SN) is the most likely candidate. We have considered nucleosynthetic yields of various SLNs (^{26}Al, ^{41}Ca, ^{60}Fe, ^{53}Mn, ^{107}Pd and ^{182}Hf) from SN of various masses to infer if all these nuclides were co-injected into the solar nebula from a single source. Based on published yields of these nulcides as well as their stable counterparts (^{27}Al, ^{40}Ca, ^{56}Fe, ^{55}Mn, ^{108}Pd and ^{180}Hf) from a 25 solar mass supernova, we have obtained the ratio of predicted to inferred solar system initial values, based on meteorite data, for a set of SLNs considering different injection mass cut and specific values of dilution factor, providing the mass fraction of injected material compared to that of the pre-existing solar nebula and suitable free decay time intervals. Results from one such calculation is shown in Figure 28. A reasonable fit is seen for most of the nuclides, except for ^{53}Mn, if we consider an injection mass cut at ~ 7.5 solar mass, a region from which freshly synthesized nuclides are not ejected due to fall back of material following SN explosion.

(R. K. Mishra and J. N. Goswami)

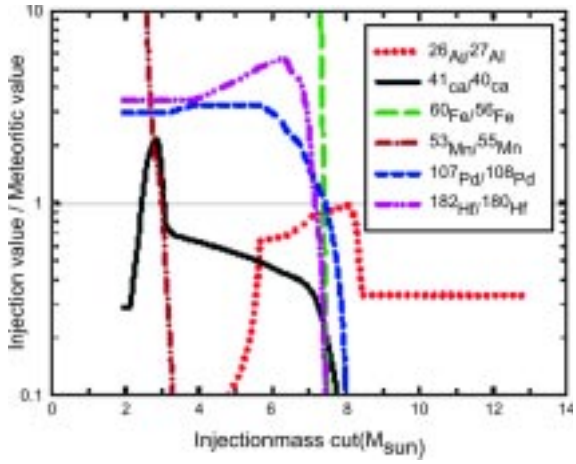

Fig.28: Expected solar system initial abundances for a set of SLNs, relative to their stable counterparts, based on published model yields from a 25 solar mass supernova, normalized to their inferred initial abundances based on meteorite data.

NEW FACILITIES

Thermo Neptune Multi-Collector Inductively Coupled Plasma Mass Spectrometer (MC-ICP-MS)

Owing to very high ionization efficiency of its plasma source, MC-ICP-MS is becoming a very powerful mass spectrometer, more specifically, for high precision study of non conventional isotopes which are difficult task with other mass spectrometers. MC-ICP-MS has been installed during December 2009 in PRL by engineers from Thermo Scientific (the instrument is shown in Figure 29). During installation, the machine was assembled and measurements were performed on NIST standards of several elements. All the measurements on standards are accurate and well within specified uncertainty.

Fig. 29. The newly installed MC-ICP-MS at PRL

In Figure 30, lead isotopic measurement on NBS SRM 981 is compared with measurements from other laboratories. After installation, Desolvating Nebulizer and Autosampler

were installed for higher sensitivity and high throughput respectively. Measurement protocols have been optimized for several elements e.g., Sr, Nd, Pb, Al, Mg, Fe, S, Ni, Mo, Si, Hg, Hf etc. We soon plan to start measurements on meteorite and planetary samples.

(Vinai K Rai and Reshmi Das)

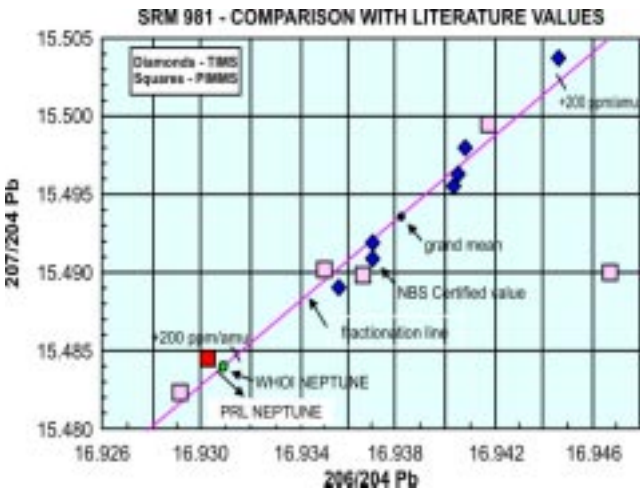

Fig. 30:A comparison of measurements on NBS SRM981 by Thermo Neptune HR-MC-ICP-MS at PRL with literature values, measured with both TIMS and Neptune. All data are aligned closely along a fractionation line with ~480 ppm/amu spread along the fractionation line.

Ne and Ar isotopic analysis by a multicollector noble gas mass spectrometer

Precise isotopic measurements of Ne and Ar are very important in the identification of minute changes that result from specific physical or nuclear processes. Cosmic ray produced ^{21}Ne in the surface rocks on Earth, nucleogenic ^{21}Ne in U, Th rich minerals, ^{36}Ar production through ^{35}Cl $(n,\gamma)^{36}$Cl$(\beta^-)^{36}$Ar, in salt deposits, Ar isotopes of trapped air in ice cores as climate markers, determination of the primordial abundance of the isotope ^{40}Ar etc. have great potential in serving as chronological tools as well as tracers to decipher physical processes in the past. Compared to the usual peak jumping techniques employed by a single collector mass spectrometer, a multi-collector mass spectrometer provides an advantage for achieving higher precision, in terms of reduced analysis time and consequently the memory effects, particularly when dealing with small gas amounts. In the PLANEX Program at PRL, we have recently procured a multi collector noble gas mass spectrometer, NOBLESSE from Nu Instruments, UK (see Figure 31). This mass spectrometer has 75° magnetic sector and modified Nier-type Ion Source. It has four fixed detectors; one Faraday and three Ion counting electron multipliers. The Faraday cup and one multiplier are behind a slit and an electrostatic deflector is used to send ion beam into one or other of the pair. Hence the three collectors (Faraday or Multiplier, and the other two multipliers) are used for multi-collection. The multi-collection is achieved by patented method of two lens arrays (called as Quad lenses, since they provide a field equivalent to an electrostatic quadrupole) placed between magnet exit pole and collectors. This beam dispersion to achieve simultaneous focus of the three isotopes on to three detectors by the quad lenses offers an advantage over mechanical adjustment of detector spacing that often results in spurts of degassing and increased background.

Fig. 31: Multi-collector noble gas mass spectrometer, recently installed at Thaltej, PRL.

At the optimium tuning, Ar sensitivity is about 1.1 A/bar at 400 µA trap current and $10^{11}\Omega$ resistor on the Faraday. We have analyzed a number of air standards of different amounts for Ne and Ar, by both peak jumping and multi collection. An excess of about $3x10^6$ atoms of ^{21}Ne can be detected with the system.

(Suruchi Goel, R.R. Mahajan and S.V.S. Murty)

Analyses of data from Chandarayaan – 1 payloads

Chandrayaan – 1, India's first Moon Mission carried three optical imaging payloads onboard. These include indigenous payloads HySI (Hyper spectral Imager) and TMC (Terrain Mapping Camera) built at SAC and Moon Mineral Mapper (M^3) from NASA. Of these, the stereo camera TMC (Spatial resolution: 5 m) is meant for topographic studies, whereas, the imaging spectrometers HySI and M3 provide compositional dependent spectral information at a very high spatial and spectral resolution (80 m and 15 nm in case of HySI, 140 m and 20 nm in case of M^3). Some results obtained from the data returned by these payloads are as under.

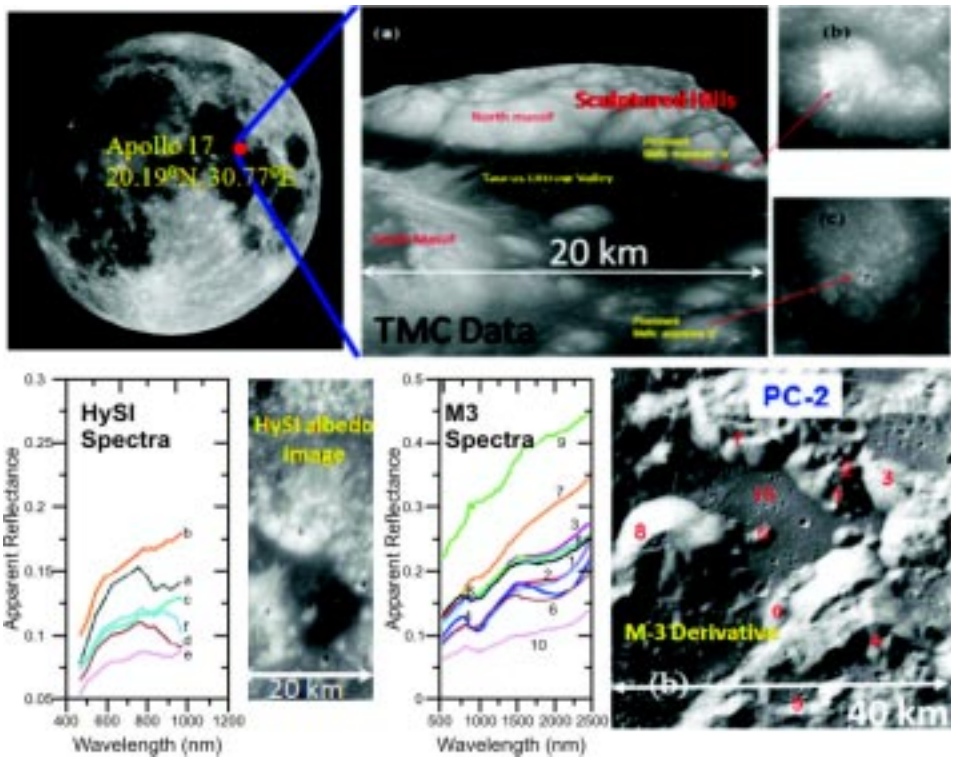

Fig.32:A mosaic showing location of Taurus-Littrow valley on moon, TMC image of the region draped over the derived DEM, showing some of the conspicuous mafic anomalies in the zoomed view, HySI albedo image and M^3 derivative (Principal Component- 3) of the region showing locations of the high altitude mafic anomalies and their corresponding reflectance spectra. Locations (10) in the M^3 image and (e) in HySI image correspond to valley floor.

a) TiO_2 Estimation and Geology of Moscoviense region from HySI data:

Spectral effects of TiO_2 on the UVVIS slope have been traditionally used to derive titanium content on Moon from reflectance data. Standard algorithm of Lucey and Co-workers, specifically meant for TiO_2 derivation from Clementine datasets has been calibrated to enable TiO_2 estimation from HySI data. Suitable spectral bands from HySI data of Moscoviense region (27.3° N, 147.9° E) on Moon have been selected for this purpose and correlations have been derived with Clementine 415 nm and 750 nm data. Resultant titanium maps have a spatial resolution of 80 meters compared to the previous best of 200 meters from Clementine data.

Further, spectral response curves of fresh craters and soils and litho-stratigraphic study of the region using superposition of craters on titanium maps have revealed greater geologic diversity in the central portion of the Moscoviense basin compared to the western edge and increase in TiO_2 content in subsequent data flows. Also, several fresh craters exhibiting high albedo and prominent mafic absorption beyond 750 nm have been spotted along the basin margins. These may be exposures of noritic lower lunar crust, pyroclastics or ancient very low titanium basalts.

(Neeraj Srivastava)

b) Integrated Study of Apollo 17 region using TMC, HySI and M^3 data:

Compositional and Topographic study of high altitude locations within Sculptured hills and Massifs surrounding Taurus-Littrow valley (Apollo 17 site) have revealed presence of numerous mafic anomalies on them (Figure 32), consistent with earlier findings from Clementine data. Further, they have been found to be morphologically

different from each other and compositionally most of them (seven out of nine) are Noritic, representing exposures of primary crustal rocks. Only one exposure (location 4, in Figure 32), located at the southwestern edge of the sculptured hill depicts distinct signature of basalt and the remaining one (location 9, in Figure 32) of crystalline plagioclase, characteristic of the primordial lunar crust. Thus, neither all the mafic anomalies are Noritic in nature as envisaged earlier based on spectral behavior of the

Clementine data nor all of them are basaltic as inferred on the basis of iron and titanium concentration, thus, revealing greater geologic complexity for the region.

(Neeraj Srivastava, J. N. Goswami, Members from SAC and M³ Team)

Discovery of Hydroxyl and Water on lunar surface

Analysis of data from the Moon Mineral Mapper (M^3) on board Chandrayaan-1 has led to the first detection of hydroxyl and water on lunar surface, a major discovery in the field of planetary sciences. M^3 is a reflectance spectrometer covering the range of wavelength from 0.4 to 3 micrometer. Distinct absorption feature near 2.8 to 3.0 micrometers has been detected when the instrument was collecting data at high latitude (> 60 degree) on either side of the lunar equator. This feature is widely seen and appears strongest at cooler high latitudes (Figure 33) and also at several fresh feldspathic craters. Our results coupled with the fact that the observed features, present in sunlit areas mapped by M^3, do not show any correlation with deep seated hydrogen abundance data inferred from neutron data in earlier Prospector mission suggest that the formation and retention of hydroxyl and water are ongoing surficial processes. We consider interactions of solar wind ions with lunar surface soils and rocks as the cause for the observed OH and H_2O on lunar surface. Our findings have been corroborated by later observations made by the Deep Impact mission and analysis of archival data obtained by this mission in 2007 and by Cassini mission in 1999.

(C. M. Pieters, J. N. Goswami, R. N. Clark et al.)

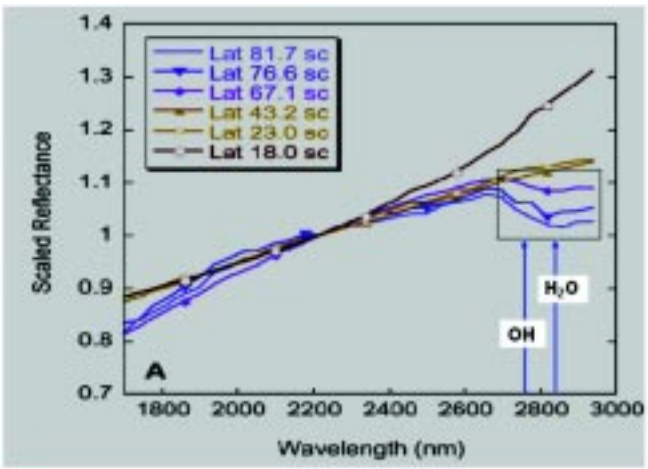

Fig.33: Reflectance spectra obtained by M^3. Strongest detection of the absorption feature near 2.8 to 3.0 micron occurs at cool higher latitudes that gradually decreases towards mid-latitudes.

PLANETARY EXPLORATION

With the experience gained from HEX payload for Chandrayaan-1, PLANEX has initiated efforts to design and build prototype payloads for orbiters and rovers of future planetary exploration missions of ISRO. Currently, three instruments and/or techniques are under development and are briefly described here.

Alpha Particle Induced X-ray Spectrometer (APIXS)

We are developing a low energy X-ray spectrometer for in situ measurement of planetary surfaces primarily focused for chandrayaan-2 rover. The working principle of this instrument is based on the irradiation of the sample surface with alpha particles and X-rays from a radioactive source (e.g. ^{244}Cm), and the measurement of characteristic X-rays emitted by sample atoms due to particle induced X-ray emission (PIXE) and X-rays florescence (XRF). In APIXS, production of characteristic X-rays due to PIXE are dominant for low Z elements and production of characteristic X-rays from high Z elements are primarily due to XRF. The APIXS technique is well suited for in situ measurements of composition of planetary surface from close proximity. Instruments similar to APIXS have been deployed in Rover for studying martian surface composition and this is the first time that such an instrument is being proposed for a lunar rover.

We have chosen to use Silicon Drift Detector (SDD) for APIXS due to its high resolution capability compared to other available detectors such as Si-PIN and CZT detectors. These detectors are available with in-built peltier coolers to provide operational temperatures around -30°C with energy resolution about 140 eV at 5.9 keV. These detectors also have space heritage.

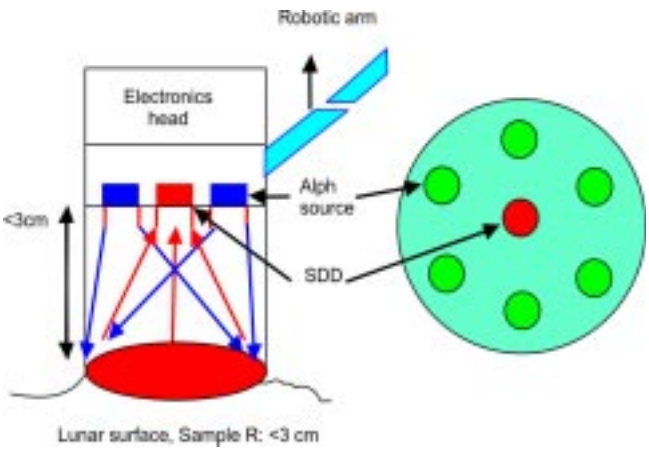

Fig. 34: Schematic of APIXS sensor head

APIXS instrument will have two packages namely APIXS sensor head and APIXS electronics package. APIXS sensor head contains a circular disc to hold 6 alpha sources and an X-ray detector (SDD) as shown in Figure 34. The alpha sources will be placed around a circular disc and the SDD will be placed at the centre of the disc. Sources and the detector are collimated such that they view same area of the lunar sample. SDD to be used in the experiment will have ~ 20 mm^2 active area with a covering of ~ 8 micron thick Be window to protect it from contamination. The distance between source/detector and the sample (lunar surface) will be less than 3cm.

APIXS electronics package will be part of rover electronics package and provides interface with the rover electronic sub-systems such as power, Data acquisition, Telecommand and Telemetry.

The estimated total mass required for APIXS instrumentation is ~ 2 Kg (instrument mass is ~ 1.2 kg and arm for instrument deployment is ~ 0.8 kg). The total power required is about 4W.

The development of electronic subsystems associated with the SDD based spectrometer has been initiated for laboratory testing. Subsystems such as shaping amplifier, peak detector, serial ADC and HV have been tested with SDD by cooling the detector at -25°C. The other subsystems preamplifier and peltier temperature controller are being tested and are being optimized for the performance. The engineering model of the proposed spectrometer with custom designed PCBs for electronic circuits is under development.

(M. Shanmugam, Y.B. Acharya and S.V.S. Murty)

Development of a $LaBr_3$:Ce Gamma Ray Spectrometer (GRS)

High energy (> 500 keV) gamma ray spectroscopy is an important technique for remote sensing studies of chemical composition of planetary surfaces, and has been used to study surface composition of the Moon, Mars and Asteroids at various spatial resolutions. In comparison to X-ray fluorescence spectrometry, compositional data from gamma spectrometry is more representative of the lunar sub-surface as gamma rays come from depths of a few centimetres to tens of centimetres whereas characteristic X-rays from major elements have a maximum interaction depth of the order of tens of microns.

We are developing a $LaBr_3$:Ce gamma ray spectrometer for future planetary orbiter mission, with the primary objective of determining the abundance and distribution of iron using the $^{56}Fe(n, \gamma)$ 7.631 and 7.646 MeV gamma lines.

We propose to use a phoswich detector consisting of a 3 inch diameter, 3 inch long $LaBr_3$:Ce crystal (available commercially as BriLanCe 380 from Saint Gobain crystals) optically coupled to a 1 inch thick BGO crystal, which surrounds the $LaBr_3$:Ce crystal. The front side of the LaBr3:Ce crystal is kept open, so that gamma photons from the source (planetary surface) can pass through without attenuation. Both detectors are optically coupled directly to a 5 inch diameter photomultiplier tube (Hamamatsu R877).

The output of the PMT will be fed into charge sensitive pre-amplifier, which converts the charge generated into a voltage pulse. The event registered in the $LaBr_3$:Ce is faster compared to BGO since the decay times of $LaBr_3$:Ce and BGO are 16 ns and 300 ns respectively. The use of pulse shape discrimination will provide information on which detector absorbed the radiation and results in substantially lower backgrounds. The outputs of the preamplifiers will be further shaped and amplified by a linear amplifier, and then processed by a single 12-bit analog to digital converter (ADC). These data will be sent to processing electronics for further processing with telemetry. The block diagram of the proposed spectrometer is shown in Figure 35 below.

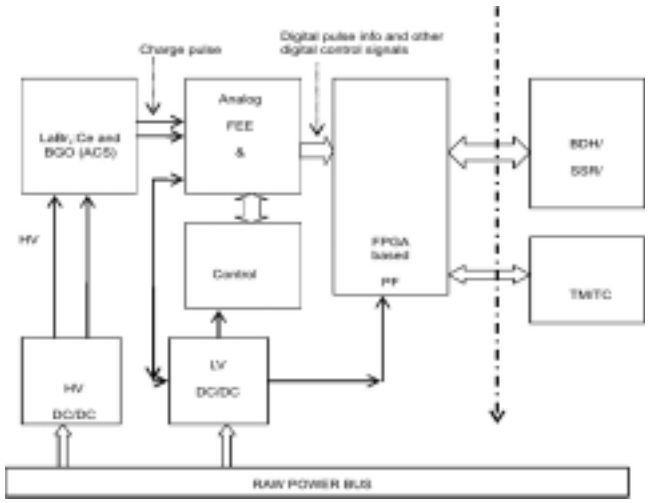

Fig. 35. Block diagram of the GRS under development

A 3 inch $LaBr_3$:Ce crystal was procured along with a 3.5 inch PMT and a preamplifier to check its suitability. We have checked the specifications of $LaBr_3$:Ce crystal using an pulse shaping amplifier, and an Ortec MCA card. Further amplification was provided by a pulse shaping amplifier whose coarse gain was set to 20 and fine gain to 0.5. The

pulse shaping time was set to 2 μs. Pulses with a pulse height between 0 and 10 V were recorded with a Ortec multi channel analyser. Pulse height spectra were measured with a ^{22}Na source. The energy resolution (FWHM) obtained at room temperature is ~ 3.5% at 511 keV, and ~ 2.2% at 1.274 MeV. Design and development of a flight worthy HV unit for PMT bias and a pulse shaping amplifier for the Front-end-electronics subsystem for GRS are in progress.

(Y. B. Acharya, D. Banerjee, S. K. Goyal and D. K. Panda)

Wireless Sensor Network for in-situ investigation of Lunar and Planetary Regoliths.

Wireless Sensor Network (WSN) is a novel technique for carrying out wide range of scientific investigations in large unfriendly planetary environments. A Wireless Sensor Network consists of a large number of tiny, battery-powered computing devices that are scattered through a physical environment to form an adhoc network with self organizing capability. WSN provides low-risk mission architecture for carrying out in-situ measurements. In PLANEX, we have initiated the development of WSN work to investigate thermal and electrical properties of lunar regolith and for detection of water. Our work involves the development of the required sensors and nodes, their demonstrartion in terrestrial environment, the communication aspects as well to demonstrate their operation in simulated lunar environment, as briefed here.

Design, Test and Verification of Custom Designed Sensor and Node

***Wireless Impedance Sensor*:** Wireless sensor network may use various types of sensors to characterize lunar Regolith and impedance sensor can be used to measure permittivity of the soil as one of the sensors. Its design was made and sensor chip was evaluated after its calibration.

Microcontroller and RF transceiver at 2.4 GHz were programmed to check wireless communication feasibility of the impedance sensor and it was demonstrated successfully in the laboratory. Development of compact wireless impedance sensor is underway Figure 36 shows plots of theoretical and measured (real and imaginary) impedances for a soil equivalent circuit and confirms that both theoretical and measured impedances match one to one throughout the measurement frequency range.

(Jayesh P. Pabari and Y. B. Acharya)

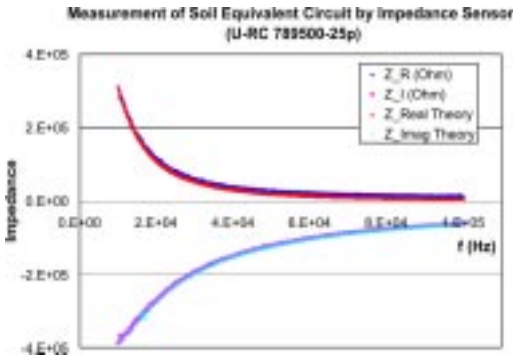

Fig. 36: Plot of Z_R (measured, blue), Z_I (measured, magenta), Z_Real (theory, yellow) and Z_Imag (theory, cyan) versus frequency showing evaluation of impedance sensor for a soil equivalent circuit.

PRL Designed Sensor Node: WSN targeted for lunar and planetary applications demands a highly optimised sensor node in terms of mass, size and power and must be rugged enough to withstand harsh environment, neccessiating custom development of sensor nodes. After careful evaluation of various platforms, sensor nodes using JENNIC wireless microcontroller have been custom-designed and developed for the purpose of testing and mock deployment. The custom node consists of a modular architecture with a processor and interface board. The processor board contains the Wireless Module while the interface board contains rest of the circuitry. This initial design (Figure 37) gives provision for using the same interface board with different modules while the final design is planned to be highly optimised with much smaller foot print. A number of self-powered stand-alone sensor nodes with varied characteristics capable of deployment in any region of our interest are designed. These nodes are self-powered using a Lithium Thionyl Chloride ($LiSOCl_2$) battery capable of operating in extreme environments and with extended lifetime.

The nodes were subjected to a series of testing and verification procedures for evaluating their performance and functionalities. Simulation tests were carried out for evaluating the battery performance, life-time and deployment scenarios of the nodes. The required firmware using necessary APIs was developed and successfully ported into the boards for wake-up and communication testing. A test for monitoring the radio performance, communication and data transfer characteristics of the sensor nodes has been carried out using sensor nodes with ceramic chip antenna and Surface Mount Antenna (SMA). The results indicate that an optimum signal quality and level is achieved up to 300 m. The performance is

better with an SMA connector than with a chip antenna. The performance of the node with respect to topography and environment was also studied. Power consumption scenario for maximum sleep time with optimised transmit and receive cycles have been worked out.

A preliminary mock deployment test was carried out at PRL-Thaltej campus using the designed nodes. Stand-alone sensor node capable of measuring electrical properties of the regolith were designed for this purpose. The sensor used in this case was the 5TE sensor capable of measuring dielectric permittivity, electrical conductivity and temperature of the soil in contact. Using these nodes, the properties of the soil have been remotely logged into a computer using a base station. This essentially depicts a scenario where one of the sensor nodes is deployed on the planetary surface and the data is logged using a base station on the rover.

(K. Durga Prasad and S.V.S. Murty)

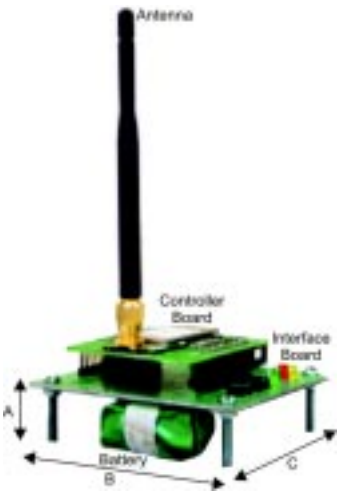

Fig. 37: Custom Node designed and fabricated at PRL. It weighs about 50 g, including the battery and has the dimensions (in cm) A(1.5), B(7) and C(6).

Lunar Radio Frequency Modeling:

Lunar Regolith properties may be studied by a wireless sensor network on surface of the Moon by using appropriate types of sensors. These sensors can measure soil properties and communicate the result, as and when ready. However, communication scenario on lunar surface is quite different as compared to that on Earth. A new wireless propagation model for communication on the Moon has been devised, which uses Digital Elevation Model (DEM) data of a site of interest on the Moon. MATLAB code of the lunar wireless model has been developed to obtain results using DEM data of desired site on the Moon. DEM data of four sites of the Moon, obtained by Terrain Mapping Camera (TMC) on board Chandrayan-1 have been used to derive area coverage patterns on the Moon. (Figure 38) shows a typical result obtained using the developed lunar wireless model.

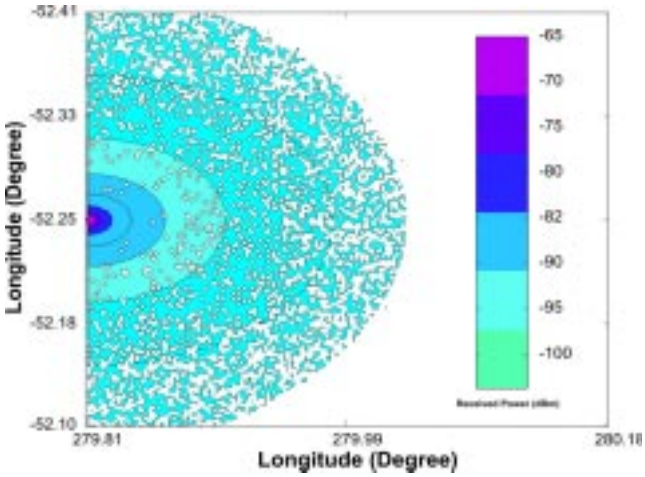

Fig. 38 Radio frequency coverage pattern of the site based on lunar wireless model.

In Figure 38 spatial resolution is 56 m in both directions and size is 164 pixels and 400 pixels in latitude and longitude directions, respectively. Such results can provide understanding of percentage area coverage for a given minimum received signal strength, potential sites for sensor deployment on the Moon assuring intact wireless link, decision whether a given sensor node can work on the Moon as far as sensitivity of the receiver is concerned and can provide suggestion for possible path of rover (carrying cluster head) to remain in contact with the nodes. DEM based results can provide more insight in to the communication scenario on the Moon and can be very useful to mission planners.

(Jayesh P. Pabari and Y. B. Acharya)

Design of Vacuum chamber:

A vacuum chamber has been fabricated in PRL workshop for studying the properties of lunar simulants under simulated lunar environment (Figure 39). The salient features of this vacuum chamber are 1) It is sealed with viton gaskets, can be baked up to ~ 150°C and can achieve 10^{-6} torr under static condition; 2) has a provision to reach low temperatures (< -100°C) on a Cu plate inside vacuum, through cooling a Cu rod by dipping it, externally in liquid nitrogen; 3) It has a large glass window for observing the processes inside the vacuum; 4) Through vacuum feedthroughs upto three thermocouples can be attached to

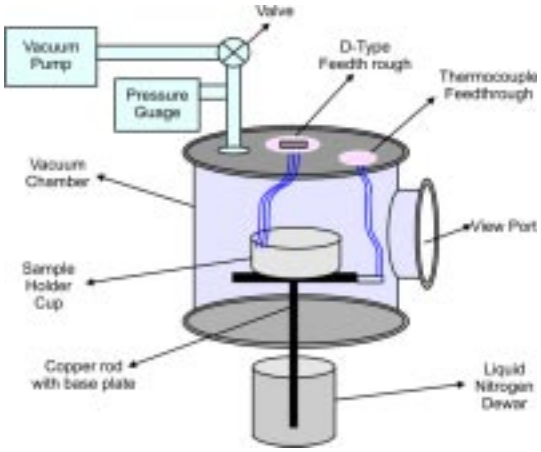

Fig. 39: A vacuum chamber inside which soil properties under simulated lunar environment can be investigated. It has a provision to reach lunar day/night temperatures through heating/ cooling through a Cu rod.

monitor temperature at different points in a soil column; 5) Also, one can connect a sensor (for example a thermal and electric sensor) and place a WSN node in the vacuum chamber. The purpose is to 1) measure simulated lunar soil properties, under simulated lunar environment (pressure and day/night temperatures) and 2) to assess the WSN performance in the lunar environment vis a vis terrestrial environment.

(S.V.S. Murty, K. Durga Prasad and H. Vaghela)

SRE-2/Dosimeter

The second version of Space capsule Recovery Experiment (SRE-2) will be launched by ISRO during late 2010. It is planned to include a space radiation monitor and dosimeter onboard this mission, which is being jointly developed by PRL and VSSC, Trivandrum. Laboratory model of the experiment was fabricated at VSSC and was brought to PRL for testing and calibration. Based on the results of tests carried out at PRL, the design of the experiment was further optimized. Preliminary design review (PDR) of this experiment has been successfully completed and the flight model is now under fabrication at VSSC. The software necessary for the analyzing data from this experiment is being developed at PRL.

(S.V. Vadawale)

Hard X-ray background from lunar surface detected by HEX

The High Energy X-ray (HEX) spectrometer experiment Chandrayaan-1 was designed to detect the hard X-rays emitted from the lunar surface in the energy range of 30 – 270 keV using an array of new generation semiconductor X-ray detector Cadmium-Zinc-Telluride (CZT). After the successful launch, the expected instrument performance of HEX was verified during the commissioning phase of Chandrayaan-1 in December 2008. The scientific operation of HEX was planned only the periods known as non-imaging season period of three months duration occurring twice a year. The first non-imaging season after launch of Chandrayaan-1 was February 2009 to April 2009 and HEX was regularly operated during this period. Due to the detector temperature constraints, HEX was operated for about 4—6 orbits per day covering the polar regions of the Moon. The resultant useful exposure time is approximately 40 hours, which is less then the integration time required to detect the γ-ray lines from the lunar surface. However, the continuum background observed by HEX agrees very well with the background expected from the Monte-Carlo simulations, if some post launch gain changes are assumed. It should be noted that this is the first measurement of hard X-ray background from the Moon.

(S.V. Vadawale on behalf of HEX team)

Modeling of X-ray fluorescence signal from lunar surface

We have submitted a proposal for Low Energy X-ray spectrometer (LEX) for the Chandrayaan-2 mission. The primary scientific objective of this experiment is to determine elemental composition of the lunar surface using the technique of X-ray fluorescence spectroscopy. In order to constrain experiment parameter such as required detector area and detector energy resolution as well as to determine the sensitivity of the experiment, we have developed a forward modeling technique to calculate the expected X-ray fluorescence spectra from the lunar surface. Our technique takes the X-ray spectra from the Sun and the concentration of various major elements in lunar surface as input and provides the expected X-ray background spectra from the lunar surface as well as intensities of the characteristic K- lines of the major elements such as Mg, Al, Si, Ti, Ca, Fe. Initial comparison of spectra obtained form our calculations with the one observed by the Chandrayaan-1/C1XS experiment (which also measures X-ray fluorescence spectra from lunar surface) shows very good agreement which corroborates our approach.

(S. V. Vadawale and D. Banerjee)

SCIENCE

Space and Atmospheric Sciences

Investigations pertaining to atmospheres and/or ionospheres of Earth and other planets are being pursued in Space and Atmospheric Sciences Division. The focus is mainly to investigate the changes in the planetary ionospheres due to eclipse events, solar disturbances and alterations in planetary atmospheres due to natural and/or man-made sources. These investigations are being carried out using state-of-the-art instruments and substantiated using models alongwith laboratory simulations. Space-borne experiments using rockets and balloon are conducted to comprehensively understand the atmospheric system.

Long-term changes in tropospheric temperatures

Long-term temperature trends over two urban agglomerations in India viz., Delhi and Kolkata, have been studied using radiosonde data of IMD. Annual and seasonal trends during 1973 - 2008 have been examined for various pressure levels up to 150 hPa in the troposphere. A cooling trend of 0.16°C/decade over Kolkata and a warming trend of 0.03°C/decade over Delhi at 925 hPa are observed. This reflects that temperature trends at this level are governed by the microclimate and local effects. Temperature trends in the 700 - 500 hPa region vary between 0.24 - 0.29°C/decade over Delhi while variability is larger over Kolkata. The maximum warming trend is observed at the 700 hPa (0.27°C/decade for Kolkata and 0.29°C/decade for Delhi) region. Seasonal trends reveal enhanced warming during winter. Previous study showed a decrease in the cooling rate from -2°C/decade during 1958-85 to -0.2°C/decade during 1970-85 at 850 hPa region. However, the present study (1973-2008) shows a warming trend over these urban locations. Similar warming trends at higher levels in the troposphere are also observed.

(Chinmay Mallik and S. Lal)

Impact of emission inventories on simulated NO_2 over India

A complex global chemical transport model (MOZART: Model for Ozone And Related Chemical Tracers) is used to simulate the effect of two emission inventories (POET: Precursor of Ozone and their Effects in Troposphere and REAS: Regional Emission Inventory in Asia) on the tropospheric columnar abundances of nitrogen dioxide (NO_2) over India. NO_2 largely controls the tropospheric ozone production and has been increasing over India in the past few years due to rapid economic growth. NO_2 emissions are primarily from anthropogenic sources involving fossil fuel combustion (i.e., motor vehicle exhaust and coal combustion). The model simulations with the European POET inventory overestimates NO_2 column over southern India compared to satellite observations, which could be due to overestimate of NO and CO emissions in POET. However, a simulation of MOZART with the REAS

shows that the NO_2 column amounts are much lower (Figure 40).

(Varun Sheel and S. Lal)

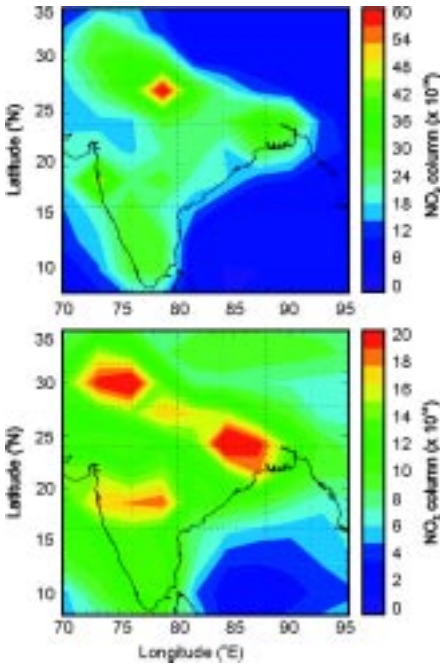

Fig.40: Model simulated tropospheric NO_2 columnar abundance (in unit of molecules/cm^2) over India from two emission inventories: POET (top panel) and REAS (bottom panel) corresponding to December, 2000.

Influence of regional pollution and long range transport on the distribution of ozone in the lower troposphere over Ahmedabad

The distribution of ozone within the atmospheric boundary layer (1-2 km) and in the lower free troposphere (2.5 - 4 km) over Ahmedabad is studied . A total of 80 ozonesonde ascents made during April 2003 to July 2007 form the basis of this study. The effects of different types of air masses on the distribution of ozone are investigated in detail using 10-days back-trajectory analysis. The back trajectories are clubbed together and are classified into three major groups namely i) long range transport region, ii) locally polluted region and iii) clean marine region. The ozone levels at Ahmedabad increase with increasing residence time (at regional sector) till 4-6 days for all seasons except winter. During winter, high levels of *in-situ* ozone and its precursors dominate, thereby, inhibiting any other effects. The average background ozone mixing ratios are found to be about 28 ppbv in the boundary layer and 42 ppbv in the free troposphere. Higher ozone levels (> 50 ppbv) during late autumn, winter and spring seasons are dominated by regionally polluted air mass whereas low ozone levels (~ 30 ppbv) during summer-monsoon are caused by marine air mass. In the lower free troposphere, the distribution of ozone is found to be affected mainly by the long range transport particularly in late spring and early summer. The ozone levels are found to be 10-27% higher in the air mass of long range transport with respect to average ozone levels.

This work is done in collaboration with Manish Naja of ARIES, Nainital.

(S. Srivastava, S. Venkataramani, T. A. Rajesh and S. Lal)

Radiative forcing and climate impact of black carbon aerosols

Black carbon (BC), among the carbonaceous aerosols, is gaining considerable significance because of its ability to influence air quality and climate on local, regional and global scales. BC mass concentrations measured in Ahmedabad varied from 2 μg m^{-3} during summer to 11 μg m^{-3} during winter and post-monsoon seasons. BC mass concentrations in Ahmedabad are governed by local sources and meteorology (boundary layer, winds, rainfall and long-range transport).

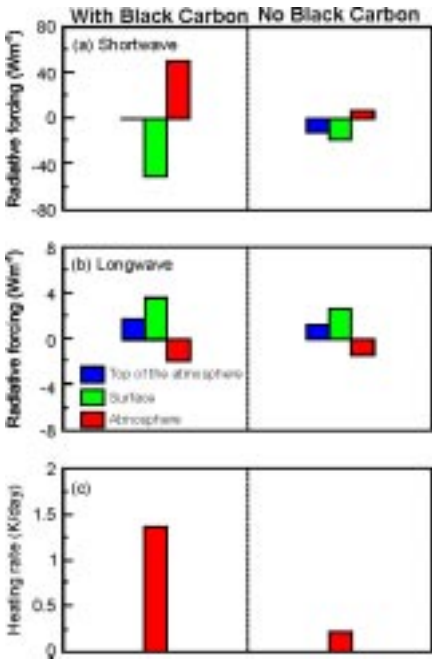

Fig.41:Aerosol radiative forcing (Wm^{-2}) at the top of the atmosphere, surface and in the atmosphere in the (a) shortwave (0.2-4.0 μm) and (b) longwave (4-40 μm) regions with and without black carbon aerosols. (c) Heating rate (Kelvin per day) for the two scenarios.

Single scattering albedo (SSA) deduced using measured BC mass concentration as input in an aerosol optical properties model varies from ~0.7 during winter and post-monsoon, to 0.93 in monsoon over Ahmedabad.

Surface and atmosphere aerosol radiative forcing in pre-monsoon and monsoon are ~50% lower than those obtained during winter and post-monsoon. It is found that when the amount of BC and water vapor are high over continental regions, the net (shortwave + longwave) atmospheric warming is higher. BC aerosols alone contribute on average 60% and 25% of shortwave and longwave atmospheric forcing respectively (Figure 41). Heating rates including BC aerosols are at least a factor of 3 higher than when BC aerosols are absent thus, highlighting the crucial role of BC aerosols in modifying the radiation budget and climate.

(S. Ramachandran, S. Kedia and T.A. Rajesh)

Aerosol optical characteristics and size distribution over different environments in south Asia: Seasonal and spatial variations

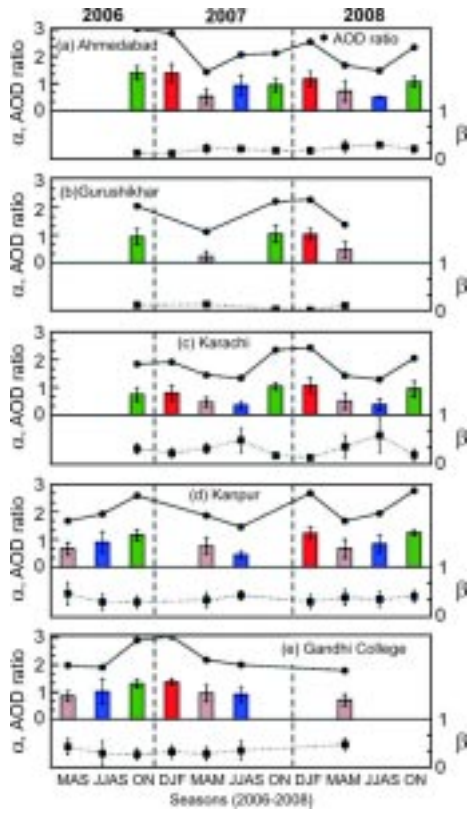

Fig.42: Variation in seasonal mean Ångström parameters (α and β) obtained from AODs measured in the wavelength range of 0.4-0.875 μm, and AOD ratio (=0.4 AOD μm/0.875 μm AOD) over (a) Ahmedabad, (b) Gurushikhar, (c) Karachi, (d) Kanpur and (e) Gandhi College during 2006-2008.

In contrast to previous attempts, aerosol data from a number of ground-based stations (Ahmedabad, Gurushikhar, Karachi, Kanpur and Gandhi College) situated in different regimes in south Asia are analyzed.

This represents different environments which help to examine the space-time variation in aerosol characteristics, and the effect of long range transport. The present study reports an important set of measurements that can be used to produce a useful characterization of the atmospheric aerosol load in this part of the world, a major regional aerosol hot spot. Ahmedabad, Gurushikhar and Karachi aerosol optical depths (AODs) are low during winter and high during summer, while in Kanpur and Gandhi College, winter AODs are higher. Ångström wavelength exponent (α) during post-monsoon and winter is higher than pre-monsoon and monsoon (Figure 42). α values are lower over Gurushikhar and Karachi (≤ 1.0) indicating the dominance of coarse mode aerosols (dust and/or sea salt). Ratio of AODs obtained at 0.4 to 0.875 μm, an indicator of the dominant aerosol size in the distribution, is higher during post-monsoon and winter when compared to pre-monsoon and monsoon in agreement with α and columnar loading (β) (Figure 42).

(S. Kedia and S. Ramachandran)

Variations in aerosol optical characteristics and radiative effects over India: Normal monsoon and drought years

Aerosols can affect clouds and precipitation, (a) by increasing the lifetime of clouds and reflectivity, thereby decreasing the precipitation and radiation reaching the surface of the Earth, and (b) by absorbing the solar radiation and re-emitting it as thermal radiation which heats the air mass may cause evaporation of cloud droplets. The indirect radiative effects of aerosols are more uncertain than the direct radiative effects (scattering and absorption of solar and terrestrial radiation). Model simulations suggest that a large decrease in the surface reaching solar flux can alter the atmospheric stability, cloud formation and reduce precipitation. Monthly mean MODerate Resolution Imaging Spectrometer (MODIS) Terra and Aqua aerosol optical depths (AODs) and Total Ozone Mapping Spectrometer (TOMS) absorbing aerosol index (AAI) obtained during 2001-2004 are utilized along with a chemical transport model and a radiative transfer model to examine seasonal and inter annual variability in aerosols, and their radiative effects over India in the context of normal monsoon and drought years. July AODs in drought years (2002 and 2004) are higher than the normal monsoon (2001 and

2003) years. AAI is also higher in drought years suggesting an increase in the abundance of absorbing aerosols. The magnitude and spatial extent of aerosol radiative forcing in April and July 2002 are higher than that of 2003 in the troposphere. Near surface heating rates are > 1 K/day during post-monsoon and winter, while it is > 0.5 K/day at 2 km in July. Such large heating rates at precipitable cloud heights have the potential to reduce the cloud cover leading to a reduction in rainfall and/or prolong the break days during monsoon.

(S. Ramachandran, R. Srivastava and S. Kedia)

Aerosol, clouds and rainfall over India and surrounding oceanic regions

Aerosols take part in the cloud formation and wield an influence on the cloud droplet size distributions. By affecting the amount, type and distribution of clouds, aerosols could alter the radiation balance of the Earth. The inter-annual and spatial variations in aerosol and cloud characteristics, water vapor and rainfall over India and the surrounding oceans during the monsoon month of July from 2000 to 2009 and their correlations have been examined, as they can provide vital clues to aerosol-climate-monsoon interaction. AOD and rainfall anomalies over India are anti-correlated. AOD anomaly is largely positive over India while rainfall anomaly is negative in 2002 (drought year). In 2003 rainfall is higher than normal and AOD is less (normal year) because of wet removal of aerosols. Absorbing aerosols are also found to be higher over India in 2002 when compared to 2003. The precipitation threshold effective radius for clouds has been observed to be 14 μm. Cloud effective radius is found to decrease to ~ 15 μm over India in July 2002 from 19 μm in 2001, thereby providing an observational evidence of the indirect effect of aerosol. Cloud effective radius and rainfall are strongly correlated over India when compared to Arabian Sea and Bay of Bengal.

(S. Ramachandran and S. Kedia)

Lidar observed temperature characteristics and its association with ozone over a sub-tropical location

Lidar observed sub-tropical middle atmospheric temperature structure over Mt. Abu revealed a prominent semi-annual oscillation (SAO) in the lower mesosphere. Heating and cooling rates are calculated and an average heating rate of about 2.5 K/month during equinoxes and a cooling rate of ~ 4 K/month during November-December are found in the mesosphere. Stratospheric temperature measured using Lidar from Mt. Abu and columnar ozone measured by Total Ozone Mapping Spectrometer (TOMS) show a good correlation (r^2 = 0.61).

(Som Sharma, S. Lal, H. Chandra and Y. B. Acharya)

Middle atmospheric thermal structure differences over sub-tropical and tropical locations.

An observational campaign was conducted during March, April and May 2004 wherein Rayleigh Lidars at Mt. Abu, (24.5^{o}N, 76.2^{o}E), which is a sub-tropical site, and at Gadanki (13.5^{o}N, 79.2^{o}E) a tropical site, were operated. Significant differences are observed in the temperature structure over these two locations. The observed differences are higher during March than in May 2004. Higher temperatures (~ 5 K) have been found in the height range of 55-65 km over both the locations during April 2004 in comparison to CIRA-86 and MSISE-90 models. Lower stratospheric temperatures have been recorded over Gadanki, as compared to model temperatures, during May 2004, whereas no such feature has been observed over Mt. Abu. A planetary wave type structure has been found in the observed temperatures over both the locations.

This work is done in collaboration with NARL, Gadanki.

(Som Sharma, H. Chandra, S. Lal and Y. B. Acharya)

Altitude-dependent effects of collisions on sodium airglow emission

Simultaneous measurements using a narrow-bandwidth (0.3 nm) airglow photometer and a sodium lidar from Gadanki (13.5^{o}N, 79.2^{o}E), reveal episodic enhancements in Na airglow intensity during 1930-0140 hrs (IST) on 18-19 March, 2007. This variation is drastically different from the average Na airglow intensity variation for that duration during that month. Although the height of peak concentration in Na atoms is at 88.5km, the Na airglow intensity variation is found to be well-correlated with the Na atom concentration variation only at the height of 93.6 km during 2310-0140 hrs. This period is closer to the measurement of mesospheric ozone by SABER instrument onboard TIMED satellite. The correlation coefficient is not significant at 88.5 km where the Na concentration peaks. Estimations of the altitude profiles of volume emission rate of Na airglow corresponding to the D2 line using measured parameters (O_3, Na) during the local post-midnight hours reveal that the peak emission altitude is different from 93.6 km. It is suggested that altitude variation in collisional quenching is needed to match the peak altitude of emission

with the altitude where correlation between Na atom concentration and Na airglow intensity is maximum. The fact that the measured atmospheric pressure reduces by a factor of ~ 2.5 as altitude changes from 88.5 to 93.6 km supports this proposition.

This work is done in collaboration with S. Sridharan, National Atmospheric Research Laboratory, Gadanki.

(S. Sarkhel, R. Sekar and D. Chakrabarty)

Neutral turbulence over equatorial mesosphere during winter

A Rohini sounding rocket carrying a Langmuir probe was flown from Thumba (8.3°N, 76.9°E), on 27 November 2005 to study the winter equatorial mesospheric neutral turbulence using electron density measurements. During winter, turbulence was observed in the entire mesosphere from 60 to 100 km. The energy dissipation rates during winter at lower altitudes (70-78 km) ranged from 0.1 to 6 W/kg and the corresponding heating rates ranged from 0.01 to 0.6 K/day, which are similar to the high-latitude winter average. In higher altitudes (83-87 km), the energy dissipation rates ranged from 10 to 1000 mW/kg and the heating rates ranged from 1 to 100 K/day. The observed winter turbulence in this altitude range is much stronger than the high-latitude winter average and is similar to that observed during summer at both, low- and high-latitudes. As the turbulence occurs in very thin layers (100-200 m), the contribution of turbulence towards heating of the winter equatorial mesosphere is significantly less in comparison to that in summer. Thus, this study shows that the winter turbulence is very weak and hence the contribution of neutral turbulence process towards heating the mesosphere is significantly less during winter.

(Uma Das and H. S. S. Sinha)

Mesospheric turbulence studies using multi-technique measurements

Rocket-borne Langmuir probe detected a spectrum of electron density irregularities, in scale sizes of 1-1000 m at 69-72, 75, and 78 km over Sriharikota on 9 July 2005. MST radar at Gadanki also detected strong scattering layers in 65-71, and 73-80 km regions, corresponding to the 3 m irregularities. Radar observations showed that at smaller scales of turbulence, the thickness of the turbulent layer was about 5-6 km with fine structures of thicknesses of 2.4 km (limited by pulse width) embedded in these layers. Rocket also detected 3 m fluctuations, which were strong (a few percent) in lower altitudes and small but clearly well above the noise level at higher altitudes. Rocket results also point to the existence of thin layers of turbulence between 100 and 300 m. The turbulence parameters estimated from the electron density fluctuations are consistent with those determined from radar observed Doppler spectra and the earlier studies.

This work is done in collaboration with NARL, Gadanki.

(H. Chandra, H.S.S Sinha, Uma Das and R.N. Misra)

Balloon-borne optical investigations of atmospheric dynamics

Atmospheric regions are intricately coupled wherein energy transfer takes place from mesosphere to the ionosphere-thermosphere regions. In order to investigate the mesospheric dynamics and its coupling to the upper atmospheric regions, a Balloon-borne optical Investigation of Regional-atmospheric Dynamics (BIRD) experiment was conducted on 08 March 2010 from Hyderabad. As part of this experiment two optical spectrographs were flown on a high altitude balloon to a height of about 34 km. Optical emissions in the UV and the visible regions that emanate from different altitudes were measured. Several ground-based experiments were operated in a campaign mode in conjunction with this experiment. Initial results show temporal variability in the optical emission rates that relate to the dynamics in the atmospheric regions. Detailed analysis is in progress to characterize the wave dynamics.

This work is done in collaboration with S. Chakrabarti of Boston University, USA, R. K. Manchanda of TIFR Balloon Facility, Hyderabad and R. Sridharan of Space Physics Laboratory, Thiruvananthapuram.

(D. Pallamraju, R. P. Singh, P. Shah, R. Narayanan and F. I. Laskar)

On deriving incident particle energies using combined optical and radar measurements

The Earth's upper atmosphere is affected by the influence of particles of solar wind origin, especially during space weather events. Estimating the energy inputs into the upper atmosphere is very essential to be able to quantify the energy budget into the upper atmosphere and also to understand the coupling between the atmospheric regions. During space weather events, the energy flux incident into

the Geospace shows significant spatial and temporal variations. While particle fluxes at high-energies (greater than a few hundreds of eV) can be known either by *in situ* measurements, or by radar-based modeling method, the information on the low-energy flux is extremely difficult to estimate. Using optical emission and radar measurements, in conjunction with modeling, influx of low-energy particles during the storm event of 30 October 2003 was derived. We find that the characteristic energies and fluxes vary between 100 eV to 5 keV and 0.5 to 160 mWm^{-2}, respectively during the 5 hours of intense magnetic disturbance on that day which expanded the auroral oval to regions over middle latitudes. Presently investigations are underway to extend this approach to higher latitudes.

(D. Pallamraju)

Investigations of equatorial ionosphere during annular solar eclipse on 15 January 2010

In order to understand the effect of conductivity changes associated with solar eclipse on the E region plasma waves a rocket flight campaign was planned and conducted during the annular solar eclipse. In addition, an investigation on the effects of winds in the E-region of equatorial ionosphere was attempted. Two RH 300 Mark II rockets were successfully launched at 1220 and at 1305 IST on 15 January 2010. The first rocket contained Langmuir and electric field probes to measure the electron densities, electron temperature, amplitude of plasma waves, and fluctuations in electric fields. The TMA vapour cloud payload in the second rocket was intended to measure the neutral winds during eclipse. The photography of the released vapour cloud was carried out using eight programmable cameras deployed at four stations in and around Thumba. The obscuration of the sun at 1220 IST on 15th was about 85%. Another rocket was launched on 16 January 2010 at 1220 IST containing Langmuir and electric field probes to obtain the control day plasma parameters. Preliminary analysis of the data indicates that the ionization on the eclipse day is reduced by 50 to 30% depending on the altitude in the 75-100 km region. Further, the signatures of plasma waves are observed at the base of E-region where sharp electron density gradients exist, indicating that the ambient electric field is directed upward. The electron density scale length is about 3 km at about 85-90 km region on both the days. Fluctuations in plasma density and electric field are found to co-exist. The amplitudes of fluctuations in plasma density and electric field are relatively less on eclipse day indicating relatively lesser electric field on this day in comparison with the control day.

(R. Sekar, Y.B. Acharya, D. Pallamraju, S.P. Gupta, R. Narayanan, M.B. Dadhania, R.P. Singh, G. Hirani, M. Bhavsar, D. Chakrabarty, S.K. Sharma, Narain Dutt, F.I. Laskar, S. Sarkhel and P. Shah)

Association of the shear in the zonal plasma flow and the development of tilted plasma plume structure during equatorial spread F

Evidence is obtained for the shear in the zonal plasma flow and for a tilted plume structure simultaneously, using collocated optical and radar measurements. A multi-wavelength photometer with a narrow band-width (0.3 nm) and a narrow field-of-view (3^{o}) was operated to measure airglow emissions from two different altitude regions in a bi-directional mode along the zonal direction. The identifiable features in the 630.0 nm airglow emission that originate from the base of the F region, moved westward while the similar features in the 777.4 nm airglow emission (Figure 43), that originate from around the peak height of the F layer, moved eastward. This indicates a shear in the zonal plasma flow.

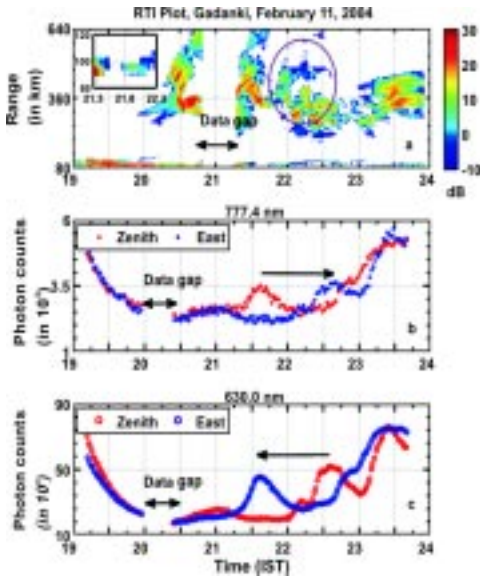

Fig.43: (a) Range-Time-Intensity (RTI) plot of the ESF structures as recorded by the Indian MST Radar on February 11, 2004. The C-shaped structure at ~2200 IST is encircled. The inset zooms-in on the disappearance of E-region irregularities during 2135-2145 IST, just prior to the occurrence of the C-shaped plasma structure. Subplots (b) and (c) depict the variations in the zenith (red) and slant (45^{o} East) columnar (blue) intensities of 777.4 nm and 630.0 nm airglow emissions respectively.

Simultaneous measurements of equatorial plasma irregularity structures using a VHF radar reveal the presence of C-shaped plume structure during the period of the sheared flow. This investigation provides experimental evidence for the existing theories.

(R. Sekar, D. Chakrabarty and D. Pallamraju)

Variation in the total electron content (TEC) over Ahmedabad during the recovery phase of a moderate geomagnetic storm

A new dual-frequency Global Ionospheric Scintillation and TEC Monitor (GISTM) was commissioned at Physical Research Laboratory in 2009. GISTM provides amplitude scintillation index (S4), single frequency carrier phase and total electron content (TEC) measurements from up to 11 GPS satellites simultaneously at L1 (1575.4 MHz) and L2 (1227.6 MHz) frequencies. Based on TEC data on magnetically quiet days during October 2009 - January 2010, quiet-time morphological variation of vertical TEC (VTEC) over Ahmedabad has been obtained. This variation is compared with the variation in VTEC obtained during the recovery phase of a geomagnetic storm that ensued after a M2 class solar flare on 17 January 2010. A decrease in VTEC is observed almost throughout the day on 21 January 2010 as a response to the geomagnetic storm. The decreased VTEC on this day is attributed to the possible change in composition, especially $[O]/[N_2]$ ratio, following the storm. This investigation brings out the signature of negative ionospheric storm over low latitudes.

This work is done in collaboration with Ms. Sowmya Kamath of Indian Institute of Space Science and Technology, Thiruvananthapuram.

(D. Chakrabarty)

Multi-technique studies of E-region plasma irregularities

Plasma density irregularities in the daytime at an off-electrojet location in India were studied using rocket-borne, VHF radar, and ionosonde observations. Langmuir probe detected weak irregularities above 98 km in scale sizes above 100 m and no noticeable irregularities at shorter scales. Spectral slope of -4 was found for scale sizes in the range of 100 m to 1 km. Radar did not detect echo at this time consistent with rocket-borne results that small scale irregularities (3 m) were absent. Strong radar echoes were seen at around 100 km before 10 LT and after 1330 LT in the form of descending echoing layer. Ionosonde observations also showed blanketing type sporadic-E with identical descending behavior.TIMED satellite measurements of neutral winds suggest that zonal winds play a crucial role in forming electron density layers, which become unstable via the gradient drift instability with background electric field and/or zonal winds.

This work is done in collaboration with NARL, Gadanki; SPL, Thiruvananthapuram, and IIG, Mumbai.

(H. Chandra, Uma Das and H.S.S Sinha)

Appearance and extension of airglow depletions

All sky imaging observations conducted so far have shown that plasma depletions are produced in the equatorial region and they reach to off-equatorial latitudes due to their vertical evolution. This development of plasma depletions from equatorial to low-, and to mid-latitudes is known as pole-ward extension. All sky observations at 630 nm and 777.4 nm from a low latitude station Kavalur (12.5°N, 78.8°E; 3.9°N geomagnetic), show that on some occasions, depletions in 630 nm images appear at the northern edge in the post sunset hours and extend towards equator in later hours, i.e. there is an equator-ward extension. Using the ionosonde data of an equatorial station Trivandrum, and an off-equatorial station Waltair, and the ratio of 777.4 nm and 630 nm airglow intensities, the F layer height gradient along the meridional direction was obtained.

This work is done in collaboration with P. K. Rajesh and J. Y. Liu of the Institute of Space Science, National Central University, Taiwan.

(H.S.S. Sinha and S.B. Banerjee)

Post-midnight depletions and GPS phase fluctuations

All sky images were taken at 630.0 and 777.4 nm emission lines over Kavalur (12.5°N, 78.8°E; 4.6°N, geomagnetic), during the solar maximum of February-April 2002. An ionosonde at the equatorial station, Trivandrum (7.6°N, 76.9°E; 1.2°S, geomagnetic) was used to monitor the ionospheric variations at the geomagnetic equator during post-sunset and post-midnight period. A collocated global positioning system (GPS) receiver was used to compare the occurrence of depletions at different hours of the nights with the corresponding GPS phase fluctuation index (Fp). Previous studies of GPS phase fluctuations have shown a single, pre-midnight peak for Fp > 200 between 2000-2100 LT, which is associated with topside plasma bubbles. Sequence of images with plasma depletions taken over Kavalur showed that they developed within the field of view in the post-midnight period (Figure 44). There appears

to be a time difference of about 1 hour between the peaks in the occurrences of plasma depletions and GPS phase fluctuations.

This work is done in collaboration with P. K. Rajesh, J. Y. Liu and W. S. Chen of the Institute of Space Science, National Central University, Taiwan and F. D. Chu of Chunghwa Telecom Company, Taiwan.

(H.S.S. Sinha, S.B. Banerjee, R.N. Misra, N.Dutt and M.B. Dadhania)

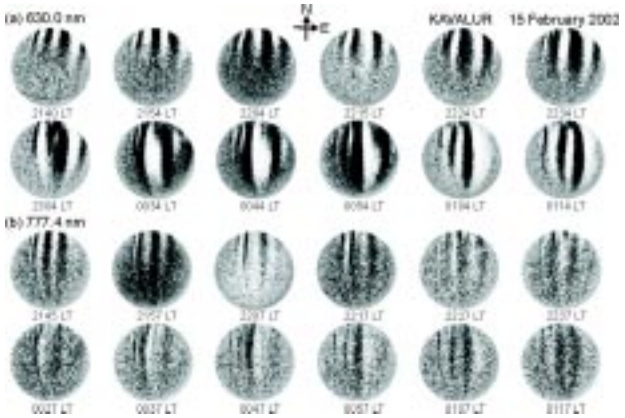

Fig. 44: Sequence of images taken over Kavalur using all sky imager revealing plasma depletions during post midnight hours

Response of solar X-ray flares on Mars: Modeling and observations

An analytical yield spectrum method is used to calculate TEC of Martian ionosphere during the period of 12-18 May, 2005. A 3-D kinetic, solar wind model (Hakamada – Akasofu - Fry version 2 (HAFV.2) is also used to predict interplanetary shock arrivals at Venus, Earth and Mars (Figure 45). Mars and Earth were on the same side from the Sun during this solar event. The composite shock has been predicted by HAFV.2 mpdel to arrive at Mars after about 60 hours while the corresponding response on Earth is seen several hours earlier. The duration of the solar flare caused enhancement in the TEC of Martian ionosphere is about one day.

This work is carried out in collaboration with S.M.P. McKenn-Lawlor, National University of Ireland, Ireland.

(S.A. Haider)

Do Meteor showers occur on Mars

Metallic ions such as Fe^+, Mg^+, Ca^+, Na^+ and Al^+ have been observed in the lower ionosphere of Earth. Although these ions are not measured in the lower ionosphere of Mars, the meteoric layer in the Mars' atmosphere occurs below the main ionization peak at ~80 km. We have analyzed 5600 electron density height profiles, which were observed by radio occultation experiment onboard Mars Global Surveyor during the period from 24 December 1998 to 9 June 2005. The preliminary analysis of these data have confirmed that metal ion layer exists at about 80-90 km, in the lower ionosphere of Mars. These observations indicate that strong meteor showers occur periodically in Mars.

This work is carried out in collaboration with Mr. Bhavin Pandya, C.U. Shah College, Ahmedabad

(S.A. Haider)

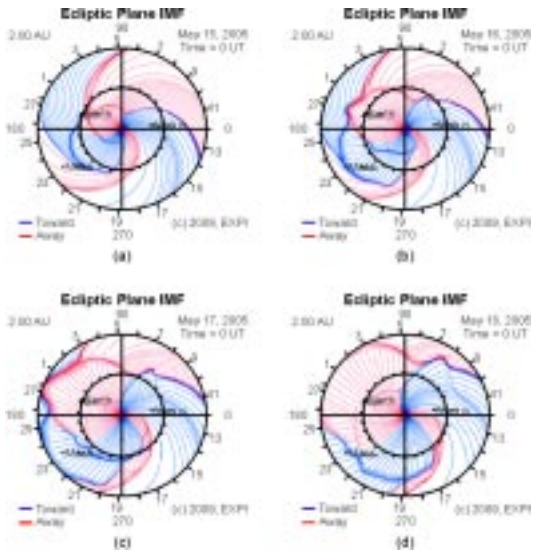

Fig. 45: Temporal sequence of planetary shock arrivals at Venus, Earth and Mars as predicted by HAFV.2 model.

Cluster Mass Spectrometry

Two types of carbon cluster sources were developed, and a mass spectrometric analysis of the clusters was carried out. One source is based on sputtering of a hollow graphite cathode in a low pressure argon discharge. The second type is based on pulsed laser ablation of a solid graphite target. Mass spectrometric analysis was done by a time-of-flight mass spectrometer, which was also developed in-house. Improvements to the flux and transport characteristics of the cluster beam are being undertaken. This set up is the first step towards the study of photochemical reactions of small clusters with a view to understanding the chemistry of particulate matter in the atmosphere.

(A.K. Saxena, S.B. Banerjee, I. A. Prajapati, K. P. Subramanian and B. Bapat)

Auger Electron Spectrometer for elemental analysis of surfaces

One of the objectives of the Chandrayaan-2 mission, consisting of an orbiter, a lander and a rover, is the determination of the elemental/chemical composition of the lunar surface at the landing site and along the rover route. Auger electron spectroscopy is one method for identifying the elemental composition, especially suited for light elements. Laboratory based Auger spectrometers are unsuited for a planetary mission because they are optimised for fixed geometries and for very short sample—analyser distances, while also being bulky. The objective is to demonstrate a compact, portable electron spectrometer for Auger Spectroscopy. A retarding potential analyser with a circular aperture and a cylindrical retarding cavity has been found to be most suited for this and a prototype instrument has been built in-house. The transmission characteristics of this analyser have been determined to be satisfactory, and efforts are now underway to obtain an electron spectrum from various solid targets bombarded by a high energy (1—3 keV) electron beam.

(B. Bapat, S. B. Banerjee and Koushik Saha)

Orientation Effects in the dissociation of small molecules

Molecules do not have a spherical symmetry, so the effect of a perturbation on a molecule should exhibit anisotropy. To determine the anisotropy of a process in a collision experiment it is necessary to know the orientation of the molecule with respect to the projectile. Since an ensemble of molecules in a collision experiment contains randomly the orientation of the axis of each molecule that undergoes fragmentation. While this is not possible in general, in the special case, when the fragmentation results in purely ionic fragments, this is possible. We performed an experiment on the molecules N_2 and CO_2 (zero dipole moment) and CO, NO (non-zero dipole moment). Projectile ions of various charge states from the Pelletron Accelerator at IUAC, Delhi were employed to investigate the expected polarisation dependence. The momentum vectors of the fragment ions were completely determined by multi-coincidence momentum imaging. Based on the momentum data, the relative orientation of the fragments within the target molecule at the fragmentation instant can be determined. Data analysis is in progress.

This work is done in collaboration with C.P. Safvan of Inter-University Accelerator Centre, Delhi.

(R.K. Kushawaha, I.A. Prajapati, Koushik Saha and B. Bapat)

Modelling the dissociation patterns of small molecular di-cations

A project has been initiated to experimentally study the dissociation dynamics of triatomic molecular di-cations created by electron impact, and follow the fragmentation sequence of excited di-cations (simultaneous, two-step or metastable) while concomitantly modelling the potential energy surfaces of these di-cations to make predictions about the fragmentation sequence and the kinetic energy release during the fragmentation. Molecular di-cations are generated by electron impact and analysed using a multi-coincidence momentum spectrometer, and data have been recorded for CO_2 and CS_2 molecules. Molecular structure calculations are in progress.

(Amrendra Pandey and B. Bapat)

Geosciences

The research activities of Geosciences Division focus on understanding the origin and evolution of the planet Earth and its various reservoirs, with special emphasis on timescales and processes. The major areas of research of the division are: Solid Earth Geochemistry, Geomorphology and Tectonics, Paleoclimate Studies, Hydrology, Aqueous Geochemistry, Oceanography and Paleo-oceanography, and Aerosol Chemistry. The methodologies followed center on the measurements of abundances and ratios of elements, radioactive isotopes, radiogenic isotopes, of light stable isotopes, and luminescence properties of materials using modern analytical tools.

Tree ring studies

Tree rings are one of the important archives for quantifying climatic variability before instrumental era. Our group use variations in the isotopic composition of wood cellulose to reconstruct past climate. Teak (Tectona grandis) is one of the few tropical species having distinct annual growth rings. Its distribution in monsoon affected south-east Asia makes it an important candidate for quantifying the past monsoon variability. Our study demonstrates oxygen isotope composition ($\delta^{18}O$) studies can be used to reconstruct past climate on the inter- and sub-annual time scales. As cellulose is sequentially laid down in a ring, the segments (Figure 46a) within the ring correspond progressively to different phases of the growing season. $\delta^{18}O$ studies of such segments provide information about environmental conditions during the entire growing season. Intra-annual (within ring) $\delta^{18}O$ analysis of several growth rings of teak samples from central India revealed a clear seasonal cycle (Figure 46b) with higher values at the ring extremities and lower values at the middle. This, when compared with the existing plant physiological model derived values and dendrometric growth pattern of teak from India revealed possibility of identifying growth occurred during pre-, main- and post-monsoon seasons. Further, relative humidity appears to control the intra-annual $\delta^{18}O$ variations rather than rainfall, and therefore past break-monsoon conditions associated with lower relative humidity, could be detected by high resolution sub-sampling of annual rings for $\delta^{18}O$ analysis. Intra-annual $\delta^{18}O$ profile of teak from southern India showed an opposite trend with lower values at the ring extremities and higher at the middle. We attribute this to ingesting of the ^{18}O enriched southwest monsoon and ^{18}O depleted northeast monsoon rains by teak during the main (June to September) and late (October to December) growing seasons, respectively. This opens up the possibility of using teak from southern India to simultaneous reconstruction of the southwest and northeast monsoon rainfall.

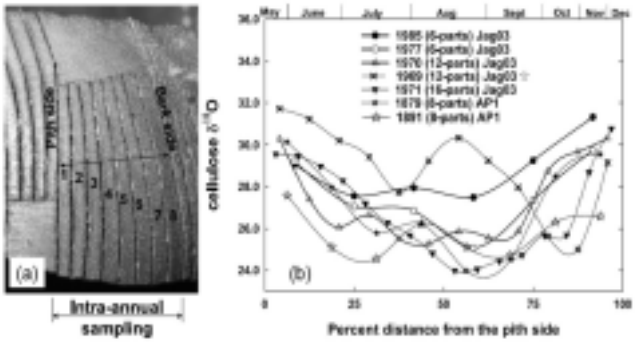

Fig.46.(a) Photograph illustrating intra-annual sampling. Arrow marks the full annual ring. Cellulose was extracted separately from such segments (numbered 1, 2 etc.) for intra-annual $\delta^{18}O$ studies. (b) Intra-annual $\delta^{18}O$ variations as a function of time of growth (top) in teak trees from central India, Jagdalpur (Jag03) and Hanamkonda (AP1). Legend represents years (A.D.) corresponding to the rings analyzed, the numbers of sub-samples and sample name. Star in the legend denotes ring that showed anomalous pattern in August 1969, a year with lower relative humidity during August.

On interannual scale, $\delta^{18}O$ variations of teak from central India showed a positive correlation ($r = 0.4$, $p < 0.01$) with ambient rainfall while teak from southern India revealed a negative correlation ($r = -0.5$, $p < 0.005$). Higher rainfall in the case of former leads to lengthening of the growing season and teak grows until a period of the lower relative humidity (post-monsoon season) leading to more evaporative enrichment of the leaf water in ^{18}O and hence higher cellulose $\delta^{18}O$ values. The plausible reasons for the negative correlation in the case of the latter could be the presence of relatively strong amount effect in the rainfall and relatively higher relative humidity conditions during the growing season in the region.

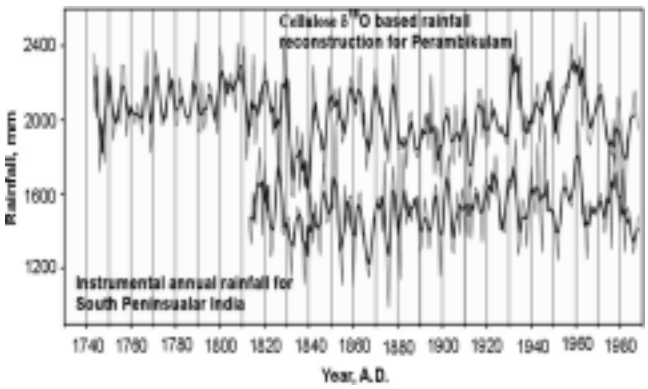

Fig.47: Rainfall reconstructed for Perambikulam using cellulose $\delta^{18}O$ record of teak from southern India (top) and rainfall record of the South Peninsular India (bottom), area below 15°N. Thick lines in both the records are three year moving averages.

The overall higher relative humidity leads to lower $\delta^{18}O$ values of teak cellulose. Rainfall of southern India was reconstructed back to 1743 A.D. (Figure 47) using the relationship between $\delta^{18}O$ record of teak from southern India and concurrent rainfall record of Palakkad. The reconstructed rainfall revealed higher rainfall during the later part (1743-1830 A.D.) of the Little Ice Age (LIA).

This work was done in collaboration with BSIP, Lucknow, IITM, Pune and UAS, Bangalore.

(S. Managave and R. Ramesh)

Isotopic Composition of Atmospheric water vapour

It is important to understand the Atmospheric Water Vapor (AMV) cycle in the changing global scenario. Stable isotopes of deuterium (D) and oxygen (^{18}O) are effective tracers of the natural hydrological processes as they fractionate during phase change, and this fractionation is very sensitive to changes in atmospheric parameters (e.g. temperature, humidity). To characterize the AWV cycle over the monsoon region a campaign was conducted for one year, April 2007 to April 2008 at the Physical Research Laboratory (PRL), Ahmedabad, India (23.03°N, 72.56°E) wherein AWV and rain water samples were collected and subjected to stable isotopic analysis.

Vapor was collected using liquid nitrogen (-196°C) using an extraction line composed of U-shaped glass traps (Figure 48) Rainwater was also collected. Stable isotopic measurements were done using a dual inlet Stable Isotope Ratio Mass spectrometer (PDZ-Europa Geo 20-20).

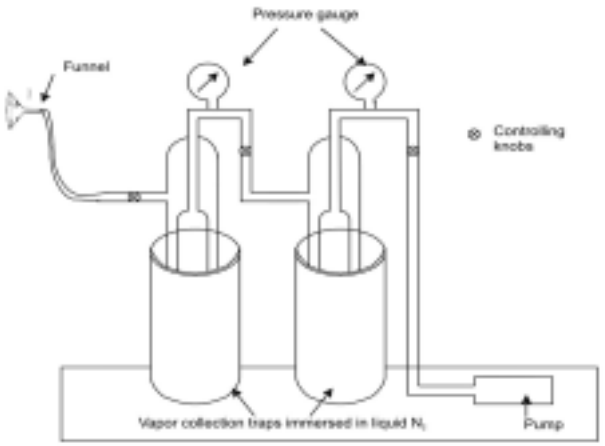

Fig. 48: Schematic diagram of water vapor collection line

Stable oxygen isotopic compositions of AWV ($\delta^{18}O_{av}$) and relative humidity (RH) values during the 2007-08 are shown in Figure 49. Between the first weeks of April and May, $\delta^{18}O$ values were higher than in the later months,

and a slight increasing trend is seen, which may be due to the increase in RH during this period (from 12 % in April to 26 % in May). A significant impact of rainwater on the local water vapor is clearly marked by a sharp decrease of ~2.9‰ in the oxygen isotopic composition of AWV ($\delta^{18}O_{av}$) and a sharp increase of ~20% in RH from May to the second week of June. During the monsoon (15 June-15 September), five major rain events were clearly traced by more negative oxygen isotopic compositions of rain ($\delta^{18}O_r$). Our results show a large effect of rainwater on the isotopic composition of AWV. During rain δ^{18}Oav was depleted than the non rainy days. It is found that for most cases AWV is ~9‰ depleted compared to that of the rain during the monsoon, while it is not so in the non-monsoon period. Short-term effect of western disturbances was also observed in $\delta^{18}O_{av}$ in February.

(R. Srivastava, R. A. Jani and R. Ramesh)

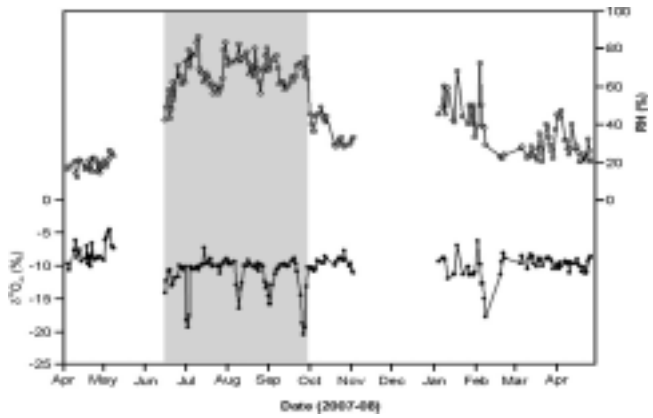

Fig. 49: Relative humidity (RH %) and stable oxygen isotopic compositions of atmospheric water vapor ($\delta^{18}O_{av}$ ‰) over Ahmedabad from April 2007-April 2008. Gray shade indicates the monsoon season. Beginning of each month is marked by a pip.

Nitrogen and carbon cycling in the Indian Ocean

The work involves the estimation of the total and new/ export production using ^{13}C and ^{15}N tracers. In the Arabian Sea, we observe that environmental conditions decide the planktonic community structure and hence the carbon and nitrogen cycling in the region. e.g. winter mixing promotes the growth of diatoms and Noctiluca, whereas, calm winds and intense sun light encourage the blooms of Trichodesmium in the region. Photo-inhibition is observed in the northeastern (NE) Arabian Sea during late winter. New productivity and f-ratios in the different parts of the NE Arabian Sea are mainly controlled by hydrodynamic and meteorological parameters like wind strength, SST, mixed layer depth and mixed layer nitrate. The mixed layer NO_3^- and the chlorophyll are functions of wind strength and the f-ratios, whose peak values lag behind the peaks in the mixed layer NO_3^-, but follow chlorophyll variations (Figure 50).

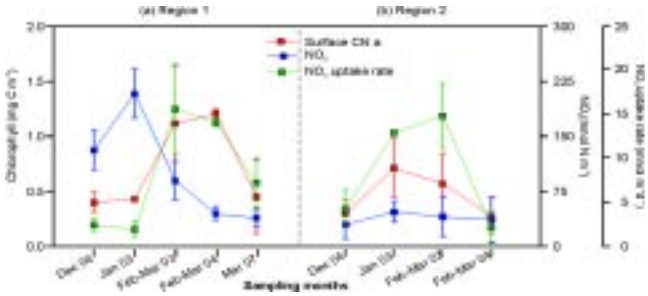

Fig 50: Mean values of surface chlorophyll, mixed layer integrated nitrate and new productivity in the Arabian Sea during different sampling periods for (a) Region 1 (north of 20°N), and (b) Region 2 (south of 20°N) . Error bar represent the 1-sigma standard deviation from the mean value. Numbers (shown with the plot) represent the number of sampling locations for the respective sampling period.

During spring, diffusive fluxes of NO_3^- across mixed layersrange from 0.51 to 1.38 mmol N-NO_3^- $m^{-2}d^{-1}$, and can account for 67% and 78% of the observed nitrogen uptake in the coastal and open ocean regions, respectively.

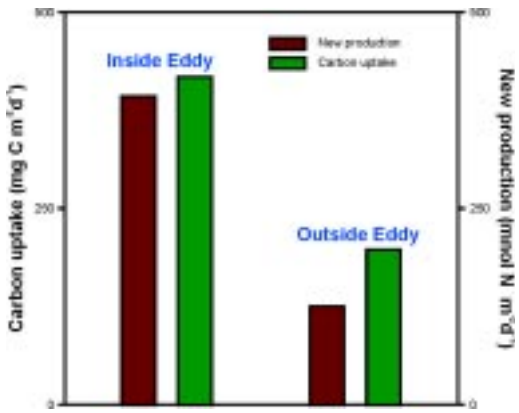

Fig 51: Carbon uptake and new productivity at locations in an eddy and just outside the eddy in the Bay of Bengal.

In the Bay of Bengal, we studied the role of eddies on the nutrient dynamics and productivity. Carbon uptake rate at location within an eddy is found to be 417 mg C $m^{-2}d^{-1}$. In contrast , carbon uptake is only 197 mg C $m^{-2}d^{-1}$ at location just outside the eddy. Similarly new productivity at location inside the eddy is observed higher (392 mmol N $m^{-2}d^{-1}$) than at location outside eddy (125 mmol N $m^{-2}d^{-1}$) (Figure 51). The results show that the supply of nutrients by such eddies can enhance the productivity in the region.

This work was done in collaboration with NIO, Goa, SAC, Ahmedabad and NCAOR, Goa.

(Naveen Gandhi, R. Ramesh)

Origin of hydrocarbons from mud volcanoes of Andaman Islands

Detailed investigations were carried out on gas samples collected from Mud Volcanoes (MVs) of the Andaman Islands, India during April and December 2009 to study the source of the methane emerging from them using molecular composition of hydrocarbons and carbon isotopic composition of methane (CH_4). Gas samples were collected from mud volcanoes at different locations from central and north Andaman in pre-evacuated glass bulbs (~ 200cc) at atmospheric pressure. A few samples were collected using "Closed Chamber Method" for flux calculations. The concentration of methane is in the range of hundreds of ppmV to percentage level. This depends on the collection time and location whereas ethane concentration is only in the range of 5-170 ppmV. The carbon isotopic composition ($\delta^{13}C$) of methane varies between -32.7 to -49.0‰. All samples are CH_4 dominated. The traditional diagram used to assess methane origin ie. $\delta^{13}C_{CH4}$ vs $C_1/(C_2+C_3)$ ratios known as "Bernard diagram" is plotted in Figure 52. The values of $\delta^{13}C$ indicate primarily the origin to be "thermogenic". But all the samples, however, fall in an ambiguous sector of the ''Bernard'' diagram, which suggests alteration due to secondary post-genetic processes. All samples have the values of $C_1/(C_2+C_3)$ ratios between 100-5500.

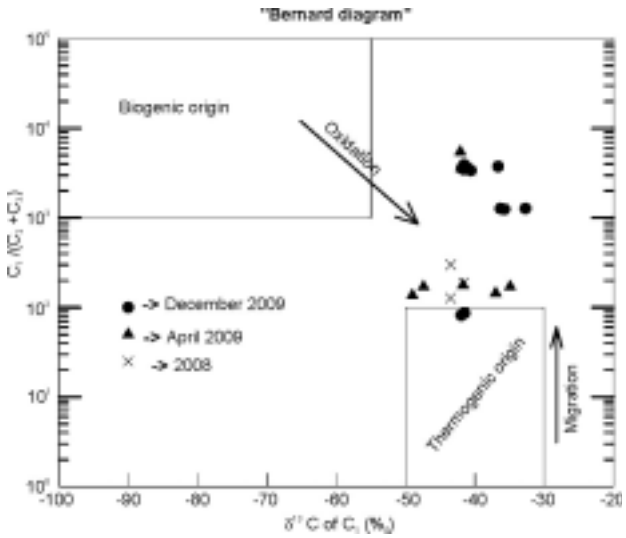

Fig. 52: Methane carbon isotopes versus hydrocarbon molecular composition diagram (Bernard plot) for mud volcanoes of central and north Andaman.

This can be explained as "Molecular fractionation by advection'. This process can explain the systematic loss of C_2+ from reservoir to surface in mud volcano gasses and hence higher values of $C_1/(C_2+C_3)$ ratios. Although these ratios indicate biogenic origin of methane, its oxidation may lead to a slight increase of $\delta^{13}C_{CH4}$, not more than 5‰. Hence such enriched values are not possible due to oxidation. The results indicate that the methane is thermogenic and there is no biodegradation of these gases, suggesting that these hydrocarbons must have come from more than 2000m deep. A good correlation between concentrations of methane and ethane from MV's of central Andaman indicates that the effect of secondary alteration during their seepage toward the surface may be insignificant. A rough estimate of gas flux from few vents in a small area (200 sq m) is calculated to be 11 tons/ year using a theoretical relationship between the size of the bubble, the frequency of the appearance and the methane flux.

(D.K. Rao, J.S. Ray and R.A. Jani)

Organic carbon in Soils

Huge amount of organic carbon (~ 1500 Gt), trapped under top 1 meter of soils is under scanner now. With rising global temperature, this natural reservoir may act as source or remain stable depending upon its regional sensitivity to ambient temperature changes. It is a challenging task to understand complex control of climate and biology on the organic carbon storage.

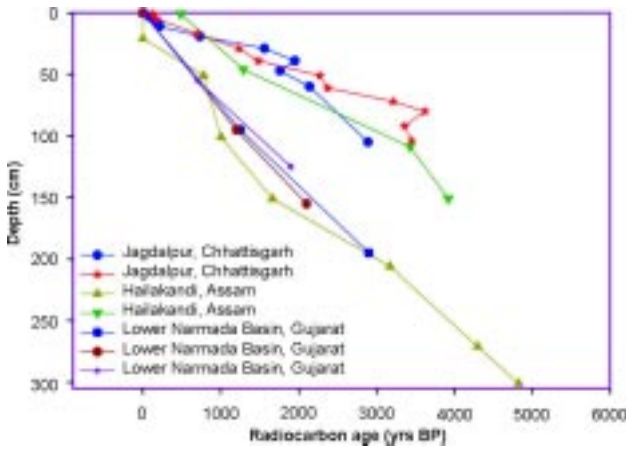

Fig. 53: Mean residence time of organic carbon for soil profiles from different climate zones.

As soil carbon is primarily derived from the atmosphere, radiocarbon can be used as a natural tracer to estimate residence time at different time scales (decades to several

thousand years). Our study based on three soil profiles collected from varying climate zones show that Mean Residence Time (MRT) of organic carbon is mainly controlled by the clay content (Figure 53). Higher clay content is favourable for carbon sequestration over longer time scales.

(A. H. Laskar, R. Ramesh and M. G. Yadava)

Fifth International Radiocarbon Inter-comparison (VIRI)

We participated in the Fifth International Radiocarbon Inter-comparison (VIRI) exercise. Eight samples of various natures were provided to ~130 laboratories to find out influence of chemical pre-treatment and radiocarbon detection procedures. Consensus values are described in Table 1. Here percent modern carbon (pmC) is defined as,

$$pmC = \left(\frac{A}{A_o} \right) \times 100$$

where A and A_o are present and initial radioactivity of the sample. Z score is used for proficiency testing and depends on x_m, the reported result, x_A, the assigned or true value for the material, σ_p, the target value for standard deviation and is given by z-score = $(x_m - x_A)/ \sigma_p$. It represents the amount of uncertainty in the results that is tolerable in relation to the purpose of the analysis. Z = 0 implies perfect result; ± 2 is good while above ± 3 is unusual and needs serious investigations. PRL results show that almost all values are within ± 2 except one sample (charcoal) which is deviated because of severe loss during pre-treatment.

(A. H. Laskar, R.Ramesh and M. G. Yadava)

Spatially Resolved Luminescence Dating

Luminescence dating generally employs mineral extracts of specific grain sizes. However in complex sediments and rocks, extraction of individual grains in not feasible. We therefore developed an imaging luminescence system that uses an electron multiplier CCD for imaging a sample in two dimensions with a unit magnification. The signal intensity of different pixels corresponds to the intensity of luminescence emitted from the different regions of sample. This instrument comprises electronics and optics developed in PRL. The optics comprises a set of achromatic doublet. An objective lens converts the light from the sample to a parallel beam. This beam is reflected on to a converging lens that creates an image of the samples on the chip EMCCD camera. Optical filters for the measurement of interference free sample luminescence are placed en-route. The optical arrangement enables freedom to move different optical elements for better focusing and easy handling. The electronics enables variable and controlled heating and optical stimulation rates, and both blue and infrared stimulation are possible. The commands for the operations to be performed is controlled by the Labview based GUI interface, developed in-house. The software provides flexibility in respect of defining various stimulation operations the choice of the stimulation source. The luminescence data can be analyzed in a program made in Matlab. The program reads a specific image format of digital image and stores it in a two dimensional array. The images

Table 1: Summary of VIRI samples and results.

Sample (PRL)	PRL Code (PRL)	pmC (Consensus)	pmC (yrs BP)	Age (yrs BP)	Consensus age	Z Score
K(wood)	PRL-3034	Not detectable	0.0576 ± 0.0062	> 40,000	61670 ± 890	-----
L(wood)	PRL-3035	76.4 ± 0.4	75.72 ± 0.04	2230 ± 50	2300 ± 5	1.7
M(wood)	PRL-3036	74.2 ± 0.5	73.90 ± 0.03	2560 ± 50	2500 ± 5	0.6
O(cellulose)	PRL-3037	99.5 ± 0.5	98.46 ± 0.04	40 ± 40	130 ± 5	2.0
R(Shell)	PRL-3038	74.1 ± 0.4	73.34 ± 0.04	1690 ± 45	1800 ± 10	1.9
S(Barley mesh)	PRL-3039	110.2 ± 0.5	109.96 ± 0.04	-----	-----	0.5
U(Humic acid)	PRL-3040	23.64 ± 0.3	23.08 ± 0.02	11930 ± 90	12120 ± 10	1.9
P(Charcoal)	PRL-3041	81.5 ± 0.4	80.46 ± 0.09	2480 ± 50	2560 ± 5	2.6

acquired in subsequent runs are aligned with respect to a base image (Natural signal) with an accuracy of ± 1 pixel using several control points in the base image and the unaligned images. The numerical value of the image pixels is used to compute the luminescence vs. dose growth curves and derive paleo-dose values. Matlab based program provides flexibility to obtain the dose values for different Region of Interest (ROI).

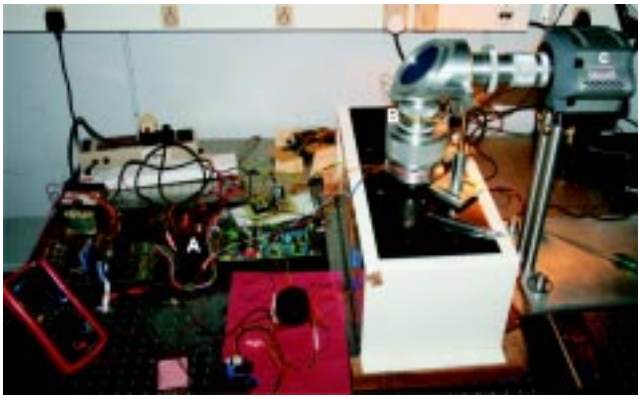

Fig. 54: A view of the spatially resolved Luminescence System developed at PRL A) Control Electronics B) Stimulation assembly and optical arrangement C) CCD Camera.

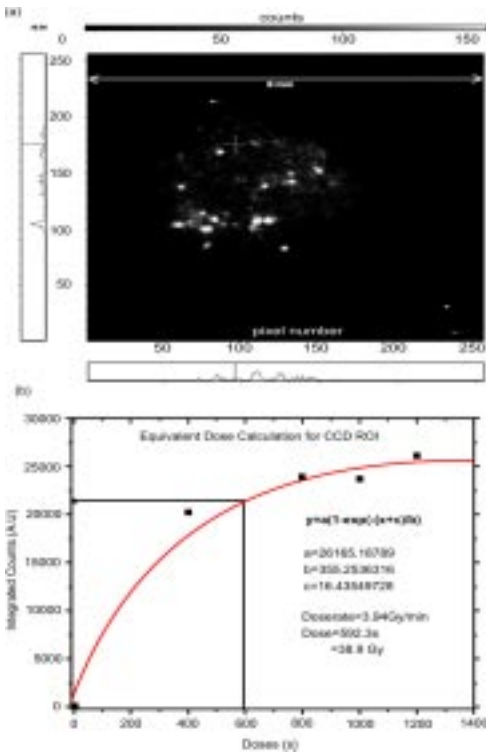

Fig. 55: (a) A CCD image from a luminescing sample and (b) the dose reconstruction using standard dosimetric protocols.

(Figure 54) shows the electronic and mechanical arrangements and (Figure 55a and b) show one of the initial trial image obtained by the new setup for a quartz sample and the dose response curve calculated using one of the ROI's. Initial test have provided good results and further refinements are being incorporated in to make the system for routine dating applications.

(N. Chauhan, P. Adhyaru, H. Vaghela and A.K. Singhvi)

Meteorite luminescence and Cosmic ray exposure ages

Meteorites are exposed to cosmic ray (CR) radiation over million year (Ma) time scales and consequently their luminescence signal builds up. The annual cosmic ray dose has so far been assumed as 0.1Gy/year. This aspects was examined in detail by considering the shielding effects using GEANT4 simulation toolkit, and by measuring linear energy transfer dependent luminescence efficiency of cosmic ray heavy charged particle. We observed that luminescence effective; cosmic ray dose rate in the interior of the meteoroid body of a pre-atmospheric radius = 9-40 cm is ~ 0.043 Gy/year. This is about 50% lower compared to the value used so far.

With such a dose rate and irradiation duration over Ma time scale, the luminescence in meteorites is expected to be either in saturation or equilibrium. Isothermal (300 °C) luminescence in red emission (650 ± 20 nm) window gave equivalent dose significantly lower than saturation dose. This suggested that the natural luminescence levels in meteorites are in equilibrium, the level of which is determined by luminescence build up by cosmic rays and its decay due to both the thermal and athermal pathways. Similar thermoluminescence glow curves of several ordinary chondritic meteorites suggested identical kinetic properties and orbital temperature and hence, identical thermal fading. Experimental results on athermal fading indicated that the fading rates (g-value in % per decade of time), decreased with exposure ages. We surmise that the decrease of athermal fading rates with CRE age is due to progressive loss of luminescence centers which results in diminishing tunneling probability. The mechanism for loss of centers could be radiation damage due to interaction of high-energy heavy charged particle with matter and high ionization density and possible creation of Schottky-Frenkel type defects. The rate at which centre concentration decreases is not known and hence the best alternative of laboratory measured g-value was considered.

The g-value exponentially decreases with time with the life time of 7.3 ± 2.5 Ma and a residual value of 2.8 ± 0.7 % per decade ($\log_{10}$ scale; Figure 56). As the g-value

decreases, equilibrium luminescence level is expected to increase. Equivalent doses of seven chondritic meteorites using red ITL signal increased with CRE ages (Figure 57). These studies suggest that the athermal fading rate and equivalent dose are the two parameters that systematically vary with CRE ages. Further studies are in progress to elucidate the mechanism of athermal loss and examine the prospects of using g - values as a surrogate for cosmic ray exposure age.

(R.H. Biswas, P. Morthekai and A.K. Singhvi)

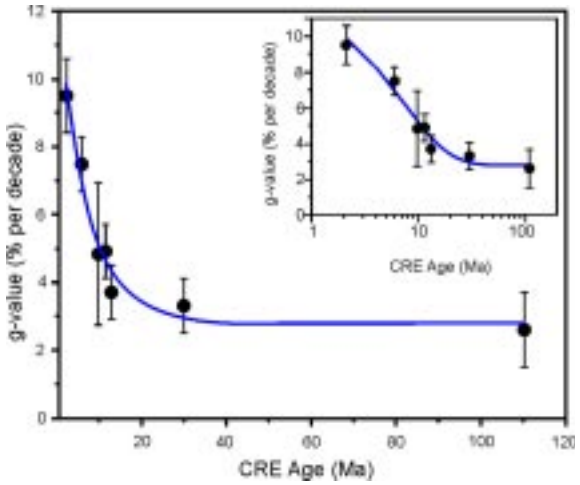

Fig. 56: Variation of athermal fading rate in (g-value per decade) with cosmic ray exposure age. The inset gives the same data on a logarithmic scale.

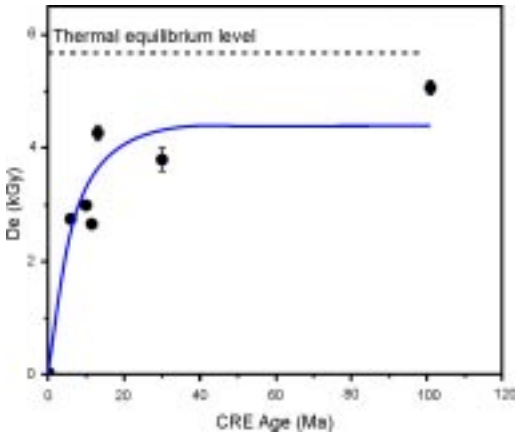

Fig. 57: Equivalent doses of Meteorites using isothermal red emission, plotted against cosmic ray exposure ages.

Athermal fading of feldspar luminescence

Feldspar is the only natural luminescence dosimeter in extra terrestrial contexts i.e., meterorites and Mars that can be used for dating. Compared to quartz, feldspar is very sensitive and provides hope for dating sequences where quartz has lower sensitivity. However, at times, feldspars suffer from 'athermal fading'. Athermal fading is the loss luminescence signal over time scales much shorter compared to the values expected from standard kinetic analysis. A widely accepted explanation for this phenomenon is that the trapped charges directly tunnelled to the luminescence centre and recombine at a rate faster than the normal decay. We explored the possibility of arriving at a sample dependent correction procedure for athermal loss of signals by taking into account the rapidity of athermal fading simultaneous to irradiation of the sample in the nature. A new mathematical apparatus has been developed to obtain the fading parameter (g') from the fading measurements and a generalized fading equation is developed such that it includes the decay over extended durations.

This work is being carried out in collaboration with Dr. Mayank Jain of Riso National Laboratory, Denmark.

(P. Morthekai and A. K. Singhvi)

Fluvial aggradations and incision in Alaknanda valley: Monsoon during the past 30,000 years.

Geomorphology, stratigraphy and optical dating was used to develop a regional model of fluvial landscape evolution in the Alaknanda valley during the last 30000 yrs. This is being depicted in Fig.58; (a) the oldest valley fill is dated to 26000 yrs and was deposited under moderate monsoon; (b) this was followed by the deposition of assorted boulders and pebbles under transitional climatic condition around 18000 yrs; (c) an accelerated phase of valley fill and the underlying hard rock incision between < 18000 yrs - > 15000 yrs occurred under weak monsoon and rapid bed rock uplift; (d) strengthened monsoon during 15000 yrs and 8000 yrs resulted in the regulated sediment flux and deposition of well graded sediment.This phase coincides with the strengthening of the monsoon following the Last Glacial Maximum and was regionally extensive in the valley and, (e) Incision of valley fill and development of terraces occurred during < 8000 yrs to 6000 yrs. This period correspond to the weak monsoon. The data compares well with regional records e.g. from (I) Guliya ice core data from Tibet where enriched $\delta^{18}O$ value corresponds to strengthened monsoon. Lake Records (filled blue vertical bars (II) Sanai lake Ganga Plain, (III) Goting Lake, upper Alaknanda catchment and (IV) Speleothems from central Himalaya, (Figure 58).

The present study demonstrated that fluvial dynamics in the Alaknanda valley was modulated by monsoon and,

the role of tectonic was subordinate, limited to providing accommodation space and post deposition modification of the fluvial landforms.

This work was done in collaboration with Prof. Y.P. Sundriyal, Naresh Rana and Shipra Chaudhary of the HNB Garhwal University, Srinagar.

(N. Juyal, and A.K. Singhvi)

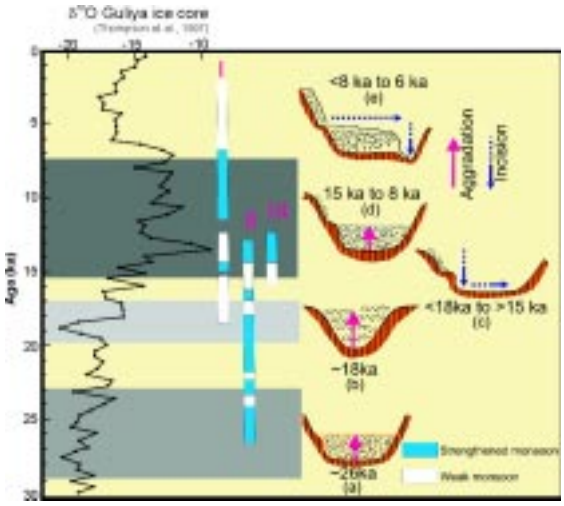

Fig. 58: Evolution of the Alaknanda basin with time. The text provides more details.

Aerosol iron solubility over Bay of Bengal: Role of anthropogenic sources and chemical processing

The chemical composition (involving water-soluble inorganic constituents, crustal elements and carbonaceous species) of size-segregated aerosols (PM_{10} and $PM_{2.5}$), collected from the marine atmospheric boundary layer (MABL) of the Bay of Bengal (BoB) during 27th Dec' 08 – 28th Jan' 09, has been studied to ascertain the factors controlling the spatio-temporal variability in the fractional solubility of aerosol iron. Based on the air-mass back-trajectory (AMBT) analyses and chemical proxies, continental outflow from the two major source regions has been identified, viz: (1) outflow from the Indo-Gangetic Plain (IGP) sampled over north-BoB (N-BoB); and (2) south-east Asian (SEA) outflow over south-BoB (S-BoB). A significant linear relationship among fractional Fe solubility [WS-Fe (%)] and nss-SO_4^{2-} over N-BoB (Figure 59a; characterized by higher abundance of aerosol iron (Fe_A) and SO_4^{2-}) provides evidence for the acid processing of mineral dust during atmospheric transport from IGP. The enhancement in the solubility of aerosol constituents is also evident from a linear increase in nss-Ca^{2+} with nss-SO_4^{2-} (Figure 59b). In contrast, a temporal shift in the winds, representing the outflow from south-east Asia and aerosol composition over south-BoB, exhibit enhanced fractional solubility of aerosol Fe (range: 11.4 to 49.7 %) associated with the lower abundance of dust (< 100 ng m^{-3} of Fe_A) and nss-SO_4^{2-} (< 15 µ g m^{-3}). These observations suggest the dominance of combustion sources (biomass burning and fossil-fuel) in dictating the aerosol iron solubility over south-Bay of Bengal. The impact of the anthropogenic sources is also ascertained based on the covariance of WS-Fe with K^+ and OC (organic carbon); as well as enrichment factor of heavy metals (Pb and Cd) associated with the outflow from south-east Asia.

(Ashwini Kumar, M.M. Sarin and Bikkina Srinivas)

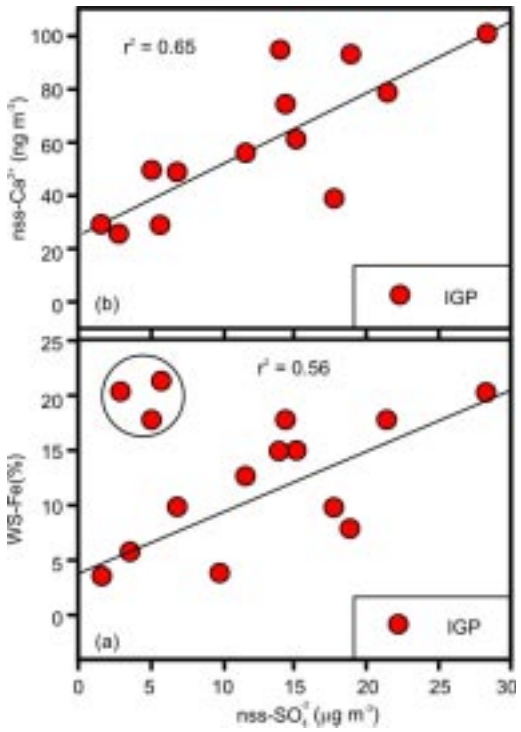

Fig. 59: (a)A linear-relationship among WS-Fe (%) and nss-SO_4^{2-} for IGP outflow, suggesting the role of chemical processing in the enhancement of fractional solubility of Fe over north-Bay of Bengal, (b) Acid uptake by mineral dust is also evident from increase in the solubility of Ca^{2+} as a function of nss-SO_4^{2-} in PM_{10}.

Atmospheric dry deposition of N, P and Fe to the Bay of Bengal

Atmospheric supply of nutrients (N, P & Fe) to the marine atmospheric boundary layer (MABL) has gained considerable interest in the recent years due to rapid increase in their anthropogenic sources and possible impact on the ocean surface biogeochemistry. As a part of the National

Programme on integrated campaign of aerosols and trace gasses radiation budget (ICARB-2009), concentrations of dissolved inorganic Nitrogen (DIN = NO_3^- + NH_4^+), Phosphorous (DIP = PO_4^{3-}) and water-soluble-Fe (Fe_{ws}) have been studied in aerosol samples collected over Bay of Bengal. The measured concentrations and dry-deposition fluxes show significant spatio-temporal variability over north and south Bay of Bengal (N-BoB & S-BoB). In N-BoB, the average dry-deposition fluxes of DIN and DIP are 50 µmol-N/m^2/day and 2.5 µmol-P/m^2/day, respectively, and that of Fe_{ws} is 1185 nmol-Fe/m^2/day. In contrast, atmospheric deposition fluxes of DIN (Av: 27.7 µmol-N/m^2/day), DIP (Av: 2.1µmol-P/m^2/day) and Fe_{ws} (Av: 565 nmol-Fe/m^2/day) are relatively low over S-BoB. The nutrient ratios N:Fe, N:P and P:Fe, in dry-deposition, over Bay of Bengal center around 80, 17.5 and 5.5 respectively and N:P ratio in atmospheric deposition is comparable to their marine Redfield ratio. A comparison of the data from Bay of Bengal suggests that the flux ratios of N: Fe, N:P are significantly lower, whereas P:Fe ratio is higher than those over north Atlantic. The enhanced supply of Fe_{ws} to the Bay of Bengal is attributed to its dominant source from biomass burning and fossil fuel combustion.

(Bikkina Srinivas, M.M. Sarin, Ashwini Kumar and R. Rengarajan)

Spatio-temporal variability in the atmospheric conversion efficiency of sulphur dioxide to sulphate

Simultaneous measurements of the surface level concentrations of sulphur dioxide (SO_2) and submicron sulphate aerosols (SO_4^{2-}) have been carried out from an urban region (Ahmedabad: 23.0^0 N, 72.6^0 E, 49m asl) and a high-altitude site (Mt. Abu: 24.6^0 N 72.7^{0}E, 1680 m asl) located in the semi-arid western India. The ratio of SO_4^{2-} to SO_x (SO_x = SO_2 + SO_4^{2-}), termed as S-ratio, has been calculated which in turn provides a measure of the conversion efficiency of SO_2 to SO_4^{2-} under different seasonal and environmental conditions. Over urban region (Ahmedabad), the average S-ratio is 0.37 and 0.55 during Aug-Sept'08 and Jan '09, respectively. In contrast, at a high altitude site (Mt. Abu), the S-ratio is 0.28 during Feb '09 and 0.18 during Sept-Oct '09. An increase in the S-ratio during the high atmospheric dust season, compared to that during the low dust season, is attributed to the enhancement in the oxidation efficiency of SO_2 due to the involvement in heterogeneous phase chemistry (in addition to the homogeneous gas phase chemistry). The temporal variability in the concentrations of SO_2 and SO_4^{2-} is shown in Figure 60. These results have important implications to the direct/ indirect atmospheric radiative effects due to sulphate aerosols on a regional scale.

(Timmy Francis and M. M. Sarin)

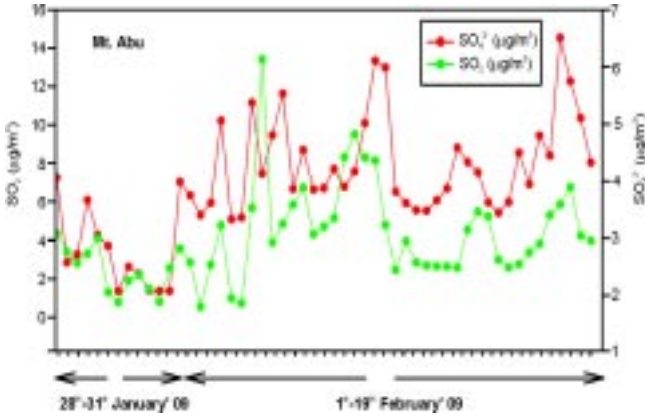

Fig. 60: SO_4^{2-} and SO_2 concentrations measured over Mt.Abu during Jan-Feb 09

Atmospheric Concentrations of Polycyclic Aromatic Hydrocarbons

One of the important classes of organic aerosols is the Polycyclic Aromatic Hydrocarbons (PAHs), emitted in the atmosphere primarily due to incomplete combustion of fossil–fuels and biomass burning. PAHs participate in photo-chemical reactions in the ambient atmosphere mainly in the gas-phase with NO_2^+ and OH^- radicals as well as with O_3. Aerosol samples ($PM_{2.5}$) were collected during winter season (Oct'08-Mar'09) and pre-monsoon season (Apr-May'09) from an urban location (Patiala: 30 N; 76 E; 250 m. amsl), characterized by widespread emissions from wood–fuel and agricultural-waste burning as well as from fossil-fuel combustion.

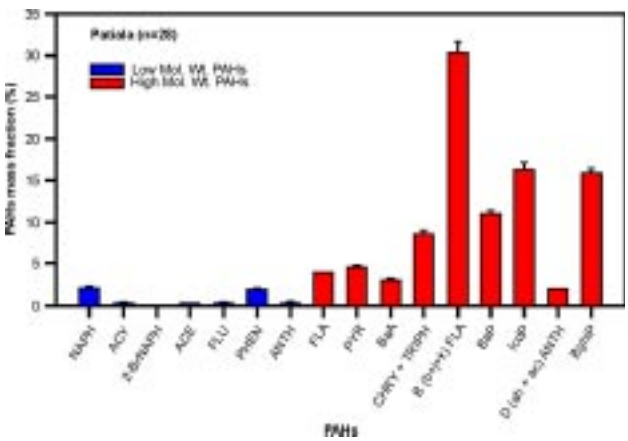

Fig. 61: Average concentration of PAHs (Dec'08-Mar' 09)

The aerosol samples collected during wintertime (Dec'08 to Mar'09) show total PAHs varying from 4.3 to 48 ng m^{-3}. The 16–PAHs (analyzed on a GC-MS) congener profile suggests that 4 to 6 rings PAHs (high molecular weight) are higher in the ambient aerosols than the PAHs with 2 to 3 rings (Figure 61). On average, 4 to 6 rings PAHs contribute about 95 % of the total PAHs. The ratios of PAH-isomers can be used as diagnostic tracers of the sources of carbonaceous aerosols.

The ratio of isomeric-PAHs, Fluoranthene / Pyrene, varied from 0.71 to 1.13 with an average value of 0.90. Another isomeric ratio of Anthracene / Phenanthrene, varied from 0.15 to 0.30 with an average value of 0.17. The ratio of third isomeric pair, Indeno (123-cd) Pyrene / Benzo (ghi) Perylene, varied from 0.68 to 1.57 (Av = 0.98). The cause for such large variability in isomer ratio is attributed to the relative dominance of fossil – fuel combustion and biomass burning sources.

This work is done in collaboration with Prof. Darshan Singh, Panjabi University, Patiala, providing logistic help for sample collection.

(Rajput Prashant, R. Rengarajan and M. M. Sarin)

Day-Night variability of EC, OC, WSOC and inorganic ions over urban site

The day- and night-time variability of EC, OC, WSOC and inorganic ions in ambient aerosols ($PM_{2.5}$ and PM_{10}), sampled from an urban site (Kanpur) in the Indo-Gangetic Plain, has been studied with an objective to understand the formation of secondary aerosols. The aerosol mass dominated by fine-mode particles ($PM_{2.5}/PM_{10}$ mass ratio = 0.46 – 0.86) and their chemical composition suggest that total carbonaceous aerosols (TCA = 1.6 * OC + EC) account for ~50% of the $PM_{2.5}$ mass; whereas mass fraction of water-soluble inorganic species (WSIS) is no more than 20%. A significant linear relation between EC, OC and K^+ and their characteristic ratios suggest biomass burning as a major source of carbonaceous aerosols. The $PM_{2.5}$ mass and concentrations of EC, OC show significant increase (~30%) during nighttime. The average WSOC/ OC ratio is significantly higher in the daytime samples (0.66 ± 0.11) compared to that in the nighttime (0.47 ± 0.07); suggesting increased contribution of secondary organic aerosols (SOA) during daytime. The mass fraction of particulate NO_3^- increases by a factor of three during nighttime indicating its secondary formation; and that of SO_4^{2-} shows enhancement (~20%) during daytime

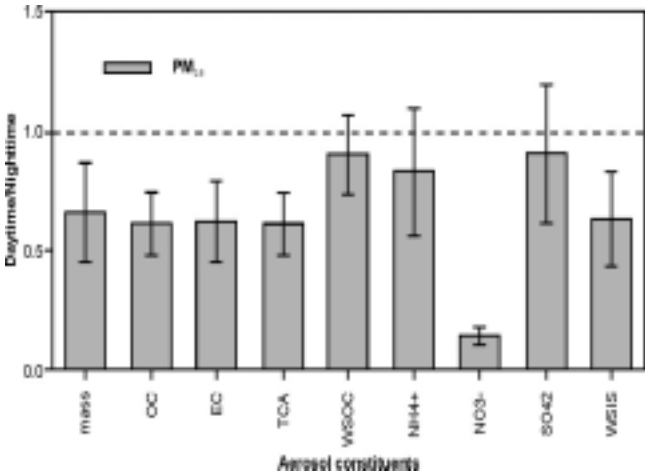

Fig. 62: Ratios of concentrations of selected chemical species in ambient aerosols in daytime and nighttime during the sampling period. The low ratios for particulate NO_3^- can be seen in contrast to ratios for other chemical species.

(Figure 62). A thick-haze event on 30th Oct 2008 (also observed by MODIS image) is marked by a factor of two-to-four increase in the concentrations of OC, EC and inorganic species.

(Logistic help for sample collection at IIT-Kanpur was provided by Dr. S.N. Tripathy)

(Kirpa Ram and M.M. Sarin)

Secondary organic aerosols and associated acidity over an urban environment

Carbonaceous aerosols (elemental carbon (EC) and organic carbon (OC)) are ubiquitous in the atmosphere and impact significantly the regional air quality and climate. The organic aerosols, emitted from both natural and anthropogenic sources are primary and secondary in nature. Estimates of secondary organic aerosol (SOA) production based on biogenic and anthropogenic volatile organic compound (VOC) precursor fluxes suggest that their dominance over primary component, but large discrepancies exist in these estimates and the inconsistencies are attributed to the poor understanding of SOA production mechanism from the precursors. The co-variation of secondary organic carbon (SOC) along with H^+ ion concentration (referred as aerosol acidity) over an urban environment has been investigated in this study. $PM_{2.5}$ samples (aerodynamic diameter < 2.5 µm) collected from Ahmedabad (23°02'N, 72°32'E) during December, 2006-January, 2007 were analysed for OC, EC, water soluble organic carbon (WSOC). pH of water extract was expressed in terms of atmospheric H_+ ion concentration which can be considered as a measure of

acidity of the deliquescent particles. SOC was estimated by EC-tracer method assuming minimum OC/EC as the primary ratio.

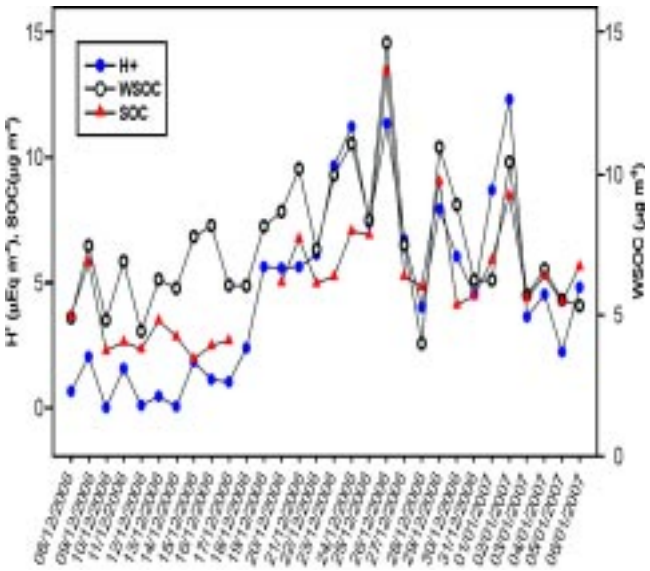

Fig. 63. H^+ ion concentration in determined from the measured pH of aerosol water extract shows significant correlation with SOC and WSOC concentrations.

During this period, $PM_{2.5}$ mass ranges from 32 to 106 mg m^{-3} (Av. = 56 mg m^{-3}). Of the total mass, inorganic salts constitute 29%, organic matter 53%, EC 5.4% and unidentified insoluble component is 21%. The OC varied from 11 to 39 mg m^{-3} (organic mass: 17 to 62 mg m^{-3}) and exhibits a linear correlation with EC indicating its major contribution from anthropogenic sources. The OC/EC ratio varies from 4.0 to 8.1 and SOC content constitutes about 25% of total OC. Water soluble organic matter (calculated from WSOC by multiplying with 1.9) is the major soluble component and ranged from 7.6 to 28 mg m^{-3} and significant fraction of SOC is expected to be water soluble. WSOC/ OC ratio varied from 0.26 to 0.52 and on an average, WSOC constitutes 41% of the total OC during the study period. H^+ ion concentration determined from the measured pH of aerosol water extract shows significant correlation with SOC concentration (Figure 63) which provides the direct evidence for the enhanced SOC formation along with acidity of the aerosols. WSOC concentration also varies linearly with H^+ ion concentration. These preliminary results suggest that the secondary organic aerosol formation at this site is favoured by the acidic nature of pre-existing aerosols on which the heterogeneous reactive uptake of VOC can occur.

(R.Rengarajan and A.K. Sudheer)

Impact of aerosol on glacier recession in Bhagirathi valley

Glaciers are the natural sensors of climate variability and provide a visible expression of climate change. Recent studies have shown that increase in green-house gases and aerosols may lead to accelerated melting of the Himalayan glaciers. Himalaya together with the Tibetan plateau has the highest concentrations of glaciers outside the polar region and provides a unique opportunity to investigate the impact of aerosols, if any, on the glacier recession (melting). Temporal changes in aerosol optical depth (AOD) between 2001-2008 obtained from Moderate Resolution Imaging Spectroradiometer (MODIS) onboard Terra satellite and the glacier recession data of Dokriani glacier in the Bhagirathi valley show a reasonable correlation (R^2 = 0.86). An increase in AOD was observed after 2005 which also coincide with the accelerated recession of the Dokriani glacier. Although the mineral aerosols increase scattering and cloud cover and re-radiation of the solar energy to space (negative forcing), however, in the lower and the middle troposphere (altitude favored by Himalayan glaciers) they can have positive forcing (warming). We hypothesize that increased AOD over the Himalayan region is one of the factors responsible for the accelerated recession of Dokriani glacier. This would imply that AOD can be used to obtain the spatial and temporal changes in microclimatic conditions in the inaccessible glaciated terrain of the Himalaya.

This work is being carried out in collaboration with Dr. D. P. Dobhal, Wadia Institute of Himalayan Geology, Dehra Dun.

(Sanat Kumar Das and Navin Juyal)

Dissolved Nd isotope composition of the Ganga: Spatial distribution of silicate weathering over the Himalaya

Spatial distribution of silicate weathering over the Himalaya (Higher vs Lesser Himalaya) and their controlling factors (temperature, vegetation, relief, rainfall etc.) are the matters of debate. In this study an effort has been made to track the spatial distribution of silicate weathering over the Himalaya using isotropic composition of the dissolved Nd of the Ganga mainstream and its various tributaries. Nd Isotopic composition in the dissolved phase of the Ganga is measured for the first time. ε_{Nd} of the mainstream Ganga varies from -14.2 to -11.5 whereas the tributaries show a range of -16.8 to -14.5 (Figure 64). Measured dissolved ε_{Nd} in the Ganga system are more radiogenic compared to that of the sediments from the same location indicating either their source variability or the fractional dissolution

of various minerals hosting Nd. ε_{Nd} of the Ganga show close affinity with the Higher Himalaya with very little contribution from the Lesser Himalaya if any, indicating the dominance of the Higher Himalaya on the silicate erosion despite the fact that the Lesser Himalaya has more conducive environment for silicate weathering such as higher temperature, vegetation, lower relief suppoting soil formation etc. Higher silicate weathering in the Higher Himalaya could be due to higher physical erosion continuously ekposing fresh mineral surfaces..

(Jayati Chatterjee and Sunil Kumar Singh)

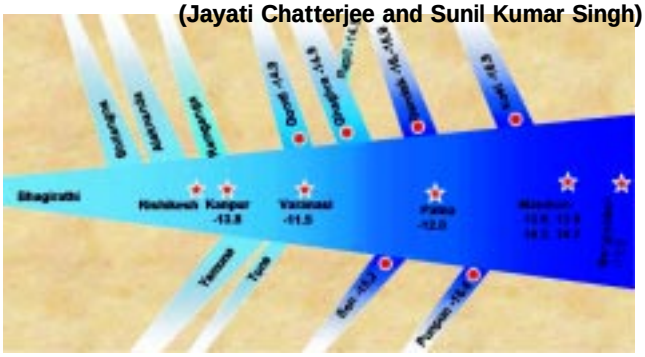

Fig. 64: Dissolved ε_{Nd} of the Ganga mainstream and its tributaries

Mo in estuaries: Impact on global oceanic budget of Mo

Dissolved Mo was analyzed in four Indian estuaries i.e. the Narmada, Tapi, Mandovi and the Hooghly falling into the Arabian Sea and the Bay of Bengal respectively. Among these four estuaries, Mo shows nonconservative mixing in the Hooghly (Figure 65) and the Mandovi with its significant removal in lower salinity ranges (0 to 15‰). Mo seems to be removed due to the local anoxia resulting from the wide spread mangrove swamp. Available data on Mo supply (2.0 -2.6 × 10^8 mol/y) to ocean and sink (1.1-1.7 × 10^8 mol/y) from ocean indicate a significant missing sink of Mo if it is in steady state with respect to input/ output. The current study provides an estimate of an additional Mo sink in the range of 0.4 to 3.1 × 10^8 mol/y caused by the presence of mangrove swamps in the worldwide oceans.

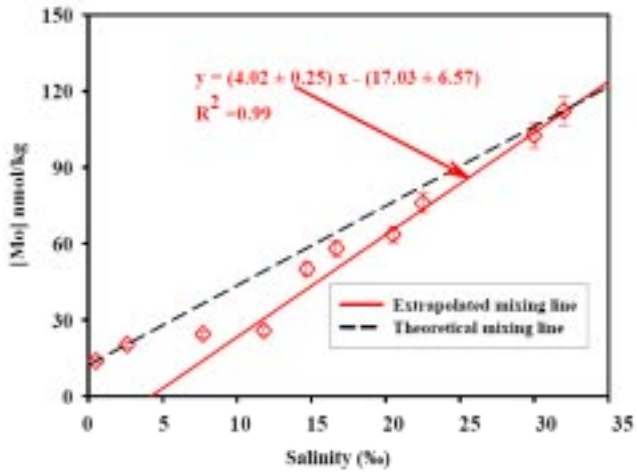

Fig. 65: Mo vs salinity in the Hooghly Estuary

This work is being done in collaboration with Mr. Sanjeev Raghav, GSI, Kolkata

(Waliur Rahaman and Sunil Kumar Singh)

Distribution of redox sensitive elements (Re, U and Mo) in the North Indian Ocean: Impact of OMZ

High productivity in the Arabian Sea (AS) leads to the formation of oxygen deficient sub-surface water where as the mid depth water of the Bay of Bengal (BoB) is equally oxygen deficient due to fresh water stratification. The impact of oxygen minimum zone (OMZ) of these water columns on the biologically important element Mo and geochemically important elements U and Re are assessed in this study. Re, U and Mo are analysed using ICP-MS in the water samples collected from several vertical water profiles in the Bay of Bengal and the Arabian Sea.

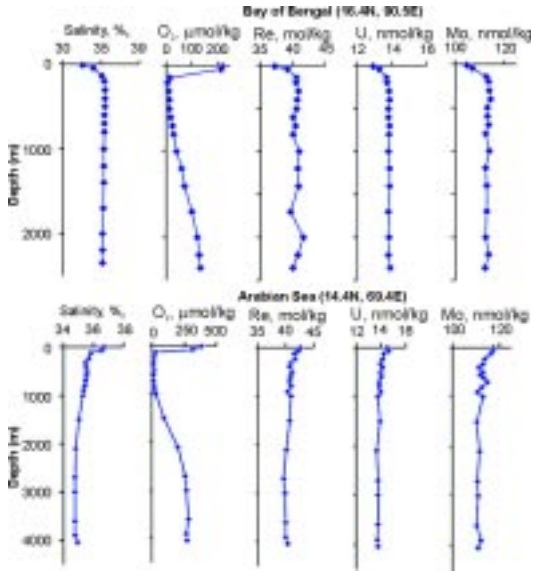

Fig. 66: Distribution of Re, U and Mo in the water columns of the BoB and the AS.

The concentrations of Re, U and Mo in the water columns of the Bay of Bengal and the Arabian Sea display similar ranges and are comparable to those reported for other open oceans. There seems to be no impact of OMZ on the dissolved Re, U and Mo in the Bay of Bengal and the Arabian Sea. The results (Figure 66) indicate very conservative behaviour of Re, U and Mo in the water columns indicating control of the factors in addition to

oxygen on the distribution of redox sensitive elements in the water column.

(Ravi Bhushan, Vineet Goswami, Satinder Pal Singh and Sunil Kumar Singh)

Dissolved ε_{Nd} in the Arabian Sea: Tracking the water masses.

Dissolved Nd isotope composition of the Seawater holds the potential to track the water masses, however its measurement is challenging owing to its low concentration in the dissolved phase. Isotope compositions of the dissolved Nd are measured using TIMS in two vertical water profiles in the Arabian Sea to track the various water masses present in the Arabian Sea. Dissolved ε_{Nd} varies from -11.4 to -7.1 in the two profiles with majority of them are around -9.0 (Figure 67).

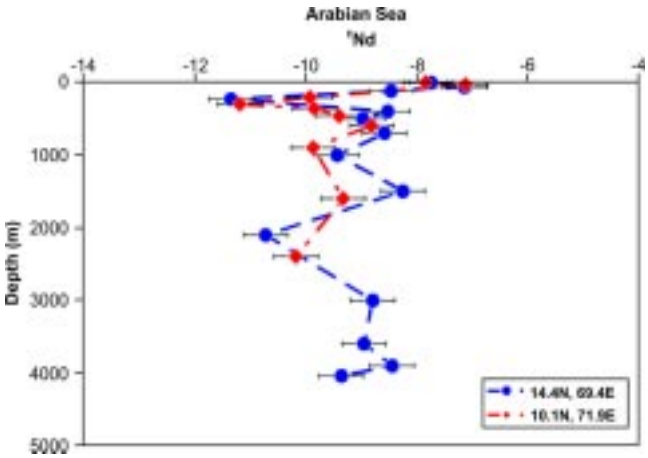

Fig. 67: Dissolved ε_{Nd} in the Arabian Sea

Surface water of both the profiles is more radiogenic indicating its atmospheric input or the impact of riverine supply from Deccan or the Indus river. ε_{Nd}at ~ 200 m water depth is least radiogenic, which could represent the Persian Gulf water.Water at ~ 2000 m show eNd of ~ -10.7 which could be Red Seawater. Except these two depths, ε_{Nd} at remaining water depths are ~ -9, similar to those reported for Antarctic Intermediate Water.

(Ravi Bhushan, Vineet Goswami, Sunil Kumar Singh)

Sr and Nd isotope composition of the sediments of the Arabian Sea: Implication to provenance of sediment and their pathways

Sr and Nd isotope composition of the silicate fraction of the sediments from a well-dated core from the southern Arabian Sea are determined to track their provenance(s) and the pathways of their transport. $^{87}Sr/^{86}Sr$ of these sediments show small variation, 0.7141 to 0.7207 whereas their ε_{Nd} vary considerably, -15.24 to -9.03. Both Sr and Nd isotope compositions of these sediments show significant temporal variation. $^{87}Sr/^{86}Sr$ of these sediments increase at ~ 20 ka and ~ 9 ka with corresponding decrease in ε_{Nd} (Figure 68).

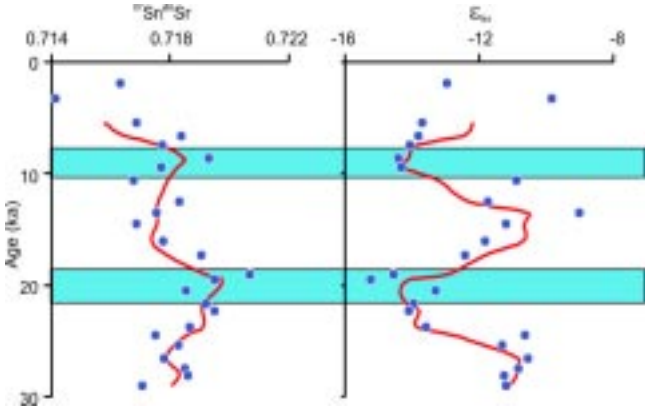

Fig. 68: Variation of $^{87}Sr/^{86}Sr$ and ε_{Nd} of the Arabian Sea sediments with age.

Excursions in Sr and Nd isotope compositions indicate significant climatic control on their sources. Higher $^{87}Sr/^{86}Sr$ and lower ε_{Nd} at ~ 20 ka could be due to increased supply of sediment from the Bay of Bengal to the core site in the Arabian Sea due to diminished SW monsoon and enhanced NE monsoon during the LGM. Excursions in Sr and Nd isotope composition at ~ 9 ka could represent the Holocene intensification of SW monsoon.

(Ravi Bhushan, Vineet Goswami, Sunil Kumar Singh)

Radiocarbon Measurements in the Northern Indian Ocean

The bomb ^{14}C has provided an additional tool to assess more precisely the time scales of various processes associated with carbon exchange among the various Earth surface reservoirs. Radiocarbon measurements in atmosphere over the ocean, in water column, in forams separated from sea sediments and in corals and shells from coasts of India were done at various locations in the northern Indian Ocean. These studies were carried out to determine air-sea exchange rate of CO_2, 'ages' of water masses and circulation time scales in the Arabian Sea and Bay of Bengal, sediment accumulation rates and ^{14}C reservoir ages. The air-sea CO_2 exchange rates in the northern Indian Ocean, as determined from the nuclear bomb produced ^{14}C inventories range from 7 to 17mol.m^{-2}.yr^{-1} (Figure 69). From the average ^{14}C derived CO_2 exchange rates and reported annual surface seawater pCO_2 values, the net flux of CO_2 from the Indian Ocean in the late 1990s has been estimated to ~ 164TgC.yr^{-1}. The entire Arabian Sea is acting as a source

of CO_2, with estimated net ocean-air CO_2 flux of ~ 174TgC.yr^{-1}. The Bay of Bengal is a sink of CO_2, the net uptake rate of atmospheric CO_2 by the entire basin has been estimated to ~ 9TgC.yr^{-1}.

(In collaboration with Dr. K. Dutta, IOP, Bhubneshwar)

(Ravi Bhushan)

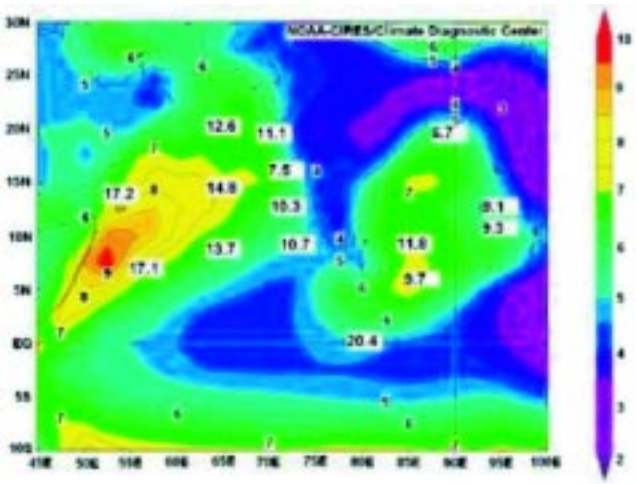

Fig. 69: Air-sea CO_2 exchange rates (moles m^{-2} yr^{-1}) in the northern Indian Ocean.

Geochemistry of Barren Island Volcanics

Barren Island (BI) (12.29°N, 93.85°E) of Andaman and Nicobar Islands, India is the only subaerial active volcano of the Andaman Subduction Zone, and is one of the northernmost volcanoes of the Indonesian Arc. Located on the Burmese plate that overrides the Indian plate, this stratovolcano is believed to have emanated from the ocean floor during the Pleistocene. It has had historic subaerial eruptions during 1787-1832 and has been active since 1991. Study of Nd-Sr isotopic, trace element, and major element characteristics of lava, scoria and ash from the volcano provides insights into the nature of the magma chamber, and the mantle source. Major element analyses of lava, scoria and ash samples reveal that most volcanics are less to moderately evolved (Mg# = 43.5-68.1) basalts or basaltic andesites of subalkalic nature (SiO_2 = 47-57 wt%, $Na_2O + K_2O$ < 5.1wt%,). The high alumina content of most samples (Al_2O_3 > 20 wt%) possibly is a result of dissolution of xenocrystic plagioclase derived from plutonic rocks present in the magma chamber. Alternatively this could indicate a shallow mantle source for these volcanics. Primitive mantle normalized trace element patterns of BI samples indicate that these lavas represent typical subduction zone magmas. They show large relative Nb, Ta and Ti depletions and strong relative enrichments in K and Pb, with lesser enrichment of Sr. $^{87}Sr/^{86}Sr$ of BI lavas vary from 0.70379 to 0.70415, and $^{143}Nd/^{144}Nd$ range from 0.512861 (ε_{Nd} = 4.4) to 0.512992 (ε_{Nd} = 6.9). These data suggest that the BI lavas are derived from a large ion lithophile depleted source, and that their mantle source is marginally enriched with respect to that of the Indian-Mid Oceanic Ridge Basalts (I-MORB). Magmas for the BI lavas appear to be the most primitive in comparison to those in all other volcanoes of the Indonesian Arc. Mixing calculations suggest that the material contribution from the Indian plate slab to the BI magma sources is < 10%. This conclusion is also supported by low Th/Ce ratios (< 0.3) of the lavas.

(Alok Kumar, J.S. Ray and A.D. Shukla)

Geochemistry of sediments from the Vindhyan Supergroup, Rajasthan

The Vindhyan Supergroup is one of the largest and thickest Proterozoic sedimentary sequences of India. Deposited in a time period in the Earth's history that witnessed the beginning of animal life, stabilization of cratons and establishment of modern plate tectonics, the Vindhyan sediments are believed to contain evidences for many of these important events and processes. The evolution of the Vindhyan Basin, which span in space from the Son Valley in the east to the Chambal Valley in the west, in term of sediment provenances and tectonic framework has not yet been understood fully.

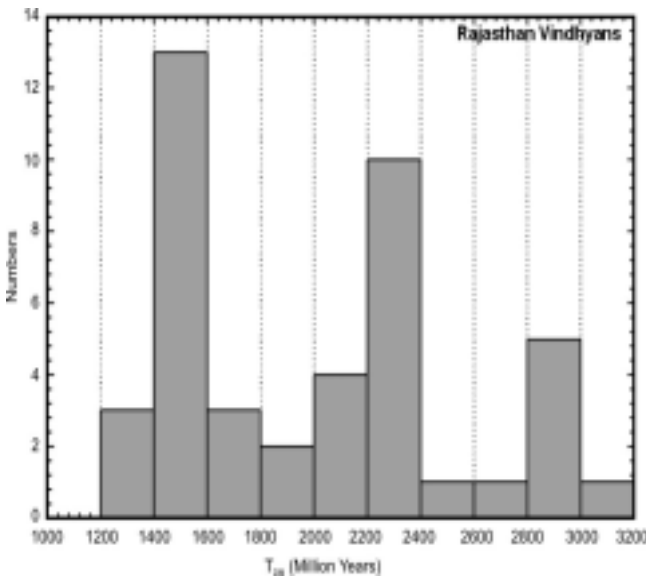

Fig. 70: Distribution of Depleted Mantle Nd model ages (T_{DM}) in the Vindhyan Supergroup.

Geochemical investigations by us using major and trace elements and Nd isotopic ratios on Vindhyan sediments from the western sector (Rajasthan) have revealed the following fascinating aspects about the evolution of this basin. Trace element (REE, Nb/Ta, Zr/Sm, and Ce/Pb) and isotopic (eNd) studies reveal that the rocks of Aravalli Supergroup have been the major source of sediments for the Vindhyans.We find that sediments from granitic gneisses of Aravalli (e.g., Berach Granite) dominate the lower Vindhyans, whereas sediments from mafic igneous rocks (e.g., Khairmalia Andesite) dominate the upper Vindhyans. Depletion of large ion lithophile elements (LILE) and depletions in Nb and Ta suggests that the mafic igneous sources were located on a magmatic arc, which hints at a subduction zone setting for the Vindhyan Basin. The distribution of Nd-model ages (T_{DM}) ages for Vindhyan formations shows two major modes, one at 2300 Ma and the other at 1500 Ma (Figure 70). Both the ages appear to be due to mixing of sediments from at least two major magmatic sources, having different ages. We believe that the older mode is a result of mixing of sediments derived from the ~2500 Ma old basement rocks (e.g., Berach granite) with those derived from younger igneous rocks, the ~1850 Ma old Hindoli Group of rocks and/or the ~2100 Ma old Khairmalia volcanics. The younger mode at 1500 Ma seems to owe its origin to the mixing of sediments derived from two igneous sources: the ~1850 Ma old Hindoli volcanics and the ~800 Ma old Malani Volcanics. The possibility of incorporation of sediments derived from the Malani Igneous Suite in the Vindhyans questions the very claim by some workers that the deposition in the basin ceased prior to 1000 Ma.

(A.D. Shukla and J.S. Ray)

Geochemical study of rosette structures in Deccan Basalts

Large radial columnar jointing structures, popularly known as rosettes, are found in some of the rubbly pahoehoe flows of Deccan Traps. Such structures have been reported from Koyna-Satara region of the Deccan, east of the Western Ghats escarpment, where some of the younger stratigraphic formations (Poladpur, Ambenali and Mahabaleshwar) are exposed at increasing elevations above sea level. Unlike the rosettes described from other basaltic provinces, rosettes from Deccan contain large (several metres across) breccia cores. Field observations, petrographic data, and geochemical data including Nd-Sr isotope data, all indicate that the breccia cores of these rosettes are blocks of the flow-top breccia crusts that became unstable and sank into these flows' molten interiors. This strongly affected the temperature distribution within the molten flow interiors, warped the isotherms around the relatively cold masses, and led to the formation of the breccia-cored rosettes. Our study shows that, whereas lava lakes actively recycle their upper crusts, multiple times, at least one such cycle of crustal overturn and "subduction" can occur, under suitable conditions, in large and thick flood basalt lava flows.

This work was done in collaboration with H.C. Sheth of IIT Bombay, Mumbai.

(J.S. Ray, A.D. Shukla and Alok Kumar)

IWIN National Programme

Comparison of isotopic composition of daily rain (DR) and ground level water vapour (GLV) has provided new insights into origin of vapour sources for rain, and rain-vapour interaction at Ahmedabad. The GLV has a steady baseline isotopic composition and no statistically distinguishable seasonal differences are discernible. The d-excess of GLV indicates that its isotopic composition has a significant contribution from kinetic evaporation of non-local water sources. During a rain event, GLV rapidly interacts with raindrops to establish isotopic equilibrium. On cessation of rainfall, the isotopic composition of GLV quickly returns to the typical baseline value. Contrary to earlier suggestions, it is observed that the amount weighted average monthly isotopic composition of local rain cannot be used to correctly estimate the average isotopic composition of ground level vapor, particularly in the dry climatic regions. Within a rainy season certain large rain events have depleted isotopic compositions compared to other equally large rain events with significantly enriched isotopic composition. The observed isotopic differences cannot be ascribed to variations in the degree or evaporation or amount of rain. This study shows that varying source regions (Arabian Sea/ Bay of Bengal) and cloud top temperature may be responsible for observed differences. It is estimated that at Ahmedabad raindrops reach the ground level undergoing an average evaporative loss of about 10% at an effective Rh of ~96% during fall from the cloud base. The experiments for collecting the ambient atmospheric water vapour revealed an unexpected kinetic fractionation effect associated with condensation of water vapour at 0ºC. Isotopic composition of liquid condensate (collected by condensation on conical metallic surface at 0ºC) was found to be unexpectedly depleted in 180 and enriched in 2H

compared to vapour (collected by complete cryogenic trapping at -78ºC). A theoretical model has been proposed envisaging: (i) kinetic fractionation during diffusive movement of different isotopologues of water from open air (Rh ~ 70%) into a supersaturated boundary layer against the concentration gradient; (ii) Equilibrium fractionation during condensation of water vapour into liquid condensate; and (iii) Evaporation of the condensed water

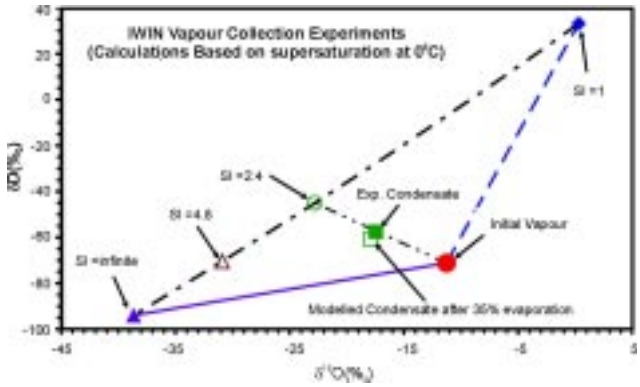

Fig. 71: Modelled isotopic composition of liquid condensate under different degree of super saturation (SI = actual vapour pressure/ saturation vapour pressure).

The model calculations (Figure 71) clearly suggests that the extent of kinetic fractionation is dependent on saturation index (SI), and consequently, on the prevalent relative humidity. The effect of temperature is not seen because the condensing surface is maintained at ~ 0ºC. This model is able to reproduce observed values of the collected liquid condensate.

(R.D. Deshpande, A.S. Maurya, M. Shah and S.K. Gupta)

Theoretical Physics

The Theoretical Physics Division has continued its activity in the fields ofparticle physics, astroparticle physics and cosmology, atomic physics, nuclear physics, quantum mechanics, non-linear dynamics and optics. Significant progress has been made in understanding mechanisms of fermion masses and mixings in extensions of the standard model of particle physics, the nature and origin of dark matter, dynamics of inflation in the early universe,strong interaction physics in matter at high densities, random matrix structure and nuclear shell model, synchronization in dynamical systems. New accurate results have been obtained in calculations involving heavy atoms. Investigations in quantum dynamics and optical vortices have yielded interesting results.

Quasi degenerate neutrinos

Type-I seesaw mechanism is the most popular mechanism for generating neutrino masses. Almost all neutrino mass models based on this mechanism lead to hierarchical neutrino masses. A novel possibility was pointed out which leads instead to quasi Dirac neutrinos. Key ingredient is the construction of an effective theory based on a flavour symmetry dictated by the Yukawa couplings of the theory. This mechanism leads to a simple and phenomenologically consistent description of neutrino masses and provides a nice possibility of generating large lepton asymmetry and measurable flavour violations.

This work was done in collaboration with Sudhir K. Vempati from Indian Institute of Science, Bangalore.

(Anjan S. Joshipura and Ketan M. Patel)

Quasi degenerate neutrinos in SO(10)

The above proposed mechanism for generating quasi degenerate neutrinos was extended to include all fermion masses within an SO(10) grand unified theory. A specific ansatz leading to quasi degenerate neutrino was proposed and was shown to lead to correct description of all fermion masses thereby leading for the first time to an SO(10) model with quasi degenerate neutrinos and type-I seesaw mechanism.

(Anjan S. Joshipura and Ketan M. Patel)

Novel two Higgs doublet models

The conventional two Higgs doublet models are characterized by the absence of (1) the tree level flavour changing neutral currents and (2) CP violating phases other than the one appearing in the quark mixing. We generalized

these models in a way that retains the desirable property (1) but contain additional phases in the charged Higgs couplings to quarks. These models were shown to follow from the study of the flavour symmetries of the quark mass matrices. The extra phases in the charged Higgs couplings were shown to lead to explanation of the possible new phases seen in the mixing of B mesons.

(Anjan S. Joshipura and Bhavik P. Kodrani)

Charged-Higgs signals from polarization of top in single-top production at LHC

Single top events, though rare, have been seen at the Tevatron. At the LHC (Large Hadron Collider), a million events are expected to be seen. In extensions of the standard model (SM) which have two Higgs doublets, an additional possibility is single-top production associated with a charged Higgs. It is proposed that a search for top polarization in such a process, measured through the secondary decay lepton productions, would be a sensitive probe of the parameters of the model. The charged-lepton azimuthal distribution, for a given value of charged-Higgs mass, is extremely sensitive to tan β, the ratio of the scalar vacuum expectation values, which characterize the model.

This work was carried out in collaboration with S.K. Rai of Oklahama State University and K. Rao of University of Helsinki.

(S.D. Rindani and Pankaj Sharma)

Polarization measurement at LHC for highly boosted quarks

The top quark, being the heaviest quark, is likely to play a special role in the understanding of the mechanism of spontaneous gauge symmetry breaking, which takes place at a scale similar to the top-quark mass. At the same time, since the top quark decays before it hadronizes, it affords a unique platform to study top polarization mechanisms, as spin information is maintained in the top decay products. Angular distributions of these decay products serve as ideal measures of top polarization. However, tops arising from possible heavy resonances predicted by several models would be highly boosted, and consequently, the decay products would be confined to a narrow cone in the direction of the top momentum. Angular distributions would thus be hard to measure. Alternative variables suggested are energy fractions of the top carried by leptons or *b* quarks. It is shown here that these variables do not necessarily measure the top polarization, unless anomalous *tbW* couplings are accounted for.

This work was done in collaboration with Rohini M. Godbole (CHEP, Indian Institute of Science, Bangalore.

(S.D. Rindani)

Common origin for visible and dark matter in the universe

The visible component of matter in our universe is mostly matter with negligible amount of antimatter. This matter-antimatter asymmetry could be generated in the early universe if there was CP violation and lepton number violation, which is again related to neutrino masses and mixing. Since the amount of visible matter is comparable to the amount of dark matter in the universe, we tried to explain the origin of both the visible and dark matter from the same mechanism and relate it to the neutrino masses and mixing. In our model, the dark matter relic density is a dark matter asymmetry generated simultaneously with the baryon asymmetry so that we can naturally understand the coincidence between the visible and dark matter. It has recently been argued that the dark matter may also be responsible for the cosmic positron and electron excesses, which can be explained naturally in the present model as the dark matter mostly decays into the leptons.

This work was done in collaboration with P. Gu from MPI-Heidelberg, Germany and H.B. Zhang from IHEP, CAS, Beijing, China.

(Utpal Sarkar)

Spontaneous Parity Violation in Supersymmetric Models

The left-right symmetric extension of the standard model of particle physics was proposed with a view to explain the origin of parity violation through spontaneous symmetry breaking. However, in the supersymmetric version of the theory, implementation of spontaneous parity breaking became very difficult. Several attempts were made to solve this problem, but all these solutions end up with some new crisis. We proposed a novel implementation of spontaneous parity breaking in supersymmetric left–right symmetric model, avoiding the problems encountered in previous studies. This implementation includes bi-triplet and singlet scalar fields, in addition to the bi-doublets which extend the Higgs sector of the Minimal Supersymmetric Standard Model (MSSM). The supersymmetric vacua of

this theory are shown to be consistent with phenomenology including the neutrino masses.

This work was done in collaboration with A. Sarkar from Institute of Physics, Bhubaneswar and U. Yajnik from Indian Institute of Technology, Mumbai.

(S. Patra and Utpal Sarkar)

Boson stars: Chemical potential and quark condensates

We have studied equilibrium solutions of a boson star in the mean field approximation using a general relativistic framework. Dynamics of the constituent matter in such a star is described by a scalar field. The statistical aspect of the matter equilibrium is investigated by incorporating the effect of finite chemical potential in equation of state. We analyze the two possible situations where the scalar field is either a composite one -suitable for describing diquark-condensates or a fundamental. We derive a generalized set of Tolman-Oppenheimer-Volkov (TOV) equations to incorporate the metric dependence of chemical potential in general relativity. It is demonstrated that the introduction of finite chemical potential can lead to a new class of the solutions where the maximum mass and radius of a star change in a significant way. In general the density profile has node like structures due to introduction of finite chemical potentials. It is shown that these nodes can be avoided by applying constraints on the values of the central pressure and central chemical potential. This in turn can reduce the parameter space available for the stable solutions.

We have shown that when the self-interaction of the condensate is negligible, the typical energy density of the star is too high to have a boson star of diquark condensates. Our results indicate, even after the effect of self-interaction is incorporated, the stable equilibrium can occur only in a low-density and high pressure regime. Thus the boson stars of diquarks are very difficult to be formed in nature.

(Jitesh R. Bhatt and V. Sreekanth)

Neutrino Condensate as Origin of Dark Energy

We propose a new solution to the origin of dark energy. We suggest that it was created dynamically from the condensate of a singlet neutrino at a late epoch of the early Universe through its effective self interaction. This singlet neutrino is also the Dirac partner of one of the three observed neutrinos, hence dark energy is related to neutrino mass. The onset of this condensate formation in the early Universe is also related to matter density and offers an explanation of the coincidence problem of why dark energy (70%) and total matter (30%) are comparable at the present time. We demonstrate this idea in a model of neutrino mass with (right-handed) singlet neutrinos and a singlet scalar.

This work was done in collaboration with B. Desai and E. Ma from University of California and G. Rajasekharan from Institute of Mathematical Sciences, Chennai.

(Jitesh R. Bhatt and Utpal Sarkar)

Hard Thermal Photons in QGP and non-ideal effects

Thermal photons are a promising tool to investigate the quark-gluon plasma formed in relativistic heavy-ion collisions. We have investigated the thermal photon production-rates using one dimensional boost-invariant second order relativistic hydrodynamics to find proper time evolution of the energy density and the temperature. The effect of bulk-viscosity and non-ideal equation of state are taken into account in a manner consistent with recent lattice QCD estimates. It is shown that the non-ideal gas equation of state i.e e-3p¹0 behaviour of the expanding plasma, which is important near the phase-transition point, can significantly slow down the hydrodynamic expansion and thereby increase the photon production-rates. Inclusion of the bulk viscosity may also have similar effect on the hydrodynamic evolution. However the effect of bulk viscosity is shown to be significantly lower than the non-ideal gas equation of state. We also analyze the interesting phenomenon of bulk viscosity induced cavitation making the hydrodynamical description invalid. It is shown that ignoring the cavitiation phenomenon can lead to a very significant over estimation of the photon flux. It is argued that this feature could be relevant in studying signature of cavitation in relativistic heavy ion collisions.

(Jitesh R. Bhatt, H. Mishra and V. Sreekanth)

Meson mass corrections to form factors in large energy effective theory and implications for semi-leptonic decays

Semi-leptonic decays of B mesons can provide clean signatures of new physics beyond the standard model of particle interactions. However, theoretical calculations are limited by hadronic uncertainties stemming from the form factors describing the hadronic transitions. It has been

found that in the cases where the final state meson associated with the lepton pair is light, significant simplification takes place and simple results for form factors are obtained. The same methodology is generally applied to the case when the final state meson is reasonably heavy due to lack of the proper knowledge of the final state meson mass corrections to the usually employed form factors and their relations. We incorporate the leading corrections in meson mass and study the relevant phenomenology. It is found that for certain observables and in certain kinematic regions, these corrections can be significant. We discuss the implications for extracting the short distance information in the presence of such correction terms for the most relevant decay modes.

(Namit Mahajan)

$B_S \to \chi_{(c0)}\varphi$ branching ratio and time dependent CP asymmetry

The mode $B_S \to \chi_{(c0)}\varphi$ is a very interesting and important one for two main reasons. First, the final state is a pure CP odd state and hence the study of time dependent CP asymmetry for this state can be used to confront the expectations from the usually employed and suggested $B_S \to J/\psi(\eta\eta')\varphi$ states. The second reason is the fact that due to the quantum numbers of $\chi_{(c0)}$ it is a scalar charmonium state), the naive estimates yield a rate that is identically zero. A similar result holds for $B \to \chi_{(c0)}K$ decays where it is found that the branching ratio is reasonably large. The current experiments and the upcoming LHCb experiment will study CP violation in the B_σ sector with high precision. This will require a precise value for the branching ratio. We calculate the decay rate including the colour octet contribution and find a large value for the branching ratio. This in turn also implies that there will be enough statistics available to perform a time dependent analysis and obtain a value for the CP violating phase β_σ. Also, because of the quantum numbers of the particles in the final state, no angular analysis will be needed, implying better efficiency. The value of ϕ_S obtained via this mode can be compared with the value obtained through the angular analysis of $B_S \to J/\psi\varphi$ rate. Any discrepancy (beyond the overall sign) will be a signal of new physics in B_σ sector or more generally $b \to s$ transitions.

This work is being done in collaboration with Rupak Datta of Institute of Mathematical Sciences, Chennai, India.

(Namit Mahajan)

TeV scale electromagnetic leptogenesis

Leptogenesis is one of the most popular and economical mechanism for generating the observed matter anti-matter asymmetry of the universe. This also provides a link between the high scale CP violation and neutrino mass. In this work we extend the standard model of particle interactions by adding three right handed neutrinos, a singly charged scalar, two scalar doublets and an extra vector-like heavy lepton. This extension allows us to have resonant electromagnetic leptogenesis at the TeV scale, where the heavy right handed neutrino decays to a light neutrino and a photon. Within this model it is possible to disentangle the neutrino masses from neutrino magnetic moments, a feature which is desirable but almost impossible to attain in most constructions. We also comment on possible signals at the LHC as a direct way to test the model.

This work is being done in collaboration with Debajyoti Choudhury of University of Delhi, Delhi, India.

(Namit Mahajan, Sudhanwa Patra and Utpal Sarkar)

Kinetics of chiral phase transition in hot and dense quark matter in the inertia dominated regime

We study the kinetics of chiral phase transition in dense matter in the context of looking for QCD critical point in relativistic heavy ion collision experiments. While most of the theoretical investigations have been so far based on equllibrium properties, the experimental situation is actually a non-equllibrium process. In this context we study the phase transition kinetics for chiral transition in dense quark matter. Using a variational method we calculate the thermodynamic potential for two flavor quark matter in Nambu Jona Lasinio model. We then use a Ginzburg Landau expansion of free energy near the transition. We then discuss the dynamics of phase transition by solving a Langevin equation with a dissipative force and study the ordering dynamics. For quench through a second order transition, the evolution of the domains proceed through a spinodal decomposition. For a quench through a first order transition, the evolution is described by a bubble nucleation followed by spinodal decomposition. The growth of domains at later times follows Allen-Chan growth law $L(t) \sim t^{1/2}$.

This work was done in collaboration with A. Singh and S. Puri from Jawaharlal Nehru University, New Delhi.

(H. Mishra)

Chiral transition with strong magnetic fields

Very strong magnetic fields $eB \sim m_p^2$ could be there in the interior of ultra dense compact astrophysical objects like neutron stars. Even stronger magnetic fields can also be produced during relativistic heavy ion collisions. In this context, we investigate the structure of QCD vacuum and chiral symmetry breaking in presence of strong magnetic fields. We also investigate the phase structure of hot quark matter along with possible strong CP violation in presence of such ultra strong magnetic fields.

This work was done in collaboration with B. Chatterjee and A. Mishra from Indian Institute of Technology, New Delhi

(H. Mishra)

Minimal Textures in Seesaw Mass Matrices and their low and high Energy Phenomenology and lepton flavour violation.

In an attempt to find minimal scenarios we study the implications of Dirac and Majorana mass matrices with texture zeros within the type I seesaw mechanism. For the Dirac mass matrices we consider 5 zero textures which we show to be the most minimal form that can successfully account for low energy phenomenology if the Majorana mass matrices are chosen minimal as well. For those, we consider both diagonal and even more minimal non-diagonal forms. The latter can be motivated e.g. by simple U(1) flavour symmetries and have two degenerate eigen values. We classify the allowed textures and discuss the ramifications for leptogenesis.

This work was done in collaboration with Werner Rodejohann from Max-Planck Institute, Heidelberg, Germany.

(Srubabati Goswami and Subrata Khan)

Large U_{e3} and Tri-bimaximal Mixing

We investigate in a model-independent way to what extent one can perturb tri-bimaximal mixing in order to generate a sizable value of U_{e3}, while at the same time keeping solar neutrino mixing near its measured value, which is close to $\sin^2\theta_{12} = 1/3$. Three straightforward breaking mechanisms to generate U_{e3} of about 0.1 are considered. For charged lepton corrections, the suppression of a sizable contribution to the 12 mixing angle can be achieved if CP violation in neutrino oscillations is almost maximal. Generation of the indicated value for the magnitude of U_{e3} of about 0.1 through renormalization group corrections requires the neutrinos to be quasi-degenerate in mass. The consistency with the allowed range 12 mixing angle together with large running of the magnitude if U_{e3} forces one of the Majorana phases to be close to p. This implies large cancellations in the effective Majorana mass governing neutrino-less double beta, constraining it to lie near its minimum allowed value. Finally, explicit breaking of the neutrino mass matrix in the inverted hierarchical and quasi-degenerate neutrino mass spectrum cases is similarly correlated with the effective Majorana mass, although to a lesser extent. The implied values for the atmospheric neutrino mixing angles are given in all cases.

This work was done in collaboration with S.T. Petcov from SISSA, Italy and S. Ray from Tata Institute of Fundamental Research, Mumbai and W. Rodejohann from Max-Planck Institute, Heidelberg, Germany.

(Srubabati Goswami)

Collective Flavor Oscillations Of Supernova Neutrinos and r-Process Nucleosynthesis

Neutrino-neutrino interactions inside core-collapse supernovae may give rise to flavor oscillations resulting into collective swap of flavors. These oscillations depend on the initial energy spectra and initial relative fluxes or initial luminosities of the neutrinos. It has been observed that departure from energy equipartition among different flavors can give rise to one or more sharp spectral swap over energy termed as splits. We study the occurrence of splits in the neutrino and antineutrino spectra varying the initial relative fluxes for different models of initial energy spectrum in both normal and inverted hierarchy. These initial relative flux variations give rise to several possible split patterns where as variation over different models of energy spectra give similar results. We explore the effect of these spectral splits on the electron fraction, Y_e, that governs r-process nucleosynthesis inside supernovae. Assuming the condition Y_e, needed for successful r-process nucleosynthesis we present exclusion plots of the initial luminosities or relative fluxes, including the effect of collective oscillations.

This work was done in collaboration with S. Chakroborty and S. Kar from Saha Institute of Nuc lear Physics, Kolkata and S. Choubey from Harishchandra Research Institute, Allahabad.

(Srubabati Goswami)

Magnetic field generation in Higgs inflation model

We study the generation of magnetic field in Higgs-inflation models where the Standard Model Higgs boson has a large coupling to the Ricci scalar. We couple the Higgs field to the Electromagnetic fields via a non- renormalizable dimension six operator suppressed by the Planck scale in the Jordan frame. We show that during Higgs inflation magnetic fields with present value 10^{-6} Gauss and comoving coherence length of 100 kpc can be generated in the Einstein frame. The problem of large back-reaction which is generic in the usual inflation models of magneto-genesis is avoided as the back-reaction is suppressed by the large Higgs-curvature coupling.

(Moumita Das and Subhendra Mohanty)

The Quantum Phase of Inflation

Inflation models can have an early phase of inflation where the evolution of the inflaton is driven by quantum fluctuations before entering the phase driven by the slope of the scalar field potential. For a Coleman-Weinberg potential this quantum phase lasts 10^{7-8} e-foldings. A long period of fluctuation driven growth of the inflation field can possibly take the inflaton to the bottom of its potential, or past the value of the field where our current horizon scale crosses the horizon. Alternatively, the inflaton could have high kinetic energy at the end of the quantum phase. All these possibilities will change inflation and the density spectrum significantly. Therefore we study these issues in the context of new inflation, chaotic inflation and natural inflation. New scenarios where cosmological relevant scales leave during the quantum phase are explored but are found to be unfeasible. A new phase of thermal fluctuation driven inflation is proposed, in which during inflation the inflaton evolution is governed by fluctuations from a sustained thermal radiation bath rather than by a scalar field potential.

This work was done in collaboration with A. Berera from the University of Edinburgh, UK.

(Raghavan Rangarajan)

Anticipatory synchronization with variable time delay and reset

When two dynamical systems are coupled they synchronize under suitable conditions. It is also possible that one system (response system) can anticipate the behaviour of the other system (drive system), i.e. the response system can predict the behaviour of the drive system. We propose a new method of anticipatory synchronization based on variable delays. The method has the advantage that the response system requires only intermittent information about the drive system. We determine the conditions under which such an anticipatory synchronization can be obtained. This gives us the maximum time for which anticipation is possible. The numerical calculations in standard systems like the Rossler and Lorenz systems are used to demonstrate the method and the results of the analysis. The method may have applications in secure communications.

(R. E. Amritkar and G. Ambika)

Estimating parameters of a nonlinear dynamical system

A new method based on a modified Newton-Raphson scheme is introduced to estimate parameters of a nonlinear dynamical system from the time series data of the variables. The method removes some of the problems associated with the standard synchronization based methods. An important achievement of this method is that it is possible to determine the exact form of dynamical equations for systems with quadratic nonlinearity.

(R. E. Amritkar)

Multifractal spectrum of a chaotic attractor

A chaotic attractor is usually characterized by its multifractal spectrum which gives a geometric measure of its complexity. We present a characterization using a minimal set of independent parameters which are uniquely determined by the underlying process that generates the attractor. The method maps the f-alpha spectrum of a chaotic attractor onto that of a general two scale Cantor measure. We show that the mapping can be done exactly for a large number of chaotic systems.

We show that the existing methods for computing the f-alpha spectrum from a time series can be improved by using a new algorithmic scheme. The scheme relies on the basic idea that the smooth convex profile of a typical f-alpha spectrum can be fitted with an analytic function involving a set of three independent parameters. While the standard existing schemes generally compute only an incomplete f-alpha spectrum, we show that this can be overcome by an algorithmic approach which is automated

to compute the f-alpha spectrum from a time series for any embedding dimension.

(R. E. Amritkar, K. P. Harikrishnan, R. Misra and G. Ambika)

Large Shell Model Description of odd-even $^{61-67}$Co and odd-odd $^{58-62}$Mn isotopes

Low-lying spectra and several high-spin states of odd-even $^{61-67}$Co isotopes are calculated in two different shell model spaces with largest dimensions ~ 20 × 10^6 in the *m*-scheme. First set of calculations have been carried out in *fp* shell valence space (full *fp* space for ^{63,65,67}Co and a truncated one for ^{61}Co) using two recently derived *fp* shell interactions namely GXPF1A and KB3G with ^{40}Ca as core. Similarly, the second set of calculations have been performed in $fpg_{9/2}$ valence space using an *fpg* effective interaction due to Sorlin *et al.*, with ^{48}Ca as core and imposing a truncation. The present calculations show that the results of GXPF1A and KB3G are reasonable for ^{61,63}Co and point out that these interactions need some modifications. For ^{65,67}Co as we move towards $N = 40$, inclusion of $g_{9/2}$ orbital is important and shell model results show that the present form of the *fpg* interaction is not suitable for neutron rich Co isotopes and further modifications of this interaction are required. A similar study has been carried out for negative parity levels in odd-odd neutron rich $^{58-62}$Mn nuclei.

(V.K.B. Kota and P.C. Srivastava)

Deformed Shell Model Results for Two Neutrino Positron Double Beta Decay of ^{84}Sr

Half-lives $T_{1/2}^{2\nu}$ for two neutrino positron double beta decay modes b^+EC/ECEC are calculated for ^{84}Se, a nucleus of current experimental interest, using deformed shell model based on Hartree-Fock states employing a modified Kuo interaction in ($^2p_{3/2}$, $^1f_{5/2}$, $^2p_{1/2}$, $^1g_{9/2}$) space. The calculated half-life for the ECEC mode is ~ 10^{25} yr and it may be possible to observe this in the near future in the planned ^{84}Sr experiments using $SrCl_2$ crystals at KyungPook National University, South Korea.

This work was done in collaboration with R. Sahu from Berhampur University, Berhampur.

(V.K.B. Kota)

Transitions in eigenvalue and wavefunction structure in (1 + 2)-body random matrix ensembles with spin

Finite interacting Fermi systems with a mean-field and a chaos generating two-body interaction are modeled by one plus two-body embedded Gaussian orthogonal ensemble of random matrices with spin degree of freedom [called EGOE(1 + 2)-**s**]. Numerical calculations are used to demonstrate that, as I, the strength of the interaction (measured in the units of the average spacing of the single particle levels defining the mean-field), increases, generically there is Poisson to GOE transition in level fluctuations, Breit-Wigner to Gaussian transition in strength functions (also called local density of states) and also a duality region where information entropy will be the same in both the mean-field and interaction defined basis. Spin dependence of the transition points I_c,I_F and I_d respectively is described using the propagator for the spectral variances and the formula for the propagator is derived. It is further established that the duality region corresponds to a region of thermalization. For this purpose, the single particle entropy defined by the occupancies of the single particle orbitals is compared with the thermodynamic entropy and information entropy for various I values and they are very close to each other at $I = I_d$. Further, the formula for the spectral variances is used to provide a simple description of some of the ground state properties of mesoscopic systems.

This work was done in collaboration with N.D. Chavda from The M.S. University of Baroda, Vadodara.

(V.K.B. Kota and Manan Vyas)

Spectral Properties of Embedded Gaussian Unitary Ensemble of Random Matrices with Wigner's *SU(4)* Symmetry

Continuing with our work on the new random matrix ensemble (for *m* fermions in W number of single particle orbitals, each four-fold degenerate) EGUE(2)-*SU(4)* introduced last year, several numerical calculations are carried out for general *SU(4)* irreps with W = 6 and 10 as appropriate for nuclear (*2s1d*) and (*2p1f*) shell nuclei. Firstly, spectral variances clearly showed, by applying the Jacquod and Stone prescription, that the EGUE(2)-*SU(4)* ensemble generates ground state structure just as the quadratic Casimir invariant (C_2) of *SU(4)*. This is further corroborated by the calculation of the expectation values of C_2[*SU(4)*] and the four periodicity in the ground state energies. Secondly, it is found that the covariances in energy centroids and spectral variances increase in magnitude considerably as we go from EGUE(2) for spinless fermions to EGUE(2) for fermions with spin to EGUE(2)-*SU(4)* implying that the differences in ensemble and spectral averages grow with increasing symmetry. Also for EGUE(2)-*SU(4)* there are, unlike for GUE, non-zero cross correlations in energy centroids and spectral variances

defined over spaces with different particle numbers and/or $Y(\Omega)$ [equivalently *SU(4)*] irreps. In the dilute limit defined by $\Omega \to \infty$, $\rho >> 1$ and $\rho/\Omega \to 0$, for the $\{4^{\rho},\pi\}$ irreps, we have derived analytical results for these correlations.

(V.K.B. Kota and Manan Vyas)

Random matrix structure of nuclear shell model Hamiltonian matrices

We have carried out a comprehensive analysis of the structure of Hamiltonian matrices based on visualization of the matrices in three dimensions as well as in terms of measures for GOE, banded and two-body random matrix ensembles (TBRE). We have considered two nuclear shell model examples, ^{22}Na with $J^{\pi}T=2^{+}0$ and ^{24}Mg with $J^{\pi}T = 0^{+}0$; (Figure 72) shows ^{22}Na *H* matrix and (Figure 73) for ^{24}Mg in a different representation. It is clearly established that the matrices are neither GOE nor banded random matrix type.

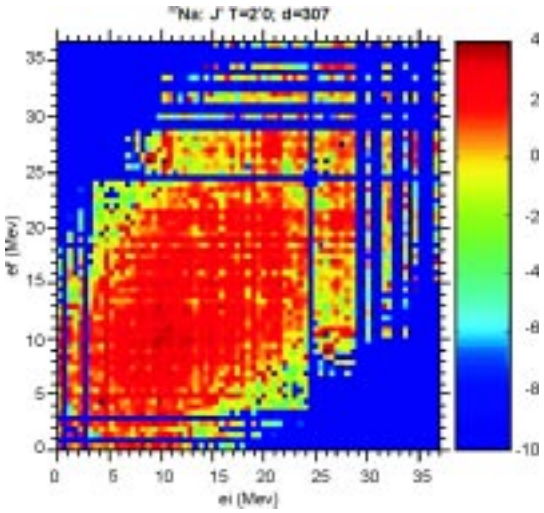

Fig. 72: Plot of squares of matrix elements averaged over an area in (e_i,e_f) plane as a function of basis state energies (e_i,e_f) for ^{22}Na nucleus. Color code for the size of the matrix elements is also shown. Clearly, the *H* matrix for ^{22}Na nucleus is neither GOE nor banded.

For the TBRE structure we have examined the correlations between diagonal elements and eigen values, fluctuations in the basis states variances and structure of the two-body part of the Hamiltonian in the eigenvalue basis. The present study, by combining with the analysis carried out by groups in Michigan and Heidelberg, conclusively established that the nuclear shell model Hamiltonians can be well represented by TBRE.

(V.K.B. Kota and Manan Vyas)

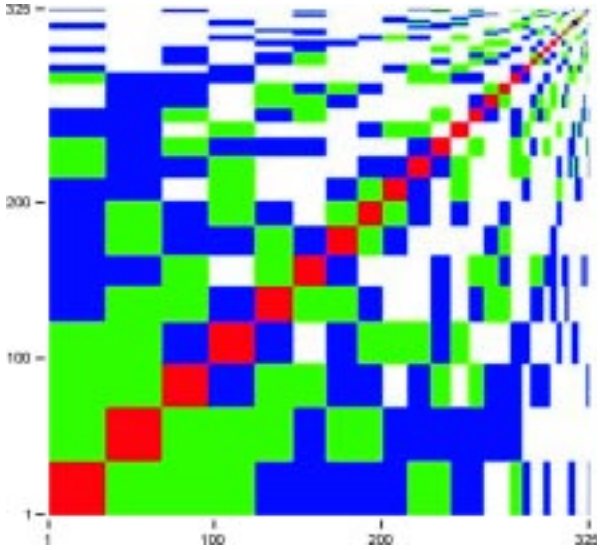

Fig. 73: Block matrix structure of the *H* matrix for ^{24}Mg displaying two-body selection rules. The diagonal blocks shown in red correspond to the region in the matrix connected by two-body interaction that does not involve change in the ccupancy of the nucleons. Similarly green(blue) correspond to change of occupancy of one(two) nucleons. Finally, white corresponds to the region forbidden by two-body selection rules.

On the calculation of inner products of Schur functions

Two methods for calculating inner products of Schur functions in terms of outer products and plethysms are implemented for large scale machine calculations. One of these is derived from a recent analysis of the *SO(8)* proton-neutron pairing model of atomic nuclei by our group. In group theory reduction of the Kronecker product of two S_n irreps into S_n irreps corresponds to inner product of Schur functions. The two methods we have used allow for generation of inner products for the Schur functions of degree up to 20 and even beyond and this represents a major advance since the tabulations by James and Kerber and Wybourne for $n \leq 9$.

This work was done in collaboration with J.A. Castilho Alcarás from Instituto de Fßsica Teórica, Universidade Estadual Paulista, UNESP, São Paulo, Brazil.

(V.K.B. Kota)

We have carried out a detailed and systematic study of the correlation energies of inert gas atoms Ne, Ar, Kr and Xe using relativistic many-body perturbation theory and relativistic coupled-cluster theory. In the relativistic coupled-cluster calculations, we implement perturbative triples and

include these in the correlation energy calculations. We then calculate the dipole polarizability of the ground states using perturbed coupled-cluster theory.

This work was done in collaboration with K.V. P. Latha from Indian Institute of Astrophysics, Bangalore.

(B. K. Mani and D. Angom)

Scattering length for fermionic alkali atoms

We examine the use of WKB approximation to determine *p*-wave scattering length. For this we solve the *p* partial wave Schrödinger equation and analyze the validity of adopting the semiclassical solution to evaluate the constant factors in the solution. We also calculate the *p*-wave scattering lengths of ^{6}Li and ^{40}K for the $a^3S_u^3$ and X^1S_g states respectively using variable phase method. The *p*-wave scattering lengths of ^{132}Cs and ^{134}Cs are also calculated. Based on our calculations, the value of the *p* wave scattering lengths of ^{6}Li and ^{40}K are $-36a_o$ and $-95a_o$ respectively.

(S. Gautam and D. Angom)

Probing CP violation with the electric dipole moment of atomic mercury

The electric dipole moment of atomic ^{199}Hg induced by the nuclear Schiff moment and tensor-pseudotensor electron-nucleus interactions has been calculated. For this, we have developed and employed a novel method based on the relativistic coupled-cluster theory. The results of our theoretical calculations combined with the latest experimental result of ^{199}Hg electric dipole moment, provide new bounds on the T reversal or CP violation parameters q_{QCD}, the tensor-pseudotensor coupling constant C_T and d_u - d_d. This is the most accurate calculation of these parameters to date. We highlight the crucial role of electron correlation effects in their interplay with the P,T violating interactions. Our results demonstrate substantial changes in the results of earlier calculations of these parameters which can be attributed to the more accurate inclusion of important correlation effects in the present work.

This work was done in collaboration with K. V. P. Latha and B. P. Das from Indian Institute of Astrophysics, Bangalore and D. Mukherjee from Indian Association for Cultivation of Science, Kolkata.

(D. Angom)

High Energy Emissions from Young Stellar Object (YSO)

X-ray emissions from Young Stellar Objects (YSO) are detected by many X-ray missions like Einstein X-ray Observatory, ROSAT Observatory etc. These missions provide a lot of important information about the X-ray properties of YSOs. However, the emission processes are not fully understood. A simple model is proposed for the generation of emissions from a Young Stellar Object on the basis of a simple interaction between the YSO and its surrounding circumstellar accretion disk containing neutral gas and the charged dust. It is assumed that the YSO has weak dipole type magnetic field and its field lines are threaded into the circumstellar disk. Considering the motion of ions and charged dust particles in presence of neutral gas, it is shown that the sheared dust-neutral gas velocities can lead to the current along the ambient magnetic field direction. This current becomes quite large and is capable of generating an electric field along the magnetic field lines. It is shown how the particles can gain energy up to MeV range and above, which can produce high-energy radiation from YSO.

(A.C. Das)

Engineering the size of the dark core of an optical vortex

An optical vortex is a light beam having a helical wave front and a zero intensity region - a dark core - in the centre when viewed in the direction of the propagation of the light beam. They can be created using computer generated holographic technique. We have studied the effect of the resolution of the computer generated hologram on the intensity profile of the vortex beam. With increase in the resolution of the grating element the intensity profile of the vortex has been found to vary in such a way that the diameter of the core goes on decreasing. This has been tested by taking the horizontal line intensity profile of the vortex beams obtained by simulation and with the experimentally recorded images.

The result we obtained suggests that in the case of vortex beams produced using computer generated holography, the vortex diameter can be controlled by simply varying the resolution of the hologram. In digital holography it is determined by the number of values stored. We suggest that this method can be used directly for controlling and confining the microscopic particles with lower refractive index than surroundings. Just by online control of the

hologram resolution, the region of confinement as well as the mobility of these particles can be controlled, after proper calibration.

(Ashok Kumar, Pravin Vaity and R. P. Singh)

Diffraction characteristics of optical vortex passing through an aperture

The diffraction of an optical vortex through an iris diaphragm which is a close approximation to a circular aperture has been investigated experimentally and theoretically. The results are compared with those obtained from the diffraction of a Gaussian beam through the same aperture. The singularity of the vortex beam is found to be consistent even after the diffraction through the aperture. We observe very interesting ball bearing sort of structures of darkness and brightness in the diffraction of the vortex and the Gaussian beams through the iris diaphragm. These structures look similar to the vortices; however by doing interferometry we have confirmed that these are not the vortices. Unlike the vortex diffraction where the centre of diffracted beam is always dark, in the case of a Gaussian beam the centre of diffracted beam may be dark or bright. The resulting interference fringes do not show any signature of the presence of singularity in the diffracted Gaussian beam.

The ball bearing sort of structures may be useful in optical trapping experiments. These structures may be utilized as a multiple trap. Moreover, in the diffracted pattern of the vortex if we trap an absorptive particle at the centre it will gain orbital angular momentum of light due to vortex and will start rotating. Meanwhile if we use the ball bearing structures as the trap centre for other particles then it would be very interesting to observe the effect of the central rotating particle on the neighboring stationary trapped particles.

(Ashok Kumar, Pravin Vaity and R. P. Singh)

Experimental study of power decay of optical vortices in photorefractive material

We have experimentally investigated decay rate of the power of optical vortices on propagation through the photorefractive crystal ($Sr_{0.61}Ba_{0.39}Nb_2O_6$: Ce). The results were compared with that of a Gaussian beam. We found that the decay rates for vortex beams are slower than that of Gaussian beam. It has also been observed that the decay rate for vortex depends on the sign as well as the magnitude of the topological charge, as the topological charge of the vortex increases the decay rate decreases.

(Pravin Vaity, Ashok Kumar and R.P. Singh)

Wave packet dynamics of a particle in an infinite potential well

Under certain conditions, the initial wave packet of some quantum systems revives after a certain time T_{rev} and at fractions m / n of that time, the initial wave packet breaks up into n replicas. This is known as the revival and fractional revival of a wave packet.

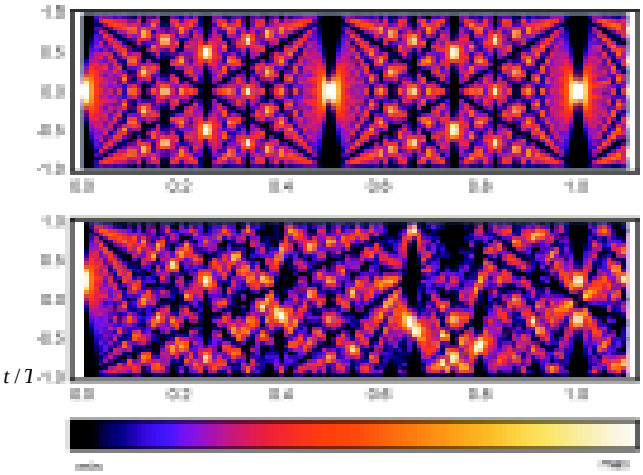

Fig.74: Space - time probability density of a particle inside an infinite potential well bounded by walls at $x=\pm b$. The horizontal and vertical axes represent the normalized variables and x / b, respectively. The initial wave packet is a Gaussian with zero mean momentum and is localized at (top figure) $x=0$ and (bottom figure) $x/b=0.25$. Note how the offset severely distorts the bottom figure. Our analytical result is, nevertheless, able to explain and reproduce the patterns in both figures.

We have made a detailed study of this phenomenon (Figure 74) for a particle in an infinite potential well bounded by walls at x = ± b. In this work, the initial wave packet can be symmetric, anti-symmetric or without any definite parity. It can be on-axis (i.e. centered at x = 0), or it may be offset from the center by an arbitrary amount Δb. The fraction m/n can be formed by having (a) m odd and n even such that $n = 0$ (mod 4), (b) m odd and n even such that $n = 2$ (mod 4), (c) m even and n odd, (d) m odd and n odd.

For the sake of clarity, we have fixed the unit of time to be the revival time T of an on-axis anti-symmetric wave packet and chosen an arbitrary time $t = (N + m/n)T$ where N is an

integer. The novelty of this work is that the fractional revival at time t for all the above scenarios can be written analytically as a finite sum of n terms only and, for each case, it depends explicity on whether the product Dn is positive or negative, integer (even or odd) or non-integer.

(J. Banerji)

Generation of Schrödinger cats and Sub-Planck sturctures in quantum states of light

The simplest quantum state of light is, perhaps, the number state $|n\rangle$ containing n photons. A particular superposition of these states produces the widely used coherent states of light. It has been known for sometime that coherent states propagating in a nonlinear (Kerr) medium generate Schrödinger cat states. In 2001, it was shown by Zurek that the Wigner distribution of these cat-like states also exhibit sub-Planck structures. Recently, we showed that Zurek's observation is valid even in the case of Kirkwood-Rihaczek distribution. Number states can also produce more complex states of light such as (a) squeezed coherent states, (b) photon-added coherent states, (c) displaced number states, and (d) displaced squeezed number states.

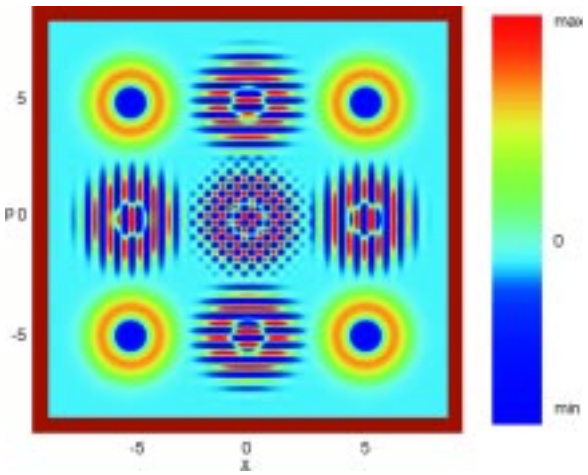

Fig.75:The Wigner distribution for a displaced number state after it has propagated through a Kerr medium for certain duration of time. The formation of cat-like states is evident from the patterns at the corners whereas the sub-Planck structures can be seen in the chess-board pattern at the centre. The horizontal and vertical axes represent the position and momentum variables $x = 0$ and p respectively.

In the present work, we consider the propagation of these complex states in a Kerr mediium, track their evolution in in phase space and compare the outcome with that for a coherent state. We show analytically that at certain instants of time, all these states generate Schrödinger cat states and exhibit sub-Planck structures in both the Wigner distribution (Figure 75) and the Kirkwood-Rihaczek distribution.

(J. Banerji)

Inelastic scattering as a probe for the level structure of the target atom/molecule

The transfer of energy in an inelastic scattering from the projectile electron to the target atom/molecule in the process of their excitation is known to lead to a small change in the wave number of the projectile.This change in the wave number, which is extremely small compared to the projectile wave number in the Born limit, has been shown here to provide information about the energy level structure of the target bound system.Such an information is obtainable from the interference effects between the elastic and inelastic scattering amplitudes. It is shown that the energy spectrum over the entire range of energies including those of the rotational and the vibrational modes are, in principle, obtainable in one shot using the electron inelastic scattering. The advantage of this technique over the usual photon spectroscopy is that it does not require different detector systems over the different energy ranges. The energy level structure of simple atomic systems are also similarly obtainable.

(R.K. Varma)

Publications in Journals

Astronomy and Astrophysics

1. Banerjee, D.P.K., Das, R.K., and Ashok, N.M., 2009, "*Near Infrared H and K band studies of the 2006 outburst of the recurrent nova RS Ophiuchi*", MNRAS, v. 399, p. 357-368.

2. Bhatt, Nipa J., Jain, Rajmal and Agarwal, Malini, 2009, "*Prediction of the Maximum Amplitude and Timing of Sunspot Cycle 24*" Solar Physics, v. 260, p. 225-232.

3. Chandra Satish, Vats, H.O., and Iyer, K.N., 2009, "*Differential coronal rotation using radio images at 17 GHz*", MNRAS Letters, v. 400, L34-L37.

4. Das, R.K., Banerjee, D.P.K., and Ashok, N.M., 2009, *"Infrared studies of Nova V2615 Ophiuchi: detection and evolution of the first overtone CO emission"*, MNRAS, v. 398, p. 375-384.

5. Dewangan, L.K., and Anandarao, B.G., 2010, *"Spitzer-IRAC imaging photometric study of the massive star forming region AFGL 437"*, MNRAS, v. 402, p. 2583-2590.

6. Jain, Rajmal, Agarwal, Malini, Kulkarni, Pradeep, 2010, "*Relationship between CME dynamics and solar flare plasma"*, Research in Astronomy and Astrophysics, v. 10, p. 473-483.

7. Joshi, U.C., Ganesh, S. and Baliyan, K.S., 2010, "*Optical polarimetry and photometry of Comet 17P/ Holmes"*, MNRAS, v. 402, p. 2744-2572.

8. Launila, O. and Banerjee, D.P.K., 2009, *"Rotational spectroscopy of AlO. Low-N transitions of astronomical interest in the X2S+ state"*, Astronomy and Astrophysics, v. 508, p. 1067-1072.

9. Naik, Sachindra, Banerjee, D.P.K., Ashok N.M., and Das R.K., 2010, *"Near-infrared observations of nova V574 Puppis"*, MNRAS, v. 404, p. 367-375.

10. Rao, A.R., Naik, Sachindra, Patil, M., Malkar, J.P. and Kalyan, Kumar, R.P.S., 2010, "*An alpha tagged X-ray source for the calibration of space borne X-ray detectors*", Nuclear Inst. and Methods in Physics Research A, v. 616, p. 55-58.

11. Singal, Ashok K., 2009, "*Maximum brightness temperature for an incoherent synchrotron source: Inverse Compton Limit - A Misnomer*", Astrophysical Journal Letters, v. 703, L109-L112.

12. Ueda, Y., Honda, K., Takahashi, H., Done, C., Shirai,

H., Fukazawa, Y., Yamaoka, K., Naik, Sachindra, Awaki, H., Ebisawa, K., Rodriguez, J., and Chaty, S, 2010, "*Suzaku Observation of GRS 1915 + 105: Evolution of Accretion Disc Structure during Limit-Cycle Oscillation*", The Astrophysical Journal, v. 713, p. 257-268.

13. Vadawale, S.V., Paul, B., Pendharkar, J., Naik, Sachindra, 2010, "*Comparative study of different scattering geometries for the proposed Indian X-ray polarization measurement experiment using Geant4*", Nuclear Inst. and Methods in Physics Research A, v.618, p.182-189.

Solar Physics

14. Artzner, G., Gosain, S. and Schmieder, B., 2010, *"A Technique for Removing Background Features in SECCHI - EUVI He II 304 A Filtergrams: Application to the Filament Eruption of 22 May 2008*", Solar Physics, v. 262, p. 437-447.

15. Cho, Kyung-Suk, Lee, Jeongwoo, Bong, Su-Chan, Kim, Yeon-Han, Joshi, Bhuwan and Park, Young-Deuk, 2009, *"A Coronal Mass Ejection and Hard X-Ray Emissions Associated with the Kink Instability"*, The Astrophysical Journal, v. 703, p. 1-7.

16. Gosain, S. and Schmieder, B., 2010, *"Estimation of width and inclination of a filament sheet using He II 304 A observations by STEREO/EUVI"*, Annales Geophysicae, v. 28, p. 149-153.

17. Gosain, S., Venkatakrishnan, P. and Tiwari, S. K., 2009, *"HINODE Observations of Coherent Lateral Motion of Penumbral Filaments During an X-Class Flare"*, The Astrophysical Journal, v. 706, p. L240-L245.

18. Gosain, S., Schmieder, B., Venkatakrishnan, P., Chandra, R., Artzner, G., 2009, *"3D Evolution of a Filament Disappearance Event Observed by STEREO"*, Solar Physics v. 259, p. 13-30.

19. Guo, Y., Schmieder, B., Bommier, V., Gosain, S., 2010, *"Magnetic Field Structures in a Facular Region Observed by THEMIS and Hinode"*, Solar Physics, v. 262, p. 35-52.

20. Joshi, A.D., Srivastava, N, and Mathew, S.K., 2010, *"Automated detection of filaments and their disappearance using full-disc Ha images"*, Solar Physics, v. 262, p. 425-436.

21. Joshi, Bhuwan, Veronig, Astrid, Cho, K.S., Bong, S.C., Somov, B.V., Moon, Y.J., 2009, *"Magnetic Reconnection During the Two-phase Evolutionof a Solar Eruptive Flare"*, The Astrophysical Journal, v. 706, p. 1438-1450.

22. Kumar, B., Mathur, S., Garcia, R.A., and Venkatakrishnan, P., 2010, *"On the flare induced high-frequency global waves in the Sun"*, The Astrophysical Journal Letters, v. 711, p. L12-L18.

23. Louis, R.E., Bellot Rubio, L.R., Mathew, S.K. and Venkatakrishnan, P., 2009, *"Supersonic Downflows in a Sunspot Light Bridge"*, Astrophysical Journal Letters, v. 704, p. L29-L33.

24. Maurya, R.A., and Ambastha, A., 2009, *"Transient Magnetic and Doppler Features Related to the White-light Flares in NOAA 10486"*, Solar Physics, v. 258, p. 31-52.

25. Maurya, R.A., Ambastha, A., and Tripathy, S.C., 2009, *"Variations in p-Mode Parameters with Changing Onset Time of a Large Flare"*, Astrophysical Journal Letters, v. 706, p. L235-L239.

26. Maurya, R.A., and Ambastha, A., 2010, *"A Technique for Automated Determination of Flare Ribbon Separation and Energy Release"*, Solar Physics, v. 262, p. 337-353.

27. Mierla, M., Inhester, B., Antunes, A., Boursier, Y., Byrne, J.P., Colaninno, R., Davila, J., de Koning, C.A., Gallagher, P.T., Gissot, S, Howard, R.A., Howard, T.A., Kramar, M, Lamy, P, Liewer, P.C., Maloney, S, Marqu´e, C, McAteer, R.T.J., Moran, T., Rodriguez, L, Srivastava, N**.,** St.Cyr, O.C., Stenborg, G., Temmer, M., 2010, *"On the 3D Reconstruction of Coronal Mass Ejections using Coronagraph Data"*, Annales Geophysicae, v. 28, p. 203-215.

28. Mathew, S.K., Zakharov, V. and Solanki, S.K., 2009, *"Stray light correction and contrast analysis of Hinode broad-band images"*, Astronomy and Astrophysics, v. 501, p. L19-L22.

29. Srivastava, N.**,** Inhester, B., Mierla, M., and Podlipnik, B., 2009, "*3D reconstruction of the leading edge of*

the May 20, 2007 partial halo CME", Solar Physics, v. 259, p. 213-225.

30. Tiwari, S.K., Venkatakrishnan, P., Gosain, S. and Joshi, J., 2009, *"Effect of Polarimetric Noise on the Estimation of Twist and Magnetic Energy of Force-Free Fields",* The Astrophysical Journal, v. 700, p. 199-208.

31. Tiwari, S.K., Venkatakrishnan, P., and Sankarasubramanian, K., 2009, *"Global Twist of Sunspot Magnetic Fields Obtained from High Resolution Vector Magnetograms",* Astrophysical Journal Letters, v. 702, p. L133-L137.

32. Venkatakrishnan, P., and Tiwari, S.K., 2009, *"On the Absence of Photospheric Net Currents in Vector Magnetograms of Sunspots Obtained From Hinode (Solar Optical Telescope/Spectro-Polarimeter)"*, Astrophysical Journal Letters, v. 706, p. L114-L119.

Planetary Sciences and PLANEX Program

33. Bhandari N., Murty, S.V.S., Mahajan, R.R., Parthasarathy, G., Shukla, P.N., Sisodia, M.S., and Rai, V.K., 2009, "*Kaprada L5(6) chondrite: chemistry, petrography, noble gases and nuclear tracks",* Planet Space Science, v. 57, p. 2048-2052.

34. Bourman, R.P., Prescott, J.R., Banerjee, D., Alley, N.F., and Buckman, S., 2010, "*Age and origin of alluvial sediments within and flanking the Mount Lofty Ranges, southern South Australia – a late Quaternary archive of climate and environmental change*", Australian Journal of Earth Sciences, v. 57, p. 175-192.

35. Das, J.P., and Murty, S.V.S., 2009, *"Cosmogenic and trapped noble gases in individual chondrules: Clues to chondrule formation",* Meteorite Planet Science v. 44, p. 1797-1818.

36. Goswami, J.N., and Murty, S.V.S., 2009, "*Planetary Sciences and Exploration: An Indian Perspective".* In "Current Trends in Science", by Indian Academy of Sciences, Bangalore, p. 457-476.

37. Huss, G.R., Meyer, B.S., Srinivasan, G., Goswami, J.N., and Sahijpal, S., 2009, "*Stellar sources of the short-lived radionuclides in the early solar system",* Geochim. Cosmochim. Acta 73, p. 4922-4945.

38. Hutcheon, I.D., Marhas, K.K., Krot, A.N., Goswami J.N., and Jones, R.H., 2009, "^{26}*Al in plagioclase-rich chondrules in carbonaceous chondrites: evidence for an extended duration of chondrule formation",* Geochim. Cosmochim. Acta, v. 73, p. 5080-5099.

39. Liu, M.C., McKeegan, K.D., Goswami, J.N., Marhas, K.K., Sahijpal, S., Ireland, T.R., and Davis, A.M., 2009, "*Isotopic records in CM hibonites: Implication for timescales of reservoir mixing in the solar nebula*", Geochim. Cosmochim. Acta, v. 73, p. 5051-5079.

40. Pabari, J.P., Acharya, Y.B., and Desai, U.B., 2009, "*Investigation of Wireless Sensor Deployment Schemes for In-Situ Measurement of Water Ice near Lunar South Pole*", Sensors & Transducers Journal, v. 111, p.86–105.

41. Pieters, C.M., Goswami, J.N., Clark, R.N., Annadurai, M., Boardman, J., Buratti, B., Combe, J.P., Dyar, M.D, Green, R., Head, J.W., Hibbitts, C., Hicks, M., Isaacson, P., Klima, R., Kramer, G., Kumar, S., Livo, E., Lundeen, S., Malaret, E., McCord, T., Mustard, J., Nettles, J., Petro, N., Runyon, C., Staid, M., Sunshine, J., Taylor, L.A., Tompkins, S. and Varanasi, P., 2009, "*Character and Spatial Distribution of OH/H2O on the Surface of the Moon Seen by M3 on Chandrayaan-1",* Science, v. 326, p. 568-572.

42. Prasad, Durga K., and Murty, S.V.S., 2009, "*LABNET "A WSN based lab automation and control network*", Journal of Instrument Society of India, v. 39, p. 172-175.

43. Prashant, Rai, Jayanta, K., Pati, Suresh, C., Patel, Ashutosh, Naik, and Dipak, Panda, 2009, "*Multi-shelled orbicular olivine gabbronorite from Leh, Jammu and Kashmir, Ladakh Himalaya*", Current Science, v. 97, p. 1769-1774.

44. Spudis, P.D., Bussey, D.B.J., Baloga, S.M., Butler, B.J., Carl, D., Carter, L.M., Chakraborty, M., Elphic, R.C., Gillis-Davis, J.J., Goswami, J.N., Heggy, E., Hillyard, M., Jensen, R., Kirk, R. L., LaVallee, D., McKerracher, P., Neish, C.D, Nozette, S., Nylund, S., Palsetia, M., Patterson, W., Robinson, M.S., Raney, R.K., Schulze, R.C., Sequeira, H., Skura, J., Thompson, T.W., Thomson, B.J., Ustinov, E.A., and Winters, H.L., 2010, "*Initial results for the north pole*

of the Moon from Mini-SAR, Chandrayaan-1 mission", Geophysical Research Letters, v. 37, p. L06204(1-6).

45. Sreekumar, P., Acharya, Y.B. et al. including Vadawale, S. February 2009, "*High Energy X-ray Spectrometer on Chandrayaan-I*", Current Science, v. 96, No. 4, p. 520-525.

Space and Atmospheric Sciences

46. Acharya, Y.B., and Goswami, V., 2009, *"Effect of Uncertainty in the Reliability of the COTS based Hardware System and its Sensitivity Analysis"*, Sensors and Transducer Journal, v. 111, pp. 1-9.

47. Chandra, H., Sharma, S., and Aung, S.W., 2009**,** ***"****Day to day variability in the critical frequency of* F_2 *layer over the anomaly crest region, Ahmedabad"*, Journal of Indian Geophysical Union, v. 13, no 4, p.217-226.

48. Das, U., Sinha, H.S.S., Sharma, S., Chandra, H., and Das, S.K., 2009, *"Fine structure of the low latitude mesospheric turbulence"*, Journal of Geophysical Research, v. 114, D10111 (1-11).

49. Haider, S.A., Abdu, M.A., Batista, I.S., Sobral, J. H.A., Sheel, V., Molina-Cuberos, G.J., Maguire, W.C., and Verigin, M.I., 2009, "*Zonal wave structures in the nighttime tropospheric density, temperature and in the D region ionosphere over Mars: Modeling and observations*", Journal of Geophysical Research, v. 114, A12315 (1-18).

50. Haider, S.A., Abdu, M.A., Batista, I.S. Sobral, J.S., Kallio, E., Maguire, W.C. and Verigin, M.I., 2009, "*On the responses to solar X-ray flare and coronal mass ejection in the ionosphere of Mars and Earth*", Geophysical Research Letters, 36, L13104, doi 10.1029/2009 GL038694.

51. Kedia, S., and Ramachandran, S., 2009, "*Variability in aerosol optical and physical characteristics over the Bay of Bengal and the Arabian Sea deduced from Angstrom exponents",* Journal of Geophysical Research, v. 114, D14207 (1-13).

52. Kumar, M., Kumar, A., Mahanti, N. C., Mallik, C., and Shukla, R. K., 2009, "*Surface flux modelling using ARIMA technique in humid subtropical monsoon area",* Journal of Atmospheric and Solar-Terrestrial Physics. v. 71, no. 12, August 2009, p. 1293-1298.

53. Kumar, M., Mallik, C., Kumar, A., Mahanti, N.C., Shekh, A.M., 2010, *"Evaluation of the boundary layer depth in semi-arid region of India"* Dynamics of Atmospheres and Oceans, v. 49, pp 96-107, doi:10.1016/ j.dynatmoce. 2009.01.002.

54. Kushawaha, R.K., Sunil Kumar, S., Prajapati, I.A., Subramanian, K.P., and Bapat, B., 2009, *"Polarization dependence in non-resonant photo-triple-ionization of* CO_2*"*, Journal Physics B: At. Mol. Opt. Phys., v. 42, p. 105201(1-5).

55. Patra, A.K., Rao, N.V., Phani Kumar, D.V., Chandra, H., Das, U., Sinha, H.S.S., Pant, T.K., and Sripathi, S., 2009, *"Off-electrojet low-latitude daytime E region plasma irregularities studied using coordinated VHF radar, ionosonde and rocket-borne observations"*, Journal of Geophysical Research, v. 114, A11301 (1-10).

56. Rastogi, R. G., and Chandra, H., 2009, *"Growth of equatorial sporadic-E during sunrise"*, Indian Journal of Radio & Space Physics, v. 38, p. 105-111.

57. Sunder Raman, R., and Ramachandran, S., 2010, "*Annual and seasonal variability of ambient aerosols over an urban region in western India*", Atmospheric Environment, v. 44, p. 1200-1208.

58. Sahu, L. K., Lal, S., Thouret, V., and Smit, H. G., 2010, *"Seasonality of tropospheric ozone and water vapor over Delhi, India: a study based on MOZAIC measurement data"*, Journal of Atmospheric Chemistry, v.62, p. 151-174.

59. Sarkhel, S., Sekar, R., Chakrabarty, D., Narayanan, R., and Sridharan, S., 2009, "*Simultaneous sodium airglow and lidar observations from India: a case study"*, Journal of Geophysical Research, v. 114, A10317 (1-7) .

60. Srivastava, S., Lal, S., Subrahamanyam, D.B., Gupta, S., Venkataramani, S., and Rajesh, T.A., 2010, *"Seasonal variability in mixed layer height and its impact on trace gas distribution over a tropical urban site: Ahmedabad"*, Atmospheric Research v. 96, p. 79-87.

Geosciences

61. Biswas, R.H., Murari, M.K., and Singhvi, A.K., 2009, "*Dose-dependent change in the optically stimulated luminescence decay of A12O3: C",* Radiation Measurements, v. 44, p. 543-547.

62. Chauhan, N., Anand, S., Selvam, P., Mayya, Y.S., and Singhvi, A.K., 2009, *"Extending the upper age limits in the Luminescence dating of sediments: A feasibility study of using large quartz grains",* Radiation Measurements, v. 44, p. 629-633.

63. Das, R., Salters, V.J.M., and Odom, A.L., 2009, *"A case for in vivo mass-independent fractionation of mercury isotopes in fish"*, Geochemistry Geophysics Geosystems, v. 10, Q11012 (1-12).

64. Dhir, R.P., Tandon, S.K., Singhvi, A.K., Kar, A., and Sareen, B.K., 2009, *"Soil Profile Modification, Genesis, Chronology and Paleo-environmental Interpretations from Paleosols in a Multi-episode Aeolian Section in Western Rajasthan",* Journal of the Indian Society of Soil Science, v. 57, p. 225-236.

65. Dhir, R.P., Singhvi, A.K., Andrews, J.E., Kar, A., Sareen, B.K., Tandon, S.K., Kailath, A., and Thomas, J.V., 2010, *"Multiple episodes of aggradation, and calcrete formation in Late Quaternary Aeolian sands, Central Thar Desert, Rajasthan, India",* Journal of Asian Earth Sciences, v. 37, p. 10-16.

66. Kumar, A., and Sarin, M.M**.,** 2009, *"Mineral aerosols from western India: Temporal variability of coarse and fine atmospheric dust and elemental characteristics",* Atmospheric Environment, v. 43, p. 4005-4013.

67. Kumar, A., and Sarin, M.M., 2010, "*Aerosol iron solubility in a semi-arid region: Temporal trend and impact of anthropogenic sources",* Tellus-B, v. 62B, p. 125-132.

68. Kumar, A., and Sarin, M.M., 2010, *"Atmospheric water-soluble constituents in fine and coarse aerosols from high-altitude site in western India: Long-range transport and seasonal variability"*. Atmospheric Environment, v. 44, p. 1245-1254.

69. Kanungo, A.K., Misra, V.N., Dutta, K., Ravi Prasad, G.V., Yadava, M.G., and Hodgins, G.W.L., (2009) "*The Radiocarbon Chronology of Kopia, an early glass manufacturing centre in India*", Archaeometry 52, v.5, p. 899-918.

70. Managave, S.R., Sheshshayee, M.S., Boragonkar, H.P., and R., Ramesh, 2010, "*Past break monsoon conditions detectable by high resolution intra-annual $\delta^{18}O$ analyses of teak rings*", Geophysical Research Letters, v. 37, p. 1-4.

71. Malik, J.N., Sahoo, A.K., Shah, A.A., Shinde, D.P., Juyal, N. and Singhvi, A.K., 2009, *"Paleoseismc evidence from trench investigation along Hajipur fault, Himalayan Frontal Thrust, NW Himalaya: Implications of the faulting pattern on landscape evolution and seismic hazard"*, Journal of Structural Geology, v.32, p.350-361.

72. Malik, J.N., Shah, A.A., Sahoo, A.K., Puhan, B., Banerjee, C., Shinde, D.P., Juyal, N., Singhvi, A.K., and Rath, S.K., 2009, "*Active fault, fault growth and segment linkage along the Janauri anticline (frontal foreland fold), NW Himalaya, India",* Tectonophysics, v.483, p.327-343.

73. Mohan, R., Shukla, S.K., Anilkumar, N., Sudhakar, M., Prakash, S., and Ramesh, R., 2009, *"Relative microalgal concentration in Prydz Bay East Antarctica duing late austral summer 2006"*, Algae, v. 24, p. 1-10.

74. Ramesh, R., and Singh, A., 2010, "*Isotopic fractionation in open systems: application to organic matter decomposition in ocean and land*", Current Science, v. 98, p. 406-411.

75. Ram, K., and Sarin, M.M., 2010, *"Spatio-temporal variability in atmospheric abundances of EC, OC and WSOC over Northern India",* Journal of Aerosol Science, v. 41, p. 88-98.

76. Ram, K., Sarin, M.M**.,** and Hegde, P., 2010, *"Long-term record of aerosol optical properties, and chemical composition from a high-altitude site (Manora Peak) in Central Himalaya"*, Atmospheric Chemistry Physics Discussion, v. 10, p. 7435-7467.

77. Ram, K., and Sarin, M.M**.,** 2009**, "***Absorption coefficient and site-specific mass absorption efficiency of elemental carbon (EC) in atmospheric aerosols over urban, rural and high-altitude sites in India"*,

Environmental Science and Technology, v. 43, p. 8233-8239.

78. Raj, R., and Yadava, M.G., 2009, "*Late Holocene uplift in the lower Narmada basin, western India*", Current Science, v. 96, p. 985-988.

79. Rastogi, N., and Sarin, M.M**.,** 2009, "*Quantitative chemical composition and characteristics of aerosols over western India: One-year record of temporal variability"*, Atmospheric Environment, v. 43, p. 3481-3488.

80. Rai, S.K., Singh, S.K., and Krishnaswami, S., 2010, *"Chemical weathering in the plain, and peninsular sub-basins of the Ganga: Impact on major ion chemistry and elemental fluxes",* Geochimica et Cosmochimica Acta, v. 74, p. 2340–2355.

81. Ray, J.S., 2009, "*Radiogenic isotopic ratio variations in carbonatites and associated alkaline silicate rocks",* Role of crustal assimilation, Journal of Petrology, v. 50, p. 1935-1954.

82. Ray, J.S., Shukla, A.D., and Dewangan, L.K., 2010, "*Carbon and oxygen isotopic compositions of Newania dolomite carbonatites, Rajasthan, India: implication for source of carbonatites",* Mineralogy and Petrology, v. 98, p. 269-282.

83. Rahaman, W., and Singh, S.K., 2009*, "Rhenium in rivers and estuaries of India: Sources, transport and behaviour",* Marine Chemistry, v. 118, p. 1-10.

84. Sano, M., Sheshshayee, M.S., Mangave, S., Ramesh, R., Sukumar R., and Sweda, T., 2010, "*Climatic Potential of Abies spectabulis from the Nepal Himalaya*", Dendrochronologia, v. 28, p. 93-98.

85. Sarkar, A., Sengupta, S., McArthur, J.M., Ravenscroft, P., Bera, M.K., Bhushan, R., Samanta, A., Agrawal, S., 2009, *"Evolution of Ganges–Brahmaputra western delta plain: Clues from sedimentology and carbon isotope",* Quaternary Science Review, v.28, p. 2564-2581.

86. Sheshshayee, M.S., Bindumadhava, H.R., Ramesh, R., Prasad, T.G., and Udayakumar, M., 2010, "*Relationship between ^{18}O enrichment in leaf biomass and stomatal conductance*", Isotopes in Environmental and Health Studies, v. 46, p. 122-129.

87. Sheth, H.C., Ray, J.S., Bhutani, R, Kumar, A., Awasthi, N., 2010, "*The latest eruption of Barren Island volcano, and some thoughts on its hazards",* logistics and geotourim aspects, Current Science, v. 98, p. 1-7.

88. Tripathy, G.R., Goswami, V., Singh, S.K., and Chakrapani, G.J*.,* 2010, *"Temporal variations in Sr and $^{87}Sr/^{86}Sr$ of the Ganga headwaters: Estimates of dissolved Sr flux to the mainstream"*, Hydrological Processes, v. 24, p. 1159–1171.

89. Tripathy, G.R., and Singh, S.K., 2010, *"Chemical erosion rates of river basins of the Ganga system in the Himalaya: Reanalysis based on inversion of dissolved major ions, Sr, and $^{87}Sr/^{86}Sr$",* Geochemistry Geophysics Geosystems, p. 1-20.

90. Tiwari, M., Ramesh, R., Bhushan, R., Sheshshayee, M.S., Somayajulu, B.L.K., Jull, A.J.T., and Burr, G.S., 2010*," Did the Indo-Asian summer monsoon decrease during the Holocene following insolation?",* Journal Quaternary Science, p. 1179-1188.

91. Tyagi, A.K., Chaudhary, S., Rana, N., Sati, S.P., and Juyal, N., 2009, *"Identifying areas of differential uplift using steepness index in the Alaknanda basin, Garhwal Himalaya, Uttrakhand"*, Current Science, v. 97, p. 1473-1477.

92. Yadav, D.N., and Sarin, M.M., 2009, *"Geo-chemical behaviour of Uranium in the Sambhar Salt Lake, Rajasthan (India): Implications to source of salt and Uranium sink"*, Aquatic Geochemistry*,* v. 15, p. 529-545.

Theoretical Physics

93. Ambika, G., and Amritkar, R.E., 2009, "*Anticipatory synchronization with variable time delay and reset*", Physical Review E, v. 79, p. 056206.

94. Amritkar, R.E., 2009, *"Estimating parameters of a nonlinear dynamical system",* Physical Review E, v. 80, p. 047202 (1-4).

95. Amritkar, R.E., and Rangarajan, G., 2009*,* "*Stability of multi-cluster synchronization*", International Journal of Bifurcation and Chaos, v. 19, p. 4263-4271.

96. Ashok, Kumar, Pravin, Vaity, Yedhu, Krishna, and Singh, R.P., 2010, *"Engineering the size of dark core of an optical vortex"*, Optics and Lasers in Engineering, v. 48, p. 276-281.

97. Bhatt, J.R., Gu, P., Sarkar, U., and Singh, S., 2009, *"Neutrino Dark Energy in Grand Unified Theories",* Physical Review D, v. 80, p. 073013 (1-14).

98. Bhatt, J.R., and Sarkar, U., 2009, "*Majorana Neutrino Superfluidity and Stability of Neutrino Dark Energy"*, Physical Review D, v. 80, p. 045016 (1-6).

99. Bhatt, J.R., Patra, S., and Sarkar, U., 2010, *"Gravitational correction to SU (5) gauge coupling unification",* Modern Physics Letters A., v. 25, p. 283-293.

100. Bhatt, J.R., Desai, B.R., Ma, E., Rajasekaran, G., and Sarkar, U, 2010, "*Neutrino Condensate as Origin of Dark Energy*", Physics Letters B, v. 687, p. 75-78.

101. Das, S., and Mohanty, S., 2009, *"Non-Gaussianity as a signature of thermal initial condition of inflation",* Physical Review D, v. 80, p. 123537 (1-8).

102. Das, S., and Mohanty, S., 2009, *"Signatureof short distance physics on inflation power spectrum and CMB anisotropy",* Journal of Cosmology and Astroparticle Physics, p. 0909 (1-9).

103. Eduard Masso, Mohanty, S., and Soumya, Rao, 2009, *"Dipolar Dark Matter"*, Physical Review D, v. 80 p. 036009 (1-8).

104. Gautam, S., and Angom, D., 2010, *"Scattering length for fermionic alkali atoms"*, European Physical Journal D, v. 56, p.173- 179.

105. Godbole, R.M., Rai, S.K., and Rindani, S.D.,2009, *"Use of transverse polarization to probe R-parity violating supersymmetry at ILC"*, Physics Letters B, v. 678, p. 395-400.

106. Goswami, S., Petcov, S.T., Ray, S., and Rodejohann, W., 2009, *"Large U_{e3} and Tri-bimaximal Mixing",* Physical Review D, v. 80, p. 0530 (13-14).

107. Goswami, S., Khan, S., and Rodejohann, W., 2009, *"Minimal Textures in Seesaw Mass Matrices and their low and high Energy Phenomenology",* Physics Letters B, v. 680, p. 255-262.

108. Gu, P., Sarkar, U, and Zhang, H.B., 2009, *"Visible and Dark Matter Genesis and Cosmic Positron and Electron Excesses",* Physical Review D, v. 80, p. 076003 (1-5).

109. Gu, P., and Sarkar, U., 2009, *"Annihilating Leptogenesis",* Physics Letters B, v. 679, p. 118-121.

110. Gu, P., He, H.J., Sarkar, U., and Zhang, H.B., 2009, *"Double Type-II Seesaw, Baryon Asymmetry and Dark Matter for Cosmic $e^{\pm}$ Excesses",* Physical Review D, v. 80, p. 053004 (1-8).

111. Gu, P., and Sarkar, U., 2010, *"Pathways to testable leptogenesis*", Modern Physics Letters A., v. 25, p. 501-509.

112. Gu, P., and Sarkar, U., 2010, "*Common Origin of Visible and Dark Universe*", Physical Review D, v. 81, p. 033001 (1-7).

113. Harikrishnan, K.P., Misra, R., Ambika, G., and Amritkar, R. E., 2009, *"Computing the multifractal spectrum from time series: An algorithmic approach",* Chaos 19, 043129 (1-9).

114. Harikrishnan, K.P., Misra, R., Ambika, G., and Amritkar, R.E., 2010, *"Parametric characterisation of a chaotic attractor using the two scale Cantor measure",* Physica D, v. 239, p. 420-427.

115. Joshipura, A.S., Kodrani, B.P., and Patel, K.M., 2009, *"Fermion Masses and Mixings in a mu-tau symmetric SO (10)",* Physical Review D, v.79, 115017 (1-11).

116. Joshipura, A.S., and Werner, Rodejohann, 2009, *"Scaling in the Neutrino Mass Matrix, mu-tau Symmetry and the See-Saw Mechanism",* Physics Letters B, v. 678, p. 276-282.

117. Joshipura, A.S., and Kodrani, B.P., 2010, *"Higgs induced FCNC as a source of new physics in b—>s transitions"*, Physical Review D, v.81, p.035013 (1-11).

118. Latha, K.V.P., Angom, D., Das, B.P., and Mukherjee, D., 2009, *"Probing CP Violation with the Electric Dipole Moment of Atomic Mercury"*, Physical Review Letters, v. 103, p. 083001 (1-4).

119. Mani, B.K., Latha, K.V.P., and Angom, D., 2009*, "Relativistic coupled-cluster calculations of 20Ne, ^{40}Ar, ^{84}Kr, and ^{129}Xe: Correlation energies and dipole polarizabilities",* Physical Review A, v. 80, p. 062505 (1-11).

120. Mahajan, Namit 2009, *"Y (4140): Possible Options"*, Physics Letters B, v. 679, p. 228-230.

121. Patra, S., Sarkar, A., Sarkar, U., and Yajnik, U., 2009, *"Spontaneous Parity Violation in a Supersymmetric Left-Right Symmetric Model",* Physics Letters B, v. 679, p. 386-389.

122. Rangarajan, R., and Sahu, N., 2009, *"Perturbative reheating and gravitino production in inflationary models"*, Physical Review D, v. 79, p. 103534 (1-7).

123. Rindani, S.D., and Sharma, P., 2009, *"Angular distributions as a probe of anomalous ZZH and γZH interactions at a linear collider with polarized beams",* Physical Review D, v. 79, p. 075007 (1-26).

124. Shukla, A., Sahu, R., and Kota, V.K.B., 2009, "*Deformed shell model results for two neutrino positron double beta decay of* ^{74}Se", Physical Review C, v. 80, p. 057305 (1-4).

125. Varma, R.K. 2010, "Observability of the effects of curl-free vector potential on the macro-scale and the nature of the transition amplitude wave" Pramana-Journal of Physics v. 74, p. 491-511.

126. Varma, R.K. 2010, "Some surprising manifestations of charged particle dynamics in a magnetic field" Jr. Plasma Phys. v. 76, p. 355-367.

127. Vyas, M., and Kota, V.K.B., 2009, "*Random matrix ensembles with random interactions: Results for EGUE (2)-SU (4)*", Pramana Journal of Physics, v. 73, p. 521-531.

128. Vyas, M, Kota, V.K.B., and Chavda, N.D., 2010, *"Transitions in eigenvalue and wave function structure in (1 + 2)-body random matrix ensembles with spin",* Physical Review E, v.81, p. 036212 (1-17).

Interdisciplinary

129. Ramachandran, S., Rengarajan, R., and Sarin, M.M., 2009, *"Atmospheric carbonaceous aerosols: issues, radiative forcing and climate impacts",* Current Science, v. 97, p. 18-20.

Publications in Proceedings of Symposia

Astronomy and Astrophysics

1. Chandrasekhar, T. and Tapas, Baug, 2009, *"Near Infrared Lunar Occultations of sources in the Galactic Centre region from Mt. Abu"*, Special Session (SPS 08) on the Galactic Plane and in depth across the spectrum, IAU General Assembly, Rio de, Janeiro, Brazil, (Abstract # SPS 08-p. 3).

2. Ganesh, S., Joshi, U.C., and Baliyan, K.S.,2009, "*Optical photo-polarimetry of infrared sources in Galactic plane fields",* Special session 8 on The Galactic Plane – in Depth and Across the Spectrum, IAU General Assembly, Riode Janeiro, Brazil, (Abstract # SpS08-p20).

3. Ganesh, S., Joshi, U.C. and K.S. Baliyan, "*Optical polarimetry of mid-infrared selected sources",* JD10 on 3D views of Cool Stellar Atmospheres, IAU General Assembly, Riode Janeiro, Brazil, August 2009 (Abstract # JD10-p7).

4. Jain, Rajmal, Rajpurohit, A.S., Agarwal, Malini, Jamwal, Rajni, Awasthi, Arun, Magnetic Coupling between the Interior and Atmosphere of the Sun, edited by S.S., Hasan, and R.J., Rutten, Astrophysics and Space Science Proceedings. ISSN 1570-6591 (Print) 1570-6605 (Online) Published by Springer Berlin Heidelberg; ISBN 978-3-642-02858-8 (Print) 978-3-642-02859-5 (Online), p.465-470, "Time-Varying Thermal Emission in Solar Flares".

5. Joshi, U.C., Fan, J.H., Ganesh, S., and Baliyan, K.S., 2009, "*Study of polarization in Oj287",* Symposium 267 on the Co-evolution of Central Black Holes and Galaxies, IAU General Assembly, Riode Janeiro, Brazil, (Abstract # S267-p18).

6. Joshi, U.C., Ganesh, S., and Baliyan, K.S., 2009, "*Optical polarimetry of comet 17P/Holmes",* Symposium 263 on the Icy Bodies of the Solar System, IAU General Assembly, Riode Janeiro, Brazil, August 2009 (Abstract # S263-p41).

7. Naik S., Joshi, V., Vadawale, S.V., and Ashok, N.M., 2010, *"Near-IR observations of the Supergiant Fast X-ray Transient (SFXT)"* IGR J17544-2619, The Astronomer's Telegram, 2475.

8. Provencal, J.L., and 55 others, including Vats, Hari Om and Baliyan, K.S., 2009, *"Preliminary XCOV26 Results for EC14012-1446"*, Journal of Physics: Conference Series 172, 012061.

9. Singal Ashok K., 2009, *"Maximum brightness*

temperature for an incoherent synchrotron source", Astrophys & Sp. Sc. Proc., Turbulence, Dynamos, Accretion Disks, Pulsars and Collective Plasma Processes, ed. S.S. Hasan, R.T. Gandhara and V. Krishnan (Springer) 273.

10. Vats, H.O., Satsih Chandra, and Iyer, K.N., 10 March, 2010, Does Coronal Rotation Period Depend on the Sunspot Number?, Magnetic coupling between the interior and atmosphere of the Sun. eds. S S Hasan and R J Rutten, Springer, P. 526-528.

Solar Physics

11. Afram, N., Unruh, Y.C., Solanki, S.K., Schüssler, M., Mathew, S.K., 2010, *"A comparison of measured and simulated solar network contrast ",* Proceedings of the International Astronomical Union, IAU Symposium v.264, p.63-65.

12. Ambastha, A., "*Dynamic Solar Corona*", Chinese Astronomical Society-IAU Joint Meeting on Suzhou, China, July 24-26, 2009.

13. Gosain, S., Bayanna, A.R., Gupta, S.K., and Ambastha, A., *"Instrument for Coronal Imaging and Spectro-polarimetry - TSE "*, July 22, 2009 China".

14. Gupta, S.K., Gosain, Bayanna, A.R., and Ambastha, A., *"Instrumentation and Control Systems for USO/ PRL TSE 2009 Expedition".*

15. Gosain, S., and Venkatakrishnan, P., 2010, *"Phase III of the USO Solar Vector Magnetograph*", in Magnetic Coupling between the Interior and Atmosphere of the Sun, p. 395-397.

16. Gosain, S., and Venkatakrishnan, P., 2009, *"A 2-dimensional Scanning Solar Vector Magnetograph at Udaipur Solar Observatory"*, Astronomical Society of the Pacific Conference Series, v. 405, p. 467.

17. Joshi, A.D., and Srivastava, N., 2010, *"Acceleration of CMEs associated with eruptive prominences"*, Proc. of *Magnetic Coupling between the Interior and Atmosphere of the Sun*, Eds. Hasan, S. and Rutten, R.J. "Astrophysics and Space Science Proceedings, Springer-Verlag, Heidelberg, Berlin", p. 485-488.

18. Kumar, B., and Venkatakrishnan, P., 2010, *"Flare driven acoustic modes in the Sun",* in the Proceedings of *Magnetic Coupling between the Interior and the Atmosphere of the Sun,* Eds. S.S. Hasan and R.J. Rutten, Astrophysics and Space Science Proceedings, Springer-Verlag, Heidelberg, Berlin, p. 405-409.

19. Kumar, B., and Venkatakrishnan, P., 2009, "*Evidence of enhanced high-frequency velocity oscillations in the Sun observed during solar flares using disk-integrated Doppler signals*", Eds. M. Dikpati, T. Arentoft, I. Gonzalez Hernandez, C. Lindsey and F. Hill, ASP Conference Proceedings, v. 416, p. 331.

20. Louis, R.E., Bellot Rubio, L.R., Mathew, S.K., Venkatakrishnan, P., 2010 *"Strong, Localized Downflows in a Sunspot Light Bridge",* Astrophysics and Space Science Proceedings, 509.

21. Maurya, R.A., and Ambastha, A., 2010, *"Flows in Flaring and Dormant Active Regions"*, in Hasan, S.; Rutten, R. J. (Eds.) Magnetic Coupling between the Interior and Atmosphere of the Sun (Astrophysics and Space Sciences Proceedings, Springer-Verlag), p. 516.

22. Maurya, R.A., and Ambastha, A., 2010, *"Magnetic and Velocity Field Changes Related to Solar Flares of October 28 and 29, 2003"*, in Hasan, S.; Rutten, R. J. (Eds.) Magnetic Coupling Between the Interior and Atmosphere of the Sun (Astrophysics and Space Sciences Proceedings, Springer-Verlag), p. 517.

23. Srivastava, N., "*CME observations from STEREO"*, Astrophysics and Space Science Proceedings series, Eds. Hasan, S.& Rutten, R. J., 2010, 308-317.

24. Tiwari, S., Venkatakrishnan, P., and Sankarasubramanian, K.,2010.*"Helicity at Photospheric and Chromospheric Heights",* in Magnetic Coupling between the Interior and the Atmosphere of the Sun'', eds. S.S. Hasan and R.J. Rutten,, Astrophysics and Space Science Proceedings, Springer- Verlag, p.443-447.

25. Tiwari, S., 2010, "*Solar Magnetic Fields,* In Souvenir *"National Seminar on Recent Advances in Helio-Physics-2010"*, p.15-17.

Planetary Sciences and PLANEX Program

26. Chauhan, P., Srivastava, N., Pieters, C.M., Ajai, Kiran kumar, A.S., Navalgund, R.R., Head, J.W., Petro, N., Runyon, C., and Goswami, J.N., 2010, "*Integrated Analysis of topographically high mafic*

exposures at Apollo -17 landing site using data from imaging sensors on Chandrayaan -1", 41st Lunar and Planetary Science Conference, Houston, (Abstract), 1606.

27. Kadlag, Y., and Marhas, K.K., 2009, "*Quasi Simultaneous Arrival (QSA) effect in nano-Secondary Ion Mass Spectrometer (nano-SIMS)"* In 11th ISMAS TRICON-2009, Ed.S.K. Aggrawal et al., p.451-452.

28. Mahajan, R.R., Murty, S.V.S. and Bartoschewitz, R., 2009, "*Noble gas and nitrogen isotopic components in CH chondrite SaU 290*". In 11th ISMAS-TRICON-2009, Ed. S.K. Aggrawal et al., p. 270-272.

29. Pabari, J.P., Acharya, Y.B., Desai, U.B., and Merchant, S.N., 2009, "*Embedded Impedance Sensor Design for Future Lunar Wireless Sensor Network with 'Chirp' Type Perturbation Signal*", Proceedings of International Conference on Signals, Systems and Automation 2009, Vallabhvidyanagar, December 28-29.

30. Prasad, Durga K., Murty, S.V.S., Shukla, P.N., and Suruchi Goel, 2009, "*Platinum group elements (PGEs) in meteorites by ICP-MS*". In 11th ISMAS-TRICON-2009, Ed. S.K. Aggrawal et al., p. 322-323.

31. Srivastava, Neeraj 2010, "*Planetary Exploration – Lecture Volume, Hyperspectra 2010",* DST sponsored Short-term Course, IIT Mumbai.

32. Suruchi, Goel, and Murty, S.V.S., 2009, "*Ne and Ar isotopic analysis by a multicollector noble gas mass spectrometer".* In 11th ISMAS-TRICON-2009, Ed. S.K. aggrawal et al., p. 273-275.

33. Suruchi, Goel, Murty, S.V.S., and Mahajan, R.R., 2009, "*Trapped Noble Gases in Iron Meteorites: First Identification of SW component in Kavarpura*", In 11th ISMAS-TRICON-2009, Ed. S.K. Aggrawal et al., p. 301-303.

Space and Atmospheric Sciences

34. Chakrabarty, D.,2009, Space Plasma Diagnostic Techniques: An ionospheric perspectiveProceedings of the SERC-DST school on Plasma Diagnostics, Institute of Plasma Research, 20-31 July.

35. Chandra, H.,Planetary atmospheres In "Heliospheric Processes", Astrophysics and Space Science Proceedings, edited by N Gopalswamy, Siraj and A Ambastha, Springer, March 2010.

36. Gupta, S.P., Spatial and temporal variations of stratospheric conductivity: An over view, p.19-20, Proceedings of DST Workshop on Electrodynamical Coupling of Atmospheric Regions, IIG, Mumbai, November 25-28, 2008.

37. Sekar, R., and Chakrabarty, D., 2008 *Effects of interplanetary electric field on low latitude ionosphere* Proceedings of the DST sponsored workshop on "Electrodynamical Coupling of Atmospheric Regions", Indian Institute of Geomagnetism.

Geosciences

38. Bhushan, R., Jull, A.J.T., Burr, G.S., 2009, *"Sediment Mobilisation in the Bay of Bengal during LGM to Holocene Transitio"*, In proceedings of the 20th International Radiocarbon Conference held at Big Island, Hawaii, USA, p. 48-49.

39. Deshpande, R.D., and Gupta, S.K., 2010 *"Groundwater dating using 14C, 4He and 4He/ 222Rn methods – A case study from North Gujarat Cambay region, India",* Proceeding of Workshop on Radon contamination in groundwater application of isotopes in groundwater studies, Central Ground Water Board (CGWB), Bangaluru p. 83-101.

40. Deshpande, R.D., and Gupta, S.K., 2009 *"IWIN National Programme for isotopic characterization of Indian Hydrological cycle: Preliminary Results"* Proceedings of the 11th ISMAS Triennial Conference, Hyderabad, November 24-28, 2009, p. 95-107.

41. Deshpande, R.D., and Gupta, S.K., 2009 *"Dissolved Noble Gases in Groundwater Hydrology",* Proceedings of the International Conference on Water, Environment, Energy and Society (WEES-2009), Allied Publishers, Vol. III, p. 1249-1259.

42. Gandhi, N. and Ramesh, R., 2009, *"Nitrogen sources for New production in the NE Arabian Sea during Spring"*, Proc. XI ISMAS Triennial International Conference on Mass Spectrometry, p. 261-263.

43. Jani, R.A., Yadava, M.G., Srivastava, R., and Ramesh, R., 2009, *"Stable isotopic signatures of rainfall events in the western India",* Proc. XI ISMAS

Triennial International Conference on Mass Spectrometry, pp 311-313.

44. Laskar, A.H., Yadava, M.G., and Ramesh, R, 2009, *"Soil carbon dynamics and its relationship to climate and vegetation",* Proc. XI ISMAS Triennial International Conference on Mass Spectrometry, p. 327-329.

45. Laskar, A.H., Yadava, M.G., and Ramesh, R., *"Stable isotopes of soil carbonates and soil organic matter: implications to paleoclimate and paleovegetation study in Gujarat, India"*, Seminar on Climate Change: causes, measures and Preparedness, University of Hyderabad, Hyderabad, August 24-26, 2009.

46. Maurya, A.S., Shah, M., Deshpande, R.D., and Gupta, S.K., 2009 *"Protocol for d18O and dD analyses of water sample using Delta V plus IRMS in CF Mode with Gas Bench II for IWIN National Programme at PRL, Ahmedabad"*, Proceedings of the 11th ISMAS Triennial Conference, p. 314-317.

47. Managave, S.R., Sheshshayee, M.S., and Ramesh, R., 2009, *"High resolution reconstruction using oxygen isotopes in teak trees"*, Proc. XI ISMAS Triennial International Conference on Mass Spectrometry, p. 533-535.

48. Managave, S.R., Sheshshayee, M.S., Borgaonkar H.P., Shah, S.K., Bhattacharyya, A., and Ramesh, R., 2009, *"Sub-annual oxygen isotope variations in Indian teak cellulose: implications to monsoon reconstruction"*, Geophysical Research Abstracts, v. 11, European Geophysical Union Meeting.

49. Rahaman W. and Singh, S.K., *"Rhenium in Indian Estuaries and high Re in the Gulf of Cambay",* Geochimica et Cosmochimica Acta, 73, A1068.

50. Rahaman W., Singh, S.K., Sinha, R., and Tandon, S.K., *"Climate-erosion coupling over the Himalaya during past ~100 ka"*, Geochimica et Cosmochimica Acta, 73, A1069.

51. Rahaman W. and Singh, S.K., *"87Sr/86Sr in Indian Estuaries: Submarine Groundwater Discharge, AGU Fall meeting*", San Francisco, USA.

52. Ram, K., and Sarin, M.M., 2009, *"Absorption properties of atmospheric aerosols from a high-altitude site in northern India"*, European Aerosol Conference-2009: Karlsruhe (Germany), T091A27.

53. Ram, K., Sarin, M.M., and Tripathi, S.N., 2009, *"One-year record of carbonaceous aerosols from urban location (Kanpur) in the Indo-Gangetic Plain (IGP)",* European Aerosol Conference-2009, Karlsruhe (Germany), T059A16.

54. Ram, K., Sudheer, A.K., and Sarin, M.M., 2009, *"Chemical characteristic of aerosols during foggy and clear days: Case study from northern India",* European Aerosol Conference-2009, Karlsruhe (Germany), T042A09 .

55. Ramesh, R., Managave, S., Yadava, M.G., and Tiwari, M., 2009, *"Paleomonsoon reconstruction using stable oxygen isotopes from various proxies from India"*, Proc. XI ISMAS Triennial International Conference on Mass Spectrometry, p. 180-184.

56. Rao, D.K., Ray, J.S., Jani, R.A., Dayal, A.M., and Patil, D.J., 2009, *"Origin of hydrocarbons from mud volcanoes of Andaman Islands: Evidence from Geochemistry"*, Pages 264-266, 11th ISMAS-TRICON.

57. Rengarajan, R., Sudheer, A.K. and Sarin, M.M., 2010 *"Secondary organic aerosols and associated acidity over an urban enviroment",* Proceedings of the IASTA-2010 conference on "Aerosols & Clouds: Climate Change Perspectives", Darjeeling, p. 522-524.

58. Satya Prakash, Ramesh, R., Rahul Mohan and Sudhakar, M., *"Is there a shift in productivity regime in the Southern Indian Ocean due to global warming?"*, National Conference on Climatic Changes during the Quaternary: Special reference to Polar Regions and Southern Ocean, NCAOR, Goa, 22-23, Oct. 2009.

59. Shetye, S.S., Sudhakar, M., Rahul Mohan and Ramesh, R., *"Early signatures of ocean acidification from Antarctic Coastal region: evidence form water column and sediment studies"*, A.P. Science Congress, A.P. Acadmi of sciences, Tirupati, Nov. 14-16, 2009.

60. Singh, A., Jani, R.A., and Ramesh, R., 2009, *"Oxygen isotope-salinity relation in the Bay of Bengal"*, Proc. XI ISMAS Triennial International Conference on Mass Spectrometry, p. 258-260.

61. Singh, S.K., Contribution from Salt: Overestimation of silicate weathering in the Ganga-Brahmaputra Basin, in Workshop on *"Anthropogenic impacts on water resources and soils: An Indo-French perspective"*, November 23-27, 2009, Bangalore, India.

62. Singh, S.K., *"Understanding the natural processes using isotope tracers",* Indian Society of Mass Spectrometry Conference, 11th ISMAS-TRICON-2009 November 24-28, 2009, Hyderabad, India.

63. Srivastava, R., Ramesh, R., and Jani, R.A., 2009, *"Stable isotope studies of atmospheric water vapour and clouds",* Proc. XI ISMAS Triennial International Conference on Mass Spectrometry, p. 530-532.

64. Srivastava, R., and Ramesh, R., *"Investigation of atmospheric water vapor cycle using stable isotopes",* 16th National Space Science Symposium, Saurashtra University Rajkot, India, 24th – 27th Feb 2010.

65. Yadava, M.G., Ramesh, R., Asmerom, Y.. and Polyak, V.J., (2008). *"Holocene Increase in the Bay Branch of the Monsoon Inferred From ä^{18}O of Speleothems From Central India"*, AGU Fall Meeting, 15-19 Dec 2008, San Francisco.

66. Yadava, M.G., Ramesh, R., Polyak, V.J., and Asmerom, Y., 2009, *"Age spans of some Indian speleothems"*, Proc. XI ISMAS Triennial International Conference on Mass Spectrometry, p. 309-310.

67. Yadava, M.G., Jani, R.A., Srivastava, R., and Ramesh, R., *"Isotopic signatures of rainfall events in western India",* Seminar on Climate Change:causes, measures and Preparedness,University of Hyderabad, Hyderabad, August 24-26, 2009.

68. Wieser, M., Schneider, T., Aeschbach-Hertig, W., Deshpande, R.D. and Gupta, S.K., 2009 *"Multi-Tracer Study of Groundwater in a Semiarid Region in Northwest India",* Abstract No. 267, Goldschmidt Conference.

Theoretical Physics

69. Jaiswal, V.K., and Singh, R.P., 2009, "*Phase singular beams generated by holographic grating: characterization of Mueller matrix"*, ICOP 2009-International Conference on Optics and Photonics Chandigarh, India, 30 October-1 November 2009, B-4.2.

70. Pravin Vaity, Ashok Kumar, and Singh, R.P., 2010, *"Experimental study of power decay of optical vortices in photorefractive material"*, National Laser Symposium, BARC Mumbai, January 13-16, 2010, CP-06-05.

Monographs/Review Articles

Astronomy and Astrophysics

1. Hari Om Vats, 2010, "Solar coronal rotation – a review of recent research", Journal of Science, 1, 27-32. (Dept. of Science & Technology, Govt. of Gujarat – Invited Review).
2. Hari Om Vats, 2009, The boundless universe, Science Reporter v. 46, p. 28-33.

Solar Physics

3. Ambastha, A., 2010, "*Solar Interior*" in Heliophysical Processes, eds. N. Gopalswamy, S. S. Hasan and A. Ambastha, Astrophysics and Space Sciences Proceedings, Springer-Verlag, Berlin, Heidelberg p. 15-34.

Book Edited:

4. Gopalswamy N., Hasan S. S. and Ambastha A. (eds.) 2010, "Heliophysical Processes", Astrophysics and Space Sciences Proceedings, Springer-Verlag, Berlin, Heidelberg.

Planetary Sciences and PLANEX Program

5. Murty S.V.S., Shyam Lal, Mahajan K.K. and Bhardwaj A., 2010, Evolution and composition of planetary atmospheres, in *"Modeling of Planetary Atmospheres" (Ed. S.A. Haider et al.)* by Mcmillan Publishers India Ltd. p. 1-82.

Space and Atmospheric Sciences

6. Haider, S. A., Sheel, V., Singh, V., Maguire, W.C. and Molina-Cuberos, G.J., 2009, "*Longitudinal Distribution of the Dayside Ionosphere of Mars at High Latitude*", in Advances in Geosciences, Eds. Anil Bhardwaj et al., v. 15, p. 25-52, World Scientific, Singapore.
7. Krishnan, R., Sheel, V., and Dash, S.K., 2010, "Dynamics of the Atmospheric General Circulation", in Modeling of Planetary Atmospheres, Eds, Haider S.A., Sheel, V., and Lal, S., Macmillan Publishers India Ltd., New Delhi, p.203-263.
8. Lal, S., 2010, "*India and Global Climate Change"*, in Science in India- Achievements and Aspirations, Eds. H. Y. Mohan Ram and P. N. Tandon, p. 231-242, INSA, New Delhi.
9. Moorthy, K.K., S.S. Babu, S.K. Satheesh, S. Lal, M.M. Sarin, and S. Ramachandran, 2009, "*Climate implications of atmospheric aerosols and trace gases"*, in Climate Sense, World Meteorological Organization (WMO), p.157-160.
10. Reddy, R.V., Das, A.C., and Haider, S.A., 2010, Chaper 3- "Magnetic Fields and Solar Wind

Interaction with Planetary Atmospheres" in Modeling of Planetary Atmospheres, Eds Haider, S.A., Varun, S., and Lal, S., by Macmillan Publishers India Ltd., p.145-202.

11. Sekar, R., Sudha. R., and Gurubarn, S., 2010, "*Terrestrial Ionosphere*", in Modeling of Planetary Atmospheres, Eds. Haider, S.A., V. Sheel and S. Lal, p. 264-307, Macmillan Publishers, India.

12. Sheel, V., Ramachandran, S., Tripathi, S.N., and Michael, M., 2010, "Chemistry and Aerosols in the Atmospheres of Earth and Mars" in Modeling of Planetary Atmospheres, Eds. Haider, S.A., Sheel, V., adn Lal, S., Macmillan Publishers India Ltd., p.83-144.

Books Edited:

13. Haider, S.A., Sheel V. and Lal, S. "Modeling of planetary atmospheres" edited by Published by Macmillan Publishers, India Ltd.

14. Kasaba, Y., Caro, G.M.M., T. Ito, P. Hartogh, C.Y.Robert Wu, Haider, S.A.,"Advances in Geosciences" editors: Vol 19 (2010), Published by World Scientific Company , Singapore.

Geosciences

15. Battarbee, R.,...Singhvi, A.K., et al., 2009, "*Science Plan and Implementation Strategy*", Past Global Changes IGBP Report No. 57, IGBP Secretariat, Stockholm. p.1-67.

16. Rengarajan, R., Soares, M., Rutgers van der Loeff, M., 2010, "*Natural radionuclides and radium isotopes*", In: Smetacek, V., Naqvi, S. W. A. (eds.), The expedition of the research vessel "Polarstern" to the Antarctic in 2009 (ANT-XXV/3 - LOHAFEX), Reports on polar and marine research, v. 613, p. 52-57.

17. Singh, A.D., Santhanam, M. S. and Ramesh, R., 2010,"*Numerical techniques*", in Modelling of Planetary Atmospheres (Eds. S.A. Haider, V. Sheel and S. Lal), Macmillan, Delhi, India, p.308-343.

18. Singhvi, A.K., Rupakumar, K., Thamban, M., Gupta, A.K., Kale, V.S., Yadav, R.R., Bhattacharyya, A., Phadtare, N.R., Roy, P.D., Chauhan, M.S., Chauhan, O.S., Chakravorty, S., Sheikh, M.M., Manzoor, N., Adnan, M., Ashraf, J., Khan, A.M., Quadir, D.A., Devkota, L.P., and Shrestha, A.B., 2009, "*Instrumental, Terrestrial and Marine Records of the Climate of South Asia During the Holocene: Present status, unresolved problem and societal aspects"*, In Global Environmental Changes in South Asia: A Regional Perspective A.P. Mitra

19. Singhvi, A.K., and Kale, V.S., 2009, "*Paleoclimate Studies in India Last Ice Age to the Present*", Indian National Science Academy I GBP - WCRP - SCOPE Series 4, New Delhi, p. 34.

20. Tiwari, M., Managave, S.R., Yadava, M.G. and Ramesh, R., 2009, "*Spatial and temporal coherence of paleomonsoon records from marine and land proxies in the Indian region during the past 30ka*", (Ed. N. Mukunda) Platinum Jubilee Special Publication of the Indian Academy of Sciences, Bangalore, p. 517-535.

21. Tiwari, M. and Ramesh, R., 2010, "*Sun:Climate coupling on sub-decadal to multi-millennial time scales*", in Heliophysical Processes, (Eds. Gopalswamy, N.K; Hasan, S.S.; Ambastha, A.) Springer Berlin Heidelberg, p. 251-269.

22. Wunnemann, B., Kotlia, B.S. and Ramesh, R. (Eds.) 2009, "*Asian monsoon variability: Selected papers, AMV-PGC Conference, Nainital*", Quaternary International, v.213, no.1-2, p. 1-90.

Theoretical Physics

23. Das, A.C., 2010, "Reconnection processes in Sun and Heliosphere" in Heliophysical Processes, Editors: N. Gopalaswamy, S.S. Hasan and A. Ambastha, Publisher: Springer, 2010. and C. Sharma (Eds), Capital Publishing Co, Delhi. p. 54-124.

PRL Publications

Technical Reports

T.A. Rajesh

1. "*Data Acquisition over Ethernet using Serial Device Server - NPort 5210*", PRL-TN-2010-96, Physical Research Laboratory, Ahmedabad, December, 2009.

Jigar Raval

2. "*The New Spacenet System at PRL*", PRL-TN-2009-94, Physical Research Laboratory, Ahmedabad, May, 2009.

Other Publications

R.S. Gupta and Hari Om Vats

1. Edited a book entitled PRL VIGYAN MALA, containing the scientific papers presented at the seminar in Hindi at PRL held on 13 March 2009.

Facilities and Services

Administration

As a part of implementation and progressive use of Hindi in PRL, the Hindi Pakhwada was celebrated at PRL from September 14 - 28, 2009. The highlights of the celebrations included word quiz, essay, elocution, Hamara Karya, self written poetry competitions. A Technical Seminar in Hindi on New frontiers in Basic and Applied Sciences was held at PRL on 23 March, 2010. 30 members presented their papers in this Seminar. Vishwa Hindi Divas was organised in PRL on 15.1.2010 and an essay competition was held on Global warming. In house magzine PRL News is being published in regular interval.

Computer Centre

To cater to the High Performance Computing needs of our scientists, Computer Centre is equipped with High Performance Compute Cluster having 20 compute nodes, (F&S1) 1 master node with 64GB RAM on each node, 10TB storage capacity and 3.2 TF peak computing performance and 2.2 TF sustained computing performance. The HPC cluster has a Backup node, I/O node, Management node, Storage node, and a Visualization node. The HPC facility is homed in a special chamber that is maintained at controlled temperature and humidity and has a dual UPS system for round the clock operation. The primary network of HPC is with Infiniband and secondary network is Gigabit. Computer Center has Dell server having 16 AMD processors, 64GB RAM with 4TB disk capacity. Centre also has four HP servers, each having four AMD processors, 4 GB RAM, 1.5 TB disk space providing computing power with large disk storage. Computer centre has also IBM Power5 4 CPU based server providing additional computing power. All these computing machines are connected to our high-speed (100/1000 Mbps) local area network (LAN) to provide easy, fast and reliable access to more than 200 PC's and a few workstations distributed throughout all the campuses of our laboratory. PRL dispensary in the colony campus opposite IIM is now connected to the Main Campus over a 10Mbps wireless link. Through this link, the PRL Medical Officers access the Dispensary database housed in the CoWAA cell in computer center. Through the same wireless link, the students and PDFs have a round the clock access to PRL LAN/Internet from their rooms via a few Wi-Fi devices installed in the buildings. Students from Thaltej Hostel also can access Internet through a Wi-Fi device installed in the common room in the hostel. The connectivity between Udaipur Solar Observatory (USO) and PRL Main Campus is 2 Mbps through BSNL – MLLN (Managed Leased Line Network). Mt.Abu is also connected to PRL main campus over 2 Mbps MLLN link provided by BSNL. Our Thaltej Campus is connected over a Optical Fiber 34 Mbps through BSNL-MLLN link. Thus, round the clock connectivity has been provided to users all the time from Thaltej, USO, and Mt. Abu. Our main campus is also connected to Thaltej via BSNL's 2 Mbps MLLN for voice communication providing intercom telephone facility

between the campuses. The Centre provides centralized virus free E-mails by automatically scanning all incoming E-mails. Anti-Spam filter has been centrally installed to fight the Spam mails. The center also provides web enabled email service. Internet authorizations, monitoring and reporting functions have been added to have optimal usage of Internet bandwidth.

F&S.1: Twenty node cluster computer at PRL with a capacity to deliver 3 TFLOPS

To cater to the High end computing needs, PRL has become resource partner of C-DAC's Grid Garuda Project. The Grid Garuda network is integrated to PRL LAN providing seamless access of Garuda resources to PRL scientists.

PRL SPACENET connectivity for Data, Intranet, and video conferencing has been established at Main Campus, USO and IR Observatory over IP to interact with ISRO centers.

Mathematical, numerical and visualization application software like IMSL, IDL, Mathematica, SigmaPlot, MATLAB, Lahey FORTARN 95, and Data Explorer etc. have also been installed to cater the needs of the scientific community.

Library & Information Services

Library plays a crucial role in facilitating research in the laboratory by making available latest books, journals, e-journals in the respective areas. In addition to procuring these, PRL Library subscribes to full-text databases like Science Direct, IOP Archive, PROLA, GSA Archive, SPIE Digital Library. As no library can be completely self-sufficient, it also provides document delivery service through ILL. The CD server housed in the library allows the students and staff to access the CDs from their desktops. In this period RFID system was implemented at USO Library too. Also, all the three libraries – Main, Thaltej and USO are now wi-fi enabled.

During 2009-10 the Library assisted the students and scientists in procuring 211 books for book grant and 37 books for personal use. The number of books added in Main, Thaltej and USO libraries was 374, Hindi books added were 102, and CDs/DVDs added were 80. In USO, 28 scientific books and 20 Hindi books were added in 2009-10 (F&S-2). As a value added service the Library informs its users about the 'Recent Arrivals' of books through email.

During 2009-10, number of visitors, visiting the library were 4512 (F&S-3) and number of documents issued were 4229. The number of ILL requests of other institutes fulfilled by PRL Library was 190 and that of requests of PRL staff fulfilled by other libraries was 275 (F&S-4). Number of Photocopies made in house were 23244 and by outside agency were 55848.

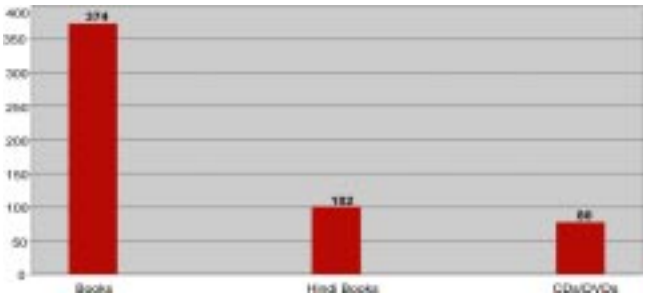

F&S.2: No of documents added to the collection in 2009-10

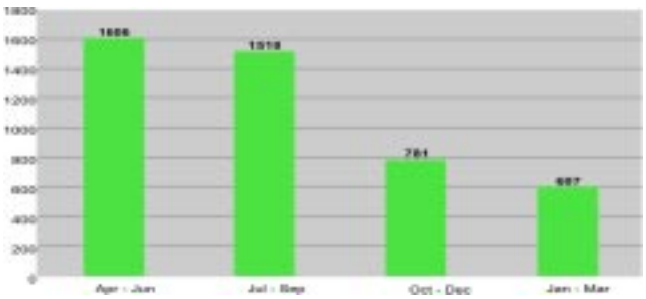

F&S.3: Footfalls in the Library during 2009-10

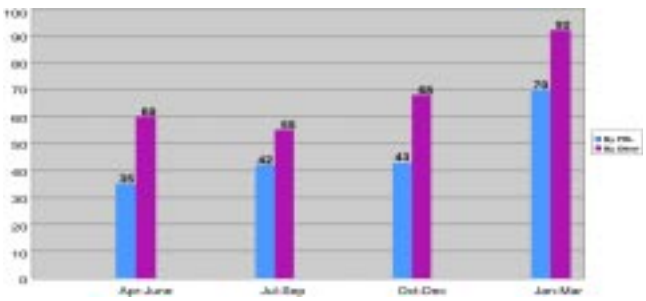

F&S.4: Inter-Library Loan requests full-filled

The library homepage gives link to 150 online journals out of the 158 journals subscribed by the library. It also

provides access to the institutional repository consisting of journal articles published by the PRL authors from 1995 to present using the Greenstone Digital Library Software (GSDL software).

A book exhibition was organized by the Library to facilitate the students and staff to procure the books for book grant in the month of July 2009 (F&S-5).

F&S.5: Book Exhibition for students, July 2009.

Workshop

PRL Workshop is a general-purpose mechanical workshop that provides extensive support to scientists and engineers. The workshop has a wide range of machines such as metal cutting machines, welding machines and CNC Lathe Machine in machine shop. The workshop plays an important role in designing, developing and manufacturing precise mechanical components and helps the scientists / engineers to establish various systems for different experimental set up. Two new machines, conventional lathe and horizontal band saw have been installed to machine heavy/bigger jobs and cutting different sections of raw material with high accuracy respectively. The workshop also carries out sheet and structural metal fabrication jobs. The high vacuum welding joints are also carried out by using TIG welding machine. The workshop is equipped with one CNC Lathe machine to carry out precise turning jobs. Various high precision jobs including optical component adapters and mounts are being fabricated at the workshop**.**

Some of the major works carried out during the year are listed below

(1) CASSEGRAIN UNIT (PARAS PROJECT)

The Cassegrain unit for PARAS project is designed, developed and fabricated in Workshop as per the requirement/ inputs given by the user. The first unit has been integrated with IR-Telescope at Mt. Abu observatory and also interfaced with High Resolution Echelle Spectrograph. The Spectrograph gets the star-light from the telescope through cassegrain unit using Fiber-Optics. The unit contains a Tip-Tilt system, an auto guider and a focal reducer to F/4.5 from F/13 for getting the light in to the fiber. All these are mounted on a precision 3 dimensional X-Y-Z Stage that can move with an accuracy of 5 microns using stepper motor drive through flexi-couplers. The unit consists of circular mounting plate to couple cassegrain housing, beam splitter, calibration unit which simulate the telescope F/13 beam and puts in the spectral lamp light into the fiber for simulation.

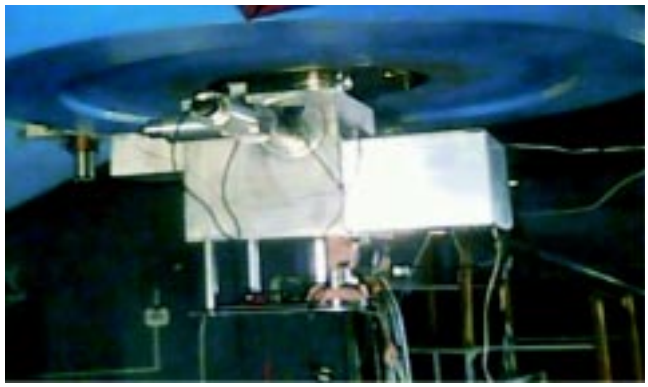

F&S.6: Cassegrain unit integrated with IR telescope at Mt Abu Observatory

Sub systems/components were machined with high accuracy of the order of 10-20 microns to achieve high precision. The components were made by using aluminum alloy material, brass, Teflon and S.S 304 material. The whole unit was mounted with telescope, interfaced with spectrograph and aligned with the system. In the first phase, the unit has been tested and preliminary results were obtained successfully. In the next phase, a better tip/tilt unit, a new Focal Reducer and a Iodine Cell inside the Cassegrain unit for higher through put will be incorporated.

F&S.7: Cassegrain unit

The workshop team has contributed substantially at work shop and also at field station Mt. Abu. The unit is shown in (F&S6 to 8).

F&S.8: Cassergrain unit with Team

(2) Shaft extension with mounting bracket for new encoder mounting on IR-TELESCOPE at Mt.Abu Observatory

Designed, developed and commissioned a new shaft extension with mounting brackets for the encoder RCN829 29bit rotary high resolution angle in telescope system with high accuracy of the order of 10 microns. The unit was installed and integrated with IR telescope for high precision and alignment requirements. It has been tested with the actual observation and found that the performance of the new encoder with the mountings has significantly improved the tracking and pointing accuracy of the telescope as shown in (F&S-9).

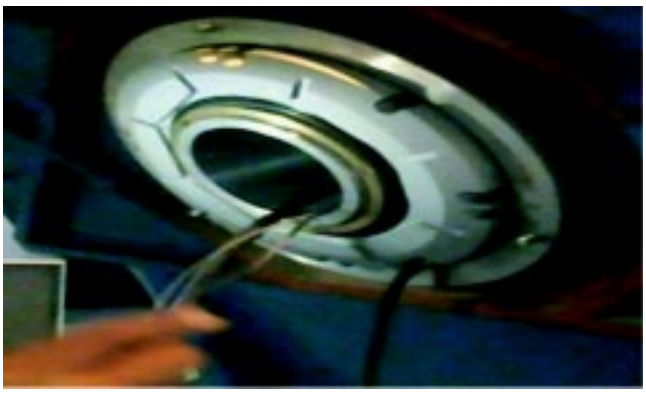

F&S.9: A new encoder integrated with main drive of the IR telescope

(3) Optical Arrangement for EMCCD Instrument (GSDN)

A subsystem of CCD based spatially resolved luminescence spectrometer has been designed. The spectrometer measures the spatially resolved luminescence emitted by a surface. The design ensures no leakage of light in to spectrometer from ambient. About 30 nos. of high power LEDs (Blue & Red) color are housed in the LED holders at an angle such that light concentrates on to the heater plate. It includes lens adjustment, mounting mirror at 45ˆ and other precise jobs. The system along with all parts and assembly is shown in (F&S-10).

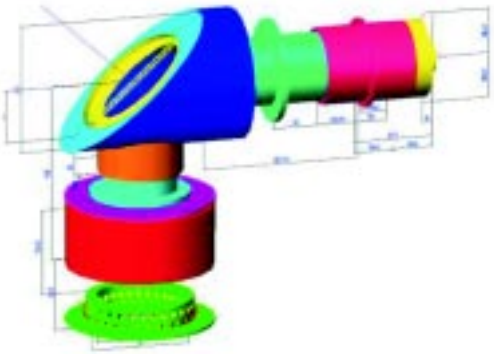

F&S.10: Optical arrangement for EM CCD Instrument

(4) Electric Field Sensor Probe (SPA/AP)

A very precise Electric Field probe Sensor has been designed and fabricated using CNC lathe machine. A special kind of face grooving tool was developed for this purpose. This type of tool for internal radius turning is not available commercially. Machining of outer Radius was being completed by using button tool. Assembly of top half and bottom half assemblies are shown in (F&S-11).

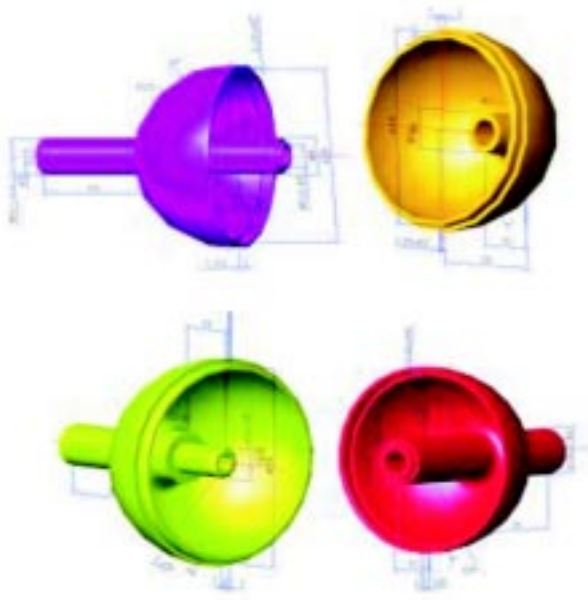

F&S.11: Electric field sensor probe

(6) Airglow Imaging System (SPA/SC)

A complete assembly of multi-wavelength airglow imager was carried out this year which is designed to characterize the three dimensional characteristics of atmospheric gravity waves. This consists of several lenses, automated filter wheel system, a highly sensitive cooled CCD detector and mechanical coupling between the filter wheel and the CCD detector. This also involves critical focusing of the lenses which is also done successfully in our workshop.

(7) Reflectron Electrode Assembly (SPA/SC)

The reflector has been made with several thin, equally-spaced, coaxially assembled rings with high transmission wire mesh at one end and a flat plate at the other. The rings will be in a potential divider arrangement, for creating the electric hence parallelism and equal spacing are critical. Total 15 thin 2mm thick Al. flanges of 120mm outer diameter and inner diameter ranging from 30mm to maximum 72 mm, were assembled with 3 studs. Also assembly consists of 51 Al. spacers and 45 Teflon spacers. An ion reflector based on the creation of a uniform retarding electric field over a large volume is needed for a Reflectron time-of-flight mass spectrometer.

(8) Laser Ablation Cluster Source (SPA/SC)

A Stainless Steel Block of Size 69mm L x 43mm W x 30mm H was designed and manufactured in workshop. The criticality involved in the manufacturing was regarding the holes which were almost on all the faces of S.S. block. A Small type cell for a laser ablation cluster source has been designed. It consists of three orthogonal channels for a laser beam, gas admittance and a target rod. The focused laser pulse ablates the target rod while the rod is constantly rotating. Gas is admitted synchronous with the laser and drives the ablated material out of the cell. Vacuum coupling of the cell to the chamber and quartz windows for the laser are provided.

Honorary Fellows

Professor J. E. Blamont

Academician V. I. Ginzburg

Professor A. M. J. Tom Gehrels

Professor D. Lal, FRS

Professor M. G. K. Menon, FRS

Professor U. R. Rao

Professor P. Crutzen

Professor K. Kasturirangan

Professor A. Hewish

Honorary Faculty

Honorary Academic Faculty

Prof. R. K. Varma, FNA, FASc, FNASc

Prof. S. Krishnaswami, FNA, FASc, FNASc, FTWAS
INSA Senior Scientist

Prof. R. G. Rastogi, FNA, FASc, FNASc
Visiting Professor

Prof. S. K. Bhattacharya, FASc, FNASc

Dr. S. K. Gupta, FNASc

Prof. A. C. Das

Prof. N. Bhandari, FNA, FASc, FNASc
INSA Honorary Scientist

Prof. D. P. Dewangan, FNASc

Dr. S. P. Gupta

Prof. Harish Chandra

Prof. H. S. S. Sinha

Honorary Technical Faculty

R. N. Misra
(Director,CSSTEAP School)

D. V. Subhedar

Academic Faculty

Name	Designation	Specialisation	Academic Qualification
Goswami J. N. *FNA, FASc, FNASc, FTWAS*	Director	Solar System Studies (Pre - Solar Processes)	Ph D, PRL, Gujarat Univ. (1978)
Ambastha A. K.	Professor	Solar Plasma Physics, Coronal Structure andPolarization	Ph D, PRL, Gujarat Univ. (1981)
Amritkar R. E. *FASc*	Professor	Nonlinear Dynamics &Chaos	Ph D, IISc, Bangalore (1978)
Ashok N. M.	Professor	Close Binary Stars, NovaeIR spectroscopy	Ph D, PRL, Gujarat Univ. (1983)
Baliyan K. S.	Associate Professor	AGNs, Comets, Atomic Physics, Milky Way	Ph D, Roorkee Univ. (1986)
Banerjee D.	Associate Professor	Thermoluminscence & Planetary Physics	Ph D, PRL, Gujarat Univ. (1996)
Banerjee D. P. K.	Professor	Novae, Be Stars,Planetary Nebulae, IR and Optical Studies	Ph D, PRL, Gujarat Univ. (1991)
Banerji J.	Professor	Classical Optics, Quantum Physics	Ph D, City Univ.(New York) (1982)
Bapat B.	Associate Professor	Atomic & Molecular Processes	Ph D, TIFR, Mumbai Univ. (1997)
Bhatt J. R.	Associate Professor	Astrophysics	Ph D, IPR, MS Univ. (1992)

Name	Designation	Specialisation	Academic Qualification
Bhushan Ravi	Scientist-SE	Oceanography and Paleoclimatology	Ph D, MS Univ.(2009)
Chakrabarty A.	Reader	Extra-solar planets, Star Formation & Instrumentation	Ph D, PRL, Gujarat Univ. (1999)
Chakrabarty D.	Scientist-SE	Upper Atmoshere and Geomagnetic Storm	Ph.D, PRL, MLS Univ. (2008)
Chandrasekhar T.	Professor	High Angular Resolution Studies, Late type stars Solar Coronal, Studies Comets	Ph D, PRL, Gujarat Univ. (1982)
Das R.	Scientist-SD	Geochemistry	Ph D, Florida State Univ.(2006)
Deshpande R. D.	Scientist-SE	Application of Environmental Tracers in Hydrology	Ph D, PRL, MS Univ. (2007)
Gosain S.	Scientist-SD	Solar Physics and Instrumentation	Ph D, MLS Univ. (2007)
Goswami S.	Associate Professor	High Energy Physics	Ph D, Calcutta Univ. (1998)
Haider S. A. *FASc*	Professor	Planetary and Cometary Atmospheres	Ph D, Banaras Univ. (1984)
Jain R.	Professor	Solar Physics	Ph D, PRL, Gujarat Univ. (1983)
Janardhan P.	Associate Professor	Solar Radio Astronomy & Space Weather	Ph D, PRL, Gujarat Univ. (1992)
Joshi B.	Scientist-SD	Solar Physics, Astronomy	Ph D, ARIES, Kumaun Univ. (2007)
Joshi U. C.	Professor	AGNs, Milky way, Star Formation and Comets	Ph D, Kumaun Univ. (1981)
Joshipura A. S. *FNA, FASc, FNASc*	Outstanding Scientist	Particle Physics	Ph D, Bombay Univ. (1979)
Juyal N.	Scientist-SE	Quaternary Geology & Paleoclimate	Ph D, M.S.Univ. (2004)
Kota V. K. B.	Senior Professor - H	Nuclear Physics	Ph D, Andhra Univ. (1977)
Kumar B.	Scientist-SD	Solar Physics	Ph D, PRL, MLS Univ. (2007)
Lal S. *FNA, FASc, FNASc*	Senior Professor	Atmospheric Chemistry and Trace Gases	Ph D, PRL, Gujarat Univ. (1982)
Mahajan N.	Reader	Particle Physics	Ph D, Delhi Univ. (2003)
Marhas K. K.	Reader	Solar System studies	Ph D, PRL, DAVV Indore (2001)
Mathew S. K.	Associate Professor	Solar Magnetic & Velocity Fields	Ph D PRL, Gujarat Univ. (1999)

Name	Designation	Specialisation	Academic Qualification
Mishra H.	Associate Professor	Strong Interaction Physics & Nuclear Astrophysics	Ph D, IOP, Utkal Univ. (1994)
Mohanty S.	Professor	Astroparticle Physics	Ph D, Wisconsin Univ. (1989)
Murty S. V. S. *FASc*	Professor	Isotope Cosmochemistry	Ph D, IIT, Kanpur (1981)
Naik S.	Reader	High Energy Astro- physics, X-ray Binaries	Ph D,TIFR,Mumbai Univ. (2003)
Panigrahi P. K.	Associate Professor	Field Theory	Ph D, Rochester Univ. (1988)
Rai V.	Reader	Stable Isotope Cosmochemistry	Ph D, PRL, MS Univ. (2001)
Pallam Raju D.	Associate Professor	Space and Atmospheric Sciences	Ph D, PRL, DAVV Indore(1996)
Ramachandran S.	Associate Professor	Atmospheric AerosolsRadiative & Climate Impacts	Ph D, PRL, MS Univ. (1996)
Ramesh R. *FNA, FASc, FNASc, FTWAS*	Senior Professor	Paleoclimatology, Oceanography & Modelling	Ph D, PRL, Gujarat Univ. (1984)
Rangarajan R.	Associate Professor	Particle Physics & Cosmology	Ph D, Univ. of California, Santa Barbara (1994)
Rao B. G. A.	Senior Professor	Star formation, Planetary Nebulae, AGB Stars and Imaging Fabry Perot Spectroscopy	Ph D, PRL, Gujarat Univ. (1978)
Ray J. S.	Associate Professor	Isotope Geochemistry	Ph D, PRL, MS Univ. (1998)
Rengarajan R.	Scientist-SE	Atmospheric aerosols & aqueous geochemistry	Ph D, PRL, MLS Univ. (2004)
Rindani S. D. *FASc, FNA, FNASc*	Senior Professor-H	Particle Physics	Ph D, IIT, Bombay (1976)
Sarin M. M. *FASc, FNA, FNASc*	Senior Professor	Geochemistry and Oceanography	Ph D, PRL, Gujarat Univ. (1985)
Sarkar U. *FNA, FASc, FNASc*	Senior Professor	Particle Physics	Ph D, Calcutta Univ. (1984)
Sekar R.	Professor	Upper Atmospheric & Ionospheric Physics	Ph D, PRL, Gujarat Univ. (1991)
Sheel V.	Reader	Modelling of Lower Atmosphere	Ph D, PRL, Gujarat Univ. (1996)
Sharma Som K.	Scientist-SE	Middle Atmosphere & Long Term Atmospheric Changes	Ph D, PRL, Gujarat Univ. (2010)
Singal A. K.	Associate Professor	Radio Astronomy & Astrophysics	Ph D, TIFR, Bombay Univ. (1986)
Singh A. D.	Associate Professor	Atomic Physics	Ph D, Bangalore Univ. (1998)
Singh R. P.	Scientist – SF	Laser Physics	Ph D, JNU, New Delhi (1994)

Name	Designation	Specialisation	Academic Qualification
Singh S. K.	Associate Professor	Isotope Geochemistry	Ph D, PRL, MS Univ. (1999)
Singhvi A. K. *FNA, FASc, FNASc, FTWAS*	Outstanding Scientist	Palaeoclimatology and Geochronology	Ph D, IIT, Kanpur (1975)
Srivastava N.	Associate Professor	Solar Physics	Ph D, PRL, Ravi Shankar Shukla Univ. (1994)
Subramanian K. P.	Associate Professor	Experimental Atomic and Molecular Physics	Ph D, PRL, Gujarat Univ. (1987)
Vadawale S. V.	Reader	High Energy Astrophysics and X - ray Spectroscopy	Ph D, TIFR, Mumbai Univ. (2003)
Vats H. O.	Associate Professor	Space Weather & RadioAstronomy	Ph D, PRL, Gujarat Univ. (1979)
Venkatakrishnan P.	Senior Professor-H	Solar Physics	Ph D, Bangalore Univ. (1984)
Yadava M. G.	Scientist-SE	Palaeoclimate, Radiocarbon dating and Stable isotopes	Ph D, PRL, DAVV Indore (2003)

Technical Faculty

Name	Designation
Acharya Y. B.	Engineer-G
Adhyaru P. R.	Engineer-SE
Dadhania M. B.	Engineer-SF
Dholakia G. G.	Scientist-SG
Dutt N.	Engineer-SF
Ganesh S.	Scientist-SE
Jokhakar D. H.	Engineer-SE
Modh K. S.	Engineer-SE
Narayanan R.	Scientist-SF
Prajapati I. A.	Scientist-SE
Rao D. K.	Scientist-SE
Shah A. B.	Engineer-SF
Shah K. J.	Scientist-SE
Shah R. R.	Engineer-SF
Singh Mahendra	Engineer-SF
Ubale G. P.	Engineer-SE
Venkataramani S.	Scientist-SE